M-405 | 2015

Sea Level Change for Norway

Past and Present Observations and Projections to 2100

NCCS report no. 1/2015

Photo: Einar Egeland

Authors

M.J.R. Simpson, J.E.Ø. Nilsen, O.R. Ravndal, K. Breili, H. Sande, H.P. Kierulf, H. Steffen, E. Jansen, M. Carson, O. Vestøl

Kartverket

NERSC Nansensenteret

Bjerknes Centre for Climate Research

Commissioned by:

Norwegian Centre for Climate Services (NCCS) is a collaboration between the Norwegian Meteorological Institute, the Norwegian Water Resources and Energy Directorate and Uni Research. The main purpose of NCCS is to provide decision makers in Norway with information relevant for climate change adaptation. In addition to the partners, the Norwegian Environment Agency is represented on the Board.

The NCCS report series includes not only reports where one or more authors are affiliated to the Centre, but also reports that the Centre has initiated. All reports in the series have undergone a review by at least one scientist associated with the Centre. Reports in this series can also be included in report series from the institutions where the main authors are affiliated.

Title: Sea Level Change for Norway Past and Present Observations and Projections to 2100	**Date:** 09.09.2015
ISSN no.: 2387-3027	**Report no.** 1/2015
Author(s): M. J. R. Simpson, J. E. Ø. Nilsen, O. R. Ravndal, K. Breili, H. Sande, H. P. Kierulf, H. Steffen, E. Jansen, M. Carson, O. Vestøl	**Classification:** ● Free ○ Restricted
Client(s): Norwegian Environment Agency	**Client's reference:** M405|2015 www.miljodirektoratet.no/20803

Abstract:

Changes to mean sea level and/or sea level extremes (e.g., storm surges) will lead to changes in coastal impacts. These changes represent a changing exposure or risk to our society. Here we try to synthesize our understanding of past and present observed sea level changes for Norway, as well as providing sea level projections up until 2100. Our primary focus is changes to mean sea level but we also give updated return heights for each coastal municipality in Norway.

We first analyse observed sea level changes from the Norwegian tide gauge network and from satellite altimetry. After the tide gauge data have been corrected for the effects of glacial isostatic adjustment, we show that 20th century sea level rise in Norwegian waters is broadly similar to the global average rise. Contributions to the observed sea level change and variability are discussed. We find that rate of sea level rise along the Norwegian coast is significantly higher for the period 1993–2014 than for the period 1960–2010. It is unclear, however, to what extent this higher rate represents natural variability rather than a sustained increase owing to global warming.

Our regional sea level projections are based on findings from the Fifth Assessment Report (AR5) of the Intergovernmental Panel for Climate Change (IPCC), and the Coupled Model Intercomparison Project phase 5 (CMIP5) output. Average projected 21st century relative sea level change in Norway is -0.10–0.35 m (5 to 95% model ranges which is the *likely* range in AR5; P>66%) for RCP2.6, -0.05–0.45 m for RCP4.5, and 0.10–0.65 m for RCP8.5. The relative sea level projections can differ as much as 0.50 m from place to place. This pattern is governed by the vertical uplift rates. Quantifying the probability of levels above the *likely* range (i.e., the upper tail of the probability distribution) remains difficult because information is lacking. And of particular concern is that the ice sheet contribution might have a skewed distribution, which would mean values in its upper tail would be quite large.

Finally, we show how the estimated return heights can be combined with our regional sea level projections to provide allowances. Allowances give the height by which an asset needs to be raised so that the probability of flooding remains preserved for a given sea level change. A possible attractive option in planning.

Keywords

Sea level change, Norway, observations, tide gauges, altimetry, land uplift, GIA, future projections, storm surges, extreme-value analysis, Hunter's method, allowances, probability distributions.

_____ Disciplinary signature

_____ Responsible signature

Sea Level Change for Norway: Past and Present Observations and Projections to 2100

Authors

Matthew J. R. Simpson[1], J. Even Ø. Nilsen[2], Oda R. Ravndal[3], Kristian Breili[1], Hilde Sande[3], Halfdan P. Kierulf[1], Holger Steffen[4], Eystein Jansen[5], Mark Carson[6], Olav Vestøl[1].

Affiliations

1. Geodetic Institute, Norwegian Mapping Authority, 3507 Hønefoss, Norway.
2. Nansen Environmental and Remote Sensing Center and Bjerknes Centre for Climate Research, Thormøhlensgt. 47, 5006 Bergen, Norway.
3. Hydrographic Service, Norwegian Mapping Authority, Professor Olav Hanssens vei 10, 4021 Stavanger, Norway.
4. Lantmäteriet, Lantmäterigatan 2C, 801 82 Gävle, Sweden.
5. Department of Earth Science at University of Bergen, and Bjerknes Centre for Climate Research, Allégt. 41, 5007 Bergen, Norway.
6. Institute of Oceanography, KlimaCampus Universität Hamburg, Bundesstraße 53, 20146 Hamburg, Germany.

Corresponding authors

Matthew J. R. Simpson (matthew.simpson@kartverket.no)

J. Even Ø. Nilsen (jan.even.nilsen@nersc.no)

Citation

Simpson, M. J. R., J. E. Ø. Nilsen, O. R. Ravndal, K. Breili, H. Sande, H. P. Kierulf, H. Steffen, E. Jansen, M. Carson and O. Vestøl (2015). Sea Level Change for Norway: Past and Present Observations and Projections to 2100. Norwegian Centre for Climate Services report 1/2015, ISSN 2387-3027, Oslo, Norway.

Other series

This report is also included in the following report series. External citation remains as above.

- NERSC Technical Report no. 356
- Norwegian Environment Agency report no. M405 | 2015

URL

This report can be downloaded at www.miljodirektoratet.no/20803

Sammendrag på norsk

Denne rapporten gir en samlet og oppdatert presentasjon av havnivåendringer i Norge ut fra tilgjengelige data. Dette inkluderer framskrivinger og ekstremverdier (stormflonivåer) for hver eneste kystkommune i Norge. Å beregne framtidige havnivåendringer krever god forståelse av mange forskjellige aspekter ved klimasystemet. Nøkkelen til denne forståelsen ligger i å kunne identifisere separate bidrag til havnivåendring, siden disse ikke bare reagerer forskjellig på den globale oppvarmingen, men også bidrar forskjellig i ulike regioner. Opprettholdelse og forbedring av både observasjonssystemer og modelleringsverktøy er nødvendig for å sikre stadig bedre framskrivinger av regionalt havnivå. I tillegg til de langsomme klimatiske endringene i det normale havnivået, undersøkes endringer i ekstremverdier (stormflonivåer) som vi allerede har erfaring med i dag. Vi oppsummerer resultatene fra rapporten i dette sammendraget.

De viktigste bidragene til havnivåendring i Norge

De viktigste bidragene til pågående og forventede endringer i globalt havnivå er varmeutvidelse og økt tilførsel av smeltevann fra verdens breer og iskapper. Ulik grad av varmeutvidelse fra sted til sted, samt endringer i tyngdefelt, vind, og havstrømmer, fører til regionale forskjeller. Også i norske farvann er hovedårsakene til den langsiktige stigningen varmeutvidelse og smeltingen av landbasert is i verden, men strandlinjen stiger langsommere her fordi landet også stiger. Hovedgrunnen til denne landhevingen er at ismassene som dekket Nord-Europa under siste istid, presset jordskorpen ned i mantelen, og tilbakejusteringen tar tusenvis av år. Ettersom landhevingen varierer langs Norskekysten, vil den opplevde havnivåendringen i form av stigende strandlinje variere tilsvarende. Effekter av endringer i havstrømmer, som også involverer vind, kan på en mellomårlig og tiårlig tidsskala gi betydelige avvik fra de langsiktige endringene.

Tidligere havnivåendringer i Norge

Da ismassene som dekket Nord-europa under siste istid, begynte å trekke seg tilbake, begynte landmassene straks å løfte seg på grunn av vektendringene. Fra tiden etter landet vårt kom til syne for 12 000 år siden finnes data som viser at havnivået relativt til land, sank med flere titalls meter over et par tusen år. Samtidig smeltet også ismasser ellers i verden og det globale havnivået steg kraftig. Derfor var tiden fram til for omtrent 6000 år siden preget av store variasjoner i havnivået langs Norges kyst. Avsmeltningen var nå stort sett fullført og det globale havnivået holdt seg mer eller mindre konstant. Men tilbakejusteringen av jordskorpen etter avsmeltningen av den nord-europeiske innlandsisen, fortsatte med omtrent konstant hastighet og medførte at det relative havnivået sank jevnt fram til moderne tid. De siste tiårene er det imidlertid observert tegn på at akselererende havnivåstigning har tatt igjen landhevingen flere steder, slik at vi i dag også her opplever havnivåstigning relativt til land.

Vannstandsmålerne langs Norskekysten gir fra slutten av 1800-tallet og fram til i dag direkte målinger av havnivået i forhold til land. Enkelte områder i Norge har opplevd fall i relativt havnivå og andre en begrenset stigning. Over perioden 1960–2010 er det observert endringer som varierer mellom 13 centimeter fall i Oslo og 6 centimeter stigning i Stavanger. Dersom

vannstandsmålingene korrigeres for landheving, kan vi beregne endring av det absolutte havnivået (dvs. i forhold til en global referanseramme). Vi har undersøkt tre perioder, 1960–2010, 1984–2014 og 1993–2014, og ser en klar økning i stigning. Gjennomsnittsverdiene for de undersøkte stasjonene er henholdsvis 1,9 mm/år, 2,4 mm/år og 3,6 mm/år i disse periodene. For den siste perioden, 1993–2014, har vi også undersøkt to datasett med høydemålinger fra satellitter, og for norskekysten er endringene estimert til 3,1 og 3,4 mm/år avhenging av hvilket datasett som legges til grunn.

Usikkerheten knyttet til disse tallene ligger i størrelseorden 0,6–0,8 mm/år og skyldes i hovedsak mulig instabilitet av den globale referanserammen. Det er også viktig å understreke at det er uklart i hvilken grad den observerte økning i havnivåstigning mellom periodene nevnt over, er en akselerasjon som forårsakes av global oppvarming, eller et uttrykk for naturlig variasjon.

Framtidig havnivå i Norge

Denne rapporten presenterer framskrivinger av relativt havnivå i Norge (dvs. relativt til land). Disse er basert på funn i den femte hovedrapporten (AR5) til FNs klimapanel (IPCC), og fra klimamodellprosjektet CMIP5. Vi vurderer de tre utslippscenariene RCP2.6, RCP4.5 og RCP8.5. Framskrivingene våre tar hensyn til regionale variasjoner i (1) havets tetthet, omfordeling av vannmasser og sirkulasjon, (2) totale masseendringer i havet og tilhørende endringer i tyngdefeltet, og (3) landheving og tilhørende endringer i tyngdefeltet. Det er anvendt egne beregninger for punkt (3). I tillegg er det gjort beregninger av endringer i tyngdefeltet pga. omfordeling av masse i havet.

Framskrivingene viser at det regionale mønsteret for relative havnivåendringer i Norge domineres av landhevingen i Skandinavia. Landhevingen medfører også at relativ havnivåstigning i Norge framskrives til å bli noe lavere enn det globale gjennomsnittet. Framskrivningenes middelverdier (mellom modellene) for endringer fra 1986–2005 til 2081–2100 er, for

- RCP2.6, mellom -10 og 30 cm, avhengig av sted.
- RCP4.5, mellom 0 og 35 cm, avhengig av sted.
- RCP8.5, mellom 15 og 55 cm, avhengig av sted.

De regionale ulikhetene, samt størrelsen på intervallene for sannsynlige endringer, kan beskrives med noen eksempler. Det legges til grunn middelverdiene (mest sannsynlige endring) for utslippsscenariet RCP8.5 og avrundes til nærmeste 10 cm:

- 20 cm med et sannsynlig intervall på -10 – 50 cm for Oslo.
- 50 cm med et sannsynlig intervall på 30 – 80 cm for Stavanger.
- 50 cm med et sannsynlig intervall på 20 – 70 cm for Bergen.
- 30 cm med et sannsynlig intervall på 10 – 60 cm for Heimsjø (Trøndelagskysten).
- 30 cm med et sannsynlig intervall på 10 – 60 cm for Tromsø.
- 40 cm med et sannsynlig intervall på 10 – 80 cm for Honningsvåg.

Framskrivningene for alle scenariene indikerer at det meste av Norge vil oppleve stigende relativt havnivå før slutten av dette århundret. Tallene over gir det generelle bildet for Norge, men framskrivningene og deres usikkerheter bør vurderes fra kommune til kommune. Det komplette tallmaterialet finnes i rapportens tillegg. Det oppgis også tall for perioden 2041–2060 og for året 2100, relativt til 1986–2005.

For tiden etter 2100 er det ikke gjort regionale framskrivinger av havnivå. Men som nevnt i AR5, er det "så godt som helt sikkert" (det høyeste konfidensnivået til IPCC) at gjennomsnittlig globalt havnivå vil fortsette å stige, og framskrivinger for 2300 spenner fra mindre enn 1 meter til mer enn 3 meter, henholdsvis for scenarier tilsvarende RCP2.6 og RCP8.5. Denne uttrykte vissheten om fortsatt stigning, uavhengig av klimagassutviklingen, er knyttet til tregheten i havets opptak av varme og tilhørende termisk ekspansjon, samt smelting av de store iskappene under et varmere framtidig klima. Det er vanskelig å beregne hva dette vil kunne bety for Norge, siden de relative bidragene kan endre seg over tid og dermed bidra annerledes langs Norskekysten enn til det globale gjennomsnittet.

Stormflo under framtidige havnivåendringer

Ekstreme høyder av havnivå opptrer som regel i forbindelse med stormflohendelser. De norske vannstandsmålerne registrerer havnivået kontinuerlig, og på bakgrunn av registreringene er det utført statistiske beregninger av returnivåer for ulike gjentaksintervaller for alle kystkommuner i Norge. Sannsynligheten for ekstremhendelser i dag, er altså kjent. For eksempel er returnivået (over middelvannstand) for et 200 års gjentaksintervall

- 1,9 meter i Oslo.
- 1,2 meter i Stavanger.
- 1,4 meter i Bergen.
- 2,1 meter i Heimsjø (Trøndelagskysten).
- 2,2 meter i Tromsø.
- 2,2 meter i Honningsvåg.

Returnivået er her det havnivået som i gjennomsnitt overstiges en gang i løpet av en 200 års periode. Returnivåer beskriver spesielle hendelser, og sannsynligheten for at de kan inntreffe er uttrykt ved gjentaksintervallet. Det komplette tallmaterialet finnes i rapportens tillegg, sammen med omregningstall til ulike kartreferansenivåer.

Framskrivinger av stormaktivitet er ansett som svært usikre, og er derfor ikke tatt i betraktning i denne rapporten. Men de ekstreme høydene vil også endre seg dersom middelvannstanden endrer seg. Returnivåene vil altså stige tilsvarende en framtidig havnivåstigning. En viktig konsekvens av den forventede havnivåstigningen i Norge, er at sannsynligheten for å overstige dagens returnivåer kan øke dramatisk. For eksempel i Stavanger og Bergen forventer vi ved RCP8.5 at dagens 200 års returnivå vil bli overskredet i 40 av de gjenstående år i dette århundre.

Når framskrivingene av de klimatiske endringene i havnivå skal legges til returnivåene for ekstremhendelser, må det tas hensyn til at framskrivningene har sannsynlighetsfordelinger

knyttet til seg. Det må altså gjøres valg med tanke på konsekvens og risiko også i forhold til havnivåendring. Vi demonstrerer som en mulig løsning, hvordan de beregnede returnivåene kan kombineres med våre regionale framskrivinger av framtidig havnivå for å angi klimapåslag. Denne typen klimapåslag angir høyden man for eksempel må løfte et gitt byggverk for at sannsynligheten for oversvømmelse ved ekstremhendelser skal forbli den samme ved en gitt endring i havnivå. Dette kan være nyttig kunnskap ved prosjektering av bygg som skal tåle framtidige havnivåendringer.

Sannsynlighet og mulig havnivåstigning utover det beregnede

Framskrivingene som presenteres i denne rapporten er, på samme måte som i AR5, angitt med et 5 til 95 % modellintervall. AR5 vurderer at framtidig havnivåendring med 66 % sannsynlighet vil ligge innenfor dette intervallet. Det finnes foreløpig ikke tilstrekkelig grunnlag for å kvantifisere sannsynlighet utenfor dette intervallet, men det bør bemerkes at eventuelle hendelser som involverer isdynamikk og påfølgende tap av landbasert is, spesielt i Antarktis, vil kunne medføre havnivåer over det beregnede intervallet.

Vi demonstrerer dette ved å benytte en skjev sannsynlighetsfordeling for bidraget fra isdynamikk i Antarktis, med grenser basert på eksisterende studier som tar høyde for kollaps av ismasser i Antarktis. Resultatet er at øvre sannsynlige grense for havnivåstigning i Norge blir betydelig høyere enn i de oppgitte framskrivingene. Kunnskapen om utviklingen i Antarktis er imidlertid svært usikker og vi gjør oppmerksom på at disse resultatene først og fremst har til hensikt å illustrere muligheten for å inkludere slike hendelser. En fullstendig beregning av havnivåstigning utenfor AR5s sannsynlige intervaller, vil måtte behandle alle bidragene på liknende måte og med et sikrere tallgrunnlag.

Abstract

Changes to mean sea level and/or sea level extremes (e.g., storm surges) will lead to changes in coastal impacts. These changes represent a changing exposure or risk to our society. Here we try to synthesize our understanding of past and present observed sea level changes for Norway, as well as providing sea level projections up until 2100. Our primary focus is changes to mean sea level but we also give updated return heights for each coastal municipality in Norway.

We first analyse observed sea level changes from the Norwegian tide gauge network and from satellite altimetry. After the tide gauge data have been corrected for the effects of glacial isostatic adjustment, we show that 20th century sea level rise in Norwegian waters is broadly similar to the global average rise. Contributions to the observed sea level change and variability are discussed. We find that rate of sea level rise along the Norwegian coast is significantly higher for the period 1993–2014 than for the period 1960–2010. It is unclear, however, to what extent this higher rate represents natural variability rather than a sustained increase owing to global warming.

Our regional sea level projections are based on findings from the Fifth Assessment Report (AR5) of the Intergovernmental Panel for Climate Change (IPCC), and the Coupled Model Intercomparison Project phase 5 (CMIP5) output. Average projected 21st century relative sea level change in Norway is -0.10–0.35 m (5 to 95% model ranges which is the *likely* range in AR5; P>66%) for RCP2.6, -0.05–0.45 m for RCP4.5, and 0.10–0.65 m for RCP8.5. The relative sea level projections can differ as much as 0.50 m from place to place. This pattern is governed by the vertical uplift rates. Quantifying the probability of levels above the *likely* range (i.e., the upper tail of the probability distribution) remains difficult because information is lacking. And of particular concern is that the ice sheet contribution might have a skewed distribution, which would mean values in its upper tail would be quite large.

Finally, we show how the estimated return heights can be combined with our regional sea level projections to provide allowances. Allowances give the height by which an asset needs to be raised so that the probability of flooding remains preserved for a given sea level change. A possible attractive option in planning.

Table of Contents

1 Introduction

In the global setting, Norway is not considered to be vulnerable to sea level rise. The coastline is largely characterized by a steep topography and rock types resistant to erosion. In addition to this, the land surface is experiencing ongoing uplift due to the loss of the large ice sheet that once covered Fennoscandia (a process known as glacial isostatic adjustment). It is well recognized that this uplift process will act to mitigate future sea level rise. These factors suggest Norway has a generally low physical vulnerability to sea level rise (Aunan and Romstad, 2008). Although this general perception may be true, there are nevertheless several reasons for wanting to gain a better understanding of future sea level changes and their associated risks. Firstly, as highlighted in a national vulnerability assessment, there are low-lying coastal areas of Norway which could be at risk owing to their important cultural and economic value (Aunan and Romstad, 2008). Secondly, it is prudent to take into account our changing climate in planning and/or adaption policy. We note that many of Norway's major cities are situated along the coast and, in recent years, some have undertaken large developments close to the shoreline. Thirdly, even if Norway may be at low risk compared to other countries, setting up a framework for how to apply the IPCC projections on a local scale is necessary and may also serve as an example for other countries.

Like in most Norwegian coastal cities, the harbour of Stavanger has a mixture of new development and cultural heritage right at the shoreline. Stavanger is likely to experience a sea level rise between 5 and 90 cm by 2100, depending on emission scenario. These numbers represent future additions to the already observed extreme levels, like the one shown here. (Photo: Jostein Berggraf, Stavanger kommune.)

For effective coastal management, it is important to understand how sea levels will change in the future. Changes to mean sea level, sea level extremes (e.g., storm surges) and/or wave events will lead to changes in coastal impacts. These changes represent a changing exposure or risk to our society. Note that in this report, we focus primarily on changes to mean sea level, i.e., the average over some period of time. We do not in any way assess the direct impacts of wave action and run-up. To be able to quantify the effect of sea level change on flood risk assessments, information on future sea levels is required in a probabilistic form (i.e., for a specific future date, an assessment is made of the probability or likelihood of a certain sea level occurring). Up until very recently, such projections for mean sea level changes were not achievable. In the Fifth Assessment Report (AR5) from the Intergovernmental Panel for Climate Change (IPCC), the authors outline how confidence in projecting sea level changes has improved (Church et al., 2013a). This has meant that probabilistic projections are now possible, but there remain significant challenges to overcome before projections of sea level change can be considered truly robust. Concerning storm surges and waves, there is generally low confidence in our ability to project regional changes of these effects. In this work we generally assume no future changes in their amplitude or frequency. However, it is important to emphasize that sea level extremes and their associated risks will nevertheless increase in combination with mean sea level rise.

The report is structured as follows. Chapter 1 outlines the motivation for the work and how we determine sea level changes. It also outlines past global sea level changes and their causes. Previous works on future projections of sea level change are described in Chapter 2, this includes the main findings of AR5 and progress since then, it also discusses earlier sea level projections for Norway. In Chapter 3 we analyze observed sea level changes in Norway from tide gauge records and satellite altimetry. Furthermore, we examine the contributions to these observed sea level changes. Chapter 4 details vertical land motion in Norway, an important component of present sea level change in Scandinavia, which we constrain using new GPS measurements and modelling. Our *regional* projections of 21st century sea level changes for Norway are given in Chapter 5. These are largely based on findings from AR5 and Coupled Model Intercomparison Project phase 5 (CMIP5) output (Taylor et al., 2012). Chapter 6 examines extreme sea levels in Norway. Here we show how storm surge return heights are determined using statistical analysis of the tide gauge observations (an example of this is the 1 in 200-year storm surge height which is currently used in Norwegian planning law). Chapter 7 looks at how our sea level projections can be combined with the storm surge statistics. We show how the frequency of flooding over a fixed elevation can dramatically increase with a change in mean sea level. And, following Hunter (2012), we present allowances which give the height by which an asset needs to be raised so that the probability of flooding remains preserved. Finally, Chapter 8 summarizes our results. Sea level projections and return heights for the coastal municipalities, as well other useful practical information, can be found in the tables of the Appendix.

1.1 Processes Affecting Sea Level

Global mean sea level (GMSL) is the sea level averaged in time, to remove unwanted variability, and then averaged over the oceans. The main contributors to GMSL changes are

changes in ocean mass, largely from land ice, and changes in ocean density (Figure 1.1). Regional differences in sea level arise due to spatial differences in ocean density change, ocean mass redistribution and circulation, atmospheric pressure and winds, as well as changes to the gravity field. When considering sea level changes at the coastline, vertical land motion must be taken into account.

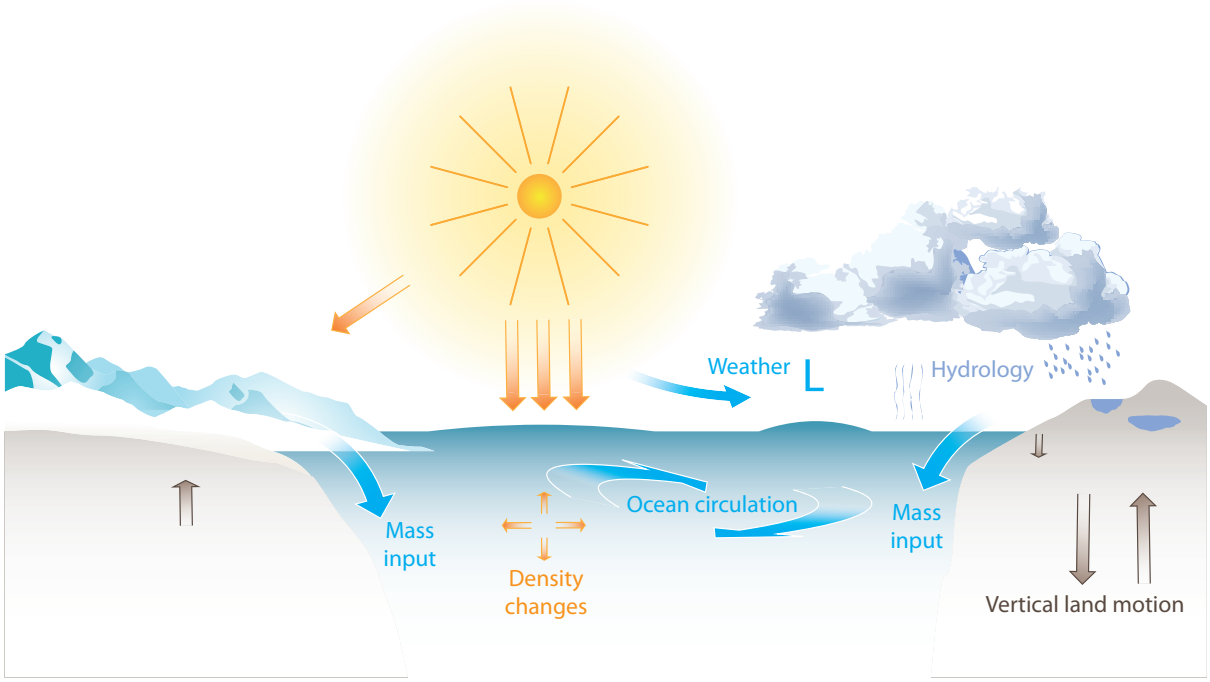

Figure 1.1 Diagram showing processes affecting sea level. Modified from Nilsen et al. (2012b; Original graphics courtesy of Haltenbanken AS).

Changes in the heat (temperature) and salt (salinity) content of seawater result in thermal expansion and haline contraction. The resulting change in sea level is referred to as a change in steric height. Warmer water expands, while more salt causes water to contract. In many areas of the oceans it is the temperature effect that dominates the steric height change. But in the cold waters of the Nordic Seas and Arctic Ocean, changes in salinity may be as important as temperature effects. Steric height variations alter the sea level by changing the volume of seawater through expansion and contraction, in contrast to adding or removing water from an ocean region.

Changes in the amount of water in the ocean, and thus its level, can be due to changes in land ice volumes (glaciers and ice sheets) or changes in the amount of liquid water stored on land. And any exchange or redistribution of mass will lead to changes in the gravity field, making the ocean surface readjust accordingly. Perhaps the best known example of this are so-called sea level 'fingerprints', which are the sea level response to rapid land ice loss. Ocean mass redistribution can also occur due to dynamic responses which are tightly connected to ocean density (i.e., steric) changes. In addition, any other physical process affecting ocean currents, in particular winds, will lead to redistribution of mass and also lead to changes in the gravity field. There are also adjustments in the earth's crust, both seafloor and land, due to any kind of mass redistribution above it.

Changes in atmospheric pressure over the oceans cause seawater to move and therefore changes the local sea level. A low-pressure system means less air mass (less weight) and the ocean surface will respond by rising. Whereas in areas of high air pressure the ocean surface is depressed. In this way, atmospheric pressure changes act to move water from areas of high air pressure to low air pressure.

In addition, a low-pressure system (a storm) is usually accompanied by winds that, through friction, sets the seawater in motion. The Norwegian coast is often subjected to incoming storms from the southwest that push water towards the shore. The higher water level associated with an individual storm is known as a storm surge. If multiple low-pressure systems arrive in relatively quick succession, then it is possible multiple storm surges can build upon each other.

Vertical land motion (VLM) must be accounted for when assessing sea level changes at the coastline. And it is the sea level with respect to the shore that is of interest for adaptation and mitigation. Throughout this report we separate between sea surface height (SSH) and relative sea level (RSL), where the latter is the sea surface relative to the seafloor, i.e., the shore (Figure 1.2). Satellite altimetry provides a measure of SSH whereas tide gauges measure RSL at the coast. VLM in Norway is dominated by the relaxation of the Earth in response to deglaciation and the eventual loss of the Fennoscandian ice sheet. The Earth is still adjusting to the removal of the weight of this ice mass (a process known as glacial isostatic adjustment, GIA) and, for the period this study is concerned with, the effect can be assumed to be essentially constant. There are a number of other physical processes which can also cause vertical movements or coastline changes. For example, tectonics, the above mentioned mass loading effects, sediment deposition or compaction, erosion, or groundwater storage changes. Generally speaking these processes are thought to be small in Norway but they can be significant in some areas and especially on local scales.

A more detailed description of the processes relevant for sea level change in Norway will be given in Chapter 3.

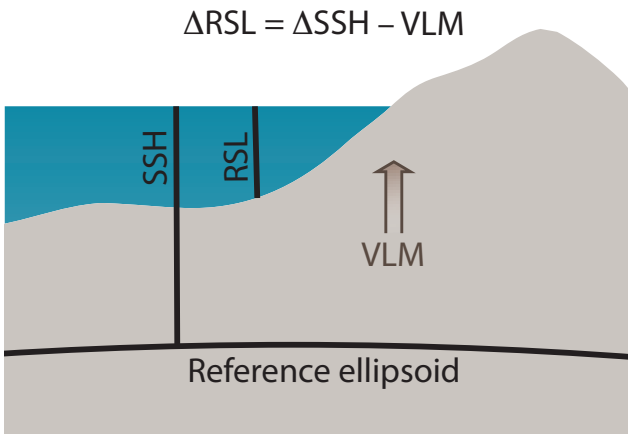

Figure 1.2 Definitions of sea surface height (SSH) and relative sea level (RSL). The SSH is relative to the reference ellipsoid, while RSL is relative to the solid Earth surface. Thus, a change in RSL is the difference between the change in SSH and the vertical land motion (VLM). Tide gauges measure RSL, while satellites measure SSH. The three variables are herein defined in a general, physical sense, i.e., including all processes that may change the actual sea surface and land uplift at any timescale.

1.2 Past Global Sea Level Changes

1.2.1 Paleoclimatic Perspectives

Present and future sea level changes may be placed into a longer time perspective by examining sea level changes during past warm periods of Earth's history and the rates of change experienced during previous periods of rapid sea level change. Sea level in these paleoclimatic periods can be calculated from reconstructed positions of earlier shorelines, from lake or bog sediments which show changes from marine to freshwater conditions, or from fossils of organisms known to live near the sea surface (e.g., corals). After dating the shoreline positions in a specific locality, one needs to correct for vertical land movement as well as known horizontal changes in the locality. Such corrections can in many places be made with high degree of certainty, hence it is possible to establish both the past height of sea level and, in some situations, also the rates of change of past sea level variations.

Mean Sea Level

During the Pliocene era (approximately 3–5 million years before present) the mean climate state of the Earth was over long periods (more than 100,000 years) significantly warmer than present. At the same time the CO_2-content of the atmosphere is estimated to have been 400–420 ppmv (parts per million by volume), i.e., a range that we are entering today. The Earth was quite similar to present in terms of the positions of continents and size and place of mountain ranges. Since the warm periods of the Pliocene had such a long duration, it is reasonable to assume that the slow acting elements of the climate system were in equilibrium during this period, which therefore can provide us with estimates of future sea level on the longer-term with a slow and steady adjustment to existing boundary conditions. Recent literature suggests that Pliocene sea levels were 20 ± 10 m above modern GMSL. But there remain significant uncertainties on the analytical errors and land motion corrections (Dutton et al., 2015). Nevertheless, the results imply that land-ice volumes in Antarctica and Greenland were significantly less in the Pliocene than now, and that the West Antarctic ice sheet and potentially marine based sections of the East Antarctic ice sheet were diminished during periods of this time (Naish et al., 2009; Pollard and DeConto, 2009; Cook et al., 2013).

The last interglacial period, approximately 130,000–120,000 years before present, was a period with mean global temperature 1–2^{o}C above pre-industrial temperatures, and a significantly enhanced warming in polar regions. At this time the Earth's orbit brought the Earth closer to the sun during Northern Hemisphere summer than now with a slightly warmer climate as a consequence. Atmospheric CO_2 levels were significantly lower than they are now, at 280–300 ppmv. Extensive data sets indicate that sea level was at least 6 m higher than now (6–9 m above modern GMSL), based on lifted marine terraces and the oxygen isotope composition of the sea (which change when global land-ice volume changes) (Kopp et al., 2009; Rohling et al., 2009; Lisiecki and Raymo, 2005; Dutton et al., 2015). Both Greenland and West Antarctic ice sheets were likely smaller than now (Dutton et al., 2015). Estimates of the steric effect of the warmer ocean indicate a contribution of at most 0.3 m (McCay et al., 2011). Most of the sea level rise must therefore be ascribed to deglaciation of mountain

glaciers and the ice sheets. These results show that polar ice sheets and associated sea levels are highly sensitive to increasing temperatures.

The termination of the last glacial period began around 20,000 years before present when global mean sea level was about 120 m below its modern level. Following this, the majority of the large continental ice sheets in the northern hemisphere melted and GMSL rapidly rose. Over the past 2000 years GMSL has been relatively constant, fluctuations within a range of ± 20 cm, and close to present-day levels (Masson-Delmotte et al., 2013). The start of the monotonic rise seen in the instrumental record began after 1900 AD.

Rates of Change

Rates of sea level change during past warm periods can offer some constraint on possible future rates. The accuracies of current dating techniques are too low to allow estimates of rates of change beyond the last interglacial. During the last interglacial, estimates of maximum rates of GMSL rise range from 20 cm/century (Blanchon et al., 2009) to 160 cm/century (Rohling et al., 2009). The present-day rate of GMSL rise is, for comparison, 30 cm/century.

Following the termination of the last glacial period, large continental ice sheets collapsed. The very high rates of GMSL rise seen during this time may help us define an upper boundary on how fast sea level may rise in a situation where the Greenland and West Antarctic ice sheets were to collapse. Reconstructed rates of change of up to 4 m/century have been estimated for shorter periods over 20,000–10,000 years before present (Bard et al., 1990; Hanebuth et al. 2000). This may be regarded as an upper bound for rates of sea level rise during intervals of ice sheet collapse, but is likely not analogous to the modern situation of a warm world with only polar ice caps, for which the upper bound is likely smaller.

1.2.2 The Instrumental Record

Observations of sea level changes from the 1700s are available from the global tide gauge network and, for the last few decades, from satellite altimetry. Tide gauges record RSL changes along the coastlines of the continents and at some islands. Satellite altimetry measures sea surface heights primarily in the open ocean.

Global Sea Level Observed by Tide Gauges

The AR5 (Rhein et al. 2013) concludes that the change in global sea level was 1.7 (1.5–1.9) mm/yr from 1901 to 2010. Hence, the longer term estimate based on tide gauges has not changed from AR4 (Meehl et al., 2007) that reported a global sea level rate of 1.8 ± 0.5 mm/yr for 1961–2003 and 1.7 ± 0.5 mm/yr over the whole 20th century. However, recent work by Hay et al. (2015) argue that previous efforts have overestimated twentieth-century GMSL rise. Using probabilistic techniques that combine tide gauge records with physics-based and modeled-derived geometries of the contributing processes, they find a rate of GMSL rise from 1901 to 1990 of 1.2 ± 0.2 mm/yr. This estimate is significantly lower than the rate of GMSL rise reported in AR5, but compares better with the estimated sum of contributions to sea level change (see Section 1.3 on closure of the 20th century sea level budget).

Other tide gauge studies have investigated the presence of nonlinear trends in global sea level changes. For example, Jevrejeva et al. (2006) determine a trend of 2.4 ± 1.0 mm/yr for the period 1993 to 2000. They find that this recent trend is similar to the observed trend between 1920 and 1945.

There is also evidence of accelerations in the tide gauge records. Jevrejeva et al. (2008) reconstruct global sea level 300 years back in time, and the time series indicates that global sea level change has accelerated by 0.01 mm/yr^2, starting at the end of the 18th century.

In Church and White (2006), altimetry data and tide gauge records are combined to reconstruct global sea level back to 1870. They find a sea level rise of 1.7 ± 0.3 mm/yr over the 20th century and reported an acceleration of 0.013 ± 0.006 mm/yr^2 for the same period. An updated analysis using five additional years with altimetry data comes to a similar conclusion; a sea level rise of 1.7 ± 0.2 mm/yr for 1900 to 2009 and an acceleration of 0.009 ± 0.003 mm/yr^2 over the same period (Church and White, 2011).

Global Sea Level Observed by Altimetry

By averaging satellite altimetry observations over the sampled ocean, GMSL rise can be estimated directly. From TOPEX/POSEIDON, Jason-1, and Jason-2, we estimate GMSL change referred to the geodetic reference frame as 2.9 mm/yr over the period January 1993 to December 2013 (see Figure 1.3). However, for understanding climate driven ocean water volume changes (essentially thermal expansion and the loss of land ice) this estimate needs to be corrected for GIA. This accounts for the effect of the ocean basins getting gradually larger as the ocean floor subsides following the last glaciation. Peltier (2009) uses GIA modelling to calculate the effect to be -0.3 mm/yr. Once this relatively small GIA correction is made, our estimate for GMSL rise becomes 3.2 mm/yr over the satellite altimetry era. This agrees well with the consensus estimate of 3.2 mm/yr (2.8 to 3.6 mm/yr) reported in Rhein et al. (2013; AR5).

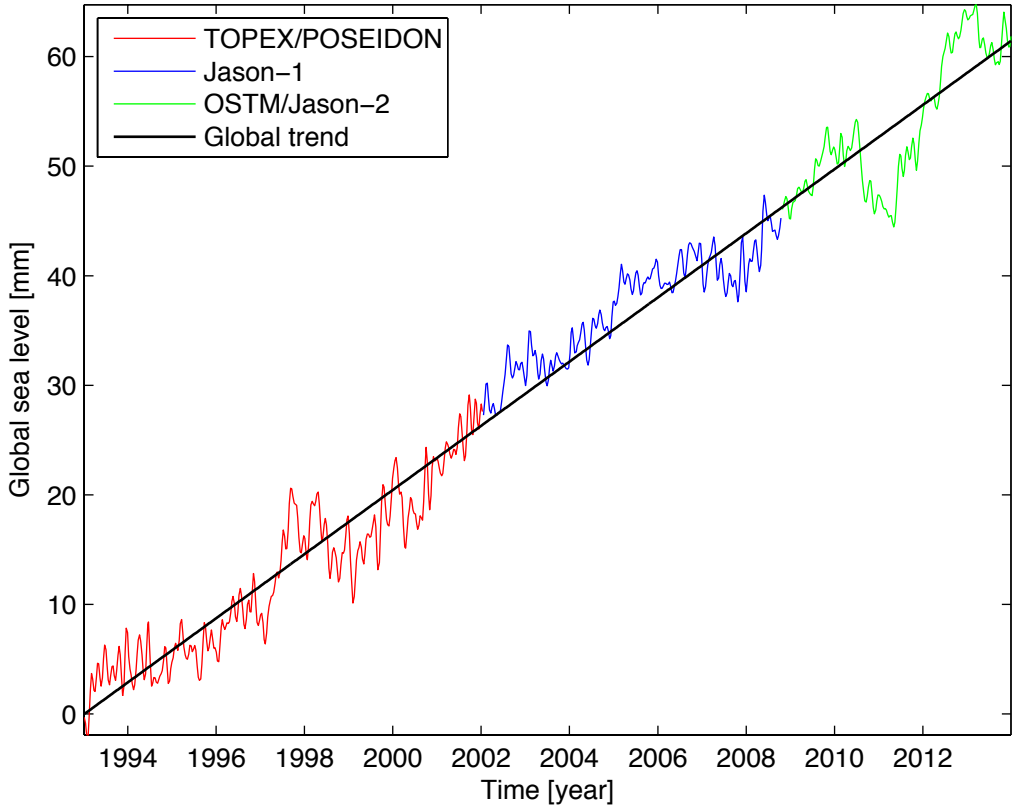

Figure 1.3 Global sea level relative to the start of the record observed by the three satellites TOPEX/POSEIDON, Jason-1 and Jason-2 from 1993 to 2014. The seasonal signal is removed from the data.

The accuracy of the rate of GMSL rise cannot be estimated from the altimetry measurements alone. Ablain et al. (2009) therefore assessed the accuracy by evaluating the models used to correct the range measurements, the accuracy of the satellite orbits, and the effect of combining several satellite altimetry missions into one time series. The authors found that these errors add up to 0.44 mm/yr for the global sea level rate estimated by combining data from TOPEX/POSEIDON and Jason-1 over 1993 to 2008. However, this error budget did not include systematic errors which may arise due to reference frame instabilities over time. Especially relevant are the reference frame's drift along the z-axis (the drifts along the x- and y-axis are negligible) and the change in scale with time. These rates are assessed to be within 0.5 mm/yr and 0.3 mm/yr, respectively (Collilieux et al. 2014). The z-rate propagates by 12% into GMSL while the scale-rate propagates 100% into GMSL (Watson et al. 2015). Added in quadrature to the uncertainty of the models, this yields a total error of 0.5 mm/yr (standard error) on the GMSL rise estimated from altimetry. Satellite altimetry is more thoroughly discussed in Section 3.3.

We notice that the recent study by Watson et al. (2015) indicates that the rates estimated from standard multimission altimetry data may be biased high due to drifts in the complex altimeter measurement system (not the reference frame changes). Using tide gauge records corrected for vertical land motion by GPS, they find individual mission bias drift estimates larger than zero for all missions. The drift is largest for the data from the TOPEX side A altimeter, i.e 1.5 mm/yr. Applying individual drift corrections, the rate of GMSL rise is reduced to 2.6 ± 0.4

mm/yr (corrected for GIA) for the period 1993 to mid-2014. Considering the uncertainty, this estimate is still within the uncertainty bounds of the consensus estimate reported in Rhein et al. (2013) and the estimate found by analyzing the data illustrated in Figure 1.3.

1.3 Contributions to Global Sea Level Rise

For the instrumental period it is possible to estimate the different contributions to sea level change in some detail. As discussed in the previous section, global mean sea level has risen at an increasing rate over the past 100 years or so. Figure 1.4 shows a summary of some results on contributions to and total observed GMSL change. The acceleration in GMSL over the past century can be seen in the increasing rates for different time periods.

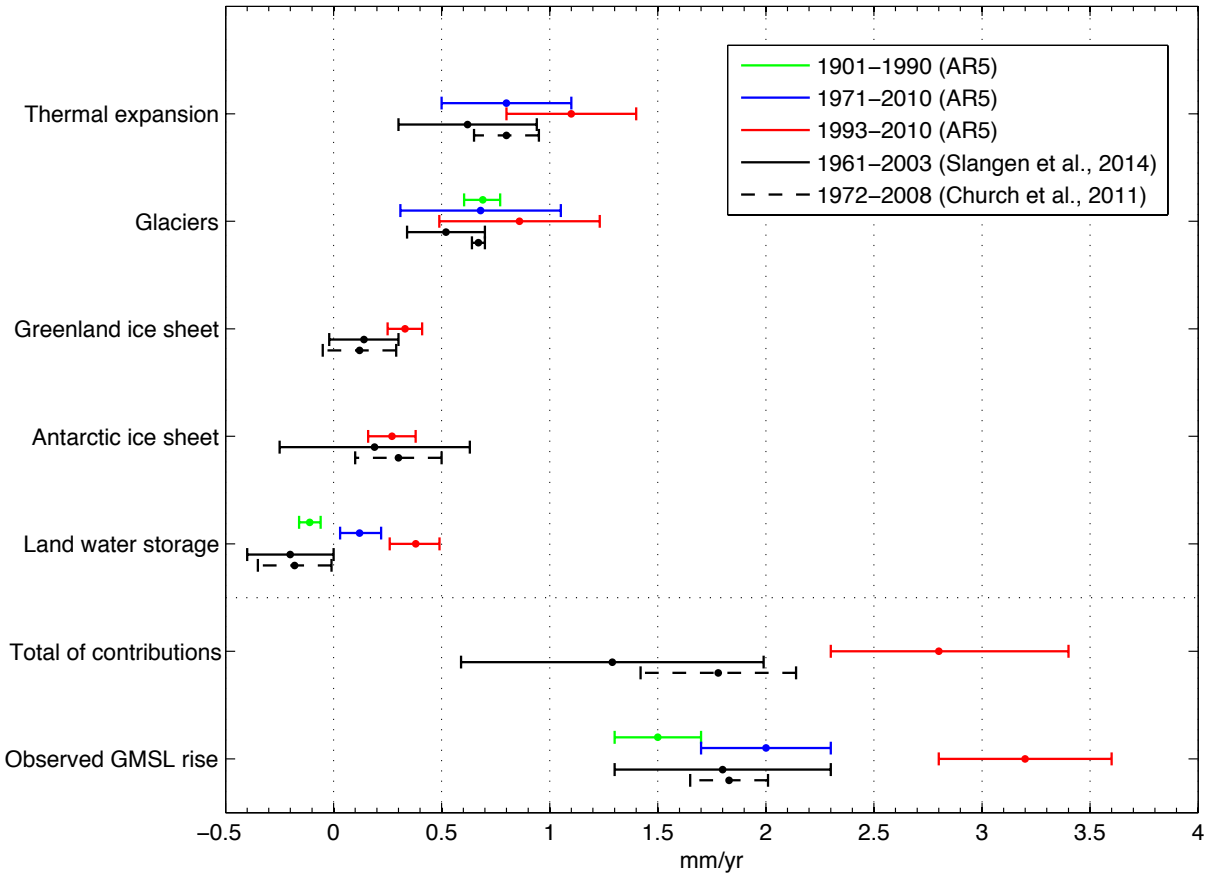

Figure 1.4 Global mean sea level (GMSL) budget (mm/yr) from observations, showing contributions from different sources over different time intervals, based on different studies. The coloured bars are based on AR5 (Church et al., 2013; their Table 13.1) with uncertainties of 5% to 95%. The additional black bars are based on Slangen et al. (2014; their Table 2) and Church et al. (2011) with one standard deviation uncertainties. The observed GMSL rise for the latter two studies are based on tide gauge measurements, and the full line estimate is from AR4 (Bindoff et al., 2007).

Almost all the assessed separate contributions have increased their rate during the previous decades. One exception is perhaps the Antarctic ice sheet, which is estimated to have contributed around 0.2–0.3 mm/yr during both the longer and shorter periods it has been assessed for. Land water storage has increased, but contributes less than 0.5 mm/yr. Some of

these changes may be due to different methods and data used in the different periods, but there is general agreement wrt. their increasing rates. The largest and approximately equal contributions have come from thermal expansion and melting of glaciers, with roughly 0.5–1.0 mm/yr each. When including ice sheets the land ice melt has been dominating (1.0–1.5 mm/yr) and seems to be gradually increasing its importance relative to thermal expansion, due to increased ice-sheet contribution over the last two decades.

In the recent years studies have managed to close the 20th century budget between the observed GMSL and the sum of contributions. The lower part of Figure 1.4 shows some comparisons. In addition to improvement of closure by new estimates of GMSL (Hay et al., 2015), efforts have also been made on improving the estimates of contributions. Slangen et al. (2014) closed the GMSL budget for 1961–2003 comparing with the AR4 GMSL estimate. The budget closure for 1972–2008 by Church et al. (2011) has slightly larger rates, but that can be explained mainly by the difference in the period studied (Slangen et al., 2014).

For the more recent altimetry period (1993–2010), AR5 reports closed budgets and point out that the estimates and agreement are of high confidence for this period. The estimates for this period by Hay et al. (2015) based on tide gauges (3.0 ± 0.7 mm/yr) also show good agreement with the consensus estimate from altimetry.

Even though closure has been achieved it is still a challenge to estimate separate contributions correctly. This is done by different methods which also involves intercomparisons of different parts of the budget. For instance, a new technique has been developed for combining full-depth steric profiles with satellite altimetry to quantify ocean mass changes (Purkey et al., 2014). Using this method, the authors calculate regional and global estimates of ocean mass trends from 1996 to 2006. The results agree well with observations from the Gravity Recovery and Climate Experiment (GRACE).

Note that budget closure is dependent on time scale. In particular, a remaining discrepancy in the budget for 1901–1990 has been attributed to both underestimation of contributions (Church et al., 2013a; Gregory et al., 2012) and overestimation of the global sea level trend (Hay et al., 2015). The focus and multiple efforts on improving estimates of GMSL and contributions to GMSL, and the following improvements in closure, mean that the physical understanding of the causes for sea level rise has improved. This provides better basis for development of models and evaluation of projections.

2 Background and Previous Work on Future Projections

The regional sea level projections that are presented in this report are largely based on the results from AR5. Hence, we first give the necessary background on AR5 terminology, methodology and global projections (Section 2.1). This is followed by a brief summary of scientific progress before and after AR5 (Section 2.2). The chapter concludes with a summary of previous reports on sea level projections for Norway (Section 2.3).

2.1 The Fifth Assessment Report of the IPCC

2.1.1 Representative Concentration Pathways

Representative Concentration Pathways (RCPs) represent different future scenarios of concentrations of greenhouse gases, aerosols, and other climate drivers. Such emission scenarios are dependent on human activities, technology development, and policies, but these factors are not assessed in AR5. Instead, different developments of atmospheric concentrations of climate drivers are prescribed in the different RCPs, spanning out several possible future developments.

The numbers identifying each RCP reflect their approximate total radiative forcing in year 2100 relative to 1750. For instance, following RCP4.5 will lead to a level of surplus heat put into the earth system of approximately 4.5 W/m^2. The advantage of having scenarios defined by physical expressions for global warming, is that it makes it possible to evaluate which pathway certain mitigation measures may lead to. In the following we will give some context to the three pathways considered in this report.

RCP8.5 is a high emission scenario, also known as a 'business as usual' scenario. There are no reductions in emissions, but instead there a tripling of CO_2 emissions by 2100, and a rapid increase in methane emissions. Global temperatures will have increased by some 3–5°C, compared to the mean 1986–2005. Results are largely unknown, but this scenario likely involves several catastrophic consequences for human civilisation.

RCP4.5 involves strong reductions in emissions. There is some increase in CO_2 emissions, but reduction is achieved around 2040, and the concentration stabilises by 2100. This pathway can be reached by creating an energy efficient society and having ambitious climate policies in most countries. By 2100 temperatures are more likely than not more than 2°C warmer. Methane emissions are stable in this scenario. It is expected that many regions will experience shortage of water, and high threat of extinction for many species.

RCP2.6 is a low emission scenario. It describes a path where emissions are reduced by 2020, and atmospheric concentrations go down from 2040. The scenario is based on expectations of reduction in use of oil, lower energy consumption in general, and a human population stabilising around 9 billion. This is the only scenario used that may secure the 'two-degree target'. Note that the concentrations today correspond to about 2.5 W/m2.

In terms of sea level, RCP2.6, RCP4.5, and RCP8.5 is projected to lead to 40 cm, 47 cm, and 63 cm global mean sea level rise over the period 1986–2005 to 2081–2100, respectively. The RCP6.0 scenario is not considered herein, since the sea level response is very similar to that of RCP4.5.

2.1.2 Models Used to Project Sea Level Change

Coupled Atmosphere–Ocean General Circulation Models (AOGCMs) used in projecting climate change have components representing the ocean, atmosphere, land, and cryosphere. They simulate changes in the climate system resulting from anthropogenic greenhouse gas and aerosol emissions, anthropogenic land use changes, as well as natural forcings such as volcanic eruptions and changes in solar irradiance. Because of the impact on ocean density and circulation, changes in surface wind stress and air–sea heat and freshwater fluxes have a big impact on changes in sea level. Ocean density, circulation and sea level are dynamically connected in AOGCMs and evolve together.

In AOGCMs, sea surface height changes are simulated relative to a time invariant topography/bathymetry and geoid, and thus do not include changes to the gravitational potential due to mass redistribution (e.g., significant ice sheet melting) or changes to the Earth's crust due to glacial isostatic adjustment. Instead, geodynamic models are used to simulate the sea level response to past and ongoing changes in mass distribution and crust, as well as ongoing atmospheric pressure changes. The sea surface height component of these calculations is based solely on water mass conservation and perturbations to gravity, and not considering ocean dynamic effects of these particular changes.

Offline model systems are also required for simulating glacier and ice-sheet changes. The two processes currently included are surface mass balance (SMB) and changes in the dynamics of ice flow. SMB is the balance between snow accumulation and ablation resulting from an ice-sheet's interaction with the atmosphere and ocean, and modelled regionally with input from AOGCMs. Models of ice-sheet dynamics represent the response of ice flow to changes at the marine boundary and internal stresses in the ice. The two effects may be simulated separately or together.

The Coupled Model Intercomparison Project phase 5 of the World Climate Research Programme (WCRP) provides a set of coordinated climate model experiments, from which model assessments in AR5 has been drawn. CMIP5 includes ‘long-term’ simulations of 20th century climate and projections for the 21st century and beyond.

2.1.3 Treatment of Uncertainties and Likely Ranges

As stated in the Technical Summary of AR5 (Stocker et al., 2013), there are two measures used for communicating the degree of certainty in the findings in AR5, which are referred to as "uncertainty" and "confidence":

- Confidence is a qualitative measure, based on the type, amount, quality, and consistence of the available evidence, weighed by agreement between the different evidence, and leading to the author team's judgement about the validity of the finding.

- Uncertainty is the quantitative measure of probability arising from statistical analysis of observations or model results.

When it has been possible to assess the uncertainty (and thus the probability), the confidence is normally deemed *high* or *very high*, and the probability expressed in verbal terms of likelihood. These terms range from *exceptionally unlikely* (0–1% probability) to *virtually certain* (99–100% probability).

The range chosen for presenting global and regional sea level projections in AR5 is the *likely* range (66–100% probability). From Stocker et al. (2013) on projections for the mid- and late 21st century:

> *"[The likely range is] calculated from projections as 5−95% model ranges. These ranges are then assessed to be likely ranges after accounting for additional uncertainties or different levels of confidence in models. For projections of global mean sea level rise confidence is medium for both time horizons."*

The reason for choosing to assess the *likely* range, may lie in the assessment that there is currently insufficient evidence to evaluate the probability of specific levels above the *likely* range (Stocker et al., 2013). Note also that "confidence" in the AR5 nomenclature is not related to the statistical term "confidence interval".

In this report, we generally present the projections as the 5−95% model ranges where possible. Other uncertainties are expressed as the standard error (SE) or one standard deviation . We reserve the first term for the precision or accuracy of calculated values (for instance the standard error of the regression analysis), whilst the latter term expresses the spread. It is worth mentioning that although a statistical uncertainty may be possible to calculate, e.g., from model spread, the result is not automatically of high confidence. For instance the performance of the numerical models may give rise to lower confidence in certain contributions to sea level change. More on this in Chapter 5.

2.1.4 Projected Contributions to Global Mean Sea Level

The processes contributing to sea level rise are modelled and estimated by different means, as discussed above, and their contributions and uncertainties to the projections can be assessed separately.

In Figure 2.1 we summarise the contributions to global mean sea level rise to 2081–2100 as given by AR5. Comparing with the observed trends (Figure 1.4) it can be seen that thermal expansion and melting of glaciers is expected to continue, and accelerate (0.1 m/100 yr = 1 mm/yr), through the century, with the former as the largest contributor. It is estimated that thermal expansion accounts for 30 to 55% and glaciers for 15 to 35%, depending on RCP (Church et al., 2013a). All contributions in the projections are higher by the end of the century than their current trends (Figure 1.4) indicate.

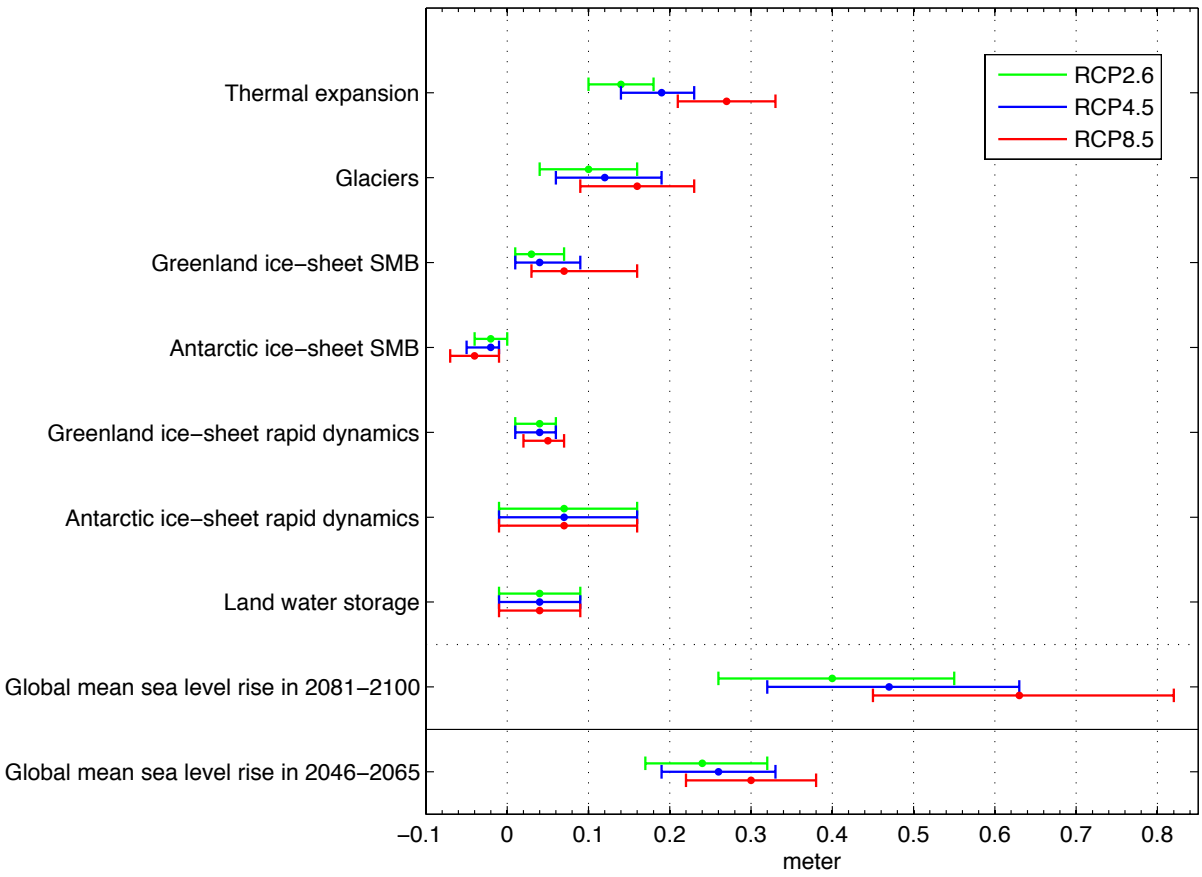

Figure 2.1 Projections of global mean sea level (GMSL) rise and its contributions over the period 1986–2005 to 2081–2100, in meters, for the three RCP scenarios considered herein. Added at the bottom are the GMSL projections for 2046–2065 (relative to 1986–2005), without contributions shown. Points are median values with likely ranges as bars. Based on AR5 (Church et al., 2013a; their Table 13.5).

The separation of ice-sheet contributions into surface mass balance (SMB) and ice-sheet dynamics, reveals more about which processes are expected to contribute. The projections indicate that Greenland will continue losing mass from its surface and dynamic ice flows at an approximately equal rate. The Antarctic ice-sheet, on the other hand, is projected to receive increased snowfall (Church et al., 2013a), leading to a negative contribution to sea level, but this is over-compensated by the ice-sheet dynamics component. The total of all land-ice contributions is somewhat higher than the contribution from thermal expansion, for all RCPs (not shown).

The projections of most components increase with increasing greenhouse gas forcing (RCP). However, it is only the thermal expansion and melting of glaciers that show a clear response to varying emissions, i.e., temperatures, during this century. The other contributions may either have a slower response to the warming or their estimates are too uncertain to show such a response. In particular, the Antarctic ice-sheet dynamics and the land water storage have large uncertainties and the same values for all RCPs.

2.1.5 Projections of Global Mean Sea Level Rise

In the Summary for Policy Makers of AR5, it is the projections of global mean surface temperature change and global mean sea level rise that is put forth as quantified with confidence (IPCC, 2013; their Table SPM.2). Global mean sea level rise for 2081–2100 relative to 1986–2005 will *likely* be in the ranges of 0.26 to 0.55 m for RCP2.6, 0.32 to 0.63 m for RCP4.5, and 0.45 to 0.82 m for RCP8.5. The numbers for 2046–2065 are also provided: 0.17 to 0.32 m for RCP2.6, 0.19 to 0.33 m for RCP4.5, and 0.22 to 0.38 m for RCP8.5.

We present the projected ranges of GMSL and their median values graphically in the lower part of Figure 2.1, and the time series in Figure 2.2. It is clear that both the median and the ranges increase with increased greenhouse gas forcing (RCPs), for both periods of the century. Comparing the mid-century with the end of century projections, the lowest emission scenario shows a slowing of the rise, the reduction scenario gives linear rise, while the high emission scenario indicates accelerated sea level rise.

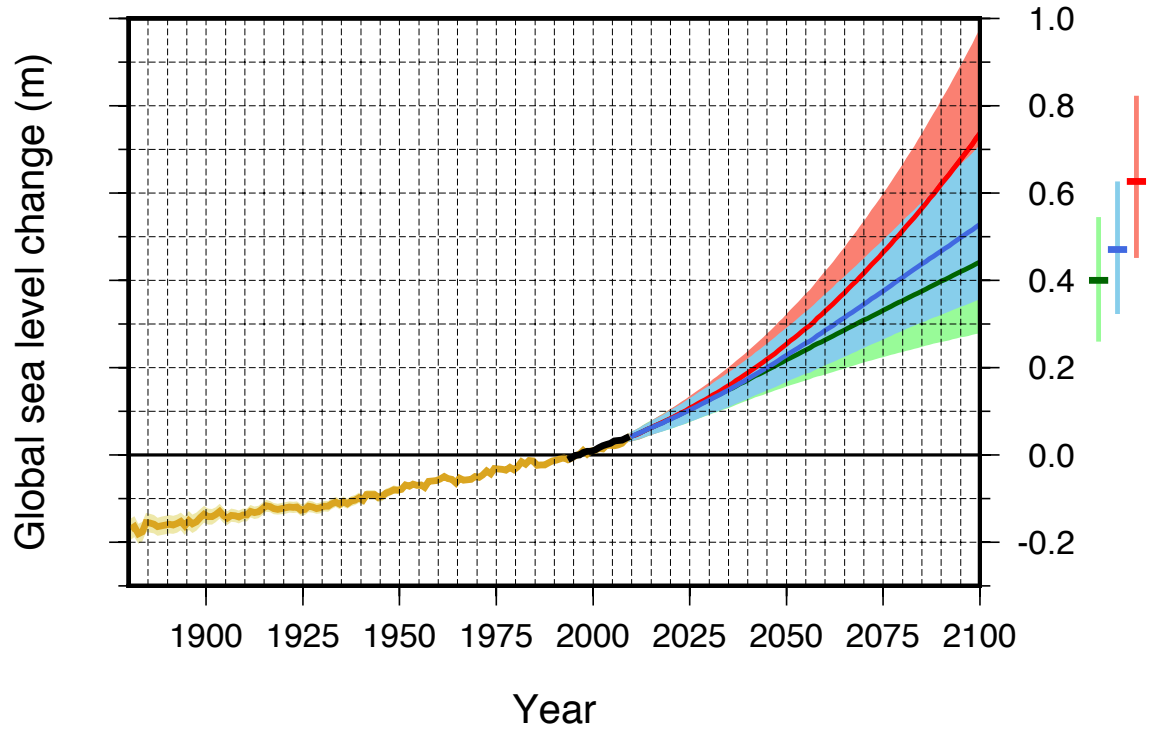

Figure 2.2 Time series of global projections for RCP2.6 (green), RCP4.5 (blue) and RCP8.5 (red) from Church et al. (2013a) with corresponding 5 to 95% ensemble spread (the likely range). The vertical bars on the right side of the panel represent the ensemble mean and ensemble spread (5 to 95%) for RSL change for 2081–2100. The tide gauge reconstruction (mustard) and altimetry observations (black) are taken from Church and White (2011) plotted with corresponding one standard deviation in brighter colour around (only visible where wider than the linewidth).

2.2 Comparison of the Fifth and the Fourth Assessment Report of the IPCC

The first IPCC assessment reports laid the fundament for much of the current understanding of sea level change. By the time of the Fourth Assessment Report (AR4), observations and understanding of the variations in the rate of global average sea level rise for the 20th century were more robust, and some of the time-variable spatial distribution of sea level could be revealed from the satellite altimeter record (Bindoff et al., 2007). Nevertheless, three central issues remained unresolved in AR4.

First, the observed sea level rise was larger than the sum of the individual contributions estimated from observations or with models, although in general the uncertainties were large enough that there was no significant contradiction. Important progress has been realised since AR4 in quantifying the observed thermal expansion component of global mean sea level rise, as well as estimating the contributions from land-based ice. The closure of the observational budget, within improved uncertainties, represents a significant advance since AR4 in physical understanding of the causes of past GMSL change. (See Section 1.3 for further details on the observational sea level budget.)

Second, there was insufficient understanding of the potential contributions from the ice sheets. In particular, AR4 recognised that existing ice-sheet models were unable to simulate the recent observations of ice-sheet accelerations and that understanding of ice-sheet dynamics was limited. The inclusion of dynamic ice-sheet responses to the ice-sheet surface mass balance, is a major advance in AR5.

Third, it was not possible to make confident projections of the regional distribution of sea level rise. As a result of the improvements in understanding and modelling, AR5 presents regional projections with likelihood and confidence assessed.

In numbers, the full range of the global sea level rise projections changed little between the previous assessment reports. There was some lowering of the upper end due to smaller GHG emissions assumed, and reductions in uncertainties. But from AR4 to AR5 the projections of sea level rise have become larger, primarily because of improved modelling of land-ice contributions. In AR4 sea level projections for 2090–2099 (compared to 1980–1999) for the full range of scenarios was 18 to 59 cm, while in AR5 the corresponding range is 26 to 82 cm (for 2081–2100 compared to 1986–2005).

On a more general note, climate models have improved since AR4. Models reproduce observed continental scale surface temperature patterns and trends over many decades, including the more rapid warming since the mid-20th century and the cooling immediately following large volcanic eruptions.

Confidence in projections of global mean sea level rise has increased since AR4 because of the improved physical understanding of the components of sea level, the improved agreement of process-based models with observations, and the inclusion of ice-sheet dynamical changes.

Finally a note on semi-empirical models (Rahmstorf, 2007; Vermeer and Rahmstorf, 2009; Grinsted et al., 2010) which were developed before AR5. Semi-empirical models project sea

level based on statistical relationships between observed GMSL change and global mean temperature changes or changes in radiative forcing. They provide an alternative approach for projecting GMSL, but with low confidence according to AR5 (Church et al., 2013a). Since we are interested in regional sea level projections, as well as assessing the different contributions to sea level, we do not pursue the use of semi-empirical models in this report.

2.3 Progress Following the Fifth Assessment Report of IPCC

There have been several areas of further progress in sea level science since the publication of AR5. Here we mention a few that relates directly to the work in this report, and refer to the sections where the themes are treated fully (and citations can be found):

1. There have been further improvements in estimates of contributions to and measurements of GMSL change, and of the closure of the GMSL budget. This involves better interpretation of coastal tide gauge data for estimating GMSL, treatment of altimetric errors, and better data coverage and methods for the full depth steric changes in the ocean (see Section 1.3). This has led to increased physical understanding of sea level processes, and is thus important for future projections.

2. There have been advances in our understanding of the behaviour of marine-based parts of the Antarctic ice sheet, at the same time as observations and modelling work suggest that some marine based sectors of the ice sheet may have started to collapse. This has implications for the confidence in the likely ranges and the probability of higher future sea levels. We take this into consideration when discussing our regional projections (Section 5.4.2).

3. Methods for quantitative risk management require a complete probability distribution. Several recent publications deal with probabilistic sea level projections that can take into account changes beyond the likely ranges given in AR5. Based on these we make our own assessment and quantification for Norway (Section 5.5).

4. In the model systems used for sea level projections there are processes still not fully understood or implemented (see Section 5.6). Several studies on such processes and their possible importance have come out since AR5. We have opted to take into account one such effect that has recently been shown to give rise to quantifiable regional differences, namely self attraction and loading (see Section 5.1.2).

2.4 Previous Studies of Future Sea Level Projections for Norway

The most up to date reports with estimates of future sea level changes for Norway are from The Norwegian Mapping Authority (NMA; Simpson et al., 2012; 2014) and from the Bjerknes Centre for Climate Research (BCCR; Nilsen et al., 2012a). The reports use different methods and different input data. Simpson et al. (2012; 2014) presented regional projections for Norway using AR4 science based on scenarios A2, A1B and B1. Land uplift estimates were taken from Kierulf et al. (2012). These results indicated that 21st century sea level changes along the Norwegian coast would be between -40 and 60% of the global mean change. The authors also provide a 'high-end' scenario. Nilsen et al. (2012a) base their

analysis mainly on ranges of future sea level rise and add estimates of different contributions and uncertainties from literature published since AR4.

In general terms, the estimates of future sea level change in Simpson et al. (2012; 2014) have larger uncertainties and a lower lower bound when compared to Nilsen et al. (2012a). The current official projections for the 21st century sea level change along the Norwegian coast (The DSB-report; Vasskog et al., 2009; also presented in Hanssen-Bauer et al., 2009) are based on the semi-empirical approach of Rahmstorf (2007), and exceed the main projections of both reports from 2012. There are also differences in how estimates are given wrt. bounds or likelihood. See discussions in the respective reports for details.

These discrepancies underline the importance of working towards truly regional sea level projections and trying to better understand the individual processes contributing to local sea level changes. In the current report we aim to provide updated and consistent estimates for future regional sea level rise in Norway.

Recently, Nilsen et al. (2013) provided a preliminary assessment of water levels (tides and extreme levels) added to projected sea level changes (of Nilsen et al., 2012a) for Norwegian municipalities (as well as an assessment of regulative, economic, and informative instruments for implementation of adaptive measures from the national to the municipal level).

2.5 Chapter Summary

Sea level science is rapidly evolving, and crucial knowledge is updated almost on a yearly basis. The fifth assessment report of the IPCC (AR5) represents a fundamental step forward in our understanding of sea level rise, to the point that regional sea level projections are now provided by the IPCC for the first time, which alone warrants updated projections for Norway. In addition, it is clear that the previous reports on future sea level in Norway, with their varying data basis and methods, need to be replaced by an up to date and concerted effort.

The foundation of the regional sea level projections in this work is the suite of projections provided by the Coupled Model Intercomparison Project phase 5 and assessed in AR5. The scenarios considered herein are RCP2.6, RCP4.5, and RCP8.5. The likely range of global sea level projections for the century (i.e., over the period 1986–2005 to 2081–2100), across all scenarios, is from 0.26 to 0.82 m. The contributions from thermal expansion and glacier melt are projected to accelerate, the Greenland Ice Sheet will continue to lose mass, and the sum of all land-ice contributions will be slightly larger than the contribution from thermal expansion.

3 Observed Sea Level Changes in Norway

In the following Chapter, we first discuss historical sea level changes derived from paleo observations (Section 3.1) and present our own analysis of sea level changes observed by the Norwegian tide gauge network (Section 3.2) and satellite altimetry (Section 3.3). Then we discuss the contributions to 20th century sea level changes along the Norwegian coast (Section 3.4).

3.1 Paleo Observations

Relative sea level in Norway can be traced back almost to the last glacial period, after which the Fennoscandian ice sheet retreated and our coastlines reemerged. From studies of sediments in lakes at different elevations, showing when lake outlets were in contact with seawater or not, an updated RSL curve for Sotra in Hordaland was reconstructed by Lohne et al. (2007). The reconstruction shows that relative sea level there has experienced an overall fall over the past ~14,500 years (Figure 3.1). Thus, it is the vertical uplift of the Earth owing to GIA that dominates the total sea level change, and this general pattern is seen in multiple paleo records across Norway.

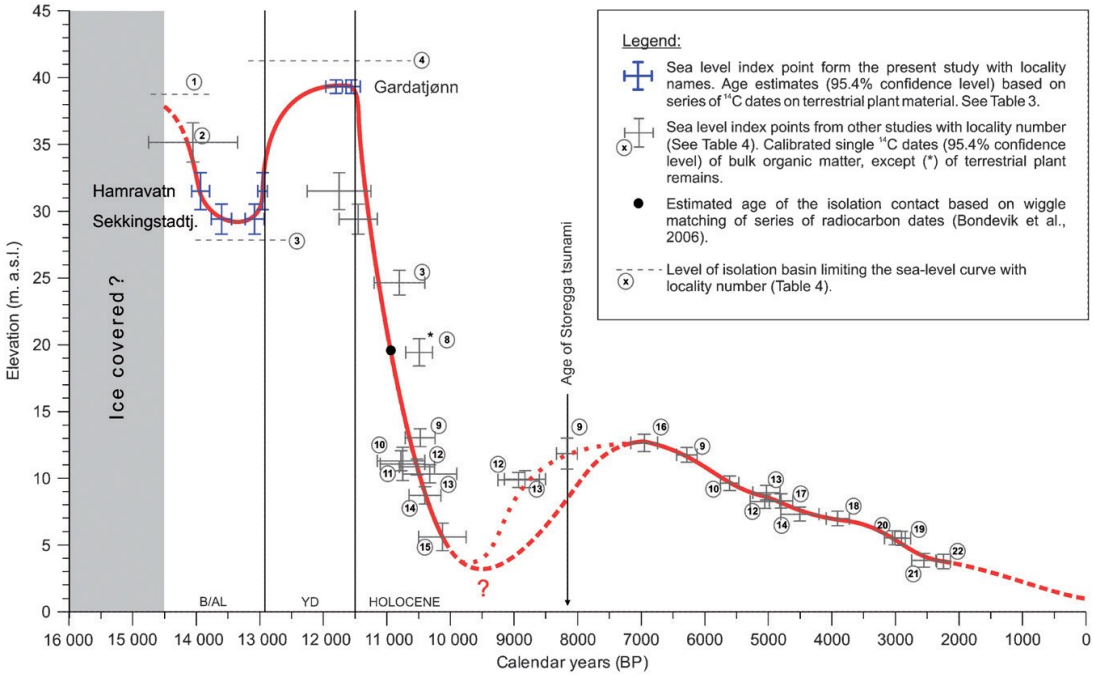

Figure 3.1 Relative sea level curve for the island of Sotra on the west coast of Norway, based on studies of lake sediments from isostatically raised lakes, during the past 14,500 years. Elevation (m.a.s.l.) refers to the lakes' height over sea level today. Crosses represent radiocarbon dates with uncertainty estimates in time and height, which the curve is drawn through. The dotted line is drawn through the actual dates, while the dashed line is considered more accurate due to probable dating errors imposed by the Storegga-tsunami 8,100 years ago. From Lohne et al. (2007).

Figure 3.1 also shows that past RSL varied on a scale of tens of meters, especially in the earlier part of the record when the margin of the ice sheet readvanced during the Younger Dryas. This reflects a complex interplay between vertical land motion due to GIA, global sea level changes, and gravitational effects. From 11,500 years before present the data show that RSL underwent a rapid fall of ~35 m largely owing to land uplift as the ice sheet melted. Following that, RSL began to rise during the early to mid-Holocene. This was because other large continental ice sheets were still melting and contributing to GMSL rise. Whereas, the rate of local land uplift was now somewhat reduced. The details of the Holocene RSL rise are, however, uncertain as the Storegga Tsunami eroded and disturbed the lake sediments in this period. But the end of this rise is constrained to ~7000 years before present (Stabell and Krzywinski, 1978). From around this date, RSL began to fall towards its modern level (Figure 3.1). Global sea level had stabilized around this time and, therefore, land uplift once again dominated the RSL response. The size of the RSL fall over this period varies from a few to 10s of meters across Norway. This reflects significant spatial variation in the vertical uplift rates and is something we also observe today (Chapter 4). Finally, we note that sea level changes in Norway over the past few thousand years (up until the start of the instrumental record) are in general poorly constrained.

3.2 Tide Gauge Records

Records from the global tide gauge network provide a useful tool for understanding 20th century sea level changes and variations in sea level over multi-decade to century time scales. Tide gauges are coupled to the solid Earth, which means that they measure sea level changes relative to land (i.e., both deflections of the Earth's surface and the ocean surface; see Figure 1.2). Thus, to derive an estimate of sea surface change (ΔSSH), the tide gauge data first needs to be corrected for vertical land motion. For Norway, vertical land motion due to GIA is an important component of contemporary relative sea level change. The land motion signal can be separated from the tide gauge records using GIA modeling and/or observations from permanent GPS stations (see Chapter 4). In addition, it is worth remembering that GIA also affects Earth's gravity field and, therefore, acts to perturb the ocean surface. This effect needs to be taken into account if the tide gauge data are to be fully "GIA corrected" and to help us understand the separate contributions to sea level change (see Tamisiea and Mitrovica, 2011; and Section 3.2.2).

The Norwegian Mapping Authority operates 23 permanent tide gauges on mainland Norway (Figure 3.2), one in Ny-Ålesund at Svalbard, and one at Jan Mayen. The tide gauges have been in service for different time periods, a few have been in operation since the late 1800s while others were only recently established in the 1990s (Table 3.1). It should be noted that the quality of the data has improved significantly over the years, as the tide gauge device as well as the recording and transmitting technology has developed. Today, the Norwegian Mapping Authority receives and broadcasts sea level data from all the tide gauges (except for Mausund) several times per hour.

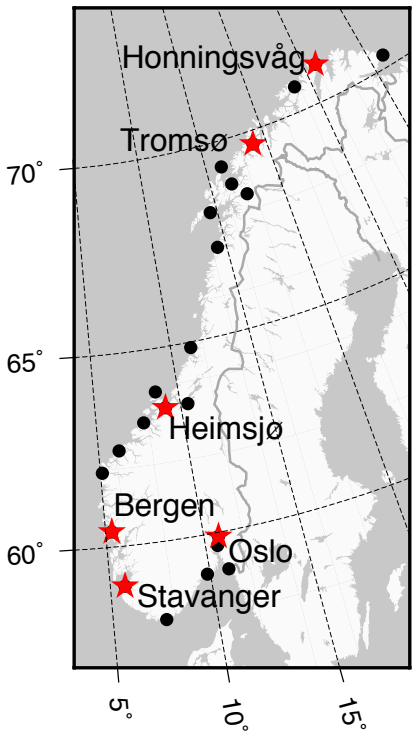

Figure 3.2 The Norwegian tide gauge network. The red stars with names indicate the sites chosen as key locations in parts of this report.

Table 3.1 Overview of the Norwegian tide gauges, ordered along the coast from north to south. The table lists longitude/latitude [degrees] of each tide gauge (from the archive of the Norwegian Mapping Authority), id-numbers in the PSMSL-archive, the start month of each record, the percentage of observations available for the periods 1960–2010, 1984–2014, and 1993–2014, and significant gaps (>= 1 year). (* : The tide gauge in Trondheim was relocated in 1990.)

Tide gauge name	Longitude (°E) Latitude (°N)	PSMSL-ID	Start yyyy.m	1960–2010 (%)	1984–2014 (%)	1993–2014 (%)	Gap
Vardø	31.104015 70.374978	1257	1969.0	60	94	95	1966.2–1984.0
Honningsvåg	25.972697 70.980318	1267	1947.7	75	94	100	1985.0–1986.0
Hammerfest	23.683227 70.664641	758	1970.5	88	99	99	1970.0–1971.0 1982.0–1983.0
Tromsø	18.961323 69.647424	680	1957.0	98	98	100	
Andenes	16.134848 69.326067	425	1938.0	52	78	100	1955.8–1974.0 1978.9–1982.0
Harstad	16.548236 68.801261	681	1952.2	94	97	100	
Narvik	17.425759 68.428286	312	1928.1	98	97	100	1940.3–1947.3

Tide gauge name	Longitude (°E) Latitude (°N)	PSMSL-ID	Start yyyy.m	1960–2010 (%)	1984–2014 (%)	1993–2014 (%)	Gap
Kabelvåg	14.482149 68.212639	45	1948.0	97	97	100	
Bodø	14.390813 67.288290	562	1949.7	89	95	99	1953.5–1954.5 1971.0–1972.0
Rørvik	11.230107 64.859456	1241	1969.7	80	99	100	
Mausund	8.665230 63.869330		1988.0	39	78	88	2005.9–2008.0
Trondheim*	10.391669 63.436484	34 1748	1945.5 1990.0	20		100	1946.5–1949.0
Heimsjø	9.101504 63.425224	313	1928.0	99	99	100	
Kristiansund	7.734352 63.113859	682	1952.4	99	98	100	
Ålesund	6.151946 62.469414	509	1945.1	98	99	100	1946.1–1951.0
Måløy	5.113310 61.933776	486	1943.5	95	99	100	1958.0–1961.0
Bergen	5.320487 60.398046	58	1915.0	98	99	100	1941.0–1943.1
Stavanger	5.730121 58.974339	47	1919.0	96	100	100	1940.0–1946.0 1970.0–1971.3
Tregde	7.554759 58.006377	302	1927.8	99	99	99	
Helgeroa	9.856379 58.995212	1113	1965.4	64	99	100	1970.0–1981.0
Oscarsborg	10.604861 59.678073	33	1872.1	90	99	100	1883.0–1953.5 1970.0–1971.0
Oslo	10.734510 59.908559	62	1885.5	95	97	100	1891.0–1914.0 1939.0–1940.0
Viker	10.949769 59.036046	1759	1990.9			100	

3.2.1 Earlier Assessments of Sea Level Rates from the Norwegian Tide Gauges

A comprehensive study of the Norwegian tide gauges is Richter et al. (2012a) (see also Section 3.4). Using EOF-analysis the authors find the leading mode of sea level variability for the Norwegian tide gauges. It shows a trend of 2.9 ± 0.3 mm/yr for 1960 to 2010 (after correcting for VLM). There are also other investigations which have included data from the Norwegian tide gauges in wider regional analyses (e.g., Douglas, 1991; Vestøl, 2006; Marcos

and Tsimplis, 2007; Henry et al., 2012; Wahl et al., 2013; Calafat et al., 2013; Dangendorf et al., 2014). We briefly summarise the findings from some of these studies here.

Vestøl (2006) finds averaged regional sea level change over Fennoscandia of 1.32 mm/yr (corrected for VLM) for 1891 to 1990. Henry et al. (2012) analyse sea level trends from the Norwegian tide gauges for 1950 to 2009, and find markedly lower rates than reported by Richter et al. (2012a). This could be due to slightly different period analysed (they opt to include data from the 1950s which generally had higher sea levels than the following decades) and/or their use of a different VLM correction. In a study of tide gauge records surrounding the North Sea, a trend of 1.6 ± 0.9 mm/yr (corrected for GIA) was found for the period 1960 to 2000 (Marcos and Tsimplis, 2007). Wahl et al. (2013) also address the North Sea region, analysing data from both tide gauges and satellite altimetry. The study presents three index time series which are the arithmetic means for each year across three subsets of GIA-corrected tide gauge records. The index time series were analyzed for a possible acceleration in regional sea level rise over the past few decades by applying Singular Spectrum Analysis (see e.g., Ghil et al., 2002). Despite a linear long-term trend of roughly 1.6 ± 0.9 mm/yr since 1900, no evidence was found for a significant acceleration in the North Sea region.

3.2.2 Analysis of the Norwegian Tide Gauges

In order to better quantify observed sea level changes along the Norwegian coast, we conduct our own analysis of tide gauge records. We use data from the Permanent Service for Mean Sea Level (Woodworth and Player, 2003) for all stations except Mausund, and follow their recommendation of only using the revised local reference datasets. These datasets are reduced to a common datum by making use of the tide gauge datum history provided by the supplying authority; this means that any shifts in the records are removed. In this study, we chose to use the monthly datasets which appear to be more complete when compared to the annual records. For Mausund we used data found in the archives of the Norwegian Mapping Authority because this tide gauge is presently not included in the PSMSL database.

To determine long-term trends from the observed RSL changes we conduct a least squares adjustment for each tide gauge (Eq. 3.1)

$$z(t) = a + bt + A_1 \sin(2\pi t - \varphi_1) + A_2 \sin(4\pi t - \varphi_2) + A_3 \sin(2\pi t/18.6 - \varphi_3) + \varepsilon(t) \ . \quad (3.1)$$

Here $z(t)$ is the observation at the epoch t, a is the intersect of the model, b is the rate of sea level change, A_1, φ_1, A_2, φ_2, A_3, φ_3 are the amplitudes and phases of the annual, semi-annual, and 18.6 year periodic variation in the time series, and ε is the error. The annual periodic term was included because visual inspection of the monthly datasets revealed significant annual variation. If not captured by the model, the annual variation increases the standard error of the estimated rate of sea level change. We also opt to include the semi-annual component. The 18.6-year periodic term is due to the Moon's nodal cycle, which is one of the components driving the tides on Earth (Baart et al. 2012). Using this model, sea level change is assumed to be constant within the study period.

The regression of the tide gauge observations is complicated by time-correlated noise. If not taken into account, the standard errors of the rates may be underestimated (Bos et al., 2013; Burgette et al., 2013). Hence, we did a preliminary fit of the model in Eq. 3.1 and investigated the sample autocorrelation function (ACF) and the sample partial autocorrelation function (PACF) of the residuals. For all tide gauges, the sample PACFs were significantly different from zero (at the 95% level) for lag one (corresponding to one month) with values of the order of 0.25 to 0.42. For greater lags, the PACF were within the significance-threshold. The sample ACFs had values of similar magnitude as the PACFs. They were significantly different from zero for lag one at all stations and close to or within the significance threshold for lags beyond one. We therefore characterize both the PACF and the ACF functions as fast decaying functions and conclude that the residuals are moderately time-correlated. This suggests that the series of errors may be described by a first order autoregressive process (AR1), i.e., the errors can be written

$$\varepsilon(t) = \Phi_1 \varepsilon(t-1) + w(t) \quad , \tag{3.2}$$

where $w(t) \sim N(0, \sigma^2)$ (white noise) and Φ_1 is the parameter of the AR1 model. This stochastic model implies that each observation is only affected by the previous observation and by white noise. The parameter Φ_1 was estimated by the Yule-Walker equations and we used the Cochrane and Orcutt's transformation to generate regression equations with uncorrelated errors (Brockwell and Davis, 2002). The resulting regression equations were then subject to an ordinary least squares adjustment. This gave rates with standard errors 20–40% larger than the standard errors of the preliminary fit, which did not take into account time-correlated noise.

We note that other stochastic models can be used to take into account time-correlated noise in tide gauge records. Bos et al. (2013) are critical of only using the AR1-model. They find that the choice of model depends on the sampling rate (monthly/annual data), the length of the record, and the location. For most tide gauges along the Norwegian coast, the Generalized Gauss Markov stochastic model performs best when applying the BIC-criterion (see any textbook on time series analysis, e.g. Brockwell and Davis, 2002). However, the AR1 model is also found to perform satisfactorily. In this report, therefore, we opt to stick with the AR1 model in our analysis because it is easy to implement. But we are aware that the AR1 model may underestimate the rate uncertainties by a factor of 1.3 to 1.5 (Bos et al., 2013).

As well as observed relative sea level rates from the tide gauges ($\dot{S}_{tg}$) we also present rates that are what we call GIA-corrected ($\dot{S}_{giacorr}$). That is, the RSL rates are adjusted for both vertical land motion ($\dot{S}_{gps/lev}$) and geoid changes associated with GIA ($\dot{S}_{geoidgia}$). The correction for VLM is based upon observations from GPS and levelling whereas the geoid change is generated from our mean GIA model (see Chapter 4 for details). The relation between these processes is defined in Eq. 3.3.

$$\dot{S}_{tg}(l,b) = -\dot{S}_{gps/lev}(l,b) + \dot{S}_{geoidgia}(l,b) + \dot{S}_{giacorr}(l,b) \, , \tag{3.3}$$

where l and b are the longitude and latitude of the tide gauge location. The GIA-corrected rates are in principle equivalent to the SSH change caused by changes in ocean mass, density, circulation etc.

We compute three sets of rates. The first set makes use of all reliable data available from 1960 to 2010. We focus on this period because we have an understanding of the different components of sea level change over this time (see Richter et al. (2012a) and Section 3.4). The second set uses data from the past 30 years (1984 to 2014) and represents present-day sea level change along the Norwegian coast. The third set covers the period 1993–2014 and is included for comparison to satellite altimetry (discussed in Section 3.3).

For each period examined, we only include tide gauges where more than 80% of the data are available (see Table 3.1), i.e., records with too short duration or with significant data gaps are excluded from the analysis. As the length of the tide gauge records varies, the three data sets include different sets of tide gauges. For the period 1960 to 2010 the tide gauges at Viker, Helgeroa, Mausund, Trondheim, Rørvik, Andenes, Honningsvåg, and Vardø are omitted from our analysis. The time series from Helgeroa, Andenes, and Vardø suffer from significant data gaps whereas the records from Viker, Mausund, Rørvik, and Honningsvåg are too short. Trondheim is omitted as the tide gauge was relocated in 1990. For 1984 to 2014 all tide gauges except Viker, Mausund, Andenes, and Vardø are used and for the same reasons as reported above. Trends are computed for 1993 to 2014 for all tide gauges where rates calculated from altimetry are also available.

The uncertainty on the GIA-corrected rates ($\sigma^2{}_{giacorr}$) is calculated as the sum of the error on the tide gauge regression ($\sigma^2{}_{tg}$), the observed VLM error ($\sigma^2{}_{gps/lev}$), the uncertainty on the reference frame's z-drift ($\sigma^2{}_{z-drift}$) and scale error ($\sigma^2{}_{scale}$), and the geoid change error ($\sigma^2{}_{geoidgia}$), as follows:

$$\sigma^2{}_{giacorr} = \sigma^2{}_{tg} + \sigma^2{}_{gps/lev} + \sigma^2{}_{z-drift} + \sigma^2{}_{scale} + \sigma^2{}_{geoidgia} \ . \qquad (3.4)$$

Note that the observed VLM error is in the range ~0.2 to 0.3 mm/yr. Reference frame errors are adopted from a recent review which concluded that the International Terrestrial Reference Frame (ITRF) is stable along each axis to better than 0.5 mm/yr (z-drift) and has a scale error of less 0.3 mm/yr (Collilieux et al. 2014). The uncertainty on the geoid change associated with GIA is very small and has a value of typically 0.03 mm/yr (see Chapter 4 for details). In general, the uncertainties vary according to the length of each time series and increase considerably when the uncertainties of VLM, the reference frame, and geoid changes are taken into account.

3.2.3 Sea Level Rates from the Norwegian Tide Gauges

Our estimated relative and GIA-corrected rates are shown in Figure 3.3, 3.4 and 3.5, and listed in Table 3.2. For the period 1960 to 2010 about half of the RSL rates computed are negative, i.e., RSL has fallen during this period as the rate of land uplift is greater than the rate of sea surface rise (Figure 3.4a and Figure 3.5a). Lowest rates are found in Oslofjorden and in the middle part of Norway. The highest rates are found along the south and west coast of Norway and at Tromsø and Hammerfest.

After correcting for GIA, all rates are positive but vary considerably (Figure 3.5a). The GIA-corrected rates range from 0.8 to 2.8 mm/yr and the spread between the tide gauges is calculated as ± 0.6 mm/yr (one standard deviation). We note that the rates at Kristiansund,

Heimsjø, and Kabelvåg stand out as low. That is, they are, i.e., 1.5 to 1.0 mm/yr below the rates observed at nearby stations. For 1960 to 2010 we calculate the weighted average sea level rise along the Norwegian coast as 1.9 ± 0.6 mm/yr (median 1.9 mm/yr). This rate of rise is similar to the rate of 20th century GMSL rise given in AR5 (Rhein et al., 2013) but a detailed comparison is not made here.

For 1984–2014 the RSL rates show a similar pattern as for 1960–2010 (Figure 3.4 and Figure 3.5). That is, for the past 30 years the pattern of RSL change is dominated by VLM. After correcting for GIA, the rates vary between 0.7 and 3.3 mm/yr. While the GIA-corrected rates observed at Kristiansund and Heimsjø appeared low for the period 1960 to 2010, we find that they are in line with the surrounding stations for the period 1984 to 2014. The rate observed at Kabelvåg, however, remains very low when compared to the other tide gauges. The cause of this apparent outlier is not known but we opt to omit this station from further analysis. With Kabelvåg excluded, the GIA-corrected rates are more uniform and have a spread of ± 0.4 mm/yr (one standard deviation). For 1984 to 2014 we calculate the weighted average sea level rise along the Norwegian coast as 2.5 ± 0.6 mm/yr (median 2.4 mm/yr).

Using Welch's t-test we determine that, in comparison to the period 1960 to 2010, the average rate of sea level rise along the Norwegian coast for 1984 to 2014 is significantly higher at the 95% level. (Note that before applying this test we recalculated the coastal averages excluding Kabelvåg and using the same set of tide gauges but found this made no difference to our earlier results).

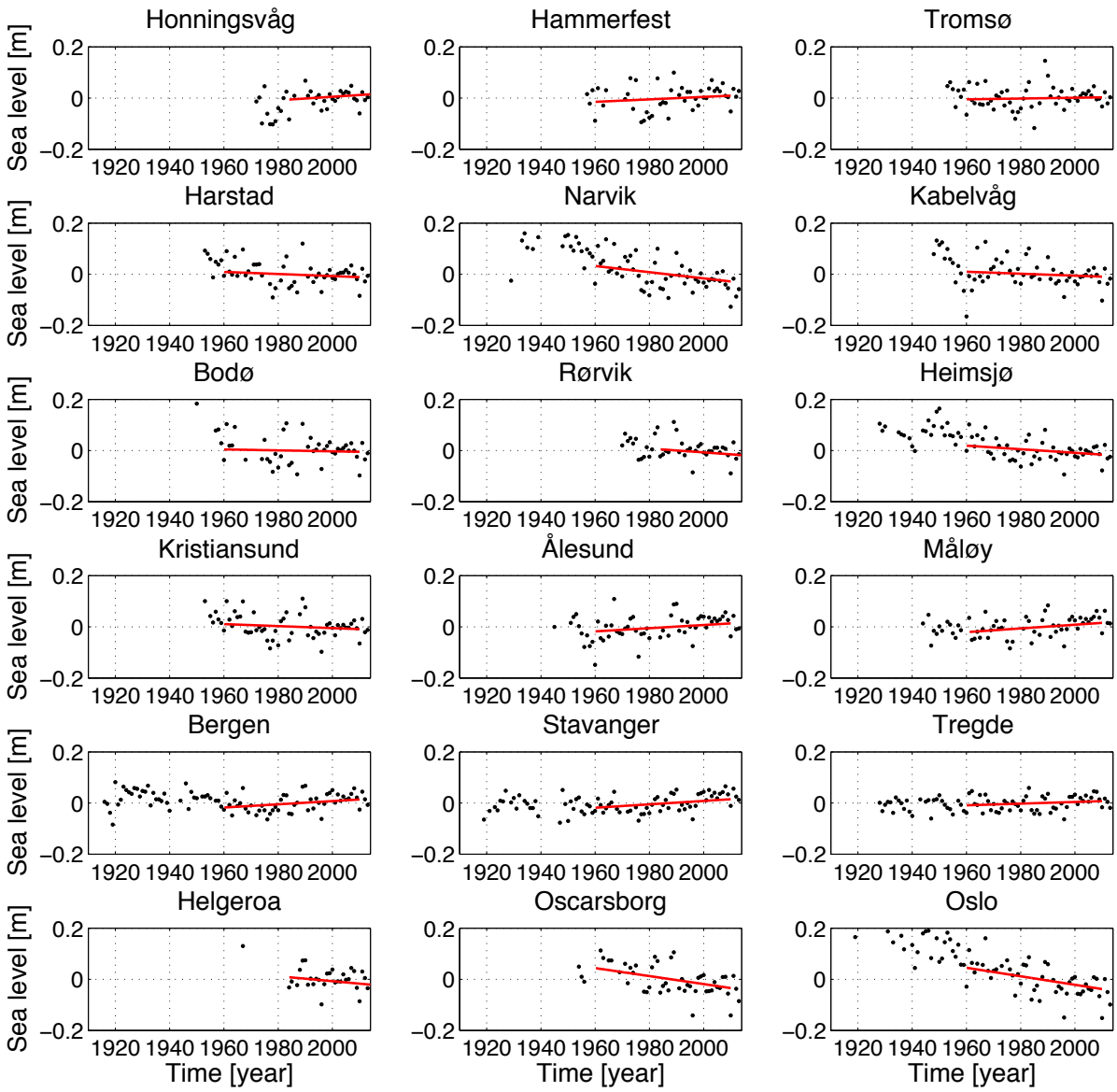

Figure 3.3 Plots of Norwegian tide gauge records of sufficiently long duration for trend estimation. Black dots are annual averages and red lines indicate trends in relative sea level estimated from the monthly data. The trend is computed for the period 1960 to 2010 where data for this period are available. Otherwise the red lines indicate trends for the period 1984 to 2014.

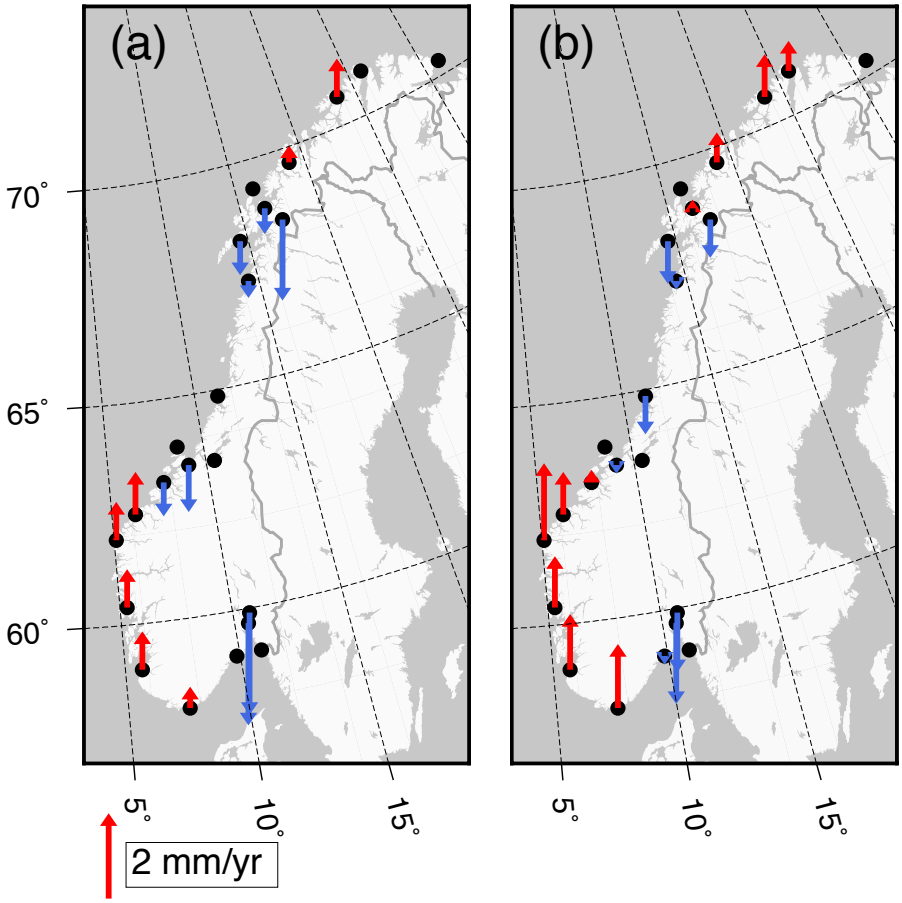

Figure 3.4 Relative sea level rates at the Norwegian tide gauges for the periods 1960–2010 (a) and 1984–2014 (b). The standard error of the rates varies from 0.2 to 0.5 mm/yr for the period 1960–2010 and from 0.5 to 1.0 mm/yr for the period 1984–2014.

a)

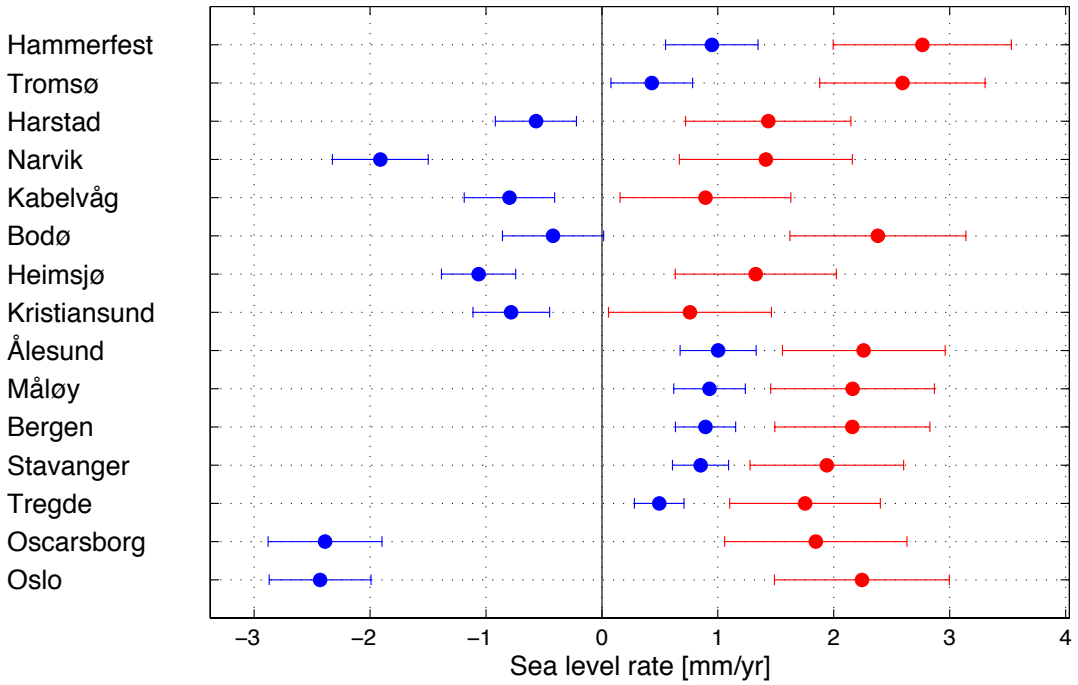

b)

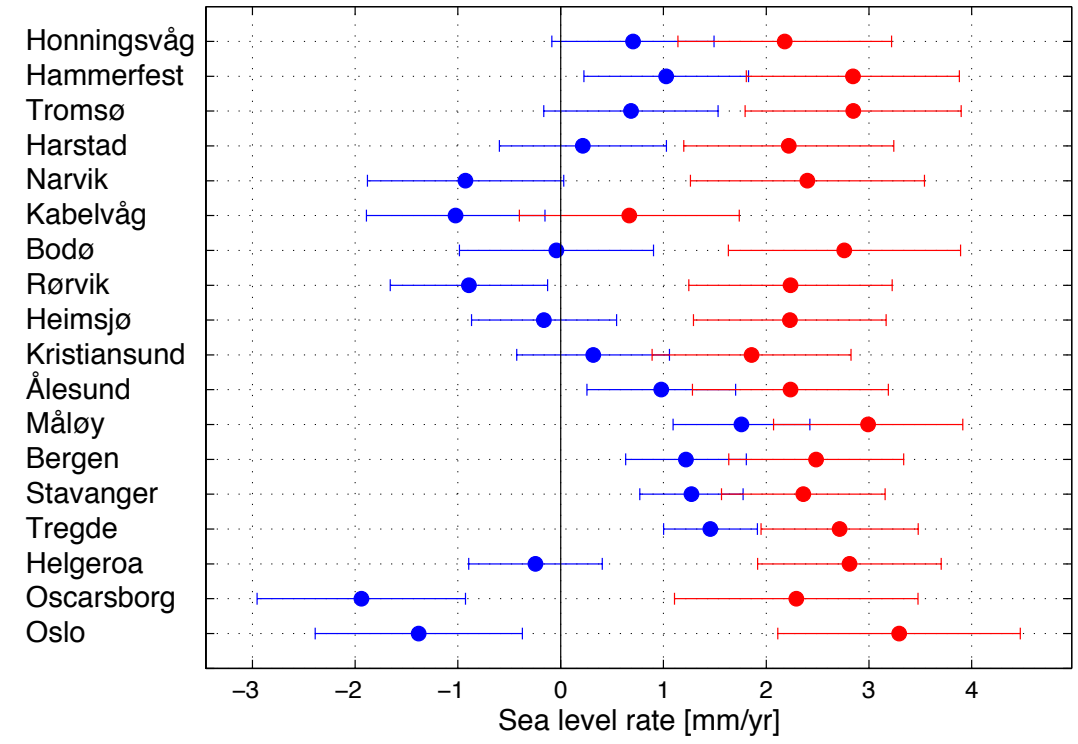

Figure 3.5 Relative (blue) and GIA-corrected (i.e., adjusted for vertical land motion as well as the gravity effect of GIA; red) sea level rates with standard errors estimated from tide gauge observations along the Norwegian coast. Rates are shown for (a) the period 1960 to 2010 and (b) the period 1984 to 2014. The stations are ordered along the coast from north to south.

Table 3.2 Observed relative sea level rates and GIA-corrected rates for selected Norwegian tide gauges, ordered along the coast from north to south. To determine the GIA-corrected sea level rates we adjusted the tide gauge observations using (1) vertical land motions estimated from a combined analysis of levelling and GPS data and (2) geoid changes generated using our mean GIA model (see Chapter 4). The weighted average of the rates is given for each period. The standard errors of the GIA-corrected rates and the weighted averages include uncertainties introduced by VLM, geoid corrections and reference frame errors. Records with too short duration or with significant data gaps are excluded from the analysis.

Tide gauge	Relative rate (mm/yr) 1960–2010	GIA-corrected rate (mm/yr) 1960–2010	Relative rate (mm/yr) 1984–2014	GIA-corrected rate (mm/yr) 1984–2014
Honningsvåg			0.7 ± 0.8	2.2 ± 1.0
Hammerfest	0.9 ± 0.4	2.8 ± 0.8	1.0 ± 0.8	2.8 ± 1.0
Tromsø	0.4 ± 0.4	2.6 ± 0.7	0.7 ± 0.8	2.8 ± 1.1
Harstad	-0.6 ± 0.3	1.4 ± 0.7	0.2 ± 0.8	2.2 ± 1.0
Narvik	-1.9 ± 0.4	1.4 ± 0.7	-0.9 ± 1.0	2.4 ± 1.1
Kabelvåg	-0.8 ± 0.4	0.9 ± 0.7	-1.0 ± 0.9	0.7 ± 1.1
Bodø	-0.4 ± 0.4	2.4 ± 0.8	0.0 ± 0.9	2.8 ± 1.1
Rørvik			-0.9 ± 0.8	2.2 ± 1.0
Heimsjø	-1.1 ± 0.3	1.3 ± 0.7	-0.2 ± 0.7	2.2 ± 0.9
Kristiansund	-0.8 ± 0.3	0.8 ± 0.7	0.3 ± 0.7	1.9 ± 1.0
Ålesund	1.0 ± 0.3	2.3 ± 0.7	1.0 ± 0.7	2.2 ± 1.0
Måløy	0.9 ± 0.3	2.2 ± 0.7	1.8 ± 0.7	3.0 ± 0.9
Bergen	0.9 ± 0.3	2.2 ± 0.7	1.2 ± 0.6	2.5 ± 0.9
Stavanger	0.9 ± 0.2	1.9 ± 0.7	1.3 ± 0.5	2.4 ± 0.8
Tregde	0.5 ± 0.2	1.8 ± 0.6	1.5 ± 0.5	2.7 ± 0.8
Helgeroa			-0.2 ± 0.6	2.8 ± 0.9
Oscarsborg	-2.4 ± 0.5	1.8 ± 0.8	-1.9 ± 1.0	2.3 ± 1.2
Oslo	-2.4 ± 0.4	2.2 ± 0.8	-1.4 ± 1.0	3.3 ± 1.2
Weighted average sea level rise		1.9 ± 0.6		2.4 ± 0.6

3.2.4 Reliability and Interpretation of Tide Gauge Records

The reliability of the rates determined from the tide gauge records is dependent on the quality of the measurements, the corrections made (e.g., VLM) and the appropriateness of the trend analysis applied. The last of these is discussed above (Section 3.2.2). If we first consider the quality of the tide gauge data themselves, we note that the recording systems and tide gauge technology have significantly improved over the lifespan of most of the tide gauges. The data quality is thus higher towards the end of the time series.

Secondly, concerning the GIA-corrected rates, it is important to ask how well vertical land motion is constrained at the tide gauge sites. VLM is not directly observed using GPS at the majority of Norwegian tide gauges. Only the tide gauges at Tregde, Andenes, and Vardø are collocated with a GPS station. At the other tide gauges, the distance to the closest reliable GPS station ranges from a few hundred meters to almost 100 km. For this reason, precise levelling data are also included in our VLM solution (see Chapter 4) which helps better constrain land motion close to some tide gauges. If GIA is the dominant contributor to VLM, then large distances (>10 km) between the tide gauge and GPS station and/or sparse levelling lines are not necessarily problematic. If local processes (e.g. subsidence) are at play, however, then this can cause localised motions at the tide gauge, GPS station or along the lines of levelling. Thus, it is somewhat unclear how well the VLM solution applied here represents actual motion at tide gauges where we lack observations.

An additional challenge is that most tide gauges in Norway are not fixed to the bedrock, local processes are especially relevant at these sites. Regular control levelling is therefore conducted between the tide gauge and a nearby benchmark located on bedrock. (this control levelling is made over short distances and is separate to the levelling measurements used in our VLM solution). If the control levelling detects a change in height between the tide gauge and the benchmark, a correction is applied to the tide gauge record. Recently it was discovered that this procedure has not been followed at Viker, Helgeroa, and Stavanger. Analysis of the levelling data indicates that these stations are sinking relative to the nearby bedrock at a rate of 0.30 (1991 to present), 0.22 (1988 to present), and 0.71 mm/yr (1988 to present), respectively. Corresponding corrections have therefore been applied to the rates presented in this report. To summarize, it is clear that VLM is poorly constrained at some tide gauge locations in Norway. Our analysis shows that the GIA-corrected rates show considerable spatial variability and, therefore, this might be in part due to errors in our VLM solution.

Finally, regarding the interpretation of our tide gauge trend analysis, it is important to be aware that the rates are extremely sensitive to the selected study period. This can be seen in Figure 3.6, which shows how the estimated rates vary for a 30-year moving window shifted in steps of 1 year from 1960 to 1984. For the tide gauges south of Trondheimsfjorden and in Tromsø, the rates vary by ~2 mm/yr. For the other tide gauges the variation is even larger, especially at Bodø, Kabelvåg, and Narvik. At Kabelvåg it seems like local effects strongly influence the earliest years of the record, the rate decreases by 4 mm/yr when changing the start year from 1960 to 1967. For all tide gauges, we find that the estimated rates can vary by more than 1 mm/yr by moving the 30-year window by just one year. These results are

indicative of strong interannual to multi-decadal variability in the tide gauge records, which is consistent with previous studies (Richter et al., 2012a; Calafat et al., 2013; Dangendorf et al., 2014). We also note that Figure 3.6 reveals patterns common to many tide gauges. For example, most tide gauges show a minimum in the rate series at 1967 and 1981. And the majority of tide gauges indicate highest rates around 1975 and for the most recent periods. This suggests that at least some of the the interannual variability in the rate estimates is due to dynamic sea level changes that have coherent spatial pattern covering most of the Norwegian coast.

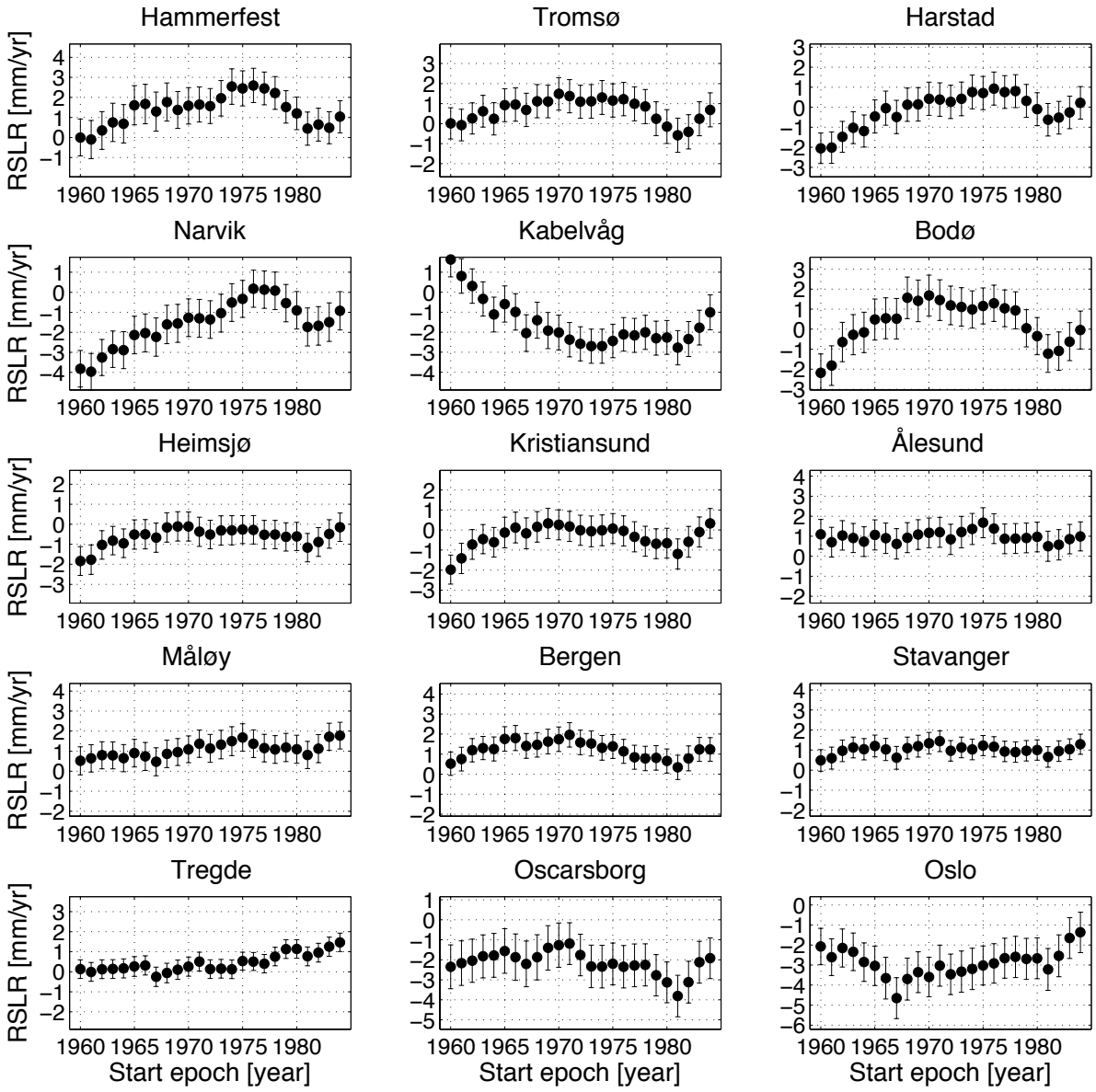

Figure 3.6 Relative sea level rates from some tide gauge records, computed for 30-year moving windows shifted in steps of 1 year as a function of the starting year of the 30-year period. The error bars indicate one standard error.

3.3 Satellite Altimetry

Over the past 20 years, satellite altimetry has been a major technique for mapping sea surface topography and measuring sea level changes. The working principle of the technique is to transmit short pulses of microwave radiation, which interact with the sea surface and are partly reflected back to the satellite. From the two-way travel time of the pulses, the distance between the satellite and the sea surface can be estimated. The sea surface height (see Figure 1.2) is computed by subtracting this distance from the height of the satellite determined in a global reference frame. Satellite altimetry is, therefore, not sensitive to the VLM changes that affect tide gauge measurements. Satellite altimetry observations have been used in a wide number of applications; in sea level change studies, mapping of ocean currents, mean sea surface determination, gravity field determination, lake level monitoring, river discharge studies, development of ocean tide models, and ENSO studies (see e.g., Beckley et al., 2007; Lysaker, 2009; Andersen and Knudsen, 1998; Hwang et al., 2005; Kouraev et al., 2004; Smith et al., 2000; Andersen et al., 2006).

Accurate sea level monitoring requires precise range measurements, precise satellite orbits (satellite positions) as well as a precise and stable reference frame. The most precise range measurements are today obtained by dual frequency radar transmitters, which directly observe the ionospheric delay, combined with microwave radiometers which measure the atmospheric water vapor delay. This allows the ranges to be determined with a precision of 3 cm (Vincent et al., 2003). Precise orbits are determined by utilizing satellite tracking systems like GPS, DORIS (Doppler Orbitography and Radio positioning Integrated by Satellite), and Satellite Laser Ranging. Using these techniques the orbits of the latest altimetry missions are determined with an accuracy better than 2 cm. Averaging the sea surface height measurements over larger regions or over the whole Earth allows us to determine changes in mean sea level with a precision of some tenths of a millimeter per year (Ablain et al., 2009). This level of accuracy requires satellite orbits defined in a reference frame that is stable over time. A drift of the origin can introduce systematic errors of several millimeters in regional sea level estimates, while a change in the scale will also influence on the global sea level. Minster et al. (2010) argue that the current version of the ITRF does not allow regional sea level to be monitored with millimeter per year accuracy.

The era of precise satellite altimetry started in 1992 with the launch of TOPEX/POSEIDON and ERS-1 (see Table 3.3 for a list of available data from the main altimetry missions). Since then, successive missions have provided more than 20 years of continuous measurements of sea level. The angle between the satellite orbit and the equatorial plane of the Earth (the orbit's inclination) controls the area observed by the satellite. The orbit of TOPEX/POSEIDON, Jason-1, and Jason-2 has an inclination which allows the ocean areas between ± 66° latitude to be observed while the satellites ERS-1, ERS-2, ENVISAT, Cryosat-2, and SARAL/AltiKa observe the ocean areas between ± 82° latitude. Data from the ERS-1 and ERS-2 satellites previously suffered from weakly determined orbits. However, recent reprocessing of the raw data from these missions means they are now more suitable for studies of sea level. Monitoring of sea level at high latitudes is now maintained by

SARAL/AltiKa and Cryosat-2. Unfortunately, the time series at high latitudes suffer from a gap between April 2002 and April 2003.

Table 3.3 Overview of the latest and some future satellite altimetry missions.

Satellite	Latitudinal boundary	Start of mission	Mission completed
ERS-1	± 82°	July 1991	June 1996
TOPEX/POSEIDON	± 66°	10 August 1992	October 2005
ERS-2	± 82°	April 1995	2004
Jason-1	± 66°	7 December 2001	June 2013
ENVISAT	± 82°	March 2002	April 2012
Jason-2	± 66°	20 June 2008	In orbit
Cryosat-2	± 88°	8 April 2010	In orbit
SARAL/AltiKa	± 82°	April 2013	In orbit
Jason-3	± 66°	2015	
Sentinel-3	± 82°	2015	
Jason-CS/Sentinel-6	± 66°	2020	

3.3.1 Regional and Coastal Altimetry

Compared to computing global sea level, it is more challenging to measure regional sea level within a smaller area like the Norwegian coast. This is because ocean variability is generally larger on regional scales due to redistribution effects like wind. In addition, regional altimetry is more sensitive to errors that are often negligible when calculating the global average. This could be errors in the ocean tide model, sea state corrections, and/or orbital errors.

For regional applications the orbital errors have a direct influence on the observed sea level rate. This was demonstrated by, e.g., Beckley et al. (2007) who computed sea level rates by using satellite orbits for TOPEX/POSEIDON in two different reference frames (CSR95 and ITRF2005). The study indicates that the sea level rates may be biased by up to 1.5 mm/yr along the Norwegian coast due to errors in the orbits. This is half the size of the present global rate and illustrates the importance of precise satellite orbits for regional sea level measurements.

Applications of satellite altimetry in coastal areas (closer than about 30 km to the land) are especially demanding. In the coastal zones, the quality of the range measurements is degraded because the radar pulses are reflected partly from land and partly from the sea. It is also more difficult to compute accurate range corrections and the tidal patterns are more complex to model. As a consequence, altimetry observations closer than ~30 km to the coast are normally not used. Hence, the estimates reported below for the Norwegian coast, do not strictly

represent sea level change at the coast. They may, therefore, deviate from estimates based on measurements from nearby tide gauges.

Recent studies, however, have demonstrated that it is possible to extract information from radar pulses in the coastal zones (see, e.g., Vignudelli et al. 2011a,b). This requires so called retracking of the radar waveforms, i.e., algorithms optimized for radar pulses backscattered from a mix of land and sea are applied. In addition, the wet tropospheric corrections must be calculated from meteorological models instead of measurements from microwave radiometers on board the altimetry satellites. Coastal altimetry products do exist for Norway, e.g., PISTACH data for Jason-2 (Mercier et al. 2010) and ENVISAT data from CTOH (Roblou et al. 2007; 2011), but the quality of these data along the Norwegian coast has not yet been assessed.

3.3.2 Analysis of Altimetry for the Norwegian Coast

To the best of our knowledge, there is no single study that focusses on sea level trends estimated from altimetry for the Norwegian coast. However, the Norwegian coast is included in several investigations that have addressed sea level change in the Arctic Ocean. In Volkov and Pujov (2012) gridded multi-mission data were analyzed using observations from the period 1992 to 2012. The gridded data were bilinearly interpolated to the positions of the Norwegian tide gauges at Kristiansund, Rørvik, Andenes, Hammerfest, Honningsvåg, and Vardø. At these locations the SSH rates were estimated as 3.5, 4.4, 4.3, 4.0, 4.0, and 4.1 mm/yr, respectively. Similar results are also reported in Henry et al. (2012) and Prandi et al. (2012). Both studies use the same multi-mission data originally compiled for studying the Arctic Ocean. In Henry et al. (2012) the average rate around 11 Norwegian tide gauges locations (from Måløy to Hammerfest) was estimated to be 4.23 mm/yr for 1993 to 2009. The authors also found that SSH changes were somewhat higher north of Sognefjorden 61°N (4 to 6 mm/yr) compared to south of the fjord (2 to 4 mm/yr). Prandi et al. (2012) examined sea level rates north of 55°N and found similar results to those reported by Henry et al. (2012). They also estimated the sea level rate for the Arctic region north of 66°N to be 3.6 ± 1.3 mm/yr for 1993 to 2009. Note that none of the above studies includes a correction for geoid changes associated with GIA (-0.2 to 0.4 mm/yr along the Norwegian coast, see Chapter 4). This is not a criticism of these investigations but, as we opt to take this effect into account, is one reason why our altimetry results are different to these other findings.

We include our own analysis of along-track observations for the Norwegian coast here. Two datasets are analyzed. The first combines observations from the three satellites TOPEX/POSEIDON, Jason-1, and Jason-2 and samples near-coastal waters (within approximately 20 km from the coastline) south of 66°N (see Figure 3.7a). The second dataset combines data from ERS-1, ERS-2, ENVISAT, and Saral/AltiKa and samples the entire Norwegian coast (see Figure 3.7b). Both datasets cover the period 1993 to 2014. The altimetry data were provided by several datacenters. For TOPEX/POSEIDON we used the generation B merged geophysical data records (GDR) distributed by NASA/JPL/PODAAC. Data from Jason-1 (GDR-C), Jason-2 (GDR-D), and SARAL/AltiKa (GDR-T) were downloaded from the AVISO portal of the Centre National d'Etudes Spatiales (ftp://avisoftp.cnes.fr/AVISO/pub/). The data from the European satellites ENVISAT (GDR

version 2) and ERS-1/2 (REAPER products) were provided by the European Space Agency and downloaded from their Earth Online portal (http://earth.esa.int).

When combining data from several missions, it is crucial to estimate possible intermission measurement biases. Biases of up to several decimeters may arise because the measurements suffer from residual errors in the observation system, the algorithms and parameters used in ground processing, and the applied range- and geophysical corrections. As a consequence, there may be an absolute bias between the true and the observed sea level and a relative bias between sea level observed by two missions. Often, the relative bias for a pair of missions is assumed to be time-invariant and can be assessed if data from a common period exist. Here, global cycle-averages were first computed for each satellite, and then differentiated in order to compute the bias. This procedure is straightforward for the first dataset because data from TOPEX/POSEIDON partly overlap in time with data from Jason-1, and data from Jason-1 overlap partly with data from Jason-2. The second dataset is more complex because the data from ENVISAT and Saral/AltiKa do not overlap in time. We therefore first compute the relative bias between ENVISAT and Jason-2, and then the bias between Saral/AltiKa and Jason-2. Finally, the bias between ENVISAT and Saral/AltiKa was computed by combining their relative biases to Jason-2.

Sea level rates were computed around tide gauges locations and in grid-points along the Norwegian coast. For each point, time series of altimetry observations were generated by computing cycle-averages for all observations within a spherical distance of 1°. Following this a least squares adjustment was used to fit the model defined in Eq. 3.1 to the time series. We also apply a correction for geoid changes associated with GIA using modelling results from Chapter 4.

The uncertainties of the regional estimates are difficult to assess. They cannot be estimated from the data alone because systematic effects dominate. We therefore combine the uncertainty from the regression (${\sigma^2}_{reg}$) with the uncertainties of known systematic effects, i.e., the error of geoid correction (${\sigma^2}_{geoidgia}$), the z-drift of the reference frame (${\sigma^2}_{z-drift}$), the scale rate of the reference frame (${\sigma^2}_{scale}$), and the models (${\sigma^2}_{models}$) used to compute the sea surface heights (e.g. the ocean tide model):

$$ {\sigma^2}_{altimetry} = {\sigma^2}_{reg} + {\sigma^2}_{geoidgia} + {\sigma^2}_{z-drift} + {\sigma^2}_{scale} + {\sigma^2}_{models} , \qquad (3.5) $$

The reference frame uncertainties are difficult to assess because the altimetry time series are defined in both ITRF2005 and CSR95 and the combined uncertainty is poorly constrained. The reference frame uncertainties applied in our tide gauge analysis are 0.5 mm/yr and 0.3 mm/yr for the z-drift and scale rate, respectively (Collilieux et al., 2014). These values are computed for ITRF2008, but we assume that the combined uncertainty for ITRF2005 and CSR95 is of the same order. The uncertainty of the models is poorly constrained for regional estimates. We therefore use the upper limit (0.44 mm/yr) of the range of the global uncertainty reported in Ablain et al. (2009), but caution that this value may be too optimistic for regional estimates. In total, the standard errors of the regional altimetry estimates are approximately 1 mm/yr.

3.3.3 Results from Altimetry for the Norwegian Coast

We list sea level rates determined from nearby altimetry for the tide gauge locations and covering the period 1993 to 2014 (Table 3.4). For comparison, the GIA-corrected tide gauge records are also included. SSH rates computed from the dataset covering the region south of 66°N (TOPEX/POSEIDON, Jason-1, and Jason-2) range from 2.8 to 4.2 and have a standard deviation of 0.4 mm/yr.

Table 3.4 Sea level rates observed by altimetry and GIA-corrected rates from tide gauge records for the period 1993 to 2014. The tide gauges are ordered along the coast from north to south. The weighted average of the rates is given for all locations and for those south of 66°N. Note that the altimetry data are corrected for geoid changes associated with GIA.

Tide gauge	GIA-corrected rate from tide gauge (mm/yr) 1993–2014	Altimetry TP,J1,J2 (mm/yr) 1993–2014	Altimetry E1,E2,EN,SARAL (mm/yr) 1993–2014
Vardø	2.7 ± 1.6		2.2 ± 1.0
Honningsvåg	2.9 ± 1.6		2.2 ± 1.0
Hammerfest	3.8 ± 1.7		2.6 ± 1.0
Tromsø	3.7 ± 1.8		3.1 ± 1.0
Andenes	3.7 ± 1.7		3.0 ± 0.9
Harstad	3.4 ± 1.7		4.0 ± 1.0
Kabelvåg	4.0 ± 1.8		4.4 ± 1.0
Bodø	3.3 ± 2.0		4.9 ± 1.2
Rørvik	4.1 ± 1.7	3.2 ± 0.8	3.3 ±1.0
Mausund	3.8 ± 1.8	3.1 ± 0.8	3.2 ± 1.0
Heimsjø	3.8 ± 1.6	4.0 ± 0.8	3.7 ± 1.0
Kristiansund	4.4 ± 1.6	3.6 ± 0.8	3.7 ± 1.0
Ålesund	3.2 ± 1.6	2.8 ± 0.8	4.1 ± 1.0
Måløy	4.5 ± 1.5	3.1 ± 0.8	3.9 ± 0.9
Bergen	3.6 ± 1.3	4.2 ± 0.8	2.4 ± 0.9
Stavanger	3.6 ± 1.3	3.5 ± 0.8	2.8 ± 1.0
Tregde	2.3 ± 1.1	3.4 ± 0.9	2.3 ± 1.0
Helgeroa	5.3 ± 1.6	3.2 ± 0.9	2.4 ± 1.1
Viker	5.0 ± 1.8	3.1 ± 0.9	2.4 ± 1.2
Weighted average sea level rise	3.6 ± 0.6		3.2 ± 0.8
Weighted average sea level rise south of 66°N	3.8 ± 0.6	3.4 ± 0.7	3.1 ± 0.7

The weighted average of the rates is found to be 3.4 ± 0.7 mm/yr for 1993 to 2014. Whereas, SSH rates computed from the dataset covering the entire Norwegian coast (ERS-1, ERS-2, ENVISAT, and SARAL/AltiKa) range from 2.2 to 4.9 mm/yr and have a standard deviation of 0.8 mm/yr. The corresponding weighted average is calculated as 3.2 ± 0.9 mm/yr. Hence, we find that the weighted averages of the altimetry datasets agree within the errors, but the spread (one standard deviation) of the second set of rates is substantially larger than that of the first set (also when only stations south of 66°N are considered).

Including the GIA-corrected tide gauge rates for comparison, we find that all weighted averages agree to within one standard error (Table 3.4). This is an encouraging result, indicating no large systematic errors in the tide gauge records, the VLM corrections applied, the inter-mission measurement biases, or the altimetry data.

Results shown in Table 3.4 and Figure 3.7 indicate substantial spatial variations in SSH changes in all datasets. The altimetry dataset covering areas south of 66°N has highest rates offshore Hordaland and at Vøringplatået (west of the slope of the continental shelf off the coast of Nordland). Whereas the dataset covering the entire Norwegian coast shows largest rates offshore Lofoten and lowest rates along the coast of Finnmark and in the Barents Sea. In general, the spatial patterns of the altimetry datasets show poor agreement (Figure 3.7). We compute the coefficient of spatial correlation between tide gauges and altimetry, and between the two sets of altimetry rates. For the GIA-corrected tide gauge rates and SSH rates from TOPEX/POSEIDON, Jason-1, and Jason-2 we find r = -0.14. While for the tide gauge rates and rates from ERS-1, ERS-2, ENVISAT, and SARAL/AltiKa it is r = 0.07. Thus, the altimetry measurements cannot explain the spatial variations seen in the GIA-corrected tide gauge records and vice versa. For areas south of 66°N, the correlation between the rates estimated from our two altimetry datasets is r = -0.08.

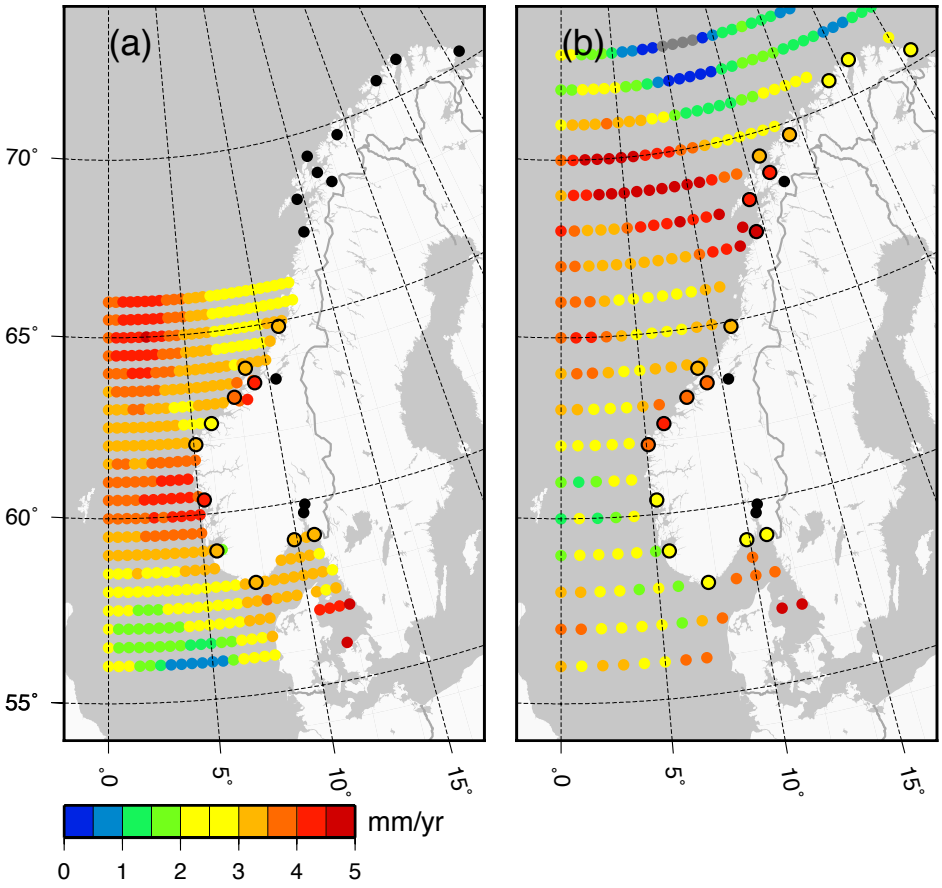

Figure 3.7 Sea surface height changes measured using satellite altimetry over the period 1993 to 2014 from (a) the TOPEX/POSEIDON, Jason-1 and Jason-2 dataset and (b) the ERS-1, ERS-2, ENVISAT, and SARAL/AltiKa dataset. For the first dataset, observations are not available above 66°N owing to the orbital inclination of the satellites. Changes in SSH were computed for individual tide gauge locations by averaging the altimetry observations within a spherical distance of 1°. The standard errors of the rates are typically 1 mm/yr. Note that the data are corrected for geoid changes associated with GIA.

Compared to the rates presented in Volkov and Pujov (2012), our sea level rate estimates differ by 0.57 to -1.42 mm/yr depending on location. The largest differences are for the northernmost stations Hammerfest, Honningsvåg, and Vardø (i.e., on the coast of Finnmark). At these stations the rates listed in Table 3.4 deviate by an average of -1.3 mm/yr when compared to Volkov and Pujov (2012). But this maybe due to the slightly different periods analysed. We note that Volkov and Pujov (2012) also present a map illustrating the pattern of SSH change including areas north of 66°N. The spatial variability shown there partly agrees with our results in Figure 3.7b, where highest rates are found west of Lofoten.

The poor correlations between the two sets of altimetry rates, the altimetry and GIA-corrected tide gauge records, and the low rates on the coast of Finnmark means we have low confidence in the ability of altimetry to monitor spatial variations in SSH changes along the Norwegian coast. At the same time, we are mindful that the altimetry satellites and tide gauges do not sample at the same locations, and are two completely different measurement concepts. It is possible that SSH changes offshore could be different to those at the coast where the tide gauges are located. Spatial variations may arise due to real oceanic signals and/or spurious spatial signals related to the altimetry measurement system. Errors in the reference frame or in

the intermission measurement biases have long spatial wavelengths or are constant. We expect, therefore, that such errors are only small contributors to the variation in the observed rates. On the other hand, errors in the corrections applied to the altimetry measurements (e.g. sea state bias corrections, tidal corrections, and corrections for atmospheric delay) may have wavelengths of shorter spatial scales.

Finally, we remark that the altimetry time series are sensitivity to the model fit to the data. For instance, omitting the 18.6 yr period in the model changed the coastal average from 3.2 to 2.6 mm/yr. This suggests that the current length of the altimetry time series is too short for assessing regional sea level changes at the millimeter per year accuracy.

3.4 Contributions to 20th Century Sea Level Change in Norway

To some extent it has been possible to quantitatively assess some of the contributions to observed sea level changes along the Norwegian coast. However, an understanding of all the physical processes is not yet complete. Two studies examining contributions to sea level change and variability at Norwegian tide gauges are Richter et al. (2012a) and Henry et al. (2012), and a global update on regional contributions can be found in Slangen et al. (2014).

The most comprehensive study of processes affecting sea level at the Norwegian tide gauges is Richter et al. (2012a). In this study, observations from 6 hydrographic stations, sea level pressure, and observed vertical land motion (Vestøl, 2006) are used to reconstruct sea level for the period 1960 to 2010. The reconstructed sea level is then compared to time series from tide gauges along the Norwegian coast providing data for the same interval. They find that the reconstruction explains 29 to 84% of the observed variability. The span in this percentage is a spatial variation as the contributions have different influence in different places (see Richter et al., 2012a; their Figure 5).

Richter et al. (2012a), Calafat et al. (2013), and Dangendorf et al. (2014) have all showed that the atmospheric pressure effect is the most important contribution to coastal sea level variability on both intra- and interannual timescales. Salinity and temperature had a slightly lesser degree of influence. For variability towards decadal timescales, the importance tends to be more equally shared among the abovementioned contributions. There is likely also a larger influence of wind driven circulation and subsequent steric changes with increasing time scales.

These results point to atmospheric influence dominating short term variability, with contributions such as the steric effects gaining importance with longer time scales. In the following we will outline the observational results regarding the contributions to long term trends.

Vertical Land Motion

Tide gauges are mounted on the land and measure relative sea level changes. Vertical land motion is clearly an important component of RSL change in Norway (a thorough assessment and description can be found in Chapter 4 and also in the above sections). Uplift rates range from 1–5 mm/yr across the Norwegian coastal municipalities (see Figure 4.6) and constitute a negative contribution to relative sea level change. The uplift pattern is essentially due to GIA;

the relaxation of the Earth in response to deglaciation and the eventual loss of the Fennoscandian ice sheet. As mentioned above, vertical land motion from GIA is considered to be a constant contribution over the timescales considered in this report, in other words a linear trend. Other potential sources of VLM are addressed in Chapter 4.

Thermosteric Signal

Richter et al. (2012a) showed that among the three contributions studied (surface air pressure, thermosteric, and halosteric sea level) the trends in Norway are strongest for the thermosteric contribution (Figure 3.8). Depending on location, the thermosteric trends are around 0.5–1.0 mm/yr for the period 1960 to 2010.

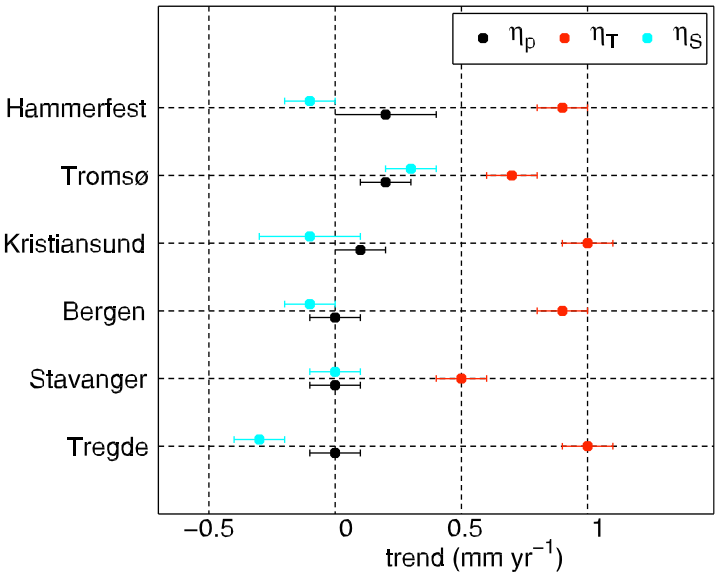

Figure 3.8 Observed trends for 1960–2010 in the surface pressure effect (in black), and the thermosteric (red) and halosteric (cyan) heights. From Richter et al. (2012a).

Halosteric Signal

The influence of freshwater on steric height trends at the coast is thought to be minimal (Henry et al. 2012; Richter et al., 2012a). Using coastal hydrographic stations, Richter et al. (2012a) found small but significant trends at Tregde (-0.3 mm/yr; Figure 3.8) and in Tromsø (0.3 mm/yr; Figure 3.8). Other evidence also points to generally small long-term halosteric sea level changes in the Arctic (Proshutinsky et al., 2004), which might not be expected as ice melt and large river runoff in that region could potentially be sources of variability in ocean salinities.

Inverted Barometer Effect

Lower surface air pressure results in higher sea level. As a rule of thumb, a 1 mbar decrease in air pressure results in a 1 cm rise in sea level. Using NCEP/NCAR monthly atmospheric surface pressure, Richter et al. (2012a) found the effect of surface air pressure trends in Norway to be negligible for the period 1960 to 2010, apart from in Tromsø (0.2 mm/yr;

Figure 3.8). This slight positive tendency towards north is supported by the observed decrease in the atmospheric pressure in the Arctic (Walsh et al., 1996). An Arctic sea level trend of 0.6 mm/yr has been attributed to air pressure changes by Proshutinsky et al. (2001; 2004), but for a shorter time period.

Wind Effects

It is hard to consistently attribute any changes in wind to sea level trends in Norway. The dominant pattern of wind variability in the northern North Atlantic and Nordic Seas (i.e., NAO) shows virtually no influence on the long-term sea level trends in Norway (Richter et al., 2012a). The pattern represents the variability of the westerlies over the North Atlantic as well as winds parallel to the Norwegian coast, and thus affects both along-slope currents and sea level on the shelf (Richter et al., 2012b; Calafat et al., 2013; Dangendorf et al., 2014). There is, however, no significant long term trend in these winds. But it should be noted that they correlate with the coastal sea level signal (the residual after removing the above mentioned effects) on monthly to decadal time scales (Richter et al., 2012a; Calafat et al., 2013; Dangendorf et al., 2014), and has a corresponding trend over the '70s and '80s. This means that changes in wind variability may give rise to decadal-scale sea level changes.

Mass Exchange between Land and Ocean

Global land ice melt (i.e., ice sheets and glaciers) is a large contributor to the global sea level rise, and its regional imprint during the previous decades may be estimated from melt rates. An estimate for a mass contribution to Norwegian sea level trends of 0.7 ± 0.2 mm/yr for 1972–2008 was made by Richter et al. (2012a) using melt rates from Church et al. (2011) and gravitational fingerprints from Mitrovica et al (2001). For the slightly earlier period 1961 to 2003, Slangen et al. (2014) estimate the regional signal from all mass input to the oceans, including ground water and dams, to be approximately 0.5–0.8 mm/yr.

Changes in the amount of liquid water stored on land will change the input of mass to the oceans. The patterns and amounts of precipitation and evaporation over ocean and land, are possible sources of such changes, but expected to be a minor contribution to long-term trends. There has, however, been some attention to changes in building of dams and changes in groundwater. Slangen et al. (2014) sums up these contributions from literature and find that globally for 1961–2003 the impoundment of water behind dams was larger than the groundwater depletion, giving a net decrease in the input to the oceans from liquid water sources. In the same way as changes in land ice masses, regional changes in liquid water storage on land change the gravitational field. For our region it is found that the liquid water changes combined with their gravitational response, gives a near-zero contribution for these four decades (Slangen et al., 2014).

For the more recent period, since 2003, GRACE provides the possibility to estimate mass changes from satellites. Riva et al. (2010) estimated the contribution to sea level in our region from land ice melt to be 0.6 ± 0.2 mm/yr during 2003–2009. The total mass exchange related regional trends, i.e., including the effect of retention of liquid water on land and the corresponding gravity effects, was estimated to 0.8 ± 0.4 mm/yr.

Ocean Mass Redistribution and Dynamics

Mass redistribution within the ocean may also add to the sea level at the coast (see Section 5.1.2). Henry et al. (2012) found a regional ocean mass trend of 2.9 ± 0.7 mm/yr for 2003–2009, which is larger than the global average ocean mass increase over the same time span, thus indicating that ocean circulation driven mass redistribution provides additional mass to our coast. Recent works suggest that the mass signal along the Norwegian coast is dynamically connected (via longshore wind forcing and coastally trapped Kelvin waves) to the sea level along the continental slope down to the Canary Islands (Calafat et al., 2013; Dangendorf et al., 2014; Hughes et al., 2015).

Richter et al. (2012a) point to the warming and freshening of the deep Nordic Seas since 1980 (Østerhus and Gammelsrød, 1999) and that steric expansion from this showed a trend of 1.3 ± 0.1 mm/yr during 1980–2006. How that quantity translates to the continental shelves and our coasts is a question of unknown baroclinic adjustments and dynamics, but it can be expected to constitute a significant contribution to coastal sea level. Fukumori et al. (2015) further point to a near uniform mass signal in the Arctic and Nordic Seas, which is, however, decoupled from the coastal regions along Norway.

Gravity Changes from Vertical Land Motion

Vertical land motion, in particular GIA, affects the Earth's gravity field (the geoid) and is therefore also a process that can perturb the ocean surface. The contributions to observed rates are thoroughly treated in Section 3.2, and mechanisms are described in more detail in Chapter 4. The geoid changes associated with GIA in our regions are modelled to be ~0.2–0.5 mm/yr (see Figure 4.5). This effect is a physical contribution to sea level rise. It is a result of land uplift, but takes no part in VLM estimates and calculations between RSL and SSH (Figure 1.2).

3.5 Chapter Summary

The relative sea level rates for the periods 1960 to 2010 and 1984 to 2014 estimated from the Norwegian tide gauge network reflect the pattern of land uplift. A fall in relative sea level is observed in Oslofjorden and in the middle of Norway, while a rise is observed along the southern and western coast of Norway and for the northernmost tide gauges. After correcting the rates for glacial isostatic adjustment (GIA), the resulting sea surface height rates are positive at all tide gauges. The coastal average is 1.9 and 2.4 mm, respectively, for the first and latter period. These are close to the global average rates for the 20th century, which also showed an increase towards the end of the century. It should be noticed that the GIA-corrected rates for an unknown reason vary considerably between the sites. However, the vertical motion of the tide gauges are in general weakly constrained.

Over the more recent period 1993–2014, the average rate of coastal sea level rise south of 66°N is estimated from two satellite altimetry datasets as 3.4 ± 0.7 mm/yr (TOPEX/POSEIDON, Jason) and as 3.1 ± 0.7 mm/yr (ERS, ENVISAT). And these numbers agree well with the rate obtained from the tide gauge network (3.8 ± 0.6 mm/yr). The rate of sea surface rise along the Norwegian coast is significantly higher for the period 1993–2014

than for the period 1960–2010. It is unclear, however, to what extent this higher rate represents natural variability rather than a sustained increase owing to global warming.

There are not enough observations available to assess all contributions to the sea level trends at the Norwegian coast. The observed changes point to warming ocean and melting land ice to be the most prominent contributors to observed sea level trends for the Norwegian coastline, as they are for the global mean. For the period 1960 to 2010, hydrographic observations show that thermal expansion contributed between 0.5 and 1 mm/yr to the trends in sea surface height while the contributions from measured change in salinity and atmospheric pressure are less than ± 0.5 mm/yr. Estimates of the regional contribution from mass input to the ocean vary between 0.5 and 0.9 mm/yr over similar periods.

The observed regional sea level trends can provide some guidance on what to expect in the near future. However, it is important to be aware that the estimated RSL rates are extremely sensitive to the selected study period, which is indicative of strong interannual to multi-decadal variability in the tide gauge records. Any extrapolation should therefore be done with caution.

4 Present-day Vertical Land Motion in Norway

There is a long history of glacial isostatic adjustment (GIA) research in Fennoscandia (Ekman, 1991). A wide variety of observations are available to us for the study of GIA, for example, paleo sea level, tide gauge, levelling and terrestrial gravity measurements. And now over the past two decades, the satellite based observation systems of GPS and the Gravity Recovery and Climate Experiment (GRACE) have provided new insights into the process of GIA (see Steffen and Wu, 2011, for a review of all the datasets).

Such observations of GIA in Fennoscandia have traditionally been used to infer details of Earth's viscosity structure and/or the region's ice history (e.g., Lambeck et al. 1998; Milne et al. 2001; 2004; Steffen and Kaufmann 2005). They also inform us on vertical land motion - an important component of present-day RSL change for Norway. The development of GPS, in particular, has enabled us to image crustal deformation to a high degree of precision. These observations show that present-day VLM across Fennoscandia is dominated by the ongoing relaxation of the Earth in response to past ice mass loss (e.g., Milne et al. 2001). While the broad pattern of land motion in Norway reflects GIA, there are a number of other physical processes which can also cause vertical movements or coastline changes. For example, tectonics, elastic loading effects, sediment deposition or compaction, erosion, or groundwater storage changes. Generally speaking these processes are thought to be small in Norway but they can be significant in some areas and especially on local scales.

In this chapter we make use of new GPS observations and GIA modeling work (Kierulf et al. 2014) as well as updated precise levelling measurements (Vestøl, 2006). We focus on the vertical component of motion as it is this, rather than horizontal movements, which is most useful for estimating present and future sea level changes. The new results are employed to determine vertical land motion, with corresponding uncertainties, for the coastal municipalities. We also show gravitational effects on sea level associated with GIA. Our findings are compared to the GIA solution applied in AR5, which is based on a combination of the ICE-5G (Peltier 2004) and ANU models (Lambeck et al. 1998 and subsequent improvements).

4.1 Permanent GPS and Levelling Networks and Analysis

The establishment of permanent GPS networks in the Nordic countries (Norway, Sweden, Finland, and Denmark) began in the early 1990s. A dense network exists in the region today, which is used for both geodynamic and geophysical studies (see Figure 4.1). Many GIA-related GPS investigations have been completed under the Baseline Inferences for Fennoscandian Rebound Observations, Sea level, and Tectonics (BIFROST) project (Scherneck et al. 1998). Crustal deformation rates from the BIFROST network have been published regularly (Scherneck et al. 1998; Milne et al. 2001; Johansson et al. 2002; Lidberg et al. 2007, 2010), largely incorporating Swedish and Finnish stations and also some Norwegian and North European stations.

The Norwegian GPS network is currently comprised of 160 permanent stations. As the network has been gradually built up over a number of years, some GPS sites have longer time series than others. This has implications for the reliability of the crustal velocities estimated from GPS observations in different parts of the network. In the first analysis of the entire Norwegian network, Kierulf et al. (2012) examined the relationship between time series length and the accuracy of the velocity estimates. The authors suggested that only vertical velocities estimated from more than 3 years of data can be considered reliable. Using this 3-year cutoff and data up until the beginning of 2011, Kierulf et al. (2012) were able to determine vertical velocities for 65 (~40%) of the 160 GPS stations in the network. In the more recent study of Kierulf et al. (2014), where they use data up until the beginning of 2013 (i.e., 2 more years of data), the authors were able to determine vertical velocities estimates for 92 (~60%) of the 160 GPS stations in the network. Thus, velocities presented in Kierulf et al. (2014) have a better spatial coverage than before and, owing to longer time series, improved accuracies.

In addition to the GPS stations which observe crustal motion in a geodetic reference frame, we also make use of repeated precise levelling data which provide a measure of relative land movements. The levelling data help us to better constrain VLM and are of particular use in areas between the GPS stations. The Norwegian levelling data have been collected over several campaigns and date from 1916 to present. Levelling lines in Norway, including the number of times they have been measured, are shown in Figure 4.1c.

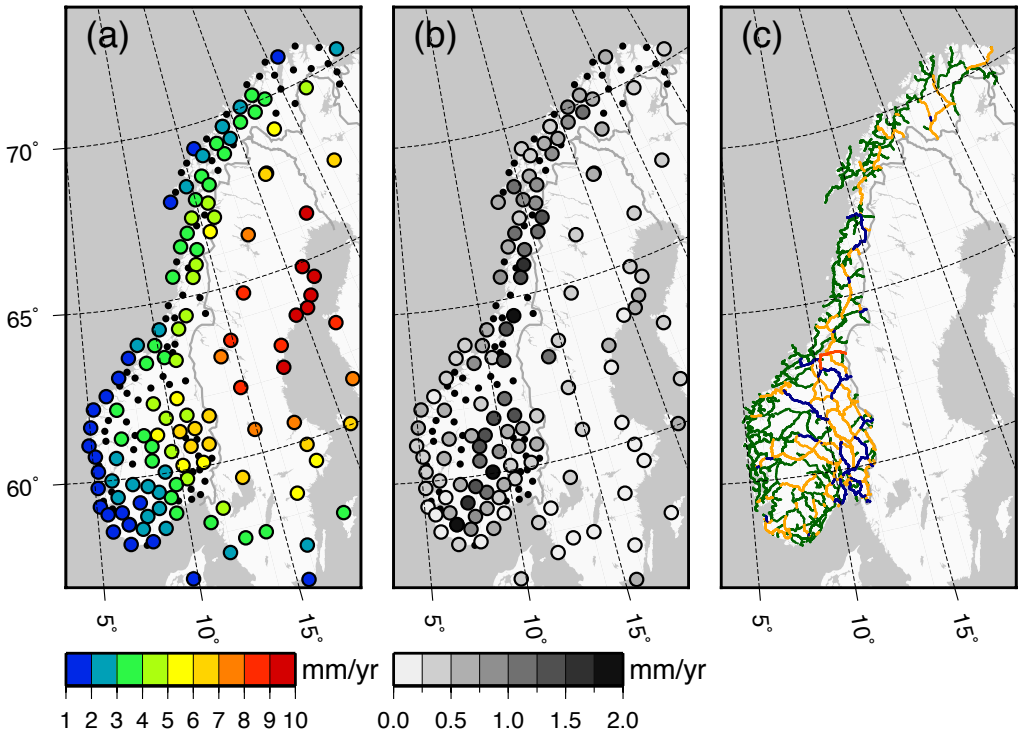

Figure 4.1 (a) Observed vertical land motion from the GPS measurements. Black dots mark stations with less than 3 years of data; these observations are not included in this study as they are considered unreliable. (b) Uncertainty on the observations (standard error) and (c) The levelling lines used. Red lines have been measured four times, orange lines three times, blue lines two times and green lines once. Levelling data from outside of Norway are included in our least-squares collocation solution but are not shown here.

4.1.1 GPS Analysis-Strategy and Determining Vertical Velocities

In their analysis Kierulf et al. (2014) employ the GAMIT/GLOBK software (Herring et al. 2011) to derive daily solutions for GPS stations across the Nordic countries. This software makes use of the so called double difference approach in which a network of GPS stations are analyzed in a single adjustment. The velocities presented here are realized in the ITRF2008 reference frame (Altamimi et al. 2011). Note that a recent review concluded that the ITRF is stable along each axis to better than 0.5 mm/yr and has a scale error of less 0.3 mm/yr (Collilieux et al. 2014). The time series analysis was performed using CATS (Williams 2008), using a combination of white noise and flicker noise. Annual and semi-annual signals are included as additional parameters in determining the vertical velocity estimates. For more information on the analysis strategy, see Kierulf et al. (2014). Note that 4 GPS stations, Tregde, Tjøme, Moldjord and Mysen, are removed from further analysis in this report as inspection of the data suggests they may be unstable.

4.2 Defining a Vertical Velocity Field for Norway

The GPS observations indicate that vertical land motion over Norway varies between 1 and 7 mm/yr. Coastal locations generally have uplift rates lower than 5 mm/yr (Figure 4.1a). The average minimum distance between the 92 Norwegian GPS stations for which we have velocities is 57 km. Thus, we consider the spatial coverage of the observations to be good, but there are coastal areas in the middle and north of Norway where we currently lack crustal velocity estimates. Note that the average minimum distance between the GPS stations and the coastal municipalities is 26 km (but can be as large as 90 km).

Figure 4.1b shows the standard errors on the observations. The GPS stations in coastal areas in the middle of Norway have higher uncertainties than elsewhere. These stations have generally shorter time series and consequently larger uncertainties. The average uncertainty on the 92 velocity estimates in Norway is ± 0.75 mm/yr (SE). In the following sections we define a vertical crustal velocity field, with corresponding uncertainties, by (1) using results from GIA modelling and (2) applying least-squares collocation to the levelling and GPS observations.

4.2.1 Glacial Isostatic Adjustment Modeling

A GIA model is generally composed of three components: a model of grounded past ice evolution (for Fennoscandia and other ice covered areas), a sea level model to compute the redistribution of ocean mass for a given ice and Earth model, and an Earth model to compute the solid Earth deformation associated with the ice-ocean loading history. Note that the sea level model is based on the ‘sea level equation’ (Farrell and Clark 1976) and includes subsequent improvements to allow for coastline migration and changes in Earth rotation (Milne and Mitrovica, 1998; Kendall et al. 2006). The GIA models are used to compute predictions of vertical land motion which are compared to the GPS observations.

In their analysis, Kierulf et al. (2014) test two different types of GIA models (finite element and normal mode) together with three different global ice models. We do not go into the

details of the analysis of Kierulf et al. (2014) but instead show results from the GIA model which they determine provides best fit to the GPS observations.

The Earth model is one-dimensional and employs the normal mode method (Wu, 1978). A Maxwell viscoelastic rheology is used and the Earth model is spherically symmetric, self-gravitating and compressible. The elastic and density structure are taken from seismic constraints (Dziewonski and Anderson, 1981) and depth parameterized with a resolution of 15–25 km. The radial viscosity structure is depth parameterized more crudely into three layers: an elastic lithosphere (i.e., very high viscosity values are assigned), an isoviscous upper mantle bounded by the base of the lithosphere and the 670 km deep seismic discontinuity, and an isoviscous lower mantle continuing below this depth to the core mantle boundary.

The ice model is made of two parts: The Fennoscandian and Barents Sea ice sheets are represented by the model of Lambeck et al. (1998), which has been shown to provide good fit to paleo sea level data from the region. For other areas of the globe, they use the ICE-3G ice sheet reconstruction of Tushingham and Peltier (1991). This is the same model setup as used in former BIFROST studies (Milne et al., 2001, 2004; Lidberg et al., 2007).

Past GIA modeling studies have used both paleo sea level data (e.g., Lambeck et al. 1998; Steffen and Kaufmann, 2005) and/or GPS observations (e.g., Milne et al. 2001, 2004; Zhao et al. 2012) to help constrain Earth model parameters. These investigations have shown that it is not yet possible to uniquely constrain Earth's viscosity structure for the Fennoscandian region. Such studies, however, are able to provide a range of Earth parameter values that satisfy the various GIA observables. Based on values from former GIA studies Kierulf et al (2014) examine laterally homogeneous Earth models bracketing 60–160 km for lithospheric thickness, (0.1–40) x 10^{20} Pa s for upper mantle viscosity and (0.1–10) x 10^{22} Pa s for lower mantle viscosity.

Results from GIA Modelling

The goodness-of-fit between the GPS observations and modelled vertical crustal velocities is tested for changes in Earth model parameters. In total 1089 Earth models are tested and the best fitting Earth model is determined to have 140 km lithospheric thickness, 7 x 10^{20} Pa s for upper mantle viscosity and 4 x 10^{21} Pa s. Predicted vertical velocities generated using the best-fit GIA model (Figure 4.2a) show a familiar pattern of land motion (e.g., Milne et al., 2001). All of mainland Norway is predicted to be uplifting; rates along the Norwegian coast vary between 1 and 5 mm/yr. Visual inspection of Figure 4.2a shows that the pattern of modelled uplift is, broadly speaking, in good agreement with the observations. At 44 of the 92 Norwegian GPS stations the model fits to within 1-sigma of the observations.

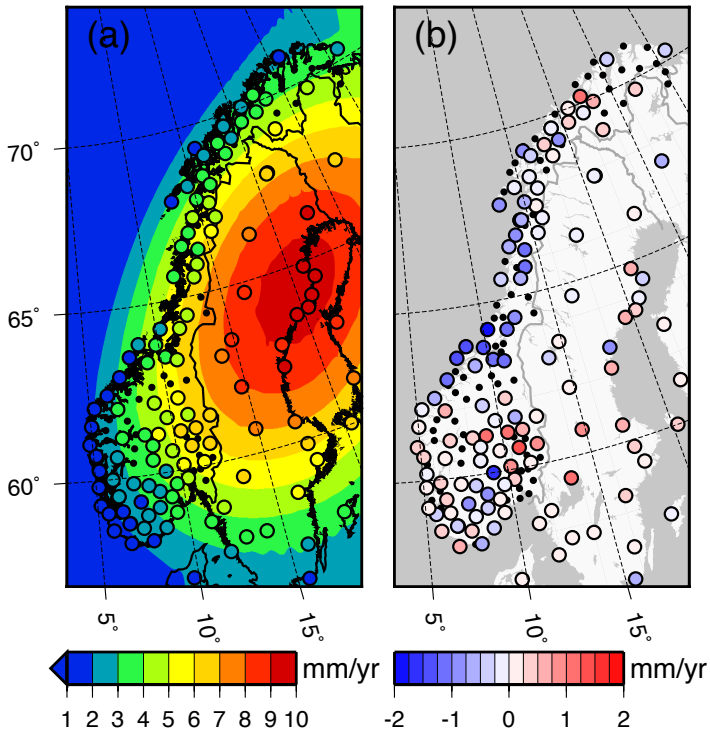

Figure 4.2 (a) Modelled vertical land motion from the best fit GIA model. The vertical velocities from the GPS observations are shown as circles (b) Residuals (observed minus modelled).

Selecting a subset of 10 stations where we have long time series and are confident in the velocity estimates, we find the RMS error between the model and GPS measurements is 0.9 mm/yr (this test is useful for a comparison later on). Residuals between the best-fit GIA model and GPS data show that the model tends to overpredict rates of uplift in the middle of Norway, around 64°N (Figure 4.2b).

In order to incorporate the GIA results within our regional sea level projections it is necessary to define a mean GIA field along with lower and upper 90% uncertainty bounds. For modelled GIA we opt to define the mean and uncertainty bounds as follows. Of the 1089 Earth models tested in the analysis of Kierulf et al. (2014) a subset of 61 are identified as having comparably good fit to the observations and classified as the best-fit models (at the one standard deviation confidence level). Using this subset of 61 models, we calculate the mean and 90% uncertainty bounds from the spread in the vertical crustal velocity field predictions (Figure 4.3). In this manner we obtain a model uncertainty which is tightly constrained to the GPS observations. This approach is preferable to simply using the full range of 1089 Earth models tested as the vertical velocity predictions are highly sensitive to the assumed Earth structure. It is important to note that the GIA uncertainty presented here only accounts for changes in Earth model parameters (i.e., it ignores possible errors in the assumed ice loading history).

In Figure 4.4 we show modelled GIA, as shown in Figure 4.3, but for the coastal municipalities. Note that the average GIA model uncertainty for the coastal municipalities is ± 0.2 mm/yr (SE).

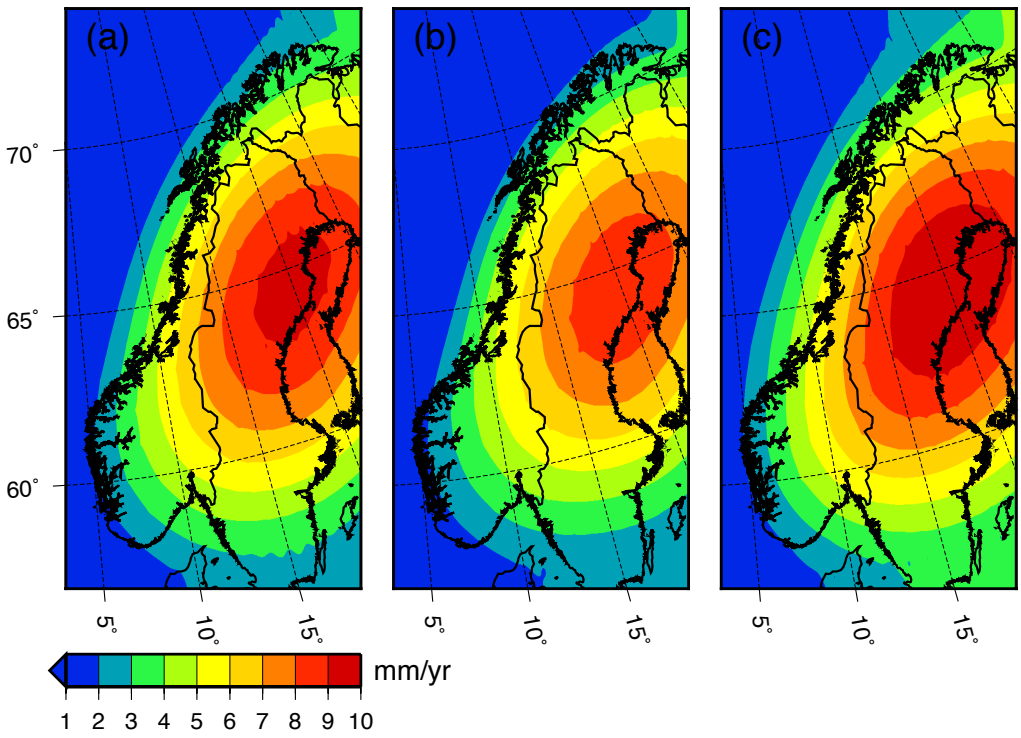

Figure 4.3 Modelled vertical land motion (mm/yr) for (a) mean (b) lower 90% uncertainty bound (p=0.05) and (c) upper 90% uncertainty bound (p=0.95).

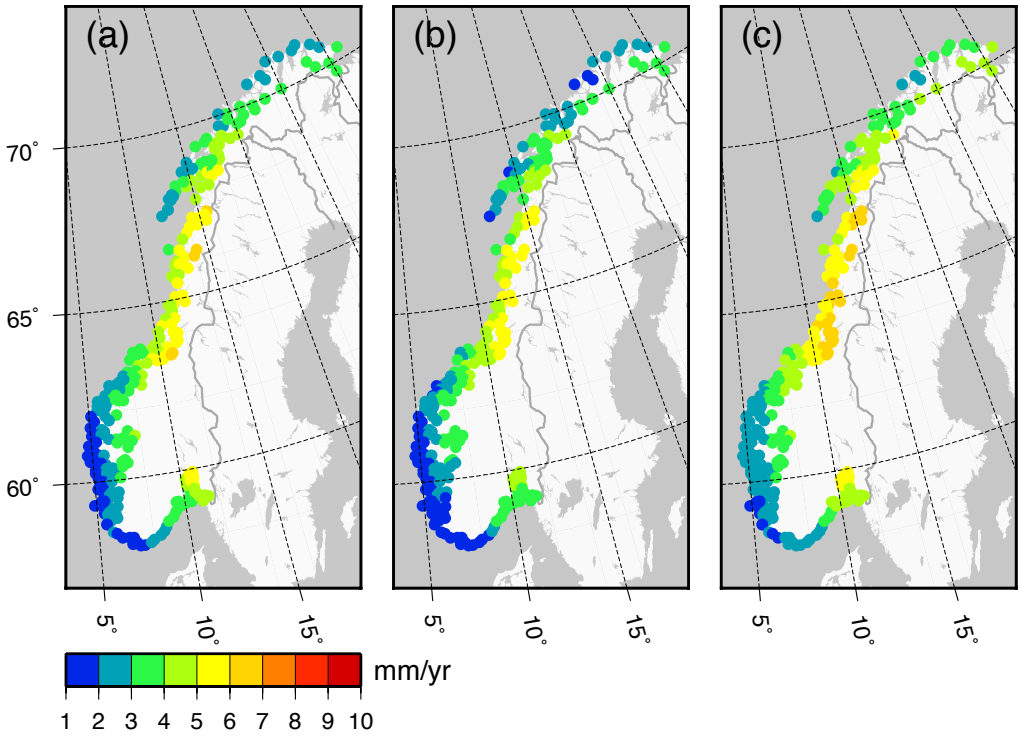

Figure 4.4 Modelled vertical land motion (mm/yr) for the municipalities for (a) mean (b) lower 90% uncertainty bound (p=0.05) and (c) upper 90% uncertainty bound (p=0.95).

Gravitational Effects on Sea Level Associated With GIA

We also take into account gravitational effects on sea level associated with GIA. These changes in the gravity field are largely driven by the movement of mantle material from the forebulge areas peripheral to Fennoscandia back towards the center as the region uplifts. The movement of mantle mass acts to increase gravitational attraction which, in turn, causes sea surface heights to increase. Such gravitational changes in Fennoscandia have been observed using both satellite gravity data from GRACE and ground-based gravity measurements (e.g., Steffen et al. 2009). Ocean surface height changes are typically between 5 and 10% of the vertical land motion signal (Tamisiea and Mitrovica, 2011) so this is a relatively small effect. Previous work has shown, based on empirical derivation, that where the vertical rates are around 10 mm/yr at the center of uplift in Fennoscandia the corresponding geoid change is 0.6 mm/yr (i.e., the sea surface change is ~6% of the land uplift signal) (Ekman and Mäkinen 1996, Vestøl 2006).

We calculate the mean field and 90% uncertainty bounds for ocean surface height changes associated with GIA (Figure 4.5). This is done with same subset of 61 Earth models used to calculate the mean and 90% uncertainty for the vertical land motion rates as above. For the mean field, modelled ocean surface changes associated with GIA vary between 0.2 and 0.5 mm/yr along the Norwegian coast (Figure 4.5a).

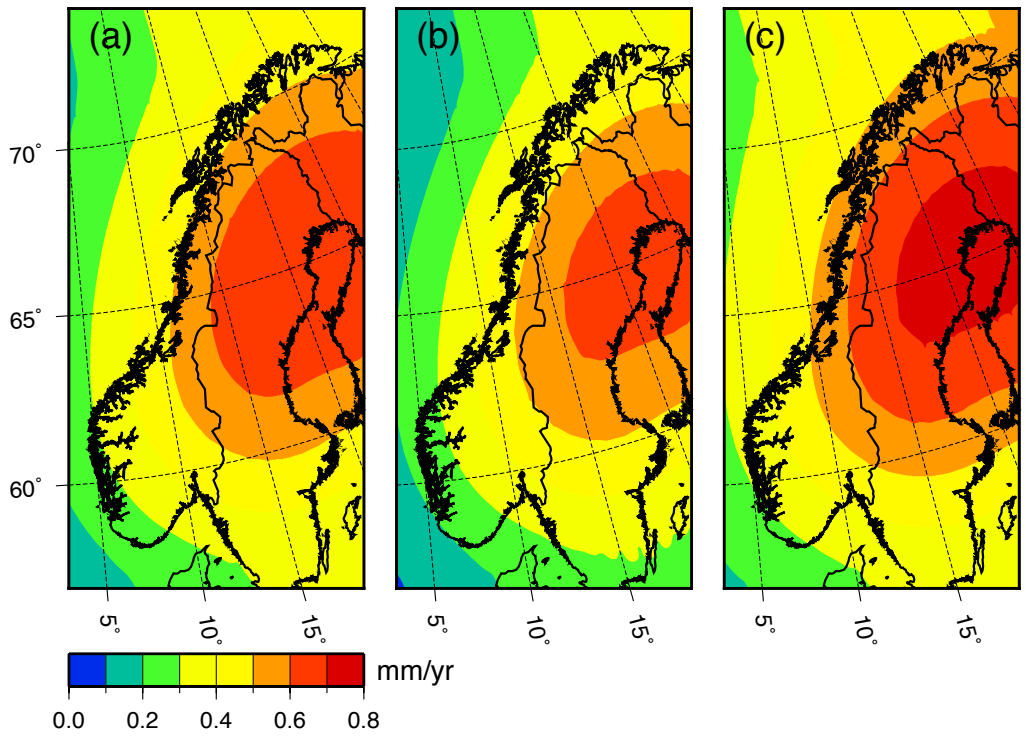

Figure 4.5 Modelled geoid changes (mm/yr) for (a) mean (b) lower 90% uncertainty bound (p=0.05) and (c) upper 90% uncertainty bound (p=0.95).

4.2.2 Least-squares Collocation

In our second approach, we base our calculation purely on geodetic observations and use a method of least-squares collocation to combine the levelling and GPS observations and determine VLM in Norway (for details on the methodology see Vestøl (2006)). Our mean VLM solution is shown in Figure 4.6a. The pattern of uplift based purely on the combined observations is broadly similar to our GIA model. And if we compare the solution to the GPS data, we find that at most coastal locations the residuals are less than ± 0.2 mm/yr (Figure 4.6b).

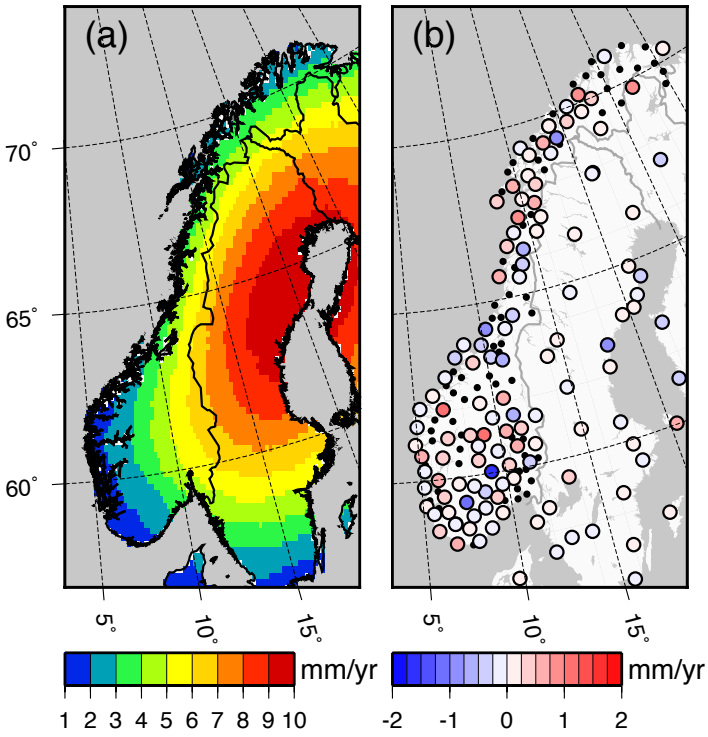

Figure 4.6 Vertical land motion (mm/yr) determined from least-squares collocation of the levelling and GPS observations for (a) our mean solution and (b) the residuals (GPS observations - mean solution).

In a test of the least-squares collocation method, we recalculate the VLM solution but omit a subset of 10 GPS stations where we have long time series and are confident in the velocity estimates (the same test as performed for the GIA model and using the same 10 GPS stations). For these 10 Norwegian stations, the RMS error between the recalculated VLM solution at the GPS observations is 0.3 mm/yr. This is an encouraging result and gives us confidence in the solution where observations are few or lacking.

From our least-squares collocation solution we calculate the mean field and 90% uncertainty bounds for the coastal municipalities (Figure 4.7). The average uncertainty for the municipalities is ± 0.2 mm/yr (SE).

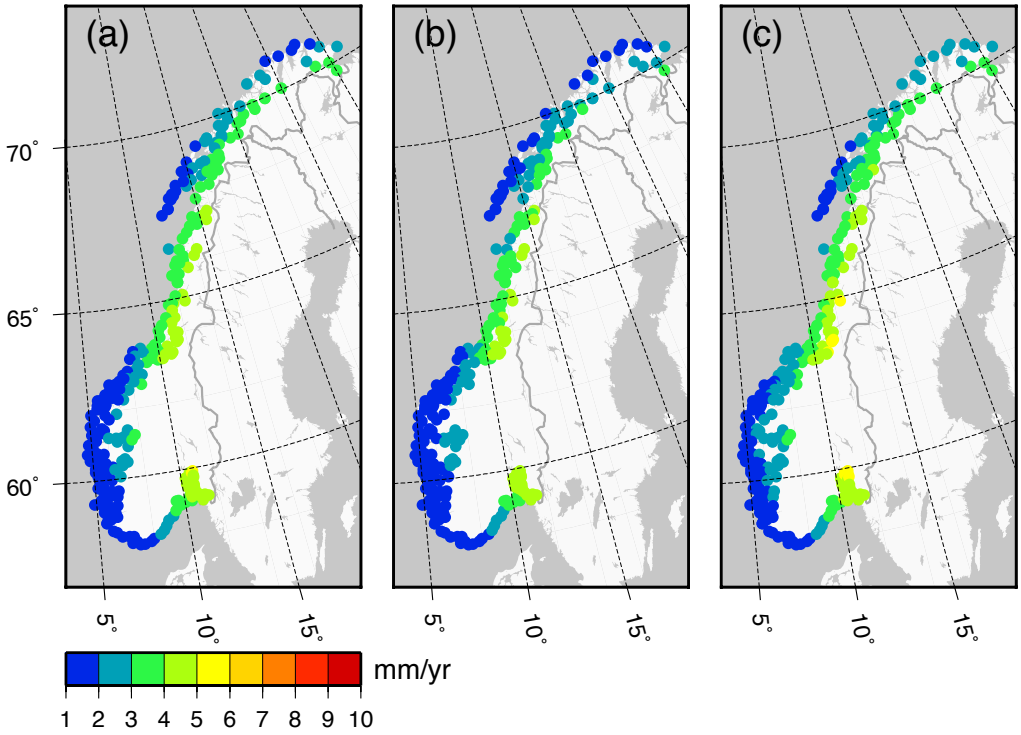

Figure 4.7 Vertical land motion (mm/yr) solution determined from least-squares collocation of the levelling and GPS observations and interpolated to the municipalities for (a) mean (b) lower 90% uncertainty bound (p=0.05) and (c) upper 90% uncertainty bound (p=0.95).

4.3 Discussion

We have shown two different approaches to predicting VLM for the coastal municipalities; (1) a GIA model that is calibrated to the GPS observations and (2) compute land motion by combining the levelling and GPS observations through least-squares collocation. It is of clear interest to determine which method best describes land motion for coastal Norway and, therefore, which is preferable when calculating future sea level changes. In a simple test, we calculated the RMS error between the two different solutions and 10 Norwegian GPS stations where we have long time series and are confident in the velocity estimates (see also above). Table 4.1 shows the results of this comparison which indicates that the least-squares collocation approach performs best, i.e., the method has a better accuracy in predicting VLM in areas where we do not have observations. Other advanced statistical techniques, for example kriging, may improve the interpolated solution and should be examined in future work.

Table 4.1 RMS error between the two different solutions and 10 Norwegian GPS observations.

	Observations – least-squares collocation	**Observations – GIA model**
RMS error (mm/yr)	0.3	0.9

Table 4.2 shows the average uncertainty for the two approaches which we find to be the same. As a consequence of the method and additional constraint of the levelling data, the average uncertainty on the least-squares collocation solution is small (0.2 mm/yr) and somewhat less than that we could expect to obtain from the GPS stations alone (the average uncertainty on the 92 GPS velocity estimates in Norway is ± 0.75 mm/yr). We also note that the uncertainties on least-squares collocation solution show far less spatial variability than otherwise suggested by the GPS observations (Figure 4.1 and 4.7). For the GIA model, the uncertainty is tightly constrained by the GPS observations and, as discussed, only accounts for changes in Earth model parameters. Better quantifying the GIA uncertainty is a challenging task but more rigorous methods are forthcoming (e.g., Tarasov et al. 2012). Finally, it is important to recognise that neither of these uncertainty estimates account for possible systematic errors in the reference frame. We address this point below.

Table 4.2 Average uncertainty on the least-squares collocation and GIA model approaches at the coastal municipalities.

	Least-squares collocation	GIA model
Standard error (mm/yr)	0.2	0.2

We opt to use the least-squares collocation solution to define our vertical velocity field for use in the sea level projections. There are a few caveats with the approach that should be highlighted. Firstly, by using the observed vertical land motion in our sea level projections, we assume that the observed rates will persist unchanged over the 21st century. We argue that this is a reasonable assumption as GIA dominates present-day vertical land motion in Norway (e.g., Milne et al. 2001, 2004; Kierulf et al. 2012, 2014; Zhao et al. 2012) and that the viscoelastic response time of the Earth is so long we would not expect any significant changes in the uplift rates over next ~100 years. Furthermore, the generally good fit between GIA model and GPS observations shows we have a good understanding of physical process causing uplift and gives us confidence that the observations can be extrapolated in this way.

As shown in Figure 4.2b, however, there are some significant misfits between the GIA model and observations. (We also expect similar differences between the GIA model and least-squares collocation solution but this is not specifically examined here). Such residuals may be explained by (1) errors in the GIA model. For example, that the ice loading is incorrect. (2) other geophysical processes contributing to vertical land motion. Recent work by Olesen et al (2013), for example, identified neotectonic deformations of around 1 mm/yr in the north of Norway. We discuss this point in more detail below. (3) errors in the GPS and/or levelling observations. As noted above, 4 GPS stations have been removed from our final results as the data suggests they may be unstable. One advantage of using the least-squares collocation approach means that, to some extent, our solution is less sensitive to outliers. These issues should be kept in mind when interpreting the results.

4.3.1 Other Processes Contributing to VLM or Coastline Changes

While the broad pattern of land motion in Norway reflects GIA, we know there are also other physical processes causing VLM and/or coastline changes. For example, tectonics, elastic loading effects, sediment deposition or compaction, erosion, or groundwater storage changes. Aunan and Romstad (2008) indicate that the soft erosive coasts in the southwest are of particular concern. It is important to keep in mind that the permanent GPS stations provide a continuous but only very localised measure of land motion. And for both the GPS and levelling networks, it is unclear how VLM may deviate in areas between the observations. In that regard, we note that satellite radar data (InSAR) looks to be a promising technique for mapping regional surface changes. Here we briefly outline some examples of land movement and coastal changes in Norway that are not related to GIA. Such local processes are not quantified in this report but, when performing risk assessments of sea level change on buildings and other assets, an evaluation of such effects may be required.

One well known example of local subsidence is the world heritage site Bryggen in Bergen. Relative to the old wharf buildings sea level has risen more than 20 cm over the last three decades, while the RSL in Bergen (relative to the bedrock) has only been rising by ~1 mm/yr (see Table 3.1). The reason for the difference is that the buildings themselves have been sinking by 6–8 mm/yr due to new drainage systems in the area which have lowered the groundwater level and caused subsequent compaction. In Oslo the sinking foundations in the harbour area (Bjørvika) has received some attention lately. A number of buildings have been founded on fillings (up to 6 m thick; Nikolaisen, 2014) that largely consist of sawdust produced by sawmills in the 18th century. This has led to compaction, during the past 50 years the resulting subsidence is estimated to have been 3–13 mm/yr.

4.3.2 Our GIA Solution and Comparison to that of AR5

Our GIA solution is used for both the interpretation of the tide gauge observations (Chapter 3) and for our sea level projections (Chapter 5). The full GIA solution, as a contribution to RSL change, is the VLM field determined from least-squares collocation added to the geoid changes generated from the GIA model. When computing uncertainties on our GIA solution, it is important to note that we include systematic errors on the reference frame's z-drift (0.5 mm/yr) and scale error (0.3 mm/yr). Taken all together the average uncertainty on our GIA solution is 0.6 mm/yr (see also Section 3.2.2 for details).

The mean GIA field in AR5 is evaluated as the mean of the ICE-5G model (Peltier 2004) and the ANU model (Lambeck et al. 1998 and subsequent improvements). These are global ice sheet reconstructions where the loading history of the ice sheets is essentially inferred from paleo sea level observations. The one standard error of the GIA field is taken as the difference between the separate models. It is important to note the the GIA model setup used in AR5 is the same as applied in Kierulf et al. (2014) and described in the above. Their solution takes into account both vertical land motion and geoid changes associated with GIA.

In Figure 4.8 we show regional changes in relative sea level rise caused by VLM and associated geoid change, both the mean GIA field applied in AR5 and our mean GIA solution. The results are presented as contributions to projected RSL change over the period 1986–

2005 to 2081–2100. Figure 4.8c shows the departure between the solutions, areas in red indicate that our solution has a less negative contribution RSL change than the mean GIA field from AR5. Differences between the solutions range from -1 cm to 18 cm with a spread of 4 cm (one standard deviation). Our mean GIA solution gives on average 4 cm higher values than that applied in AR5; i.e., our mean GIA solution indicates on average a less negative contribution to sea level.

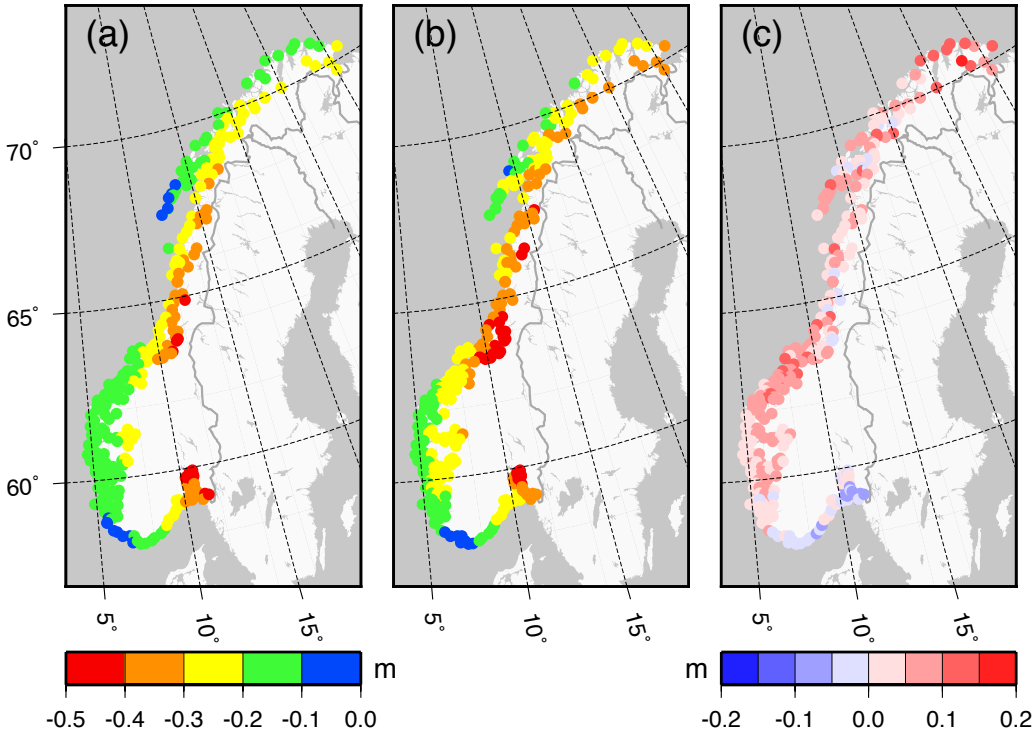

Figure 4.8 Regional relative sea level change (m) due to GIA and associated gravitational effects over the period 1986–2005 to 2081–2100 for (a) our mean GIA solution (b) AR5 mean and (c) the difference between the two solutions (a–b).

Figure 4.9 shows the difference between the future RSL contribution from our GIA solution and that used in AR5 at key locations, here we include the 90% uncertainty bounds. Note that the average uncertainty at the coastal municipalities on our GIA solution is 19 cm. Whereas, the uncertainty on the AR5 GIA field is 20 cm. Comparison of the different approaches shows that the AR5 uncertainty is smaller than ours in some locations (e.g., Oslo) and much larger in others (e.g., Tromsø). We find that the mean AR5 GIA solutions lies within our 90% uncertainty bounds for 270 of the 290 municipalities (~90%).

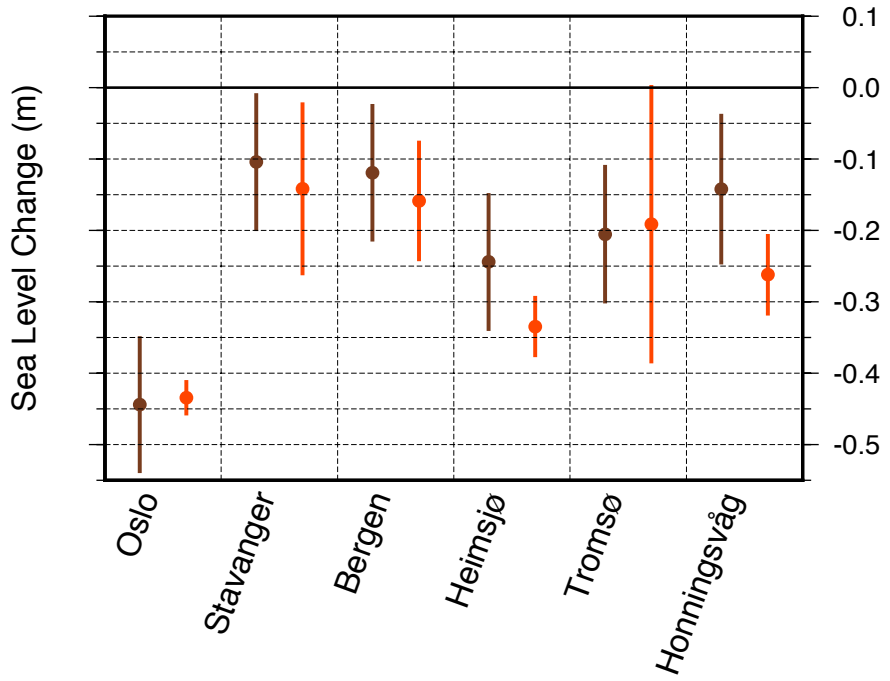

Figure 4.9 Regional relative sea level change (m) due to GIA and associated gravitational effects over the period 1986–2005 to 2081–2100 for our GIA solution (brown) and AR5 (red). Dots show mean values and vertical bars the 5 to 95% uncertainty.

4.4 Chapter Summary

Observations and modelling show that the process of glacial isostatic adjustment (GIA) dominates vertical land motion in Norway. In our analysis we make use of new GPS data, which have better spatial coverage than before, and updated levelling measurements. The observations are combined using least-squares collocation to determine land motion rates across Norway. This method performs well in areas where observations are sparse or lacking. We find uplift rates for the coastal municipalities vary between 1 and 5 mm/yr with an average uncertainty of 0.6 mm/yr (standard error and includes reference frame uncertainties)

By using the observed vertical land motion in our sea level projections, we assume that the observed rates will persist unchanged over the 21st century. The broad agreement between the GIA model and GPS observations shows we have a good understanding of the physical process causing uplift and gives us confidence that the observations can be extrapolated in this way. In order that our GIA solution can be incorporated in the sea level projections and/or used to correct the tide gauge observations, we take into account gravitational effects on sea level associated with GIA. These changes vary between 0.2 and 0.5 mm/yr along the Norwegian coast so this is a relatively small effect.

Finally, as a contribution to projected sea level over the period 1986–2005 to 2081–2100, our GIA solution appears to be broadly similar to that used in AR5. The average difference between the solutions at the coastal municipalities is 4 cm. However, we notice that the uncertainties on the solutions differ largely at some locations. We have more confidence in

our GIA solution, the values and uncertainties being essentially based upon the GPS and levelling observations.

5 Projected 21st Century Sea Level Changes for Norway

In this chapter we present regional sea level projections for Norway. Observations show that past sea level changes have been spatially variable, so we expect that future changes will also be of this nature (Milne et al. 2009). Regional sea level can be substantially different from global mean changes owing to spatial variations in (1) ocean density, ocean mass redistribution and circulation (2) mass exchange between land and ocean, and (3) vertical land motion. In addition, all three types of regional changes have associated gravitational effects on sea level. In the following, we present regional sea level projections for Norway using findings largely from AR5 and CMIP5 model output. We show results for RCP2.6, RCP4.5 and RCP8.5. The difference between our results and those shown in AR5 are that we adopt a new VLM field with corresponding gravity changes (from Chapter 4) and include an estimate of sea level changes owing to the gravitational effects of ocean mass redistribution (Richter et al. 2013).

In contrast to earlier IPCC reports, sea level projections given in AR5 are probabilistic. That is, the projections have been assigned a probability (or likelihood; see Section 2.1.3). This is now possible because our confidence in projecting sea level has increased. As detailed in Section 2.2, this is due to (1) our improved understanding of observed and modelled 20th century global sea level changes (e.g., Gregory et al., 2012) and (2) progress made with quantifying ice-dynamic contributions (e.g., Nick et al., 2013). AR5 assess that future global sea level rise is *likely* (P > 66%) to be within the range of the projections. In other words, they assess that there is up to a 17% probability that future sea level will lie above the range of the projections. Owing to insufficient and inconsistent evidence, however, the AR5 authors refrain from trying to quantify the probability of levels above the *likely* range (i.e., the upper tail of the probability distribution).

Not having information on the upper tail of the sea level projections presents a problem for their use in practical applications. Understanding of such low probability but potentially large impact future sea level changes is important for coastal management. Of particular concern is that the ice sheet contribution might have a skewed distribution, which would mean values in its upper tail would be quite large (e.g., Bamber and Aspinall, 2013). Furthermore, not having this information makes the combination of the projections with information on sea level extremes problematic. In Chapter 7, we show how this could be done using the method of Hunter (2012), but this methodology requires knowledge (or an assumption) about the upper tail of projected sea level change. For these reasons we believe that it is worthwhile exploring future sea level changes above the *likely* ranges.

5.1 Computing Regional Sea Level Projections from CMIP5 Model Output

As outlined in Section 2.1.2, AOGCMs have components representing the ocean, atmosphere, land and cryosphere. They simulate sea surface height changes relative to the geoid resulting

from natural and anthropogenic forcings. Ocean density, mass redistribution, circulation and sea level are simulated together in the AOGCMs. However, projections of the glacier and ice sheet mass contributions are currently dealt with offline. The method used to compute regional sea level projections from CMIP5 model output is dealt with in the supplementary material of AR5 (Church et al., 2013b). Here we briefly outline how the regional sea level projections are calculated along with their associated uncertainties. We pay special attention to the treatment of GIA and the gravitational effects of ocean mass redistribution, which are either treated differently or not considered in AR5.

Sea surface height data are available from the CMIP5 database. These data provide regional projections of sea surface changes owing to changes in ocean density, mass redistribution and circulation. Both the projected regional changes and the global thermal expansion time series are corrected for a control drift. Results from the individual models are interpolated to a 1 x 1 degree grid using a bilinear technique in the open ocean and a simpler nearest-neighbor interpolation close to the coast. Model time series consists of annual values. For RCP2.6 there are 16 different model runs available to contribute to the model ensemble. Whereas, for both RCP4.5 and RCP8.5 there are 21 (Table 5.1). See Table 3 in Church et al. (2013b) for details of the different models employed.

Table 5.1 Number of AOGCMs available for the model ensemble.

	RCP2.6	RCP4.5	RCP8.5
AOGCMs available	16	21	21

It is important to note that, unlike in AR5, the contribution from changes in atmospheric pressure is not considered separately here. This contribution, known as the inverse barometer effect, is instead combined with the projected ocean density, ocean mass redistribution and circulation fields from the AOGCMs. The inverse barometer effect is relatively small, it is projected to be positive in the Arctic regions, up to 1.5 cm for RCP4.5 and 2.5 cm for RCP8.5 (Yin et al. 2010). But likely less than this along most of the Norwegian coast.

The other contributions to regional sea level are GIA and ocean mass changes. (The GIA component is described in Chapter 4). Ocean mass changes are divided into the separate SMB and dynamic ice sheet components from Greenland and Antarctic, glaciers and the land water storage contribution.

It is has long been recognised that changes in the distribution of mass on the Earth's surface produces a non-uniform sea level pattern due to gravitational changes (Woodward, 1888). However, while the formalization of this theory has been established for several decades in the 'sea level equation' (Farrell and Clark 1976), it is not until recently that concerted efforts have been made to include non-uniform ocean mass changes into projections. Note that the sea level model applied in AR5 includes updates to allow for coastline migration and changes in Earth rotation (Milne and Mitrovica, 1998; Kendall et al. 2006). This sea level model is applied to the separate ocean mass contributions to compute regional sea level owing to gravitational and rotational changes.

5.1.1 Combining the Uncertainties

For the sea surface height CMIP5 model data the uncertainties are computed from the multi model ensemble spread (this is the *steric/dyn* signal given below). The ice sheet, glacier and land water storage regional uncertainties are calculated by multiplying their global uncertainties by the respective normalized 'sea level equation' patterns. The methods used to compute uncertainties associated with GIA (*obsvlm* and *geoidgia*) are given in Chapter 4. Gravitational effects on sea level due to ocean mass redistribution (*sal*) are described in the following section. To combine the uncertainties, contributions that correlate with global warming have correlated uncertainties, so they are added linearly. Other contributions are assumed to be uncorrelated and are thus added in quadrature. The regional uncertainty is found by (adapted from Church et al., 2013b):

$$\sigma_{total}^2 = \left(\sigma_{\frac{steric}{dyn}} + \sigma_{antsmb} + \sigma_{greensmb}\right)^2 + \sigma_{glaciers}^2 + \sigma_{obsvlm}^2 + \sigma_{geoidgia}^2 + \sigma_{grdwater}^2 + \sigma_{antdyn}^2 + \sigma_{greendyn}^2 + \sigma_{sal}^2 \quad (5.1)$$

steric/dyn = Global thermal expansion uncertainty and uncertainty associated with changes in ocean density, mass redistribution and circulation changes from the AOGCMs. Includes the inverse barometer effect uncertainty.

antsmb = Antarctic ice sheet SMB uncertainty.

greensmb = Greenland ice sheet SMB uncertainty.

glaciers = glacier uncertainty.

obsvlm = observed vertical land motion uncertainty. (here includes reference frame errors).

geoidgia = modelled geoid changes owing to GIA uncertainty.

grdwater = land water storage uncertainty.

antdyn = Antarctic ice sheet rapid dynamics uncertainty.

greendyn = Greenland ice sheet rapid dynamics uncertainty.

sal = self-attraction and loading uncertainty (gravitational effects of ocean mass redistribution).

Note that for each contribution σ is the standard error except for *grdwater*, *antdyn* and *greendyn*. These have uniform probability distributions in the global projections and, therefore, the half-range of their distributions was used as σ.

5.1.2 Self-attraction and Loading

Steric changes lead to dynamic changes, which includes the redistribution of mass in the ocean. This has the same consequences for the gravity field as mass exchanges with land areas (ice melt and hydrology). Thus, an increase in mass in a region of the ocean will result in attraction of additional water to that particular region.

A particular type of region is the shelf areas of the world. Having relatively shallow depths, e.g., thermal expansion results in more limited changes to the sea level than it may in the open oceans. Since large sea level differences will be evened out by water flow (dynamics), there is a redistribution of mass, from deep areas to shallow areas. In detail, the basic mechanism behind dynamical response/movement of mass is the development of horizontal pressure gradients. A net pressure gradient increase between shallow areas and deep areas can only be achieved by increasing the mass in the same depth interval as the water on the shelf, not by steric expansion of the same shallow water column alone. However, since steric changes in the deep of the oceans result in lifting of the local water column, a pressure gradient develops and mass is shifted onto the shelf areas. Since changes in heat and freshwater content in the deep oceans are usually slow, this effect is of importance when considering long term trends and climate change.

Another effect that can give mass changes on shelves, is changes in the currents that usually follow the continental shelves. Due to the dynamical balance between the Coriolis effect and the pressure gradient, any current in the northern hemisphere will have higher water to the right (on the shelf side) and the height is dependent on the speed of the flow. Variability in the speed of the current, e.g., the Norwegian Atlantic Current, contributes to variability in the sea level in the North Sea and Norwegian continental shelf and coast. This variability is a shorter term variability, but may have importance for decadal predictions.

In more broad terms, the full interplay between steric effects, changing pressure gradients, and dynamic changes, leads to mass redistribution between ocean regions. And shelf areas and coasts are in particular sensitive in this respect.

If mass has increased on a continental shelf, the gravity field will change accordingly, increasing the horizontal gravitational pull towards that region, thus attracting *additional* water. This is the same effect as discussed above, in the context of land ice melt and land hydrology. Although one may think so, the additional mass of water in the ocean region in question is not free to readjust to the 'old' gravity field. It is in a similar manner as the mass trapped on land, held in place by the pressure forces from the density field and dynamics, and instead constitute a new gravity field. This effect is called self-attraction. As with mass changes on land, the Earth's crust responds to the load of mass on it. Shelf mass loading will suppress the solid earth, leading to a slight reduction of the increase in relative sea level.

The magnitude of the resulting additional sea level rise is relatively small, but not negligible. In a study of the 21st century projections by the earth system model NorESM, the self-attraction and loading contribution along the Norwegian coast is found to range from 1–2 cm for RCP2.6–8.5 (Richter et al., 2013). Although small, the effect is of the same order of magnitude as other projected contributions to RSL change along the Norwegian coast (see, e.g., Figure 5.2). We therefore opt to include self-attraction and loading into our projections.

In climate models with realistic steric and dynamic representation, the shelf mass loading effect is part of the dynamic response. But thus far, the subsequent self-attraction and loading has to be calculated diagnostically and 'off-line' from the mass fields or indirectly from the steric/dyn fields. Self-attraction and loading is not included in the CMIP5 projections nor treated in AR5.

We base our calculations on the CMIP5 *steric/dyn* fields, thus including whichever mass redistributing effect that is resolved and present in the climate projections. Since an analysis of self-attraction and loading is not available for all the CMIP5 models separately, we choose to apply the fractional relations found by Richter et al. (2013) (Figure 5.1) to the *steric/dyn* fields.

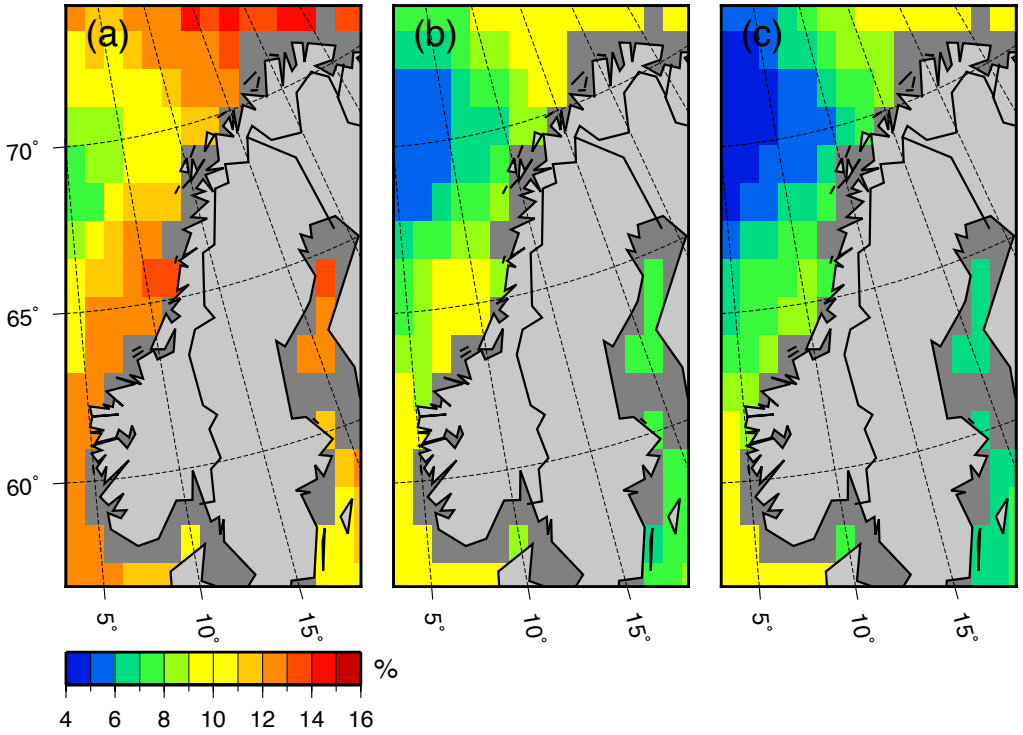

Figure 5.1 Self-attraction and loading effect as percentage of the steric/dyn component of sea level rise for the scenarios (a) RCP2.6 (b) RCP4.5 and (c) RCP8.5. Data from Richter et al. (2013).

The fractions are applied to the regionally gridded CMIP5 steric/dyn component. Note that these percentages are originally found for the projected change over the century, from 2006–2015 to 2091–2100, and thus do not provide information on time evolution. Here we assume that that the SAL effect scales linearly with the steric/dyn time series.

5.2 Analysis of Contributions to 21st Century Sea Level Changes for Norway

The separate contributions to projected sea level are shown in Figures 5.2 and 5.3 for RCP4.5. This shows that the largest projected contributions and also largest uncertainties are from rapid ice dynamics in Antarctica, the steric/dyn signal and observed vertical land motion (Figure 5.2). We note that the observed vertical land motion signal shows the largest variation between the six tide gauge sites examined, indicating that this signal will dominate the pattern of 21st century sea level changes along the Norwegian coast. The steric/dyn and glacier projections contribute to the spatial variability to a lesser extent.

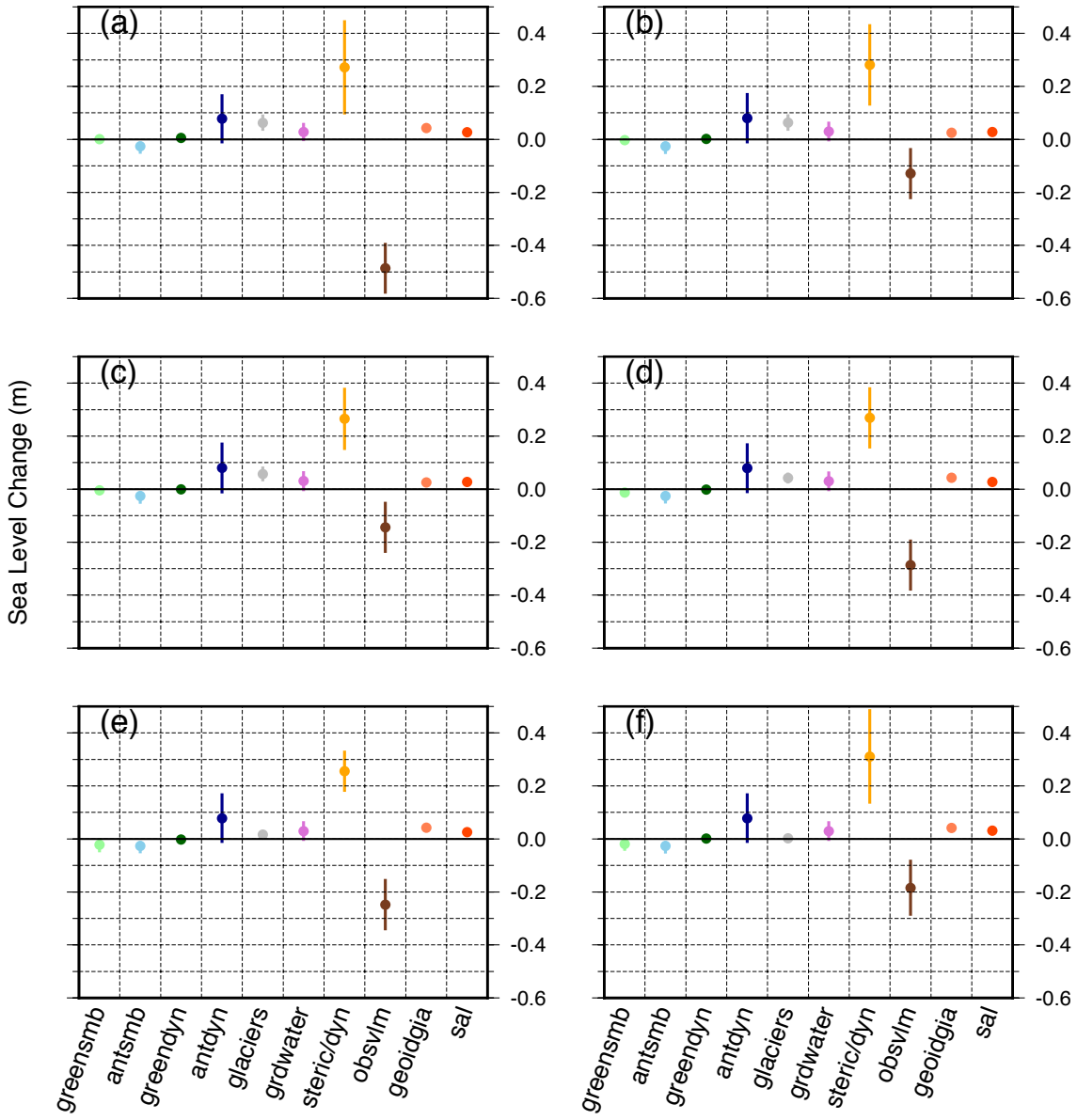

Figure 5.2 Contributions to projected relative sea level change for RCP4.5 over the period 1986–2005 to 2081–2100 for the six key locations (a) Oslo (b) Stavanger (c) Bergen (d) Heimsjø (e) Tromsø and (f) Honningsvåg. The ensemble mean and -spread (5 to 95%) are shown by the circles and vertical bars, respectively.

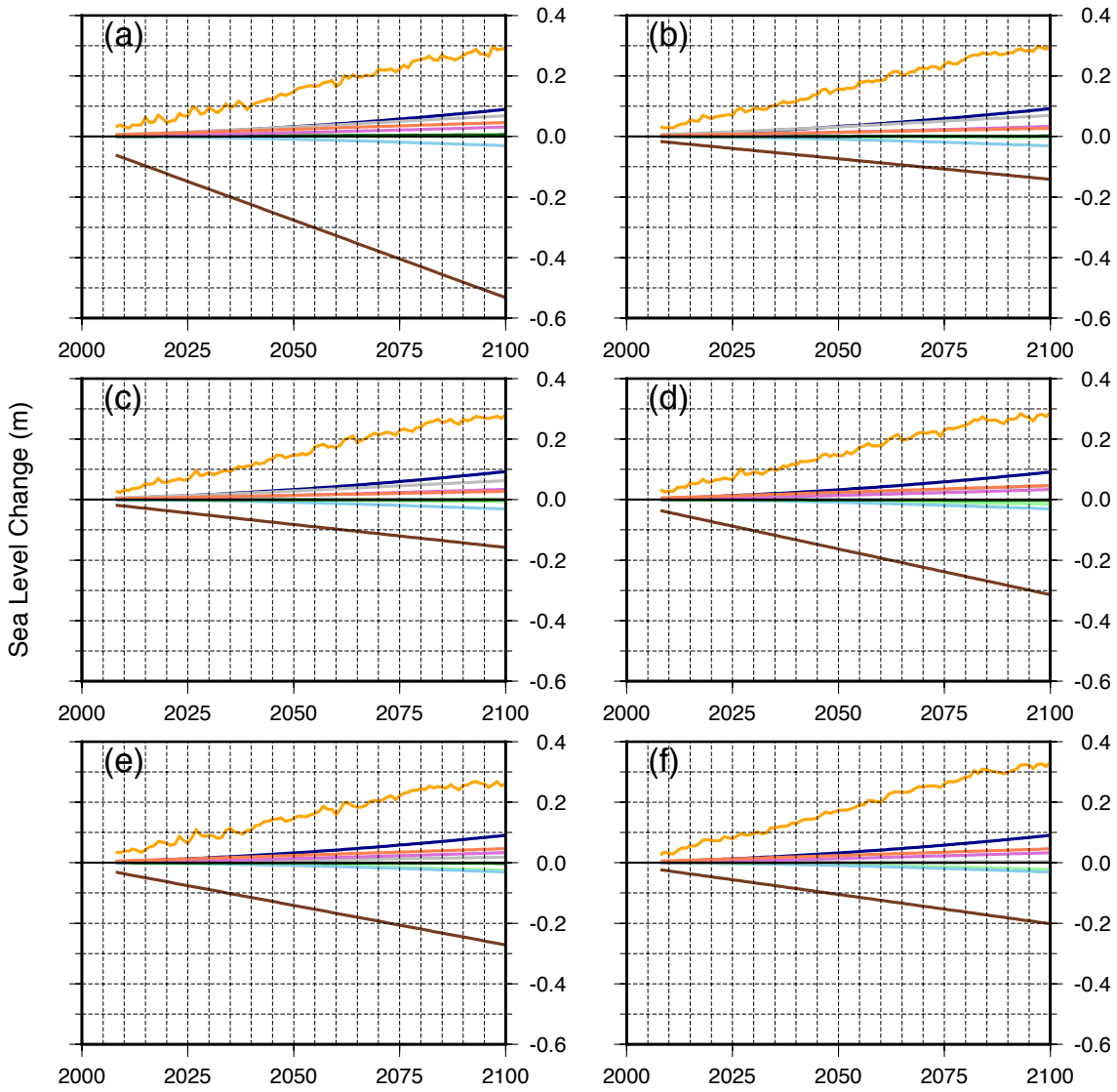

Figure 5.3 Time series for the contributions to projected ensemble mean relative sea level change for RCP4.5 for the six key locations (a) Oslo (b) Stavanger (c) Bergen (d) Heimsjø (e) Tromsø and (f) Honningsvåg. The colours for the separate contributions are the same as in Figure 5.2.

Examination of the projected time series (Figure 5.3) shows the steric/dyn signal exhibits interannual variability. This is due to changes in heat uptake and wind stress, which is simulated by the AOGCMs. The time series of contributions from glaciers and ice sheets show no variability as these are constructed using simple mathematical functions. Greenland SMB changes, for example, are based on a polynomial formula derived from modelling work which predicts mass changes from the projected temperature change (Fettweis et al., 2013).

The separate contributions can also be compared to their respective global mean contributions. We show the projected RSL change ensemble mean as a percentage of the global mean of the contribution in Figure 5.4. In the following subsections we go into more detail as to why these patterns emerge. We focus on regional sea level changes owing to (1) land ice changes and (2) steric and dynamic ocean processes.

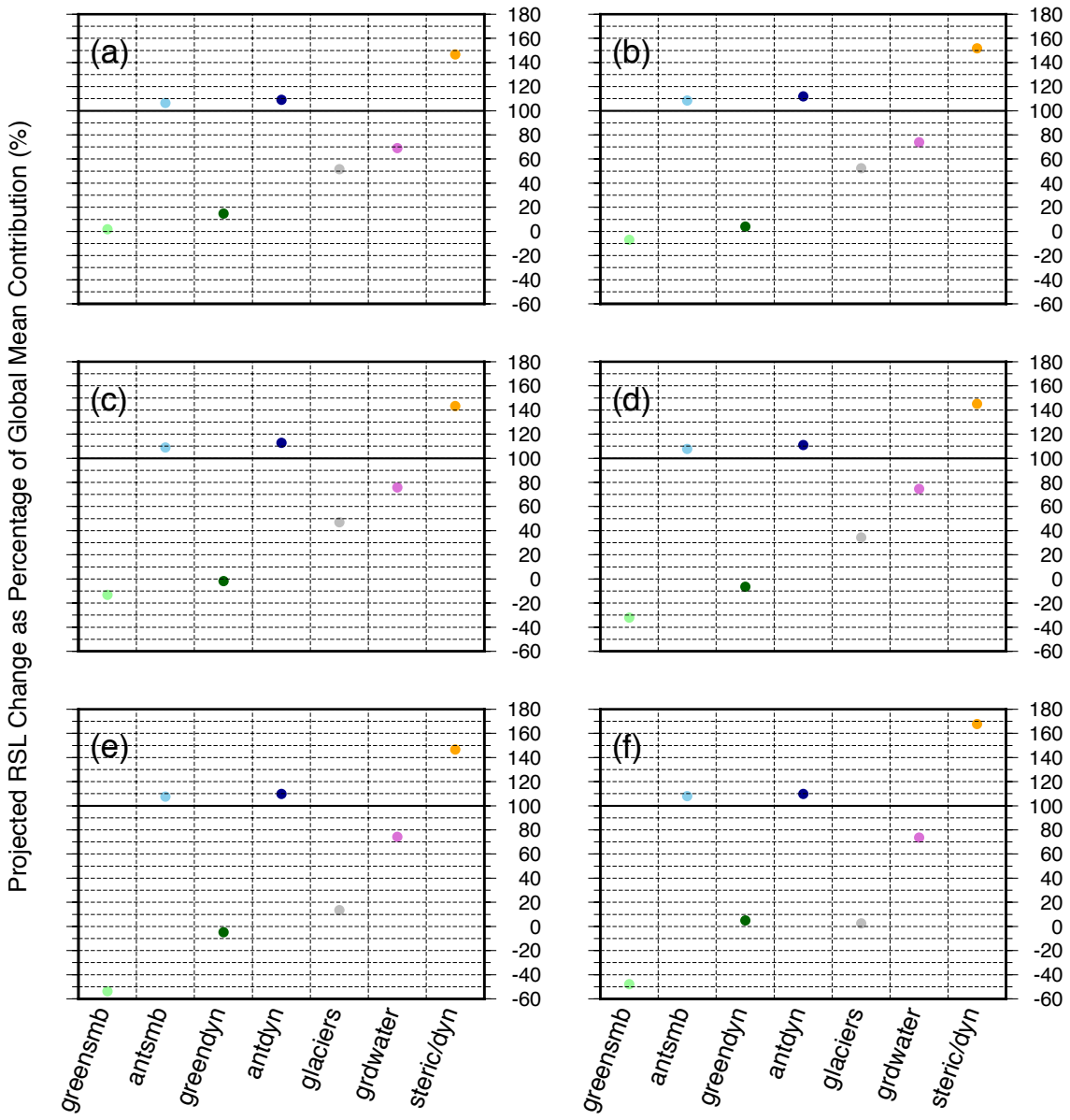

Figure 5.4 Contributions to projected relative sea level change for RCP4.5 over the period 1986–2005 to 2081–2100 for the six key locations (a) Oslo (b) Stavanger (c) Bergen (d) Heimsjø (e) Tromsø and (f) Honningsvåg. Here the projected RSL change ensemble mean is expressed as a percentage of the global mean of each contribution (100% = same as global mean).

5.2.1 Projected Regional Sea Levels Owing to Changes in Land Ice

Changes in the distribution of mass on the Earth's surface produces a non-uniform sea level pattern due to gravitational changes (Farrell and Clark 1976). This sea level response is often referred to as a 'fingerprint' as it can be used to identify the source and size of ice mass variations. As both the elastic Earth response and ocean surface perturbation scales linearly with the surface loading change, non-uniform sea level changes can be normalized by the ice mass loss (e.g., Mitrovica et al., 2001). Here we present the normalized patterns for projected changes in Greenland SMB (Figure 5.5), Antarctic SMB (Figure 5.6) and glaciers (Figure 5.7) as computed in AR5.

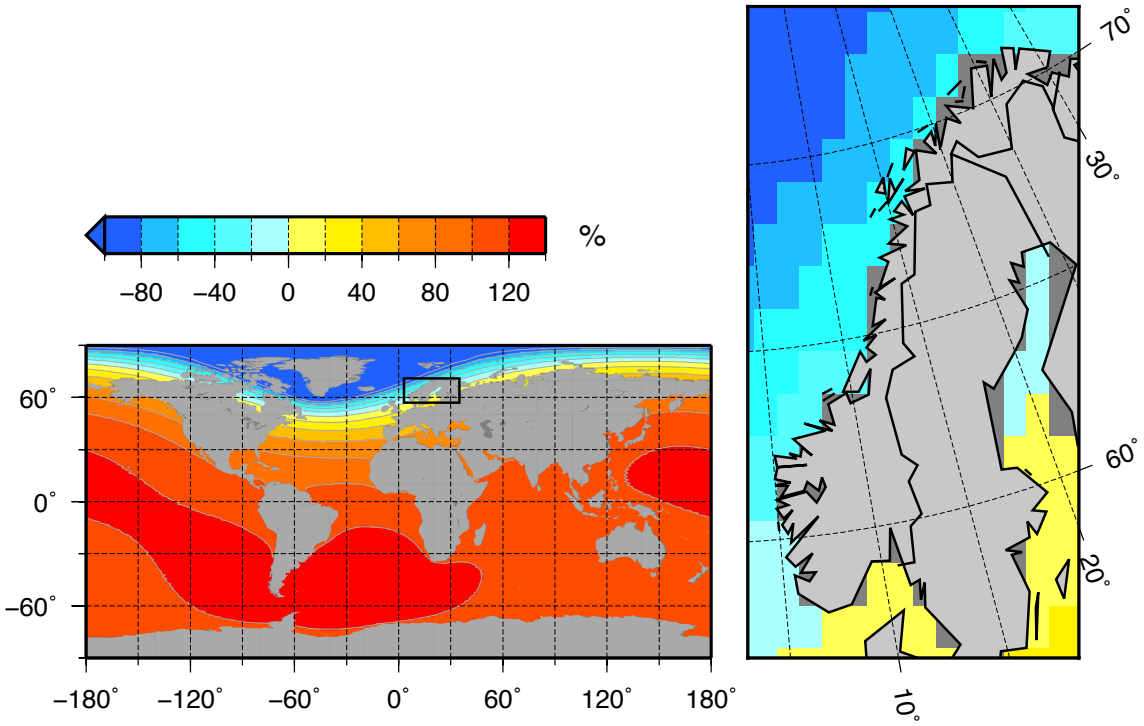

Figure 5.5 Normalized Greenland SMB regional sea level response.

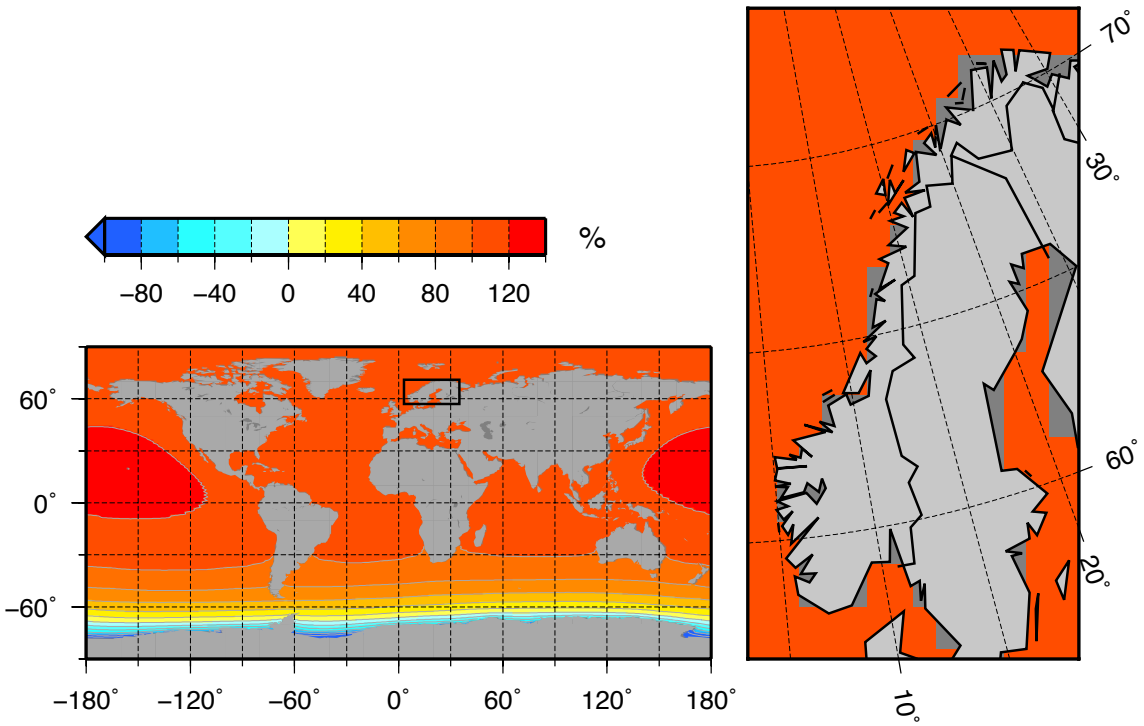

Figure 5.6 Normalized Antarctic SMB regional sea level response.

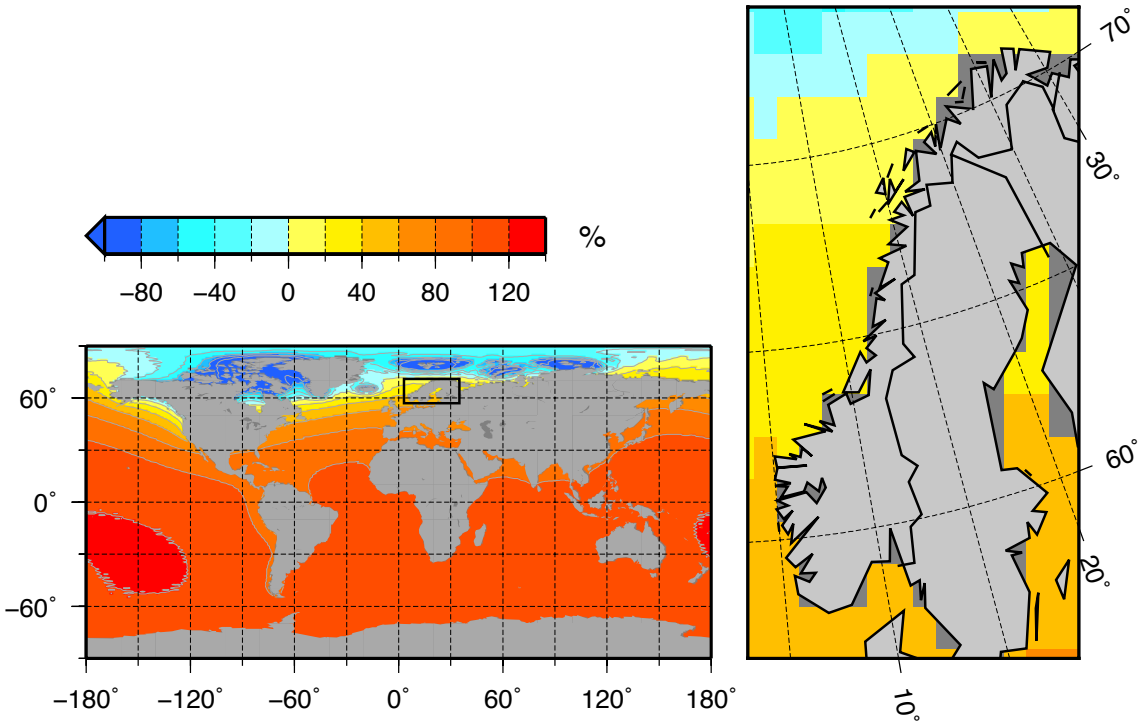

Figure 5.7 Normalized glacier regional sea level response.

As Norway sits in the near field of Greenland, the projections indicate a small or even negative sea level change along the coast (Figure 5.5). That is, they show that owing to gravitational changes, Norway is predicted to experience a sea level change between -40 and 10% of the global average sea level rise due to Greenland SMB mass loss. In AR5 it is assumed that SMB changes occur uniformly over the ice sheets. Whereas, rapid ice dynamic changes are taken to be more localised. For Greenland dynamical losses are assumed to occur roughly in the South and West (sea level response not shown here). This may be important because studies have shown that sea level around Norway is very sensitive to the pattern of Greenland ice mass change (Tamisiea and Mitrovica, 2011; Simpson et al., 2014).

On the other hand, ice mass losses in Antarctica are predicted to produce an above average sea level change for the Norway (~110% of the global average for uniform SMB changes; Figure 5.6). Note that dynamical changes are assumed to occur on the Antarctic Peninsula, Amundsen Sea Embayment, and some East Antarctic glaciers (figure of sea level response not shown). For glaciers, the sea level response is calculated for each area (e.g., Canadian Arctic), and then averaged for the model ensemble. Glacier changes lead to a strong north-south gradient (0 to 60%) along the Norwegian coast (Figure 5.7).

5.2.2 Projected Regional Sea Levels due to Steric and Ocean Dynamic Changes

Results from the AOGCMs indicate an above average steric/dyn sea level rise for Norway over the 21st century but with relatively large uncertainties attached to the projections (Figure 5.2 and 5.8). We note the results from the CMIP5 ensemble indicate that areas that are projected to have above average sea level change coincide with areas that have larger uncertainties (Yin, 2012). And that appears to be the case for Norway. Past modeling studies

have focused on identifying the contributing factors to regional differences in projected ocean density and circulation changes (e.g., Landerer et al. 2007; Katsman et al. 2008; Yin et al. 2010; Pardaens et al. 2011). These generally show that in the nearby North Atlantic positive thermosteric changes are partially compensated by a negative halosteric signal. Whereas, in the Arctic Ocean, the halosteric term is positive and dominates due to ocean freshening. Related to these steric changes is a mass redistribution term which could be important for the shallow shelf seas around Norway (see Section 5.1.2).

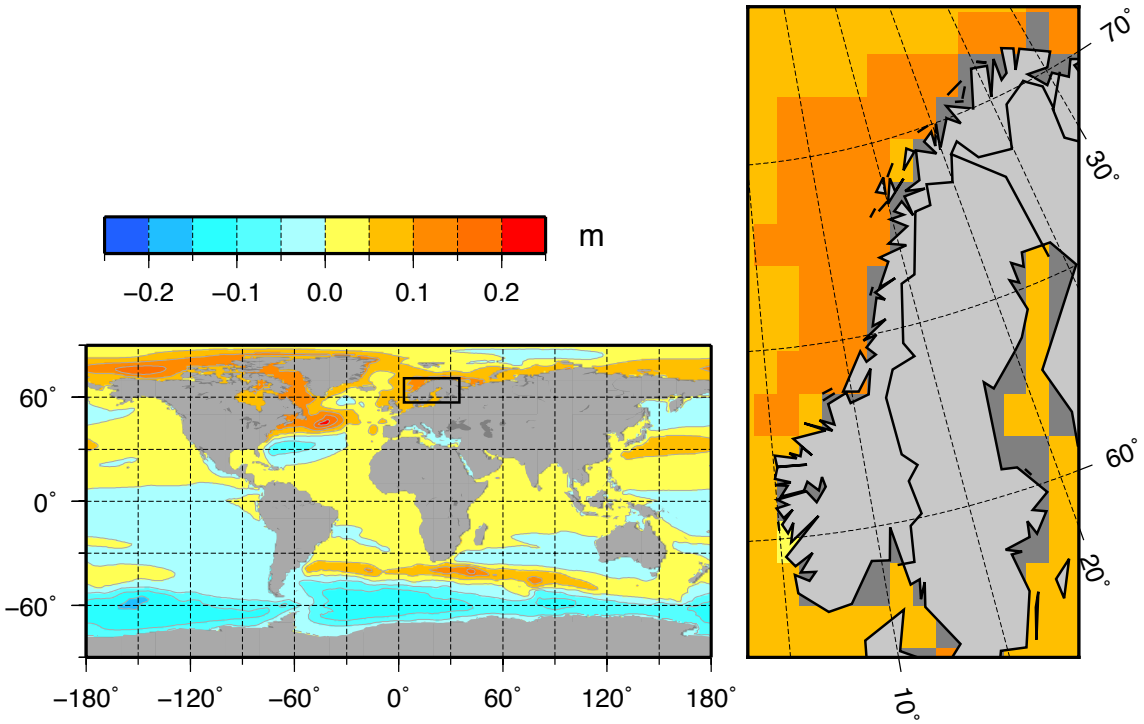

Figure 5.8 Projected mean steric/dyn sea level change for RCP4.5 over the period 1986–2005 to 2081–2100. Projected global thermal expansion (~0.19 m) has been removed.

5.3 Updated Regional Sea Level Projections

Here we present our regional relative sea level projections (Figure 5.9). The projections take account of changes to the contributions given above (Section 5.1.1). Our projections show, unsurprisingly, that the *pattern* of twenty-first century relative sea level changes for Norway is governed by GIA. For all RCPs, projected mean changes indicate that the majority of Norway will experience a RSL rise over the period 1986–2005 to 2081–2100. Thus, it is ocean mass changes and dynamic and steric sea level changes that will dominate the future RSL response.

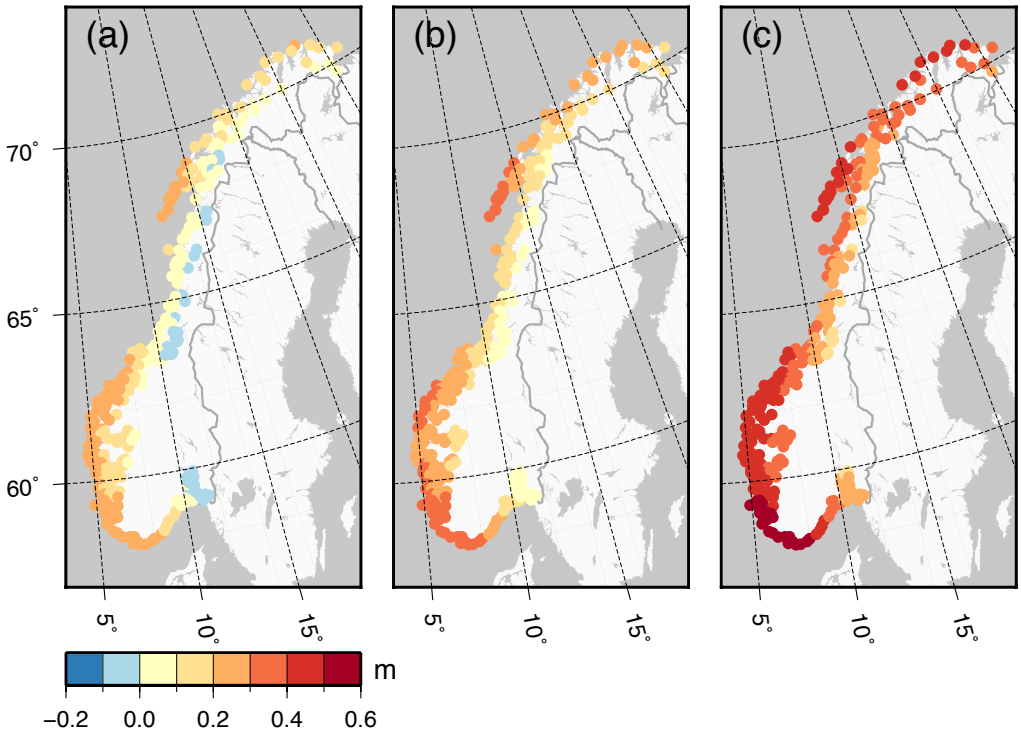

Figure 5.9 Projected ensemble mean regional relative sea level change (m) over the period 1986–2005 to 2081–2100 for (a) RCP2.6 (b) RCP4.5 and (c) RCP8.5.

Projected mean relative sea level changes along the Norwegian coast over the period 1986–2005 to 2081–2100 are for RCP2.6 between -0.10 and 0.30 m, for RCP4.5 between 0.00 and 0.35 m and for RCP 8.5 between 0.10 and 0.55 m. Expressed as a percentage of global mean change, mean regional RSL changes for Norway are for RCP2.6 from -30 to 70% (global mean change of 0.4 m), for RCP4.5 from -10 to 75% (global mean change of 0.47 m) and for RCP8.5 from 20 to 85% (global mean change of 0.63 m). Thus, for all RCPs the mean regional relative sea level change is projected to be below the global mean.

Over the period 1986–2005 to 2081–2100 the average mean regional relative sea level change for the coastal municipalities is for RCP2.6 0.1 m (90% uncertainty bounds are -0.10 to 0.35 m), for RCP4.5 0.2 m (-0.05 to 0.45 m) and for RCP8.5 0.35 m (0.10 to 0.65 m). Figure 5.10 shows the mean and uncertainty bounds for RCP4.5. If we ignore the effects of GIA, i.e., we look at the projected sea surface height change, these numbers are for RCP2.6 0.35 m (0.15 to 0.55 m), for RCP4.5 0.4 m (0.20 to 0.65 m) and for RCP8.5 0.6 m (0.30 to 0.85). For the different RCPs the projected SSH changes are between 80 and 90% of the global mean change. This is because the projected above average input from steric/dyn sea level changes and the rapid ice dynamic contribution from Antarctica are more than compensated for by the below average contributions from Greenland and glaciers. We note that differences between the RCPs for our regional relative sea level projections for Norway are similar to the differences between the RCPs for projected global mean sea level change.

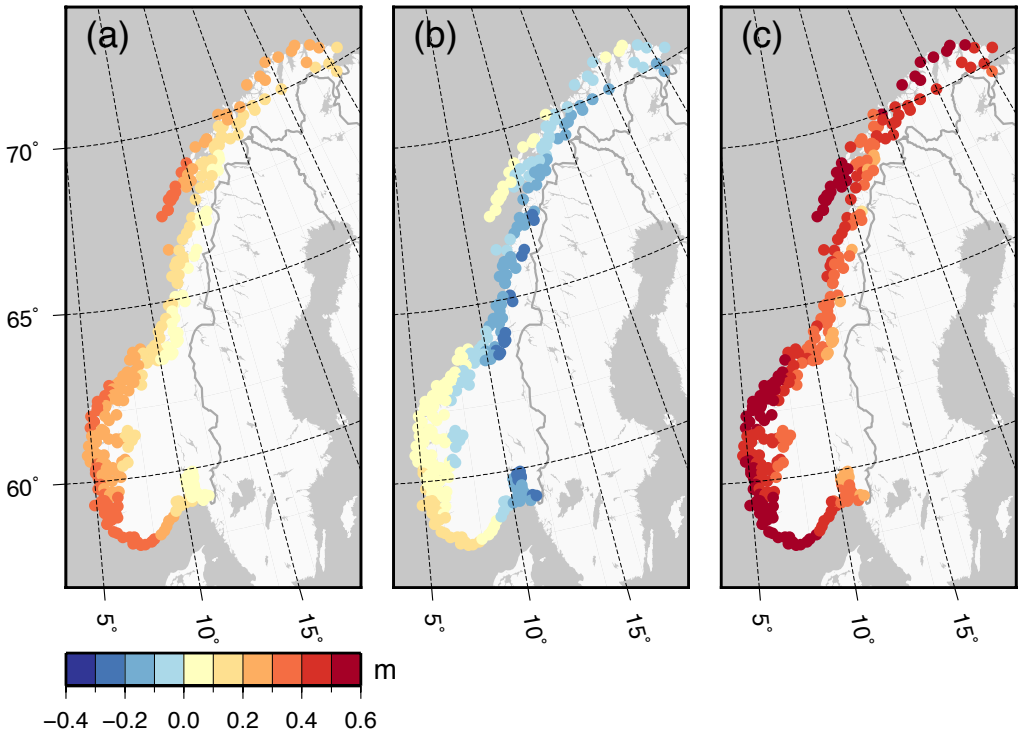

Figure 5.10 Projected regional relative sea level change (m) over the period 1986–2005 to 2081–2100 for RCP4.5 and for the model ensemble (a) mean (b) lower 90% uncertainty bound and (c) upper 90% uncertainty bound.

Examining the projected RSL time series (Figure 5.11) shows that there are only small differences between the RCPs up until 2050. Going towards 2100 the separate projections from the RCPs begin to diverge but there are still large overlaps between their respective uncertainties. In fact, inspection of the vertical bars in Figure 5.11 shows that differences between the ensemble means for the different RCPs are somewhat smaller than the projections ensemble spread (5 to 95%).

The reasons for this become apparent when we examine the contributions from rapid ice dynamics in Antarctica, the steric/dyn signal and vertical land motion. These are the largest contributions to projected RSL change in Norway and, in general, the contributions with the largest uncertainties. Firstly, we note the rapid ice dynamic contribution from Antarctica is the same for all RCPs (i.e., it is RCP independent; See Figure 2.1). AR5 assess that the scientific community is currently unable to quantify how Antarctic rapid ice dynamics relate to emission scenario, but such a dependency is expected to exist (see also Section 5.6). Secondly, we see that there is considerable overlap between the steric/dyn uncertainties for the different RCPs owing to the relatively large ensemble spread. For the period 1986–2005 to 2081–2100 the ensemble spread (5 to 95%) for the steric/dyn contribution is projected to be 0.05 to 0.35 m for RCP2.6, 0.13 to 0.43 m for RCP4.5 and 0.25 to 0.63 for RCP8.5. These values are for the average projected change across the Norwegian coastal municipalities. Thirdly, the contribution from vertical land motion is based upon the extrapolation of observed rates from the permanent GPS stations. We make this assumption on the understanding that GIA dominates vertical land motion in Norway (Chapter 4). This

contribution is, therefore, clearly not related to present-day climate change and is also RCP independent.

As the rate of sea surface rise is projected to increase over the twenty-first century, we opt to show RSL changes towards the end of the century in Table 5.2.

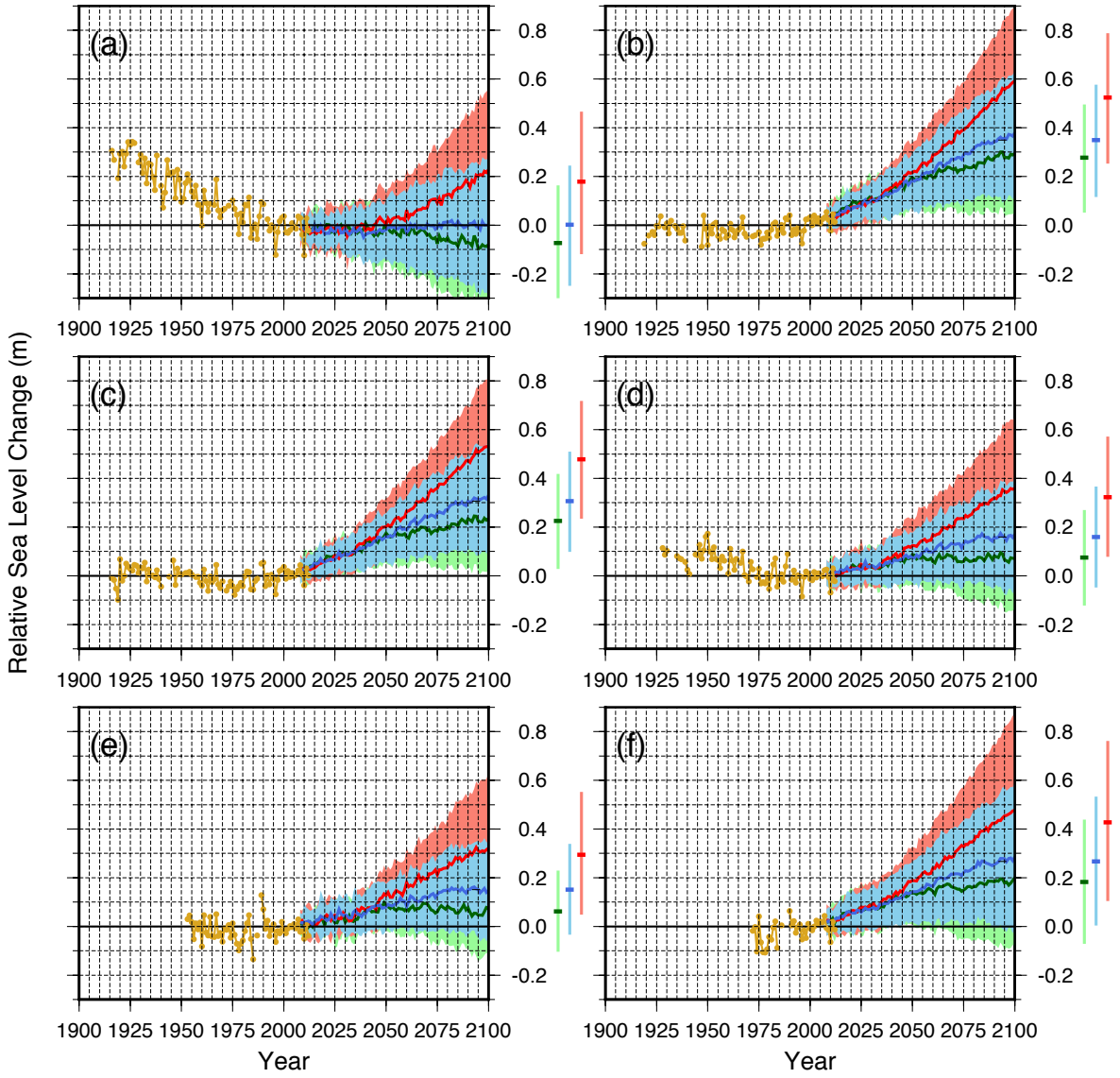

Figure 5.11 Relative sea level projections for RCP2.6 (green), RCP4.5 (blue) and RCP8.5 (red) for the six key locations (a) Oslo (b) Stavanger (c) Bergen (d) Heimsjø (e) Tromsø and (f) Honningsvåg. The vertical bars on the right side of the panels represent the ensemble mean and ensemble spread (5 to 95%) for RSL change for 2081–2100. Annual mean tide gauge observations are shown in yellow.

Table 5.2 Comparison of mean relative sea level projections at six key locations for the period 1986–2005 to 2081–2100 and the period 1986–2005 to 2100. The 5 to 95% ensemble spread is given in the parentheses. Units are in centimetres.

Location	RCP2.6		RCP4.5		RCP8.5	
	2081–2100	2100	2081–2100	2100	2081–2100	2100
Oslo	-7 (-31 to 16)	-8 (-36 to 19)	0 (-25 to 24)	0 (-29 to 28)	18 (-12 to 47)	23 (-11 to 56)
Stavanger	28 (5 to 50)	30 (4 to 54)	35 (12 to 58)	38 (12 to 64)	52 (25 to 79)	59 (28 to 90)
Bergen	23 (3 to 42)	24 (2 to 45)	31 (10 to 51)	33 (11 to 55)	48 (23 to 72)	53 (26 to 80)
Heimsjø	7 (-17 to 27)	7 (-14 to 28)	16 (-5 to 37)	17 (-6 to 40)	30 (8 to 57)	36 (8 to 65)
Tromsø	6 (-10 to 23)	8 (-11 to 27)	15 (-3 to 34)	15 (-5 to 35)	29 (5 to 55)	32 (3 to 63)
Honningsvåg	18 (-7 to 44)	20 (-8 to 48)	27 (0 to 53)	28 (2 to 59)	43 (10 to 76)	48 (11 to 86)

Table 5.3 and Figure 5.12 show the projected rates of sea level change, these show considerable variability owing to interannual to decadal variability in the projected time series. For 2081–2100 we find that projected mean rates for RCP2.6 and RCP4.5 are broadly similar and around 0 to 2 mm/yr. Whereas, for RCP8.5 mean rates are higher for the same period, and approach 10 mm/yr in many areas.

Table 5.3 Rates of projected relative sea level change over the period 1986–2005 to 2081–2100 at six key locations. The 5 to 95% ensemble spread is given in the parentheses. Units are in mm/yr.

Location	RCP2.6	RCP4.5	RCP8.5
	2081–2100	2081–2100	2081–2100
Oslo	-0.7 (-3.4 to 2.0)	-0.2 (-3.7 to 3.1)	5.6 (0.7 to 10.3)
Stavanger	2.4 (-0.2 to 5.0)	2.6 (-0.4 to 5.6)	8.0 (3.5 to 12.5)
Bergen	1.4 (-1.1 to 3.9)	1.9 (-0.1 to 3.9)	6.9 (2.7 to 11.1)
Heimsjø	-0.4 (-3.1 to 2.3)	-0.1 (-2.8 to 2.7)	4.4 (0.0 to 9.0)
Tromsø	-0.7 (-2.6 to 1.2)	-0.3 (-1.7 to 1.2)	3.2 (-0.9 to 7.7)
Honningsvåg	1.1 (-1.8 to 3.9)	1.7 (-2.4 to 5.9)	6.0 (0.3 to 12.1)

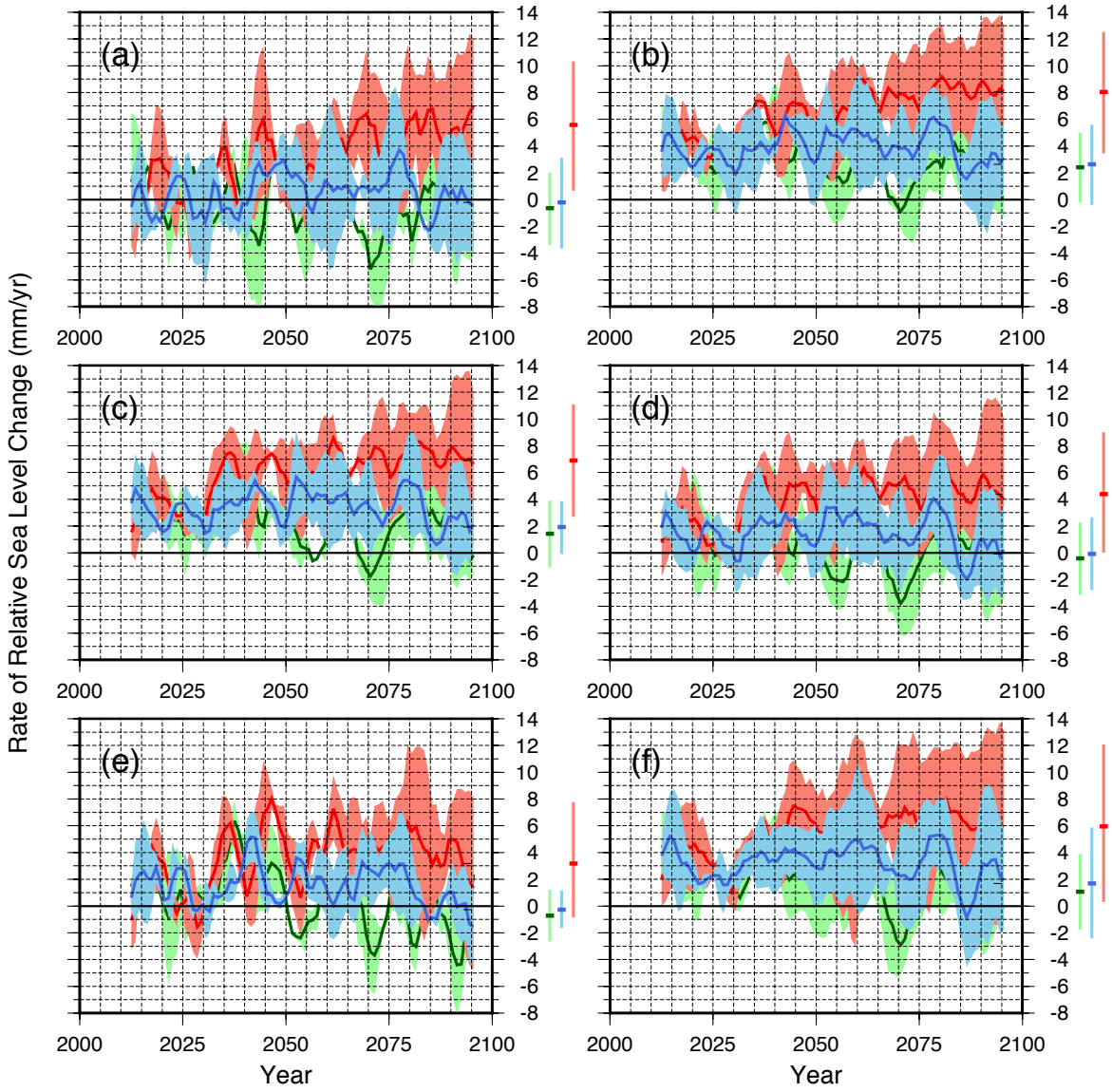

Figure 5.12 Projected rates of sea level change for RCP2.6 (green), RCP4.5 (blue) and RCP8.5 (red) for the six key locations (a) Oslo (b) Stavanger (c) Bergen (d) Heimsjø (e) Tromsø and (f) Honningsvåg. Rates are calculated as linear trends over a 10-year moving window, the x-axis represents the mid-point of each window. The vertical bars on the right side of the panels represent the ensemble mean and ensemble spread (5 to 95%) for rates calculated for the period 2081 to 2100.

5.4 Uncertainties of the Regional Sea Level Projections

In general there are three sources for uncertainties in climate projections:

Emissions scenario uncertainty: This is handled by calculating projections for different representative concentration pathways (RCPs, see Section 2.1.1.)

Natural variability: The natural or internal variability inherent in the earth system, on different time scales.

Model uncertainty: This is usually estimated using the model ensemble spread but does not necessarily represent the full uncertainties. Structural errors, for example, systematic errors and/or errors due to processes poorly represented or absent from the model setup cannot be quantified from the ensemble spread.

In the following we discuss natural variability and model uncertainties in more detail.

5.4.1 Natural Variability

Emission scenario uncertainty and statistical model uncertainty are what can be quantified from the model simulations, and thus are used as uncertainty bounds on the projections. The natural variability may be represented by the ensemble spread if the models are able to simulate the processes behind it in the real world. However, for climate models natural variability of the earth system can only be expected to be partly represented. This is in particular true for regional projections. For the same reason the interannual to decadal variability found in model runs cannot be considered fully representative of natural variability either. Thus, the actual natural variability may very well be of similar magnitude or larger than the ensemble spread, in which case the uncertainty of the projections is better represented by the observed natural variability. See Deser et al (2012) for an overview of this theme.

The observed variability is clearly that which is associated with our current climate state, but it may well be that natural variability changes its character with future climate change. Some indications that natural variability is not likely to weaken can be found in modelled ocean variability (CMIP5), which shows a projected increase in interannual to decadal sea level variability in our region (Church et al., 2013a). From this it can be assumed that the current observed natural variability represents a minimum uncertainty for the projections.

The natural variability can be seen by examining the time series of observations. Thus with the existing measurements from tide gauges, this analysis is possible on a local scale. Here we are interested in the interannual to decadal variability as the projections are given as annual values. Variability on shorter timescales is discussed in Chapter 6. Richter et al (2012a; their Figure 6a) show that the variability found in the Norwegian tide gauges generally increases with longer time scales and reaches highest amplitudes (~10 cm) at 10 years periodicity. This is a clear indication that decadal sea level variability is a significant factor along the Norwegian coast.

Indications that decadal sea level variability is important can be also be seen from our analysis in Chapter 3 (Figure 3.6) and from the annual mean tide gauge observations (Figure 5.11). After detrending the annual mean time series, we find the 5–95% spread in the

observations to be ± 4–11 cm, depending on location. Note that these results are insensitive as to whether the data are detrended using a linear trend or a best-fit polynomial. From this quick analysis we conclude that a general minimum error on the projections of ±10 cm should be applied.

The regional sea level projections as shown in Figure 5.11 indicate that for the near future the ensemble spread is less than the observed internal variability. Furthermore, as mentioned in Section 5.3, the scenario uncertainty is also small up until 2050. Hence, we can conclude that for the first couple of decades or so, the uncertainties may be better represented by the observed interannual to decadal variability.

5.4.2 Model Uncertainty

Returning to the model uncertainty, we noted earlier that AR5 assesses that future global sea level rise is *likely* (P > 66%) to be within the 5 to 95% range of the projections. This assessment reflects the level of scientific understanding of sea level and confidence in our ability to project sea level changes. It is important to recognize that we have different levels of understanding (and confidence) for the separate contributions to projected sea level change. For example, AR5 assess that there is *high confidence* in projecting Greenland SMB changes but *low confidence* in projecting instabilities at the grounding line of the Antarctic ice sheets. The methods used to project the separate contributions and their respective uncertainties are also different.

The collapse of the marine-based sectors of the Antarctic ice sheet are considered by AR5 to be the only potential contributor that could cause GMSL to rise substantially above the *likely* range. For Norway, the Antarctic ice sheet is of concern because the gravitational effect of land ice loss results in an above average sea level rise in our region (as opposed to the Greenland ice sheet which will have a negligible or even negative contribution; see Figure 5.4 and Figure 5.6). In AR5 the *antdyn* contribution is largely constructed using results from Little et al. (2013a,b), in which the authors apply a range of linear growth rates to present-day SMB and outflow observations of the Antarctic sectors. Here we first review possible high-end contributions from the Antarctic ice sheets and, in the following section, show how this information might be incorporated into our sea level projections.

Large future contributions from the marine portions of the Antarctic ice sheets are possible due to inherent instabilities or threshold behaviour (see Alley et al. (2015) for a review). To briefly summarise the problem at hand, most of the West Antarctic Ice Sheet and parts of the East Antarctic Ice Sheet are grounded below sea level. The depth of the bedrock deepens, often dramatically, towards the centre of these ice sheets. And it is well understood that the grounding line of an ice sheet will undergo an unstable retreat on such inward-sloping bedrock features. Of particular concern at the moment are the ice shelves that border Antarctica which act to buttress the grounded ice sheet. In some areas oceanic and atmospheric warming are causing the ice shelves to thin and, once they are reduced, this leads to an acceleration in the flow of the ice and can trigger grounding line retreat. If the grounding line then retreats into the more extensive areas of inward-sloping bedrock then a collapse may be initiated.

In the years following AR5 there have been advances in our understanding of the behaviour of the marine-based parts of the ice sheet (e.g., Favier et al., 2014; Joughin et al., 2014; Rignot et al., 2014), as well as recent efforts towards further quantification of future contributions from Antarctica as a whole (e.g., van den Berk and Drijfout, 2014; Levermann et al., 2014). Observations show that a number of glaciers in West Antarctica have recently undergone widespread grounding line retreat (Rignot et al., 2014). The authors also point out that there are no major bedrock obstacles to prevent further retreat. One of these glaciers, the Thwaites Glacier, is believed crucial to the stability of the large West Antarctic Ice Sheet. New modelling of the Thwaites Glacier shows good agreement with the observed losses and, furthermore, indicates that the early stages of a collapse may have begun (Joughin et al., 2014). However, it should be noted that the simulations show that losses over the 21st century will be within the *likely* ranges given in AR5 for this area of the ice sheet. Rapid losses (>1 mm/yr) are not expected before 200–900 years from now. These results give an indication of what will probably happen over the 21st century (i.e., rather somewhat less than 1 mm/yr) but, we stress, the amounts and timing of these potential future contributions from Antarctica are still very uncertain. It therefore cannot be ruled out that this vulnerable area of the ice sheet will contribute more over shorter timescales (Alley et al., 2015).

In the absence of physical understanding and, in an effort to quantify future contributions from Antarctica as a whole, other researchers have used expert assessments (e.g. Bamber and Aspinall, 2013) or extrapolated the observations in some manner. Van den Berk and Drijfout (2014) construct a time dependent storyline for high-end losses which includes a collapse of the West Antarctic Ice Sheet early this century and large increases from glaciers in East Antarctica and on the Antarctic Peninsula. In this scenario Antarctica contributes to sea level with 0.10 m by 2050 and 0.49 m by 2100. The estimate includes basal melt and iceberg calving (SMB is assumed to be in equilibrium and unchanging). These storylines are based on the high-end scenario of Katsman et al. (2011) which had an Antarctic ice-dynamic contribution of 0.49 m by 2100. Finally, we want to highlight that a significant weakness in the estimates of timing related to future Antarctic changes is the uncertainty attached to the oceanic forcing. In a study of the entire of Antarctica, Levermann et al (2014) examined this issue by combining the uncertainties in the future climatic forcing, the (modelled) ocean response, and the ice sheet model response. They also found an upper 90% probability bound on 21st century ice loss of 0.23 m and 0.37 m of global sea level equivalent for RCP2.6 and RCP8.5, respectively. However, as the authors point out, this should only be considered a first approach of quantification of Antarctica's future dynamic contribution to sea level rise, due to the many known shortcomings of the models and the approach in general.

To summarise, although the amounts and timing of potential ice sheet collapses are very poorly constrained, it is possible to draw some information from the recent assessments about what a high-end contribution from Antarctica might look like during this century. We will use this information below to consider sea level projections beyond the *likely* ranges given in AR5.

5.5 Sea Level Projections Beyond the Likely Ranges

Several recent publications have shown how you might deal with probabilistic sea level projections that take into account changes beyond the *likely* ranges given in AR5 (e.g. de Vries et al., 2014; Kopp et al., 2014). We make our own assessment and quantification here but caution that these results are preliminary and based on rather subjective choices. Following de Vries et al. (2014) we use a Monte Carlo sampling approach to combine the uncertainties on the separate projected contributions to sea level change. (This is also the approach taken in AR5 to compute global sea level rise). In our simplified method, we take 100 000 random samples from the probability distributions of the separate contributions. We choose a random normal variable to select samples from the *steric/dyn*, *greensmb* and *antsmb* ranges. That is, these contributions are assumed to be perfectly correlated as in Eq. 5.1. The other contributions are assumed as independent but are given different shaped probability distributions as detailed in AR5. For example, *antdyn* has a uniform distribution. We compute a global mean, 5 and 95% bounds that lie within a few centimetres of those presented in AR5 (Figure 5.13).

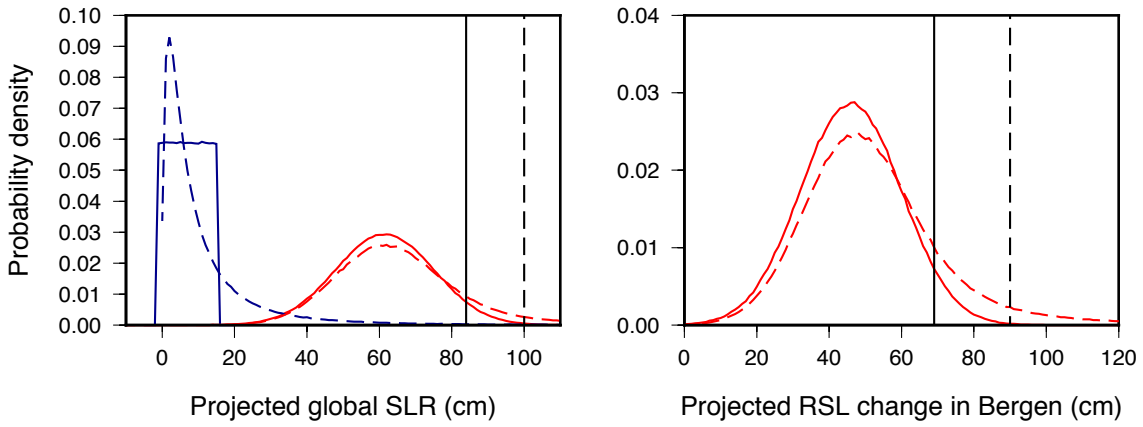

Figure 5.13 (left panel) probability density functions for projected Antarctic ice dynamics assuming a uniform distribution as in AR5 (solid blue line) and a lognormal distribution with the same mean but 0.4 m assumed to be the 95% upper bound (dashed blue line). Corresponding projected global SLR for 2081–2100 is shown in red for RCP8.5. Vertical lines are the corresponding 95% upper bounds. (right panel) corresponding probability density functions for projected RSL change in Bergen for RCP8.5.

The reason we opt to use this sampling method is because it can be simply used to illustrate the effect of changing the shape of the probability distribution for any one component can have on the total sea level rise. In Section 5.4.2 we reviewed possible high-end contributions from the ice sheets, which indicated that a large contribution from Antarctica is at least physically plausible if some marine based sectors begin to collapse. Here we assume that a 0.4 m increase from Antarctic ice dynamics over the period 1986–2006 to 2081–2100 corresponds to the upper 95% probability bound. Note that the mean value is unchanged. The probability distribution is assumed to be lognormal (large upper tail). Unsurprisingly, including this lognormal distribution acts to skew projected GMSL rise towards higher values. The same can be said for the regional projections, in our example we show that for

projected RSL change in Bergen the 95% bound increases from around 0.7 to 0.9 m (see Figure 5.13). We would expect a similar +0.2 m increase for other locations along the Norwegian coast. Other higher percentiles are shown in Table 5.4. We find that our results agree to within ~0.1 m of those given in Kopp et al. (2014), in which other components (e.g. glaciers, Greenland) and their corresponding uncertainties above the *likely* ranges are also included. These results indicate that, for Norway at least, it is the contribution from the Antarctic ice sheets that dominates the tail of the distribution. In our judgement and based on current (post AR5) understanding, then a sea level rise in Norway upwards of ~0.5 m above the *likely* ranges remains a plausible but low probability event. Finally, we caution that the levels and percentiles presented here are highly uncertain, i.e., they should not be considered fixed.

Table 5.4 Estimated sea level changes over the period 1986–2005 to 2081–2100 for the skewed Antarctic contribution in Bergen (which is taken to be ~110% of the global average owing to gravitational effects) and for the total relative sea level change in Bergen. Numbers in brackets give sea level change above the likely ranges.

	95-percentile	97-percentile	99-percentile
Antarctica	0.45 m	0.55 m	0.9 m
Total RSL in Bergen	0.9 (+0.2) m	1 (+0.3) m	1.4 (+0.7) m

5.6 Discussion

Here we discuss two interlinking issues (1) how to reduce the model uncertainty on the projections and (2) processes that are not taken into account in our analysis. Reducing the model uncertainty on the projections depends on our ability to reduce uncertainties from ice dynamics in Antarctica, the steric/dyn signal and observed vertical land motion. These contributions have the largest projected contributions and also largest uncertainties along the Norwegian coast (see Figure 5.2). For a discussion of vertical land motion and GIA see Chapter 4.

Projections of rapid ice dynamic changes are still at an early stage of development. For example, processes such as ice stream dynamics, basal sliding and ice-ocean interactions are either poorly represented or absent from the model setup. However, good progress has been made on including higher-order stresses and improved resolution in ice sheet models. We note that estimates given in AR5 are, for Greenland, essentially based on flowline modelling (Nick et al., 2013) and, for Antarctica, largely based upon the extrapolation of observations (Little et al., 2013a,b). As mentioned, these contributions are partially RCP independent in our projections, but such a dependency is expected to exist. It is going to take time to incorporate all the physical processes into continental-scale ice sheet models. And to couple these ice sheet models with the AOGCMs.

Concerning the uncertainty on the regional steric/dyn signal, it is known that there are several processes relevant for sea level that are not adequately represented by the climate models (Church et al., 2013a), and it has been shown that model uncertainty is dominating over both

internal variability and scenario differences in the CMIP5 projections (Little et al., 2015). The model spread of a regional projection may be reduced significantly by eliminating the few models that deviate most from the mean (Little et al., 2015), but this does little to improve the confidence, as there may still be systematic biases in the remaining models due to inadequately represented processes. Instead we can examine the ability of the models to replicate the observed mean dynamic topography and trends in sea level and hydrography. If the models are able to adequately reproduce the observed patterns, then it gives us increased confidence in their suitability for projecting sea level changes for the Norwegian coast. It also allows us to eliminate models from the ensemble, thus reducing the associated uncertainty, if they fail to adequately reproduce the observations (e.g., Simpson et al. 2014). We do not perform such an analysis in this report but recommend that it be done in future.

With respect to confidence in the steric/dyn signal used in this report, in AR5 it is emphasized that the understanding of the steric/dyn uncertainty is poor, and medium confidence is assigned to the likely ranges of regional projections (Church et al., 2013a). Most coastal regions of the North Atlantic, including Norway, has larger model spread compared to the rest of the world, thus there is no reason to assume any higher confidence here. Furthermore, a recent comparison of a suite of AOGCMs and sea level observations also point to the North Atlantic as a place where model errors are large (Griffies et al., 2014).

One particular effect the AOGCMs used here do not include is the effect of ocean freshening and associated ocean surface changes arising from land ice melt. In 50-year coupled atmosphere-ocean model simulations carried out for a steady Greenland melting of about 2 mm/yr global sea level equivalent, Stammer et al. (2011) found a steric/dynamic response with changes of the order of 5–10 cm in our regions. In an earlier ocean modelling study, an Antarctic contribution was also examined, but the sea level signals were found to not escape the Southern Ocean (Stammer, 2008). Van den Berk and Drijfout (2014) applied their updated melt scenarios from both ice sheets to a climate model in an RCP8.5 experiment, but found no significant steric/dynamic response to this along the Norwegian coast.

These effects are not only limited to advection of and interaction with a surface signal of halosteric height. Freshening of the ocean has the potential to change thermohaline circulation (hence the name). As elaborated on in Section 5.1.2, changes in slope currents like for instance the Norwegian Atlantic Current, an important part of the Atlantic Meridional Overturning Circulation (AMOC), has direct effects on sea level on the continental shelves and coasts. On the other hand, a reduced overturning circulation would mean warmer deep oceans and stronger shelf mass loading (Section 5.1.2). All in all, the complete picture cannot be assessed without including all the thermohaline changes in the modelling, as well as improving the internal representation of the thermohaline processes in ocean models.

5.8 Chapter Summary

We have presented regional sea level projections for Norway using model output from the Coupled Model Intercomparison Project phase 5 (CMIP5) and for the emission scenarios RCP2.6, RCP4.5 and RCP8.5. Our projections show that the *pattern* of twenty-first century

relative sea level changes for Norway is governed by glacial isostatic adjustment. Projected mean sea level changes along the Norwegian coast over the period 1986–2005 to 2081–2100 are for RCP2.6 between -0.1 and 0.3 m, for RCP4.5 between 0 and 0.35 m and for RCP 8.5 between 0.1 and 0.55 m. For all RCPs projected mean changes indicate that the majority of Norway will experience a relative sea level rise (but one below the global mean rise). Thus, it is clear that climate driven sea level rise will dominate over land motion changes over the next 100 years.

The projected time series show that there are only small differences between the RCPs up until 2050. As a side note, the uncertainties on the projections are probably best represented by the observed natural variability for the first few decades (i.e., approximately ± 0.1 m around today's mean sea level). In the latter half of the twenty-first century the separate projections from the RCPs begin to diverge but there are still large overlaps between their respective uncertainties.

The projections presented here are given with corresponding 5 to 95% ensemble spread. These ranges are defined as the *likely* ranges in AR5 (P > 66%). Quantifying the probability of levels above the *likely* range (i.e., the upper tail of the probability distribution) remains difficult because information is lacking. Of particular concern is that the ice sheet contribution might have a skewed distribution, which would mean values in the upper tail of its probability distribution would be quite large. And for Norway, it is the Antarctic ice sheets that are of most interest because the gravitational effect of land ice loss results in an above average sea level rise in our region. Recent research indicates that the early stages of collapse may have begun in some marine-based parts of Antarctica but losses are expected to be moderate over this century. These results give an indication of what will probably happen over the next 100 years but, we stress, the amounts and timing of these potential future contributions from Antarctica are still very uncertain. Lastly, we note that it is unclear how future changes in Antarctica relate to emission scenario.

6 Extreme Sea Levels along the Coast of Norway

When adapting to sea level change, it is important to know which level to be concerned about. In the above we have focussed on mean sea level. For practical purposes, however, it is clear that shorter-term water level changes need to be taken into account. Tides occur on a daily basis but their heights vary on a range of timescales (the different tidal constituents) and also along the coast. And when quantifying coastal impacts and risk, the even higher extreme sea levels associated with storm surges need to be considered.

In this chapter we first review the evidence for possible changes in the frequency and amplitude of sea level extremes. We go on to present improved and updated estimates of storm surge return heights based on a statistical analysis of the tide gauge observations (an example of which is the 1 in 200–year storm surge height which is currently used in Norwegian planning law). Extreme water levels are provided for almost every coastal municipality of Norway.

6.1 Storm Surges

Storm surges occur when a low-pressure weather system and increased surface wind stress simultaneously contribute to increased sea level and push water up against a coast. This is a complicated process where the strength of the storm, its track and speed, as well as details in the coastline and bottom relief, act in concert.

The storm surge contributes to a water level that is considerable higher than the astronomical tide, but whether or not the resulting water level is substantial also depends on the tidal regime. In the southern part of Norway the weather effect dominates the astronomical tide, here storm surges can have consequences regardless of the tides. Whereas, in the western and northern parts of Norway the amplitude of the astronomical tide can be larger than the storm surge height. In these areas a storm surge occurring during low tide has little or no impact. High tides are higher in the days around a full or new moon (called the spring period) than in the days around a half moon (neap period). In northern Norway it is generally only storm surges that occur in a spring period that will have large consequences. Here a storm surge during a neap period will typically result in a water level comparable to a normal high tide in a spring period.

6.1.2 On Possible Changes in the Frequency and Amplitude of Sea Level Extremes

Changes in sea level extremes can arise due to changes in storminess and/or the wave climate and wave setup. Here we are especially interested in changes that are significantly different to the mean sea level change, as these are clearly important when assessing future impacts.

If we first consider the tide gauge records, we find that the picture is somewhat mixed. Some Norwegian tide gauges indicate a small but statistically significant positive late 20th century trend in storm surge heights when compared to the mean sea level change, while others

indicate a negative or insignificant trend (Menéndez and Woodworth, 2010). On storminess, we note that measurements show a +0.1 m/s per year increase in wind speeds along mid to southern Norway during 1979 to 2008 (Vautard et al., 2010). However, this is a short period of time. In a recent IPCC-report, Trenberth et al. (2007) show that there has been no significant trend in storminess over Great Britain, the North Sea, or the Nordic Seas throughout the last century (1880–2003). Possible changes in storm tracks should be evaluated because of their importance for the direction of winds, how often weather systems hit the coast, and where they hit. Earlier assessments have shown that storm tracks have moved northward from the 1960s to the 1990s (e.g., Trenberth et al., 2007). It is important to note that the tracks in question are often defined from the signature of storms in the higher atmosphere, as part of the general atmospheric circulation with its advection of heat etc., but for storm surges the important factors are wind and pressure at the surface. There is no reason to believe that this often mentioned shift necessarily affects storm surges.

Projections of wind and wave climate, relevant indicators for changes in storm surges, show in general little expected change in our regions. Sterl et al. (2009) forced a storm surge model with wind data from an ensemble of 17 climate model runs for 1950–2100. The authors found no significant change in the direction of strong winds (near gale winds or more) in southern and western Norway over this period. Debernard and Røed (2008) performed a similar study based on the moderate IPCC scenarios and projected a weak (2–6%) increase in storm surges along the Norwegian coast. But the authors also point out that storm surge events are extremely dependent on the local conditions (topography and the movement of the storms). More recent model studies project little change in wave climate, however, the same studies also caution that confidence in projections of waves and storm surges is very low (e.g., Hemer et al., 2013).

In the special IPCC report on extreme events (Seneviratne et al., 2012) the following is concluded:

> *"The relatively low number of studies of extreme winds, combined with the weaknesses of the simulations of extreme winds, and the large differences in methods, regions, and models used to develop projections of strong winds, leads to low confidence in projections of strong winds. Confidence in projections of a poleward shift in storm tracks is medium. IPCC has little confidence in regional projections since the models only have partial representation of the relevant processes."*

6.2 Other Factors Affecting Short Term Variability in Sea Level

Here we note there is growing evidence that future changes in the tidal regime need to be considered in coastal risk assessments. A recent global investigation of tide gauge records shows that in many places there are statistical significant trends in the tide levels (Mawdsley et al., 2015). The causes of these changes are not well understood. Modeling studies indicate that changes in mean sea level will cause changes in the tides (e.g. Pickering et al., 2012). Results from the investigation of Pickering et al. (2012) indicate that tidal changes over the North Sea and close to Norway would be both spatially variable and nonlinear. Furthermore, any changes in the tides caused by mean sea level changes will also have implications for

future storm surge heights (Arns et al., 2015). We suggest that these issues are investigated for Norway in future work.

Most factors mentioned above will vary in time and space, and can result in large and mostly unpredictable variability in local water levels. This is especially true for ocean currents, air pressure, wind, and their combination, storm surges. In addition, water temperatures and freshwater content have been shown to govern variability down to monthly timescales (see Section 3.4 above and Richter et al., 2012a). It is not possible to estimate the effect of all these factors individually from place to place and at different times, but it is always possible to base the analysis on statistics of their joint effect, i.e., the water level that has been observed for several decades. These statistics describe the past variability and it is reasonable to assume they describe the normal occurrence of different water levels. From a coastal defense perspective, the most interesting of these are the extreme water levels.

6.3 Methodology for Calculating Return Periods for Extreme Water Levels

Knowledge of extreme high and low water levels is important for planning purposes, coastal management, and for informing the general public. We often specify these levels in terms of return period. An extreme water level with a return period of 20 years will in average occur once every 20 years or, equivalently, has a 5% probability of occurring any given year. Note that the extreme water level with a return period of 20 years is often referred to as the 20-year return height. The extreme levels are in general estimated using statistical analysis of tide gauge data. By using an appropriate statistical method, and a time series of water level data from a tide gauge which is sufficiently long, we are able to estimate extreme levels with a return periods longer than the actual length of the data series.

Different statistical methods can be used to estimate the return periods of the various water levels. Here we use the *Average conditional exceedance rate* (ACER) method for estimating the return levels. This is the method used for calculating the offical return heights for Norway (Sande and Ravndal, 2015). Other popular methods include the *Gumbel* method, which is a *Generalized extreme value* (GEV) method, and the *Peaks over threshold* (POT) method. Comparisons of the alternative methodologies have found that that the ACER method is suitable for estimating water level return periods for Norway and, furthermore, that it provides certain advantages compared to the classical methods (Haug, 2012; Skjong et al., 2013).

In the following we give a brief introduction to the ACER method and how it is used for estimating water level return period. For a more detailed overview of the method, the reader is referred to Næss and Gaidai (2009) and Skjong et al. (2013). The work presented here is a continuation of the work by Haug (2012), and a more complete description can also be found there.

6.3.1 The ACER Method

The difference between the ACER method and many of the classical methods, is that the ACER method focuses on the exceedance rates of the water level instead of only the maxima

yearly values. This means that one attempts to fit a curve to all peaks exceeding a certain level. This makes the method less sensitive to gaps of missing data and outliers than some other methods. The ACER method also takes into account the dependency of the data, that is, that several subsequent peaks exceeding some level might be from the same extreme event. Working with extreme water levels, this means that two subsequent high waters exceeding the given level are likely to be caused by the same storm surge as the storm surge often persists over more than one tidal cycle. Thus, we calculate the rate of which peaks exceed a given level given the condition that the previous peaks did not exceed; hence, we get a conditional exceeding rate.

More precisely, and technically speaking, one defines the ACER function $\epsilon_k(\eta)$ as the rate at which the water level crosses the threshold η given $k-1$ previous non-exceedances. The ACER method attempts to capture the sub-asymptotic behavior of the data by assuming that sub-asymptotically this function is given by

$$\epsilon_k(\eta) = q_k(\eta)\exp(-a_k(\eta - b_k)^{c_k}), \quad \eta \geq \eta_1 \tag{6.1}$$

for a given level $\eta_1$called the tail marker. In practice, the function $q_k(\eta)$ is varying slowly compared to the exponential function when η is large, and it is therefore replaced by a constant value q_k.

We assume that one year of water level data is one realization of the process. The conditional exceedance rate is calculated for discrete levels of η and the average is taken as the estimate. Since the conditional upcrossings are assumed to be independent for a high enough value of k, the ACER function is calculated for different values of k and the value of k for which the process starts to converge is chosen. For water level data this happens for $k = 3$. A curve with the form given by Eq. (6.1) is then fitted to the estimated ACER functions, determining the parameters q_k, b_k, a_k and c_k. The confidence intervals are found in a similar way, by fitting curves to the lower and upper confidence bounds of the estimate of the ACER function. The different return heights can now be estimated by extrapolating the fitted curve to high values of η. The return height z_m where m is the return period (for instance 20, 200, ... years) is given by the following formula

$$z_m = b_k + \left[\frac{1}{a_k}\left(\ln(q_k N) - \ln\left[-\ln\left(1-\frac{1}{m}\right)\right]\right)\right]^{\frac{1}{c_k}} \quad , \tag{6.2}$$

where N is the average number of peaks in the data during one year.

6.4 Return Periods for Extreme Water Levels in Norway

6.4.1 Return Heights at the Tide Gauges

The return heights for each of the Norwegian tide gauges are normally updated every 5 years. This ensures that changes in (1) the frequency and height of the extreme levels as well as (2) the mean RSL change are taken into account. And, as a practical consideration, updating the levels every 5 years also means they are kept stable enough to be used by the general public and the local and national authorities. The return heights used in this report are the official levels from July 2015 (Sande and Ravndal, 2015).

The ACER method (with *k* equal to 3) has been used to estimate return heights with confidence intervals for each of the permanent tide gauges, except Mausund. The 20, 200 and 1000-year return heights are given in Table 6.1 together with the first year of data used for each tide gauge. Figure 6.1 shows all return heights with confidence intervals for the six key locations. All observed time series have been detrended before the analyses. The mean sea level used as a reference level is based on observations from 1996 to 2014. The longest time series are 100 years, the shortest only 24 years (see Chapter 3 for details).

Table 6.1 Return heights for permanent tide gauges, given in meters above mean sea level (1996–2014). The 5 and 95% confidence levels are given in parentheses.

Tide gauge	Start	20 year return height	200 year return height	1000 year return height
Vardø	1947	2.19 (2.12, 2.26)	2.37 (2.28, 2.46)	2.48 (2.37, 2.58)
Honningsvåg	1970	2.01 (1.90, 2.08)	2.21 (2.05, 2.30)	2.33 (2.14, 2.44)
Hammerfest	1957	2.01 (1.91, 2.07)	2.19 (2.03, 2.27)	2.29 (2.11, 2.39)
Tromsø	1952	2.03 (1.97, 2.07)	2.21 (2.13, 2.26)	2.32 (2.22, 2.37)
Harstad	1952	1.75 (1.68, 1.79)	1.92 (1.82, 1.98)	2.03 (1.91, 2.09)
Andenes	1991	1.84 (1.70, 1.93)	2.08 (1.88, 2.20)	2.23 (1.99, 2.38)
Kabelvåg	1988	2.45 (2.30, 2.54)	2.71 (2.49, 2.82)	2.87 (2.60, 3.00)
Narvik	1931	2.59 (2.46, 2.65)	2.85 (2.65, 2.94)	3.02 (2.77, 3.11)
Bodø	1949	2.25 (2.16, 2.31)	2.47 (2.35, 2.55)	2.61 (2.47, 2.69)
Rørvik	1969	2.08 (1.95, 2.14)	2.30 (2.12, 2.38)	2.43 (2.22, 2.53)
Trondheim	1989	2.21 (2.10, 2.27)	2.38 (2.24, 2.45)	2.49 (2.33, 2.57)
Heimsjø	1928	1.94 (1.87, 1.99)	2.10 (2.00, 2.17)	2.20 (2.08, 2.28)
Kristiansund	1962	1.80 (1.72, 1.84)	1.96 (1.85, 2.02)	2.06 (1.93, 2.13)
Ålesund	1961	1.70 (1.60, 1.76)	1.88 (1.73, 1.95)	1.98 (1.80, 2.07)
Måløy	1943	1.53 (1.48, 1.57)	1.66 (1.60, 1.71)	1.74 (1.66, 1.80)
Bergen	1915	1.29 (1.25, 1.32)	1.41 (1.35, 1.46)	1.48 (1.41, 1.54)
Stavanger	1919	1.01 (0.95, 1.04)	1.15 (1.06, 1.19)	1.23 (1.13, 1.29)
Tregde	1927	0.95 (0.89, 1.00)	1.12 (1.01, 1.19)	1.23 (1.09, 1.32)
Helgeroa	1965	1.26 (1.12, 1.34)	1.51 (1.29, 1.62)	1.67 (1.39, 1.81)
Oslo	1914	1.53 (1.39, 1.62)	1.86 (1.62, 1.99)	2.09 (1.77, 2.25)
Oscarsborg	1953	1.42 (1.29, 1.50)	1.67 (1.49, 1.76)	1.83 (1.61, 1.93)
Viker	1990	1.39 (1.18, 1.52)	1.66 (1.35, 1.84)	1.83 (1.46, 2.05)

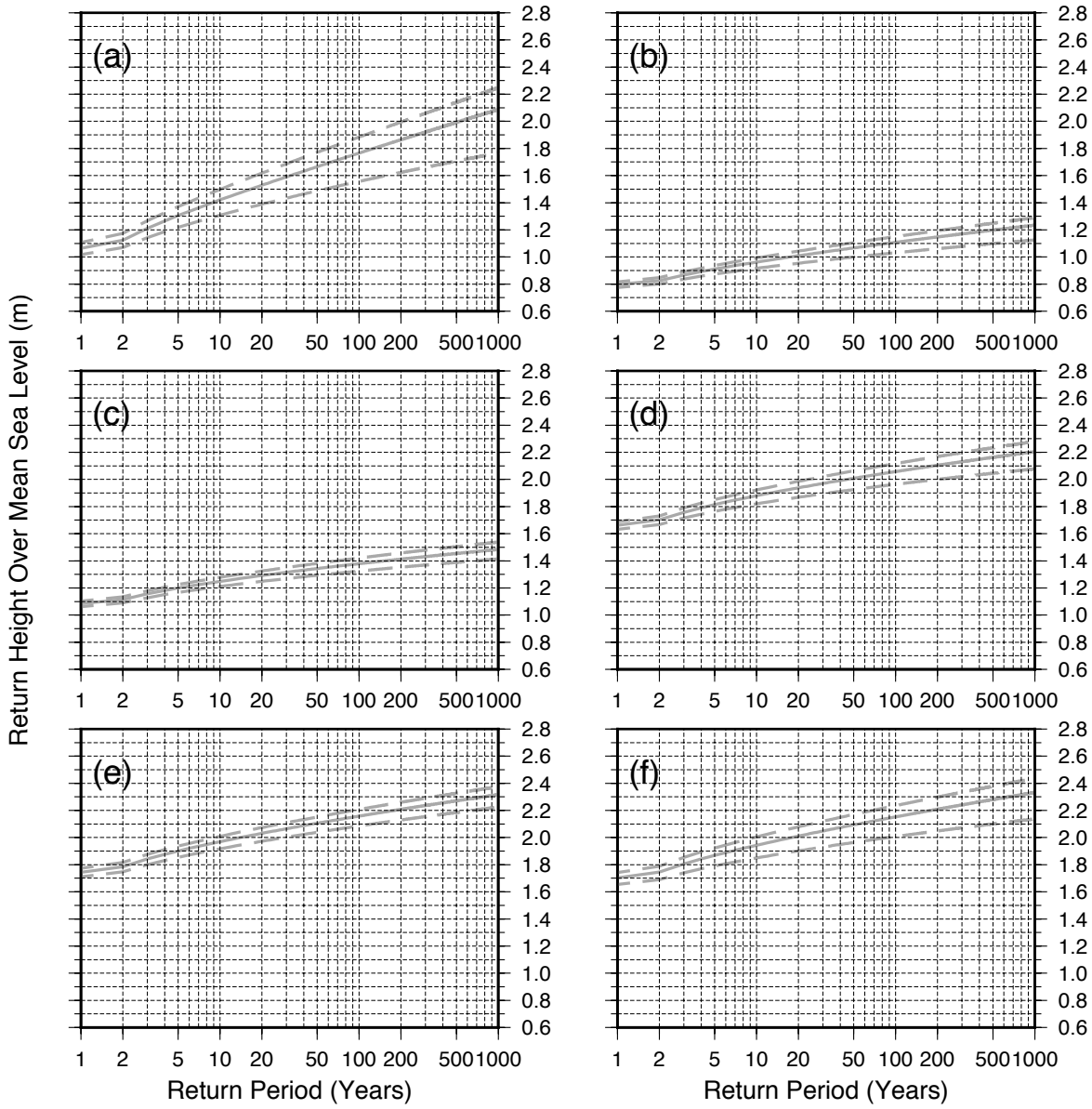

Figure 6.1 Return heights for the six key locations (a) Oslo, (b) Stavanger, (c) Bergen, (d) Heimsjø, (e) Tromsø, and (f) Honningsvåg. Dashed lines are the 5 and 95% confidence intervals.

6.4.2 Estimates for the Municipalities

In the above section, we described the methodology used for determining the extreme water levels for the tide gauges (Table 6.1). Since the amplitude and time of the tide vary significantly along the Norwegian coast, the return heights calculated for a particular tide gauge cannot simply be applied to another point of the coastline. Hence, we need to be able to extrapolate these extreme water levels along the coast. In addition to the permanent tide gauges, the Norwegian Mapping Authority also has several hundred shorter data series available from temporary tide gauges, dating from the beginning of the 20th century to present-day. These data series are analyzed so that the relationship between the tidal behavior in the area of the temporary tide gauge and that of the permanent tide gauge can be quantified. Oceanographic and local knowledge is also taken into account in the extrapolation. Following

this procedure, the Norwegian coastline has been divided into zones of similar tidal properties.

Clearly water levels and particularly the extreme water levels are not only dependent on the astronomical tide. An important contribution to the total water level is the meteorological effect. The meteorological conditions affecting the water level are large-scale phenomena and we expect them to have a similar effect on the water level over a large area and to vary smoothly. When extrapolating the water level to a point away from the permanent tide gauge, therefore, the astronomical tide first is determined using the tidal zones as described above and then added to the meteorological effect as seen at the closest permanent tide gauge.

To obtain return heights away from the permanent tide gauge, we use the above approach to produce adjusted time series for each zone, these are then analyzed using the ACER-method as detailed above. Tests have shown that the phase shift of the astronomical tide does not change the distributions of the extreme water levels. Thus, only the amplitude factor is used to produce the adjusted time series. When applying the ACER method to an adjusted series for a given tidal zone, we use the same k value as for the closest permanent tidal gauge. The return heights for areas along the coast are presented in Table A.1.2.

By analyzing the adjusted time series, we are able to present return heights for most parts of the coast, but not all. For some regions we lack sufficient knowledge about the tides to define the tidal zones and estimate the return levels. This can be the case in fjords and bays with narrow straits, which are known to cause a shift in the tidal phase and a reduction in its amplitude. In these regions, we are dependent on readings from temporary tide gauges, and there are still some regions missing appropriate data.

The southwest coast is influenced by an amphidromic point, this is a point where there is almost no tide. This area is therefore characterized by small tidal variations, but the tidal pattern is complex and difficult to adjust for. In addition, we do not have nearby recordings of the meteorological effect which in many cases dominates over the astronomical tide. Tidal predictions and adjusted time series are therefore normally not available for the area between Lista and Tananger. However, by using data from temporary tide gauges and the records from the nearby permanent tide gauges in Stavanger and Tregde, we observe that the frequency and the heights of the extreme events only vary slightly along the coast. We can thus use the adjusted time series to obtain return heights for these areas even though these time series cannot be used for tidal predictions. The return heights given in this area will have larger uncertainties than the return heights presented for the rest of the coast.

6.4.3 Comparison of Extreme Levels along the Coast

As the amplitude of the tide varies significantly along the coast of Norway, it is interesting to consider the extreme levels relative to highest astronomical tide (HAT) instead of the mean sea level. The highest astronomical tide is the highest possible tidal level due to astronomical conditions, not including weather effects (see Appendix A.1 for details on reference levels). By giving the return heights with respect to this level, we can compare the return heights along the coast without having to take into account the amplitude of the tide. The figure below shows how the 200-year return height given to mean sea level (Figure 6.2a) varies

along the Norwegian coast in a similar way as HAT varies (Figure 6.2b). Removing most of the tidal variation by giving the 200-year return height as meters above HAT (Figure 6.2c) gives a different and more accurate picture of how the return heights differ along the coast. The return heights are higher in the south-eastern part of Norway as well as along the stretch from Rørvik to Lofoten, than in the western part and north of Lofoten. This is caused by the topography and meteorological conditions.

When considering the significance of extreme levels and storm surges, it is therefore relevant to take into account the highest astronomical tide and not only consider the return heights relative to mean sea level.

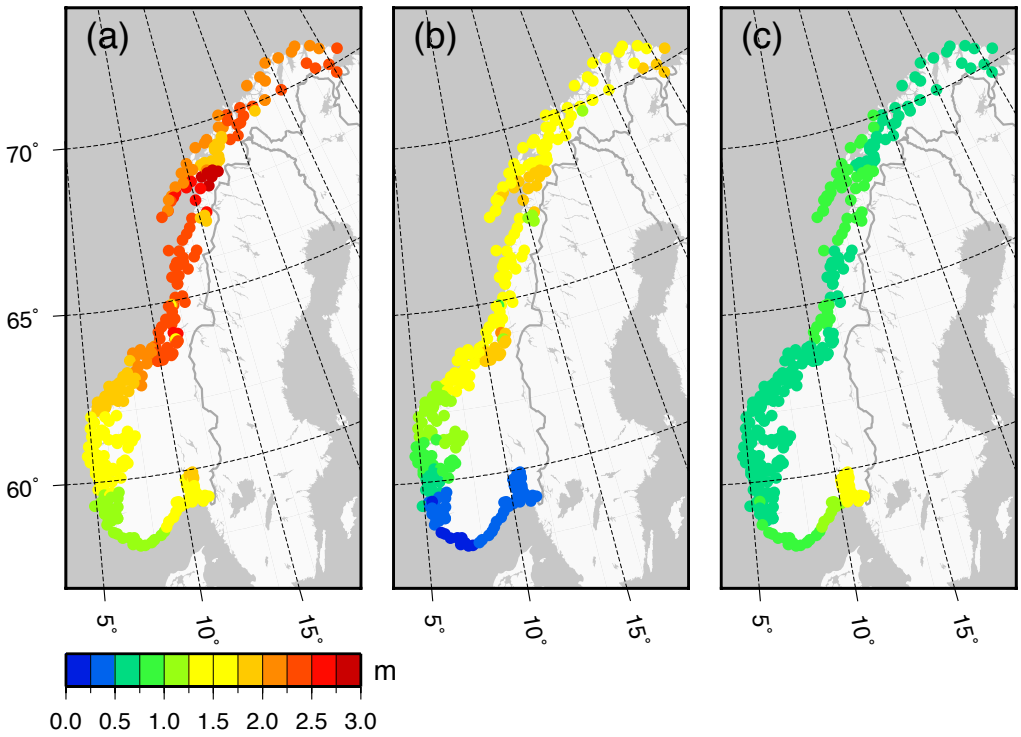

Figure 6.2 Water levels along the coast: (a) the 200 year return levels in meters above mean sea level, (b) highest astronomical tide (HAT) in meters above mean sea level, and (c) the 200 year return height in meters above HAT in order to compare the significance of the extreme levels.

6.5 Chapter Summary

Knowledge of future extreme water levels is important for planning purposes, coastal management, and for informing the general public. Return heights are calculated using statistical analysis of tide gauge data. Here we opt to use the *average conditional exceedance rate* (ACER) method as it allows for use of more data and is less sensitive to outliers and data gaps when compared to other classical methods. (The levels given here are the official return heights for Norway). The analysis is performed on the entire record for 22 out of 23 tide gauges along the Norwegian coast. The tide gauge records vary in length, but they are all sufficiently long for extreme value analysis.

To obtain return heights for all coastal municipalities, time series from the tide gauges have been extrapolated to the surrounding areas. This is done using data from temporary tide gauges and, in addition, oceanographic and local knowledge is taken into account. For some regions, however, we lack sufficient information to define the tidal zones and estimate the return levels. An example of such a problematic area is the stretch of coast from Tananger to Lista (southwest Norway). We have made an attempt at estimating the return heights for this region, but there remain some locations where we are currently unable to provide extreme levels as the tidal patterns are too poorly understood. Nevertheless, we are able to provide return heights with associated confidence levels for the vast majority of places along the coast.

On possible changes in the frequency and amplitude of sea level extremes, we note that observations of extreme sea levels for Norway give a rather mixed picture. But for a few locations there is an indication of a small but statistically significant positive late 20th century trend in storm surge heights when compared to the mean sea level change. Measured changes in storminess suggest an insignificant change or small increase in wind speeds over the same period. Projections of storm surge changes are in general of low confidence. But of the projections available, they suggest a weak increase in future storm surge heights along the Norwegian coast. We do not attempt to estimate any such future changes at coastal locations here, as this is somewhat beyond the scope of this report. Finally, we note there is growing evidence that future changes in the tidal regime need to be considered in coastal risk assessments.

7 Combining Storm Surge Statistics with Sea Level Projections

In this chapter we explore how the sea level projections might be used in a practical sense. In the first part (Section 7.1) we look at how our sea level projections can be combined with the storm surge statistics to provide 'allowances' (Hunter 2012). Allowances give the height by which an asset needs to be raised so that the probability of flooding remains preserved for an uncertain future sea level change. And we adapt this approach for use with our preferred ACER method for calculating the return heights in Chapter 6.

In the second part of the chapter (Section 7.2) we examine what the implications of mean sea level changes are for changes in the return heights. We show how the frequency of flooding over a fixed elevation can dramatically increase with a change in mean sea level. We finish by discussing how our sea level projections might be used by decision makers or in coastal management.

7.1 Method of Hunter

When the sea level increases, the observed effect will in general be related to the change in the frequency of extreme events. This does not imply that the frequency of the extreme events themselves change, but that a level previously attained with a certain frequency will be attained more or less often due to the change in sea level. The response to this would be to raise an extreme level with a certain allowance so that the probability of flooding remains preserved under the given change of sea level. This choice of this allowance often becomes a subjective choice, where the mean sea level change and its confidence interval are not used to its full potential. Hunter (2012) proposes a new method for calculating this allowance. This approach combines the projected sea level rise with extreme-value theory to give an allowance that ensures that the frequency of events exceeding a given level remains constant.

In Hunter et al. (2013) this approach was used to calculate allowances for a set of worldwide locations, using regional sea level projections based on numbers from AR4 and a Gumbel distribution for the estimation of extreme events. It is important to recognise the assumptions made in calculating the allowances as they are also valid in our analysis below. That is, it is assumed that there are no significant changes in time of the frequency and amplitude of storm surges, the tides and/or the wave setup (see Chapter 6 for discussion of these points). Finally, we note that Hunter et al. (2013) emphasize that the allowance given is based on the chosen probability distribution (here we only go as far as examining the normal distribution) and attempts to be a practical solution for coastal management. We discuss these issues below.

Here we attempt to apply the method of Hunter (2012) to the Norwegian coast. We make use of our regional sea level projections from Chapter 5, and our estimated return heights as described in Chapter 6. We start by looking at how we can adapt Hunter's approach for use with our preferred ACER method (see Chapter 6) and then go on to calculate allowances for the Norwegian coastal municipalities. We end this chapter with some comments and suggestions for future work.

7.1.1 Developing the Hunter Framework for Use with the ACER Method

We define the expected number of exceedances of a level z over a given time period to be given by

$$N_{AC} = Nq\exp(-a(z-b)^c) \tag{7.1}$$

where *N, q, a, b* and *c* are the ACER parameters for a given *k* as described in Chapter 6. We now assume that mean sea level is raised by $\Delta z + z'$, where Δz is the mean value of the sea level rise and z' is a random variable with a probability distribution given by $P(z')$ and a zero mean. As our level z has now been reduced by $\Delta z + z'$, we try to find how much we have to raise this level with in order to keep the same exceedance rate as z had before this rise of the mean sea level. This amount will be the allowance A. We denote the overall number of excedances of the level $z - \Delta z - z' + A$ as $N_{ov,AC}$, that is

$$N_{ov,AC} = \int_{-\infty}^{\infty} P(z')Nq\,\exp(-a(z-\Delta z - z' + A - b)^c)dz' \tag{7.2}$$

The objective is to calculate the allowance A so that $N_{ov,AC} = N_{AC}$, that is, the expected number of exceedances before and after the sea level rise remains constant. By manipulating Eq. (7.2) we obtain

$$N_{ov,AC} = Nq\,\exp(-a(z-b)^c)\int_{-\infty}^{\infty} P(z')\,\exp(a(z-b)^c)\,\exp(-a(z-\Delta z - z' + A - b)^c)dz' \tag{7.3}$$

thus, we have $N_{ov,AC} = N_{AC}$ if

$$\int_{-\infty}^{\infty} P(z')\,\exp(a(z-b)^c)\,\exp(-a(z-\Delta z - z' + A - b)^c)dz' = 1 \tag{7.4}$$

Following Hunter et al. (2013) we would like to write Eq. (7.4) in the form

$$A = \Delta z + \cdots \tag{7.5}$$

This cannot be done analytically when based on the ACER method but Eq. (7.4) can however be solved numerically by using appropriate software. Also, it is not possible to eliminate the return level z from this expression, as it is when based on the Gumbel method. For the ACER method, therefore, we lose the advantage of the approach by Hunter (2012) that the allowance remains the same for any level z given.

In a preliminary test of the method and its application to Norway, we examine the case of a future sea level rise assuming a normal uncertainty distribution with zero mean and a standard error σ such that

$$P(z') = \frac{1}{\sigma\sqrt{2\pi}}\exp\left(-\frac{z'^2}{2\sigma^2}\right) \tag{7.6}$$

7.1.2 Results for Allowances

By using our regional sea level projections (Chapter 5) and the ACER parameters found for each tidal zone (Chapter 6), we obtain the allowances given in Tables 7.1–7.3 and Figures 7.1–7.2. In our preliminary tests we look at two alternatives using a normal distribution: (1)

that the model range given in Chapter 5 does in fact correspond to the 5 and 95% probability bounds and (2) that the model spread being defined as the *likely* range in AR5 (P > 66%) correspond to the 17 and 83% probability bounds. We note that the latter appears to be the general interpretation of the model ranges in post-AR5 literature (e.g. Kopp et al., 2014) and is our favoured approach. We stress that these are just some preliminary tests of the method when calculating allowances. Furthermore, the method should clearly be tested using other probability distributions of different shapes and sizes (most obviously a skewed distribution, see Section 5.5). We discuss these issues below.

The difference between the two sets of allowances calculated here is simply the difference in the spread of the sea level projections. For the allowances computed using the model range as the 5 to 95% probability bounds then the allowance generally lies around the mark of the standard error above the mean (allowances are never below the mean and not above the 95% bound). Whereas, when calculating allowances using the model range as the 17 to 83% probability bounds then the allowances generally lie above the mark of the standard error above the mean and are sometimes larger than the 95% bound. There are also differences depending on which RCP and which return height is chosen (Tables 7.1–7.3). We note that the pattern of the allowances (Figures 7.1–7.2) reflects the spatial differences in both the RSL projections and return height statistics.

Table 7.1 Allowances (in cm) calculated for six key locations using the 20-year return heights and projected mean relative sea level change over the period 1986–2005 to 2081–2100. The 5 to 95% ensemble spread is given in parentheses. Allowances are given for two different choices of the level of likelihood assigned to the ensemble spread.

Location	RCP 2.6			RCP 4.5			RCP 8.5		
	Sea level change	Allowance for 20 year return height		Sea level change	Allowance for 20 year return height		Sea level change	Allowance for 20 year return height	
	2081–2100	5–95%	17–83%	2081–2100	5–95%	17–83%	2081–2100	5–95%	17–83%
Oslo	-7 (-31, 16)	6	20	0 (-25, 24)	14	28	18 (-11, 47)	34	54
Stavanger	28 (5, 50)	39	59	35 (12, 58)	48	69	52 (25, 79)	69	96
Bergen	23 (3, 42)	33	48	31 (10, 51)	42	59	48 (23, 72)	63	85
Heimsjø	7 (-17, 27)	11	24	16 (-5, 37)	20	35	30 (8, 57)	40	60
Tromsø	6 (-10, 23)	30	53	15 (-3, 34)	38	62	29 (5, 55)	60	93
Honningsvåg	18 (-7, 44)	32	53	27 (0, 53)	41	63	43 (10, 76)	64	96

Table 7.2 Allowances (in cm) calculated for six key locations using the 200-year return heights and projected mean relative sea level change over the period 1986–2005 to 2081–2100. The 5 to 95% ensemble spread is given in parentheses. Allowances are given for two different choices of the level of likelihood assigned to the ensemble spread.

Location	RCP 2.6			RCP 4.5			RCP 8.5		
	Sea level change	Allowance for 200 year return height		Sea level change	Allowance for 200 year return height		Sea level change	Allowance for 200 year return height	
	2081–2100	5–95%	17–83%	2081–2100	5–95%	17–83%	2081–2100	5–95%	17–83%
Oslo	-7 (-31, 16)	7	22	0 (-25, 24)	14	31	18 (-11, 47)	35	56
Stavanger	28 (5, 50)	41	65	35 (12, 58)	50	75	52 (25, 79)	72	104
Bergen	23 (3, 42)	35	54	31 (10, 51)	44	65	48 (23, 72)	66	93
Heimsjø	7 (-17, 27)	12	28	16 (-5, 37)	22	40	30 (8, 57)	42	66
Tromsø	6 (-10, 23)	33	61	15 (-3, 34)	41	71	29 (5, 55)	65	105
Honningsvåg	18 (-7, 44)	34	59	27 (0, 53)	43	70	43 (10, 76)	68	106

Table 7.3 Allowances (in cm) calculated for six key locations using the 1000-year return heights and projected mean relative sea level change over the period 1986–2005 to 2081–2100. The 5 to 95% ensemble spread is given in parentheses. Allowances are given for two different choices of the level of likelihood assigned to the ensemble spread.

Location	RCP 2.6			RCP 4.5			RCP 8.5		
	Sea level change	Allowance for 1000 year return height		Sea level change	Allowance for 1000 year return height		Sea level change	Allowance for 1000 year return height	
	2081–2100	5–95%	17–83%	2081–2100	5–95%	17–83%	2081–2100	5–95%	17–83%
Oslo	-7 (-31, 16)	7	23	0 (-25, 24)	15	32	18 (-11, 47)	36	58
Stavanger	28 (5, 50)	42	68	35 (12, 58)	51	78	52 (25, 79)	74	108
Bergen	23 (3, 42)	36	58	31 (10, 51)	46	70	48 (23, 72)	68	97
Heimsjø	7 (-17, 27)	13	31	16 (-5, 37)	23	43	30 (8, 57)	44	71
Tromsø	6 (-10, 23)	35	66	15 (-3, 34)	43	76	29 (5, 55)	68	112
Honningsvåg	18 (-7, 44)	36	63	27 (0, 53)	45	73	43 (10, 76)	70	112

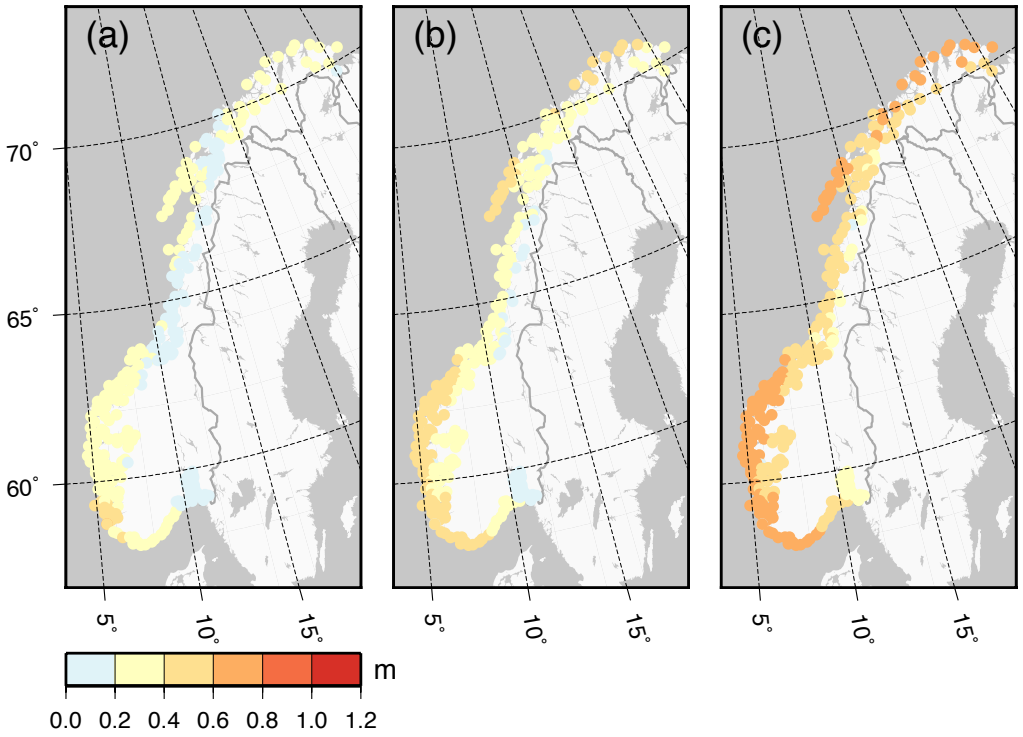

Figure 7.1 Allowances (m) calculated using the 200-year return heights and projected relative sea level change over the period 1986–2005 to 2081–2100 for (a) RCP2.6 (b) RCP4.5 and (c) RCP8.5. We assume that the model range corresponds to the 5 to 95% probability bounds and fit a normal distribution.

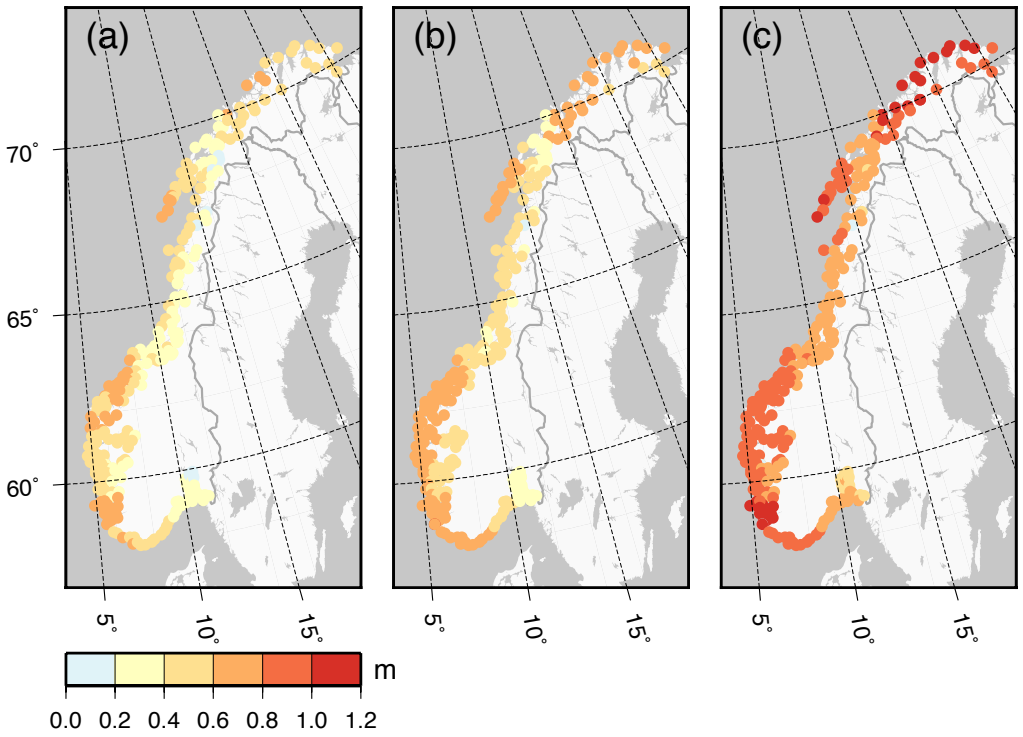

Figure 7.2 Allowances (m) calculated using the 200-year return heights and projected relative sea level change over the period 1986–2005 to 2081–2100 for (a) RCP2.6 (b) RCP4.5 and (c) RCP8.5. We assume that the model range corresponds to the 17 to 83% probability bounds and fit a normal distribution.

7.2 Changes in Return Heights

Here we first show changes in return heights after adding our twenty-first century mean relative sea level projections (Figure 7.3). We also show how the likelihood of exceeding the present 200-year and 1000-year return height can be dramatically increased with sea level rise (Figures 7.4 and 7.5). Changes in the likelihood are dependent on both the projected sea level change and the statistics of the observed sea level extremes (i.e., the spread between the different return heights which determines the gradients of the lines shown in Figure 7.3). For Oslo, which has a relatively *small* projected sea level change but has relatively *large* differences between the return heights, we expect only small changes in the frequency of exceedance. However, for Stavanger and Bergen, the reverse is true and we therefore expect a large increase in the frequency of exceedance.

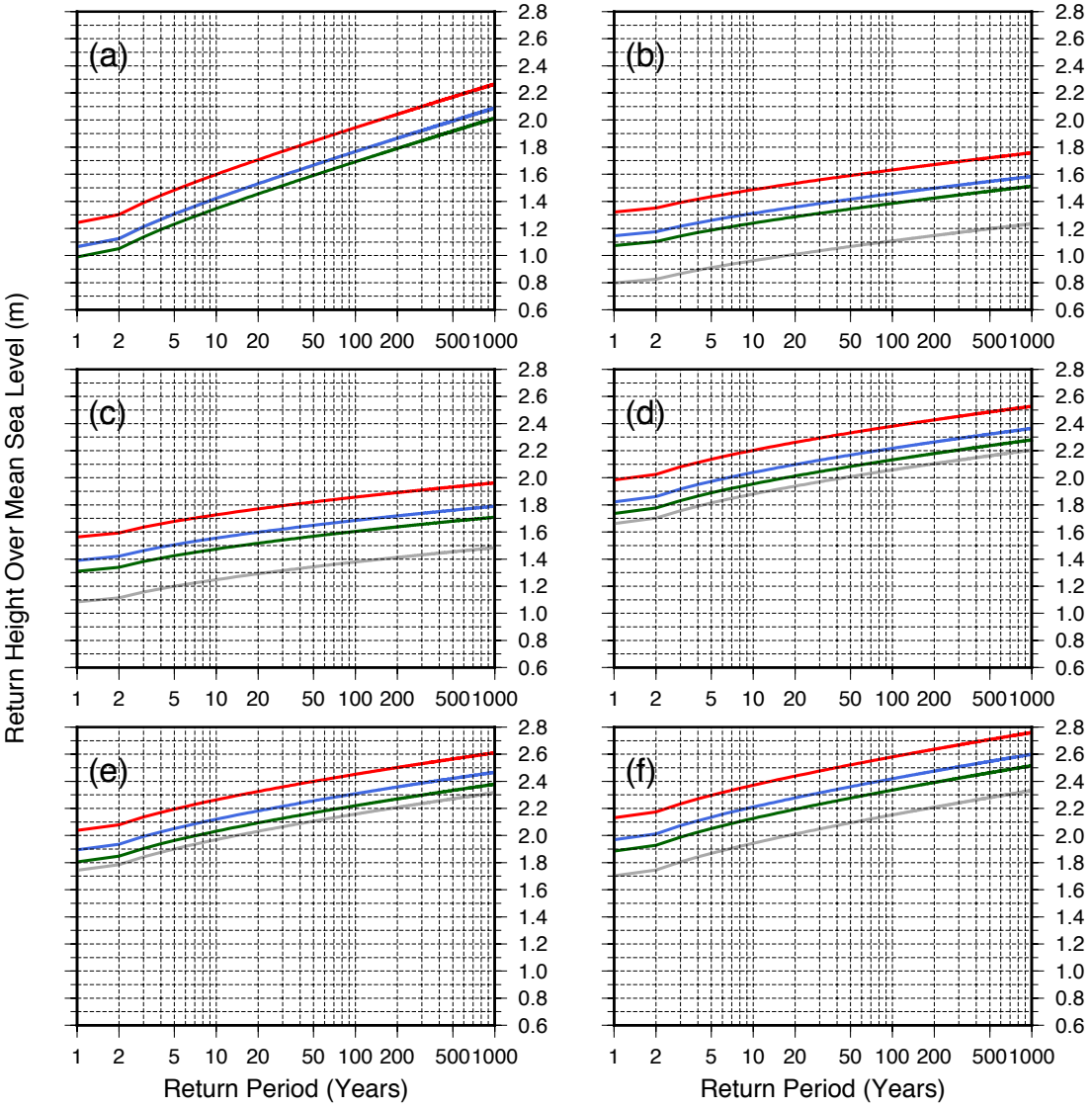

Figure 7.3 Return levels for stationary sea level (grey) and for mean relative sea level projections over the period 1986–2005 to 2081–2100 for RCP2.6 (green), RCP4.5 (blue) and RCP8.5 (red) at the six key locations (a) Oslo (b) Stavanger (c) Bergen (d) Heimsjø (e) Tromsø and (f) Honningsvåg.

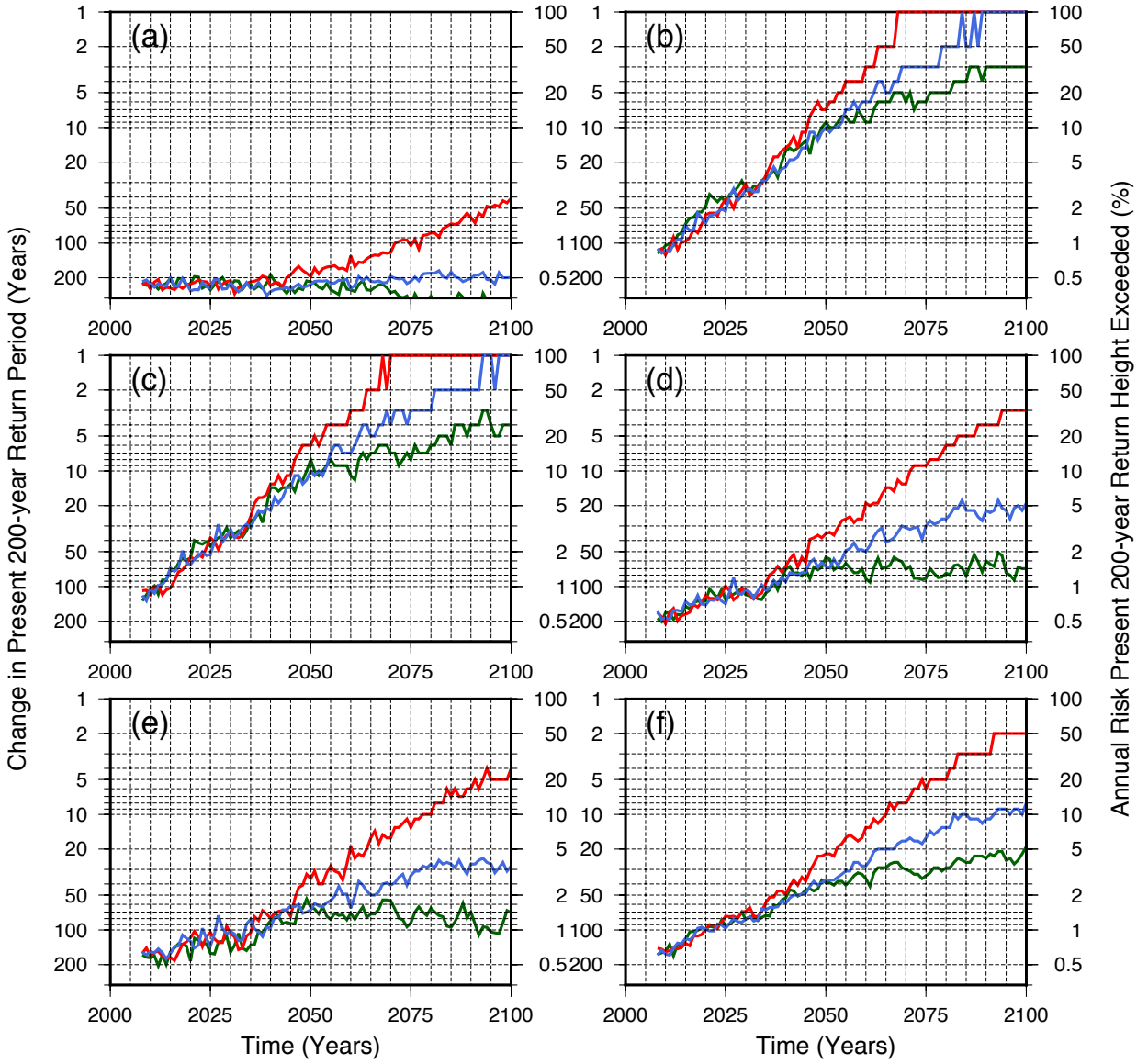

Figure 7.4 Changes in the 200-year return period (or risk) for the mean relative sea level projection for RCP2.6 (green), RCP4.5 (blue) and RCP8.5 (red) and at the locations (a) Oslo (b) Stavanger (c) Bergen (d) Heimsjø (e) Tromsø and (f) Honningsvåg.

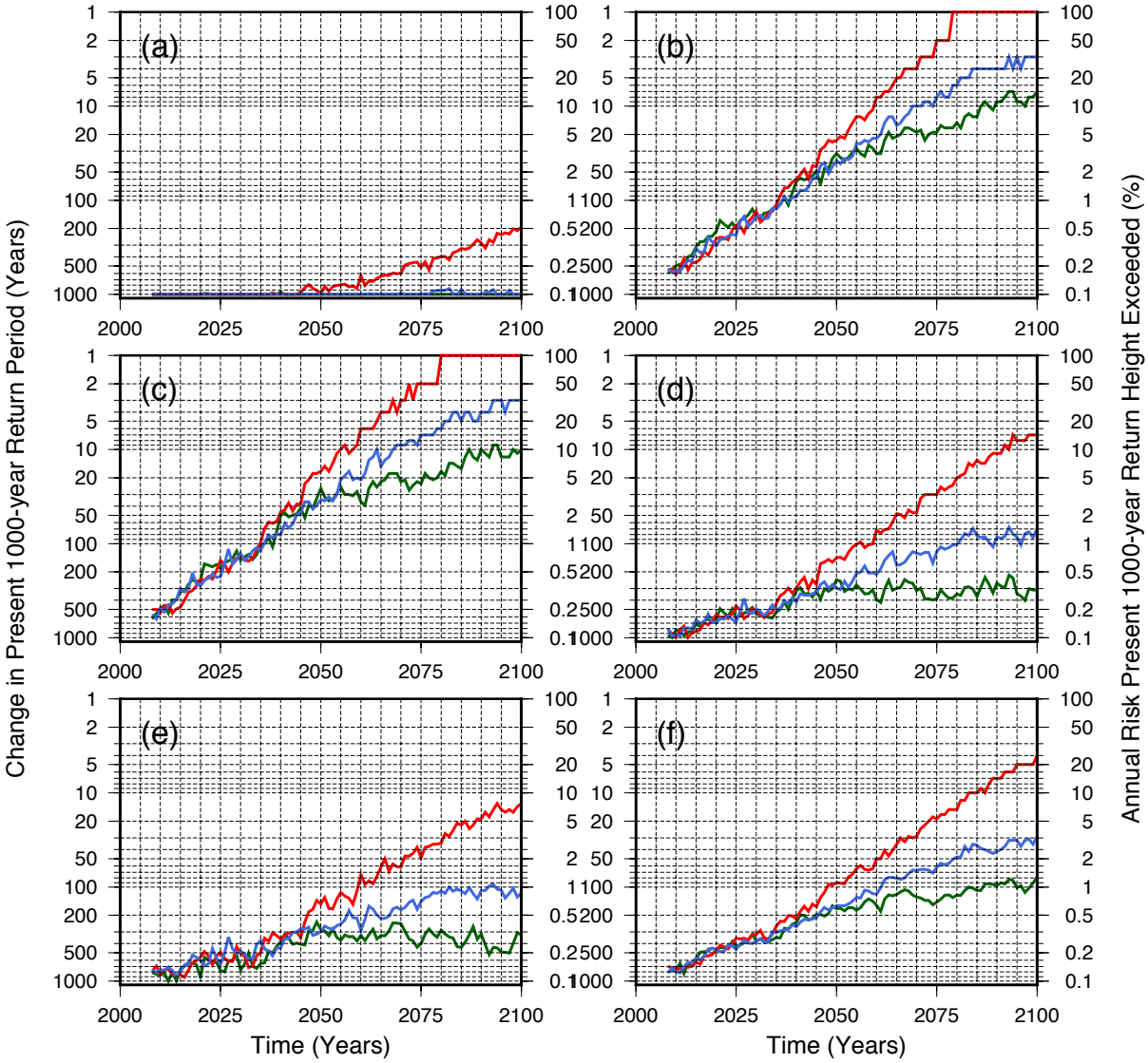

Figure 7.5 Changes in the 1000-year return period (or risk) for the mean relative sea level projection for RCP2.6 (green), RCP4.5 (blue) and RCP8.5 (red) at the six key locations (a) Oslo (b) Stavanger (c) Bergen (d) Heimsjø (e) Tromsø and (f) Honningsvåg.

For each year between 2001 and 2100 we calculate the probability (likelihood) that the present return height will be exceeded (see also Kopp et al., 2014). This is done only using the mean RSL projections for all RCPs, we assume no RSL change over the reference period 1986–2005. The method used here is not as by Hunter (2012). Simply, the annual probabilities are summed over the period of interest to give an estimate of the number years where the present return height is exceeded (note that it is possible the height is exceeded multiple times in any one year). The results are presented in Table 7.4 (for the 20-year return height), Table 7.5 (200-year return height) and Table 7.6 (1000-year return height). For Bergen and Stavanger we expect that the 200-year return height will be exceeded in ~40 of the years between 2001 and 2100 for RCP8.5.

Table 7.4 Expected number of years that the present-day 20-year return height is exceeded for the periods 2001–2050 and 2001–2100, at six key locations.

2001–2050	No RSL change	RCP2.6	RCP4.5	RCP8.5
Oslo	2.5	2.4	2.4	2.6
Stavanger	2.5	14.1	14.3	19.4
Bergen	2.5	11.6	11.0	15.7
Heimsjø	2.5	3.8	4.0	4.8
Tromsø	2.5	3.9	4.4	5.0
Honningsvåg	2.5	6.7	6.7	8.4
2001–2100	**No RSL change**	**RCP2.6**	**RCP4.5**	**RCP8.5**
Oslo	5.0	4.2	4.9	8.5
Stavanger	5.0	56.1	57.3	62.4
Bergen	5.0	42.8	52.0	58.7
Heimsjø	5.0	7.5	11.7	31.7
Tromsø	5.0	8.1	12.2	27.9
Honningsvåg	5.0	18.9	28.0	46.5

Table 7.5 Expected number of years that present-day 200-year return height is exceeded for the period 2001–2100, at six key locations.

2001–2100	No RSL change	RCP2.6	RCP4.5	RCP8.5
Oslo	0.5	0.5	0.5	1.0
Stavanger	0.5	11.1	22.2	38.1
Bergen	0.5	7.8	15.3	37.7
Heimsjø	0.5	0.9	1.5	5.7
Tromsø	0.5	1.0	1.6	4.5
Honningsvåg	0.5	2.7	4.6	13.3

Table 7.6 Expected number of years that present-day 1000-year return height is exceeded for the period 2001–2100, at six key locations.

2001–2100	No RSL change	RCP2.6	RCP4.5	RCP8.5
Oslo	0.1	0.1	0.1	0.2
Stavanger	0.1	3.2	6.5	25.8
Bergen	0.1	2.2	5.4	24.4
Heimsjø	0.1	0.2	0.3	1.7
Tromsø	0.1	0.2	0.4	1.2
Honningsvåg	0.1	0.6	1.2	4.4

7.3 Discussion

Here we briefly discuss how the information in this report might be used by decision makers and/or in coastal management. For a country like Norway, which has a generally low physical vulnerability to sea level rise, then using the allowances as described above might be an attractive option in planning. We have made some preliminary tests of the method by

assuming that our regional sea level projections are normally distributed and then by fitting this distribution to the model spread (*likely* range) as presented in Chapter 5.

The AR5 assesses that future global sea level rise is *likely* (P > 66%) to be within the 5 to 95% range of the projections. Our understanding is that a sensible interpretation of this is that the model ranges we present in Chapter 5 and in the Appendix (Tables A.2.1–A.2.3) correspond to approximately the 17 and 83% probability bounds. As mentioned, of particular concern is that the ice sheet contribution might have a skewed distribution, which would mean values in its upper tail would be quite large. Indeed, there appears a growing consensus in the glaciological community that skewed distributions should be taken into account (e.g. Levermann et al., 2014; Alley et al., 2015). This would also presumably result in higher allowances than those presented above.

Understanding of such low probability but potentially large impact future sea level changes is clearly important for coastal management. For flood risk assessments, therefore, then it seems prudent to try and take this information into account. A good starting point would be to use the numbers given in Chapter 5 (Table 5.4). That is, given possible rapid future losses in Antarctica, then the probability distribution for sea level change in Norway can be approximated as lognormal with values in the upper tail 0.2 m (95%), 0.3 m (97%) and 0.7 m (99%) above the *likely* ranges. Again, we caution that these higher levels and percentiles are highly uncertain.

7.4 Chapter Summary

Allowances give the height by which an asset needs to be raised so that the probability of flooding remains preserved for a given sea level change. We have adapted the framework of Hunter (2012) to be able to calculate allowances using the return heights estimated from the average conditional exceedance rate (ACER) method. A disadvantage of using the ACER method (as opposed to the Gumbel method) is that our allowances are dependent on the return height of interest. We emphasize that the allowances presented here are given based on the chosen probability distribution on the projection and are a preliminary test of the method. In future work the method should be tested using other probability distributions of different shapes and sizes (most obviously a skewed distribution).

Finally, we note that the likelihood of exceeding the present-day return heights can increase dramatically with sea level rise. Changes in the likelihood are dependent on both the projected sea level change and the statistics of the observed sea level extremes. For Oslo, which has a relatively *small* projected sea level change but has relatively *large* differences between the return heights, we expect only small changes in the frequency of exceedance. However, for Stavanger and Bergen, the reverse is true and we therefore expect a large increase in the frequency of exceedance. In these cities we expect that the present-day 200-year return height will be exceeded in ~40 of the years between 2001 and 2100 for RCP8.5.

8 Summary

Projecting future sea level change is a challenging task as it requires a sound understanding of many different aspects of the Earth-climate system. Key to improving our understanding of sea level is being able to identify the separate contributions to regional sea level change. This means maintaining and improving sea level observing systems for Norway. Doing this would enable further model testing and, one would hope, lead to increased confidence in our ability to project the components of regional sea level change. The findings from our report can be summarized as follows:

Paleo observations show that Norway has a complex sea level history. The spatial pattern of sea level changes over the past 12,000 years largely reflects the rebound of the solid Earth in response to past ice mass loss. This process driving vertical land motion, glacial isostatic adjustment, is ongoing and is an important component of past, present and future sea level change for Norway.

The Norwegian tide gauge network provides data on relative sea level changes from the late 1800s up until today. Over the 20th century, some areas of Norway experienced an overall sea level fall while others underwent a limited rise (values somewhat below the global mean rise). The pattern of regional sea level change appears to be largely governed by vertical land motion. After correcting the tide gauge measurements for the effects of GIA, we estimate that the average rate of sea surface rise along the Norwegian coast is 1.9 ± 0.2 mm/yr for 1960 to 2010. In general, we note that 20th century sea level rise in our ocean regions is similar to the global average.

Over the more recent period 1993–2014, the average rate of coastal sea level rise south of 66°N is estimated from two satellite altimetry datasets as 3.1 ± 0.7 mm/yr and 3.4 ± 0.7 mm/yr. These numbers agree well with the rate obtained from the tide gauge network (3.8 ± 0.6 mm/yr). The rate of sea surface rise along the Norwegian coast is significantly higher for the period 1993–2014 than for the period 1960–2010. It is unclear, however, to what extent this higher rate represents natural variability rather than a sustained increase owing to global warming.

Our regional sea level projections are based on findings from AR5 and CMIP5 model output. The projections take into account spatial variations in: (1) ocean density, ocean mass redistribution, and dynamics; (2) ocean mass changes and associated gravitational effects on sea level; and (3) vertical land motion and associated gravitational effects on sea level. Our projections show, unsurprisingly, that the *pattern* of twenty-first century relative sea level changes for Norway is governed by vertical land motion from glacial isostatic adjustment. Projected mean sea level changes along the Norwegian coast over the period 1986–2005 to 2081–2100 are for the following emission scenarios:

- RCP2.6 between -0.10 and 0.30 m, depending on location
- RCP4.5 between 0.00 and 0.35 m, depending on location
- RCP8.5 between 0.15 and 0.55 m, depending on location

For all RCPs projected mean changes indicate that the majority of Norway will experience a relative sea level rise (but below the global mean rise). Thus, it seems clear that climate driven sea level rise will dominate over land motion changes over the next 100 years. And this represents a reversal of the late-Holocene trend of relative sea level fall. By the end of the 21st century, rates of relative sea level rise are *likely* to approach ~10 mm/yr for RCP8.5 in most parts of Norway.

The projections presented here are given with corresponding 5 to 95% model ranges which are defined as the *likely* range in AR5 (P > 66%). Quantifying the probability of levels above the *likely* range (i.e., the upper tail of the probability distribution) remains difficult because information is lacking. Of particular concern is that the ice sheet contribution might have a skewed distribution, which would mean values in its upper tail would be quite large. We therefore make an attempt at including this information into our projections as it seems prudent to try and account for this possibility. Recent research suggests that the early stages of collapse may have begun in some marine-based parts of Antarctica but losses are expected to be moderate over this century. These results give an indication of what will happen over the next 100 years but, we stress, the amounts and timing of these potential future contributions are still very uncertain.

Regional sea level change beyond 2100 is not dealt with is report. However, it is clear sea level will continue to rise after this time owing to the long response times of the oceans and ice sheets. Evidence from the paleo record shows that with even moderate warming, that is, temperatures close to those we observe today, the Greenland and Antarctic ice sheets contributed to a multi-meter sea level rise above present-day levels.

Our present-day return heights for extreme sea levels are calculated using statistical analysis (the ACER method) of the observations from the Norwegian tide gauge network. The ACER method provides certain advantages compared to the other classical methods used for estimating return heights. Concerning possible changes in sea level extremes by 2100, there is generally low confidence in our ability to project regional changes of these effects. Observations of extreme sea levels for Norway give a rather mixed picture. But for a few locations there is an indication of a small but statistically significant positive late 20th century trend in storm surge heights when compared to the mean sea level change. We do not attempt to estimate any such future changes at coastal locations here.

The estimated return heights can be combined with our regional sea level projections to provide allowances. Allowances give the height by which an asset needs to be raised so that the probability of flooding remains preserved for a given sea level change. Using allowances might be an attractive option in planning and we have made some preliminary tests here. Finally, we note that changes in the likelihood of flooding are dependent on both the projected sea level change and the statistics of the observed sea level extremes. The likelihood of exceeding present-day return heights can be dramatically increased with sea level rise.

Acknowledgements

We wish to express our gratitude to colleagues who have helped us with making this report: The reviewers who gave us valuable guidance on an earlier version of the manuscript, Sönke Dangendorf, Caroline Katsman, Antony Long, Ben Marzeion, Arvid Næss, Kristin Richter, Lars Petter Røed; The reference group that gave feedback on the first draft of the report, Jens Debernard, Jon Ove Hagen, Inger Hanssen-Bauer, Hege Hisdal; and the colleagues who have contributed with discussions and comments on parts of the report as we wrote, Mats Bentsen, Helge Drange, Mari Hegland Halvorsen, Anders Levermann, Asgeir Sorteberg, Tor Tørresen, and Aksel Voldsund.

Kristin Richter is thanked for providing her results on the self attraction and loading used to include this effect in our projections. The Permanent Service for Mean Sea Level (PSMSL) provided monthly tide gauge observations.

We are grateful to Ingrid Våset for help with the layout and style of the report.

The report is commissioned by the Norwegian Environment Agency under the auspices of the Norwegian Centre for Climate Services.

Bibliography

Alley, R.B., S. Anandakrishnan. K. Christianson, H.J. Horgan, A. Muto, B.R. Parizek, D. Pollard and R.T. Walker (2015). Oceanic forcing of ice-sheet retreat: West Antarctica and more. Ann. Rev. Earth Plan. Sci., 43, 7.1-7.25.

Altamimi Z, Collilieux X, Me´tivier L (2011) ITRF2008: an improved solution of the international terrestrial reference frame. J Geod 85(8):457–473. doi:10.1007/s00190–011-0444-4

Ablain, M., Cazenave, A., Valladeau, G. and Guinehut, S. (2009). A new assessment of the error budget of global mean sea level rate estimated by satellite altimetry over 1993-2008. Ocean Science. 5, pp. 193-201.

Andersen, O. B. and Knudsen, P. (1998). Global marine gravity field from the ERS-1 and Geosat geodetic mission altimetry, Journal of Geophysical Research, 103(C4), pp. 8129–8137.

Andersen, O., Egbert, G., Erofeeva, S. and Ray, R. (2006). Non-linear tides in shallow water regions from multi-mission satellite altimetry & the Andersen 06 Global Ocean Tide Model. In: AGU WPGM meeting, Beijing, China.

Arns, A., T. Wahl, S. Dangendorf and J. Jensen (2014). The impact of sea level rise on storm surge water levels in the northern part of the German Bight, Coast. Eng., doi: 10.1016/j.coastaleng.2014.12.002.

Aunan, K. and Romstad, B. (2008). Strong coasts and vulnerable communities: potential implications of accelerated sea-level rise for Norway. Journal of Coastal Research, 24(2), 403–409. West Palm Beach (Florida), ISSN 0749-0208.

Baart, F., van Gelder, P. H. A. J. M., de Ronde, J., van Koningsveld, M., and Wouters, B. (2012). The effect of the 18.6-Year Lunar Nodal Cycle on Regional Sea-Level Rise Estimates. Journal of Coastal Research, 28(2), pp. 511-516.

Bamber, J.L. and W.P. Aspinall (2013). An expert judgement assessment of future sea level rise from the ice sheets. Nature Climate Change, 3, p. 424–427, doi: 10.1038/nclimate1778.

Bard, E., B. Hamelin, and R. G. Fairbanks, 1990: U-Th ages obtained by mass spectrometry in corals from Barbados: sea level during the past 130,000 years. Nature, 346, 456-458.

Beckley, B. D., Lemoine, F. G., Luthcke, S. B., Ray, R. D., and Zelensky, N. P. (2007). A reassessment of global and regional mean sea level trends from TOPEX and Jason-1 altimetry based on revised reference frame and orbits, Geophysical Research Letters, 34, L14608.

Bindoff, N. L., Willebrand, J., Artale, V., Cazenave, A., Gregory, J., Gulev, S., Hanawa, K., Quéré, C. L., Levitus, S., Nojiri, Y., Shum, C. K., Talley, L. D., and Unnikrishnan, A.: Observations:Oceanic Climate Change and Sea Level, in: Climate Change 2007: The Physical Science Basis. Contribution of Working Group I to the Fourth Assessment Report of the Intergovernmental Panel on Climate Change, edited by: Solomon, S., Qin, D., Manning, M., Chen, Z., Marquis, M., Averyt, K. B., Tignor, M., and Miller, H. L., Cambridge University Press, Cambridge, UK and New York, NY, USA, 2007.

Blanchon, P., A. Eisenhauer, J. Fietzke, and V. Liebetrau, 2009: Rapid sea level rise and reef back-stepping at the close of the last interglacial highstand. Nature, 458, 881-884.

Bos, M.S., Williams, S. D. P., Araújo, I. B. and Bastos, L. (2013). The effect of temporal correlated noise on the sea level rate and acceleration uncertainty. Geophysical Journal International. 196(3),1423-1430, doi: 10.1093/gji/ggt481.

Brockwell, P. J. and Davis, R. A. (2002). Introduction to Time Series and Forecasting. Springer. ISBN: 0-387-95351-5

Burgette, R. J., Watson, C. S., Church, J. A., White, N. J., Tregoning, P., and Coleman, R. (2013). Characterizing and minimizing the effects of noise in tide gauge time series: relative and geocentric sea level rise around Australia. Geophysical Journal International. 194, 719-736.

Calafat, F. M., D. P. Chambers, and M. N. Tsimplis (2013). Inter-annual to decadal sea-level variability in the coastal zones of the Norwegian and Siberian Seas: The role of atmospheric forcing, J. Geophys. Res. Oceans, 118, 1287–1301, doi:10.1002/jgrc.20106.

Church, J. A. and White, N. J. (2006). A 20th century acceleration in global sea-level rise. Geophysical Research Letters, 33, L01602.

Church, J. A. and White, N. J. (2011). Sea-Level Rise from the Late 19th to the Early 21st Century. Surv. Geophys, 32, 585-602, doi:10.1007/s10712-011-9119-1.

Church, J. A., White, N. J., Konikow, L. F., Domingues, C. M., Cogley, J. G., Rignot, E., Gregory, J. M., van den Broeke, M. R., Monaghan, A. J., and Velicogna, I. (2011), Revisiting the Earth's sea-level and energy budgets from 1961 to 2008, Geophys. Res. Lett., 38, L18601, doi:10.1029/2011GL048794.

Church, J.A., P.U. Clark, A. Cazenave, J.M. Gregory, S. Jevrejeva, A. Levermann, M.A. Merrifield, G.A. Milne, R.S. Nerem, P.D. Nunn, A.J. Payne, W.T. Pfeffer, D. Stammer and A.S. Unnikrishnan (2013a): Sea Level Change. In: Climate Change 2013: The Physical Science Basis. Contribution of Working Group I

to the Fifth Assessment Report of the Intergovernmental Panel on Climate Change [Stocker, T.F., D. Qin, G.-K. Plattner, M. Tignor, S.K. Allen, J. Boschung, A. Nauels, Y. Xia, V. Bex and P.M. Midgley (eds.)]. Cambridge University Press, Cambridge, United Kingdom and New York, NY, USA.

Church, J.A., P.U. Clark, A. Cazenave, J.M. Gregory, S. Jevrejeva, A. Levermann, M.A. Merrifield, G.A. Milne, R.S. Nerem, P.D. Nunn, A.J. Payne, W.T. Pfeffer, D. Stammer and A.S. Unnikrishnan, (2013b): Sea Level Change Supplementary Material. In: Climate Change 2013: The Physical Science Basis. Contribution of Working Group I to the Fifth Assessment Report of the Intergovernmental Panel on Climate Change [Stocker, T.F., D. Qin, G.-K. Plattner, M. Tignor, S.K. Allen, J. Boschung, A. Nauels, Y. Xia, V. Bex and P.M. Midgley (eds.)]. Available from www.climatechange2013.org and www.ipcc.ch.

Collilieux X et al. 2014 External evaluation of the terrestrial reference frame: report of the taskforce of the IAG sub-commission 1.2. In Earth on the edge: science for a sustainable planet (eds C Rizos, P Willis), pp. 197–202. Berlin, Germany: Springer.

Cook, C. P. et al. (2013). Dynamic behaviour of the East Antarctic ice sheet during Pliocene warmth. Nature Geoscience 6(9), doi:10.1038/ngeo1889.

Dangendorf, S., F. M. Calafat, A. Arns, T. Wahl, I. D. Haigh, and J. Jensen (2014). Mean sea level variability in the North Sea: Processes and implications, J. Geophys. Res. Oceans, 119, 6820–6841, doi:10.1002/2014JC009901.

Debernard, J. B. and Røed, L. P. (2008). Future wind, wave and storm surge climate in the Northern Seas: a revisit, Tellus, 60A, 472–438, doi:10.1111/j/1600–0870.2008.00312.x.

Deser, C., R. Knutti, S. Solomon and A. S. Phillips (2012). Communication of the role of natural variability in future North American climate. Nature Climate Change, 2, doi: 10.1038/NCLIMATE1562.

de Vries, H., C. Katsman and S. Drijfhout (2014). Constructing scenarios of regional sea level change using global temperature pathways. Environ. Res. Lett. 9, doi:10.1088/1748-9326/9/11/115007.

Douglas, B. C. (1991). Global Sea Level Rise. Journal of Geophysical Research, 96(C4), 6981-6992.

Dutton, A., A.E. Carlson, A.J. Long, G.A. Milne, P.U. Clark, R. DeConto, B.P. Horton, S. Rahmstorf, M.E. Raymo (2015). Sea-level rise due to polar ice-sheet mass loss during past warm periods. Science 349 (6244). doi: 10.1126/science.aaa4019.

Dziewonski AM, Anderson DL (1981) Preliminary reference Earth model. Phys Earth Planet Inter 25(4):297–356. doi:10.1016/0031-9201(81)90046-7

Ekman, M.,1991. A concise history of post glacial land uplift research (from its beginning to 1950). Terra Nova 3,358–365,doi:10.1111/j.1365-3121.1991.tb00163.x.

Ekman, M., Mäkinen,J., 1996. Recent post glacial rebound, gravity change and mantle flow in Fennoscandia. Geophys.J.Int. 126,229–234, doi:10.1111/j.1365-246X.1996.tb05281.x.

Farrell, W. E., and J. A. Clark, 1976: On postglacial sea level. Geophys. J. R. Astron. Soc., 46, 647–667.

Favier L, Durand G, Cornford SL, Gudmundsson GH, Gagliardini O, et al. 2014. Retreat of Pine Island Glacier controlled by marine ice-sheet instability. Nat. Clim. Change 4:117–21

Fettweis, X., B. Franco, M. Tedesco, J. H. van Angelen, J. T. M. Lenaerts, M. R. van den Broeke, and H. Gallee, 2013: Estimating Greenland ice sheet surface mass balance contribution to future sea level rise using the regional atmospheric model MAR. Cryosphere, 7, 469–489.

Fukumori, I., O. Wang, W. Llovel, I. Fenty, G. Forget (2015). A near-uniform fluctuation of ocean bottom pressure and sea level across the deep ocean basins of the Arctic Ocean and the Nordic Seas, Progress in Oceanography, 134, doi:10.1016/j.pocean.2015.01.013.

Ghil, M., Allen, M.R., Dettinger, M.D., Ide, K., Kondrashov, D., Mann, M.E., Robertson, A.W., Saunders, A., Tian, Y., Varadi, F., Yiou, P. (2002). Advanced spectral methods for climatic time series. Reviews of Geophysics, 40 (1).

Gregory, J. M., White, N. J., Church, J. A., Bierkens, M. F. P., Box, J. E., van den Broeke, M. R., Cogley, J. G., Fettweis, X., Hanna, E., Huybrechts, P., Konikow, L. F., Leclercq, P.W., Marzeion, B., Oerlemans, J., Tamisiea, M. E., Wada, Y., Wake, L. M., and Van de Wal, R. S. W. (2012). Twentieth-century global-mean sea-level rise: is the whole greater than the sum of the parts? J. Climate, 26, doi:10.1175/JCLI-D-12-00319.1.

Griffies S.M., et al. (2014). An assessment of global and regional sea level for years 1993–2007 in a suite of interannual CORE-II simulations. Ocean Modelling, 78, doi: 10.1016/j.ocemod.2014.03.004.

Grinsted, A., J. C. Moore, and S. Jevrejeva (2010). Reconstructing sea level from paleo and projected temperatures 200 to 2100 AD. Clim. Dyn., 34, 461–472.

Hanebuth, T., K. Stattegger, and P. M. Grootes, 2000: Rapid Flooding of the Sunda Shelf: A Late-Glacial Sea level Record. Science, 288, 1033-1035.

Hanssen-Bauer, I. et al. (2009), Klima i Norge 2100. Bakgrunnsmateriale til NOU Klimatilplassing, Norsk klimasenter, september 2009, Oslo

Haug, Even (2012). Extreme value analysis of sea level observations. Technical Report of the Norwegian Mapping Authority, Hydrographic Service.
Hay, C.C., E. Morrow, R.E. Kopp, and J.X. Mitrovica (2015). Probabilistic reanalysis of twentieth-century sea-level rise, Nature, vol. 517, doi:10.1038/nature14093.
Hemer, M. A., Y. Fan, N. Mori, A. Semedo, X. L.Wang (2013). Projected changes in wave climate from a multi-model ensemble. Nature Climate Change. Doi: 10.1038/NCLIMATE1791.
Henry, O., Prandi, P., Llovel, W., Cazenave, A., Jevrejeva, S., Stammer, D., Meyssignac, B., and Koldunov. N. (2012). Tide gauge-based sea level variations since 1950 along the Norwegian and Russian coasts of the Arctic Ocean: Contribution of the steric and mass components. Journal of Geophysical Research, 117.
Herring, T., R. King, and S. McClusky (2011), Introduction to GAMIT/GLOBK release 10.4, Tech. Rep., Mass Inst. of Technol., Cambridge, U. K.
Hughes, C. W., R. J. Bingham, V. Roussenov, J. Williams, and P. L. Woodworth (2015). The effect of Mediterranean exchange flow on European time mean sea level, Geophys. Res. Lett., 42, 466–474, doi:10.1002/2014GL062654.
Hunter, J. (2012), A simple technique for estimating an allowance for uncertain sea-level rise. Climatic Change, 113, 239-252. Doi: 10.1007/s10584-011-0332-1.
Hunter, J.R., Church, J.A., White, N.J, Zhang, X. (2013) Towards a global regionally varying allowance for sea-level rise. Ocean Engineering, 71, 17-27. Doi: 10.1016/j.oceaneng.2012.12.041
Hwang, C., Peng, M.-F., Ning, J., Luo, J. and Sui, C.-H. (2005). Lake level variations in China from TOPEX/Poseidon altimetry: data quality assessment and links to precipitation and ENSO, Geophysical Journal International, 161, pp. 1–11.
IHO, Hydrographic dictionary (S-32),online publication of the printed 5th edition, 1994, retrieved October 21, 2014 from http://hd.iho.int/en/index.php/Main_Page
IPCC (2013): Summary for Policymakers. In: Climate Change 2013: The Physical Science Basis. Contribution of Working Group I to the Fifth Assessment Report of the Intergovernmental Panel on Climate Change [Stocker, T.F., D. Qin, G.-K. Plattner, M. Tignor, S.K. Allen, J. Boschung, A. Nauels, Y. Xia, V. Bex and P.M. Midgley (eds.)]. Cambridge University Press, Cambridge, United Kingdom and New York, NY, USA.
Jevrejeva, S., Grinsted, A., Moore, J. C. and Holgate, S. (2006). Nonlinear trends and multiyear cycles in sea level records. Journal of Geophysical Research, 111, C09012.
Jevrejeva, S., Moore, J. C., Grinsted, A. and Woodworth, P. L. (2008). Recent global sea level acceleration started over 200 years ago? Geophysical Research Letters, 35, L08715.
Johansson, J., et al. (2002), Continous GPS measurements of postglacial adjustment in Fennoscandia 1. Geodetic result, J. Geophys. Res.,107(B8), 2157, doi:10.1029/2001JB000400.
Joughin, I., B. E. Smith, B. Medley (2014). Marine Ice Sheet Collapse Potentially Under Way for the Thwaites Glacier Basin, West Antarctica. Science, 244, doi: 10.1126/science.1249055.
Katsman CA, Hazeleger W, Drijfhout SS, van Oldenborgh GJ, Burgers G (2008) Climate scenarios of sea level rise for the northeast Atlantic Ocean: a study including the effects of ocean dynamics and gravity changes induced by ice melt. Clim Change. doi:10.1007/s10584-008-9442-9
Kendall, R., Latychev, K., Mitrovica, J.X., Davis, J.E., and Tamisiea, M. (2006). Decontaminating tide gauge records for the influence of Glacial Isostatic Adjustment: the potential impact of 3-D Earth structure, Geophys. Res. Lett., 33, L24318, doi:10.1029/2006GL028448.
Kierulf, H. P., M. Ouassou, M. J. R. Simpson, and O. Vestøl (2012), A continuous velocity field for Norway, J. Geod., 87, 337–349, doi:10.1007/s00190-012-0603-2.
Kierulf, H. P., H. Steffen, M. J. R. Simpson, M. Lidberg, P. Wu, and H. Wang (2014), A GPS velocity field for Fennoscandia and a consistent comparison to glacial isostatic adjustment models, J. Geophys. Res. Solid Earth, 119, doi:10.1002/2013JB010889.
Kopp, R. et al. (2009), Probabilistic assessment of sea level during the last interglacial stage. Nature, doi:10.1038/nature08686.
Kopp, R. E., R. M. Horton, C. M. Little, J. X. Mitrovica, M. Oppenheimer, D. J. Rasmussen, B. H. Strauss, and C. Tebaldi (2014), Probabilistic 21st and 22nd century sea-level projections at a global network of tide-gauge sites, Earth's Future, 2, 383–406, doi:10.1002/2014EF000239.
Kouraev, A. V., Zakharova, E. A., Samain, O., Mognard, N. M. and Cazenave, A. (2004). Ob' river discharge from TOPEX/Poseidon satellite altimetry (1992-2002), Remote Sensing of Environment, 93, pp. 238–245.
Lambeck K, Smither C, Johnston P (1998) Sea-level change, glacial rebound and mantle viscosity for northern Europe. Geophys J Int 134:102–144
Landerer FW, Jungclaus JH, Marotzke J (2007) Regional dynamic and steric sea level change in response to the IPCC-A1B scenario. J Phys Oceanogr 37:296–312

Levermann, A., Winkelmann, R., Nowicki, S., Fastook, J. L., Frieler, K., Greve, R., Hellmer, H. H., Martin, M. A., Meinshausen, M., Mengel, M., Payne, A. J., Pollard, D., Sato, T., Timmermann, R., Wang, W. L., and Bindschadler, R. A. (2014). Projecting Antarctic ice discharge using response functions from SeaRISE ice-sheet models, Earth Syst. Dynam., 5, 271-293, doi:10.5194/esd-5-271-2014.

Lidberg, M., J. Johansson, H. G. Scherneck, and J. Davis (2007), An improved and extended GPS-derived velocity field for the glacial isostatic adjustment in Fennoscandia, J. Geod., 81(3), 213–230, doi:10.1007/s00190-006-0102-4.

Lidberg, M., J. M. Johansson, H. G. Scherneck, and G. A. Milne (2010), Recent results based on continuous GPS observations of the GIA process in Fennoscandia from BIFROST, J. Geodyn., 50(1), 8–18, doi:10.1016/j.jog.2009.11.010.

Lisiecki, L., and M. Raymo, 2005: A Pliocene-Pleistocene stack of 57 globally distributed benthic δ18O records. Paleoceanography, 20, PA1003.

Little, C. M., Oppenheimer, M., and Urban, N. M. (2013a). Upper bounds on twenty-first-century Antarctic ice loss assessed using a probabilistic framework, Nat. Clim. Change, 3, 654–659, doi:10.1038/nclimate1845.

Little, C. M., Urban, N. M., and Oppenheimer, M. (2013b). Probabilistic framework for assessing the ice sheet contribution to sea level change., Proc. Natl. Acad. Sci. USA, 110, 3264–3269.

Little, C., R.M. Horton, R.E. Kopp, M. Oppenheimer, S. Yip (2014). Uncertainty in Twenty-First-Century CMIP5 Sea Level Projections. J. Climate, 28, doi: 10.1175/JCLI-D-14-00453.1.

Lohne, Ø. S., S. Bondevik, J. Mangerud, J. I. Svendsen (2007). Sea-level fluctuations imply that the Younger Dryas ice-sheet expansion in western Norway commenced during the Allerød. Quaternary Science Reviews 26, doi: 10.1016/j.quascirev.2007.04.008.

Lysaker, D. I. (2009). Mean dynamic topography (MDT) and geostrophic surface currents in the Fram Strait derived from geodetic data, Marine Geodesy, 32(1), 42-63, doi: 10.1080/01490410802662029.

Masson-Delmotte, V., M. Schulz, A. Abe-Ouchi, J. Beer, A. Ganopolski, J.F. González Rouco, E. Jansen, K. Lambeck, J. Luterbacher, T. Naish, T. Osborn, B. Otto-Bliesner, T. Quinn, R. Ramesh, M. Rojas, X. Shao and A. Timmermann (2013). Information from Paleoclimate Archives. In: Climate Change 2013: The Physical Science Basis. Contribution of Working Group I to the Fifth Assessment Report of the Intergovernmental Panel on Climate Change [Stocker, T.F., D. Qin, G.-K. Plattner, M. Tignor, S.K. Allen, J. Boschung, A. Nauels, Y. Xia, V. Bex and P.M. Midgley (eds.)]. Cambridge University Press, Cambridge, United Kingdom and New York, NY, USA.

Marcos, M. and Tsimplis, M. N. (2007). Forcing of coastal sea level rise patterns in the North Atlantic and the Mediterranean Sea. Geophysical Research Letters, 34, L18604.

Mawdsley, R.J., I.D. Haigh and N.C. Wells (2015). Global secular changes in different tidal high water, low water and range levels. Earth's Future, 3 (2), doi: 10.1002/2014EF000282.

McKay, N. P., J. T. Overpeck, and B. L. Otto-Bliesner, 2011: The role of ocean thermal expansion in Last Interglacial sea level rise. Geophysical Research Letters, 38, L14605.

Meehl GA, Stocker TF, Collins WD, Friedlingstein P, Gaye A, Gregory J, Kitoh A, Knutti R, Murphy J, Noda A, Raper S, Watterson I, Weaver A, Zhao ZC (2007) Global climate projections. In: Solomon S, Qin D, Manning M, Chen Z, Marquis M, Averyt KB, Tignor M, Miller HL (eds), Climate change 2007: the physical science basis. Contribution of working group I to the 4th assessment report of the intergovernmental panel on climate change. Cambridge University Press, Cambridge.

Menéndez, M., and P. L. Woodworth (2010), Changes in extreme high water levels based on a quasi‐global tide‐gauge data set, J. Geophys. Res., 115, C10011, doi:10.1029/2009JC005997.

Mercier, F., Rosmorduc, V., Carrere, L., & Thibaut, P. (2010). Coastal and Hydrology Altimetry product (PISTACH) handbook, CLS-DOS-NT-10-246, SALP-MUP-OP-16031-CN, 01/00, Version 1.0, October 4th.

Milne, G. A., and J. X. Mitrovica, 1998: Postglacial sea-level change on a rotating Earth. Geophys. J. Int., 133, 1–19.

Milne GA, Davis JL, Mitrovica JX, Scherneck H-G, Johansson JM, Vermeer M, Koivula H (2001) Space-geodetic constraints on glacial isostatic adjustment in Fennoscandia. Science 291:2381–2385. doi:10.1126/science.1057022

Milne GA, Mitrovica JX, Scherneck HG, Davis JL, Johansson JM (2004) Continuous GPS measurements of postglacial adjustment in Fennoscandia: 2. modeling results. J Geophys Res 109(B02412). doi:10.1029/2003JB002619

Milne GA, Gehrels WR, Hughes CW, Tamisiea ME (2009) Identifying the causes for sea-level change. Nat Geosci 2:471–478. doi:10.1038/NGEO544

Minster, J. B., Z. Altamimi, G. Blewitt, W. E. Carter, A. Cazenave, H. Dragert, T. A. Herring, K. M. Larson, J. C. Ries, D. T. Sandwell, J. M. Wahr, J. L. Davis, D. A. Feary, L. A. Shanley, N. D. Rogers, C. R. Gibbs, J. E. Edkin (2010). Precise Geodetic Infrastructure: National Requirements for a Shared

Resource. The National Academies Press. ISBN 978-0-309-15811-4. Available at http://www.nap.edu/openbook.php?record_id=12954.
Mitrovica, J. X., M. E. Tamisiea, J. L. Davis, and G. A. Milne (2001), Recent mass balance of polar ice sheets inferred from patterns of global sea-level change, Nature, 409, 1026–1029.
Næss, A. and Gaidai, O. (2009) Estimation of extreme values from sampled time series. Structural Safety, 31, 325-334, doi: 10.1016/j.strusafe.2008.06.021
Naish, T., et al., 2009: Obliquity-paced Pliocene West Antarctic ice sheet oscillations. Nature, 458, 322-384.
Nick, F. M., et al., 2013: Future sea-level rise from Greenland's major outlet glaciers in a warming climate. Nature, 497, 235–238.
Nilsen, J.E.Ø., H. Drange, K. Richter, E. Jansen, A. Nesje (2012a). Changes in the past, present, and future sea level on the coast of Norway. NERSC Special Report 89, Bergen, Norway. 48 pp. Available at http://www.nersc.no/node/14468
Nilsen, J.E.Ø., H. Drange, K. Richter (2012b). Havnivået stiger. In 2°C - Status fra klimavitenskapen, No 1, November 2012, Norway, p 20-21.
Nilsen, J.E.Ø., K. Larsen, K. Harvold, V. Martens, T. Rauken and J. Taylor. (2013). Kulturminner og havnivåstigning (Cultural Heritage and Sea Level Rise). *CIENS-rapport* 1-2013, Oslo, Norway. 52 pp. Available at http://www.ciens.no/Data/0/227.pdf.
Olesen, O., H. P. Kierulf, M. Brönner, E. Dalsegg, O. Fredin, and T. Solbakk (2013), Deep weathering, neotectonics and strandflat formation in Nordland, northern Norway, Norwegian J. Geol., 93(3-4), 189–213.
Pardaens AK, Gregory JM, Lowe JA (2011) A model study of factors influencing projected changes in regional sea level over the twenty-first century. Clim Dyn 36:2015–2033. doi:10.1007/s00382-009-0738-x
Peltier, W. R., 2004: Global glacial isostasy and the surface of the ice-age earth: The ICE-5G (VM2) model and GRACE. Annu. Rev. Earth Planet. Sci., 32, 111–149.
Peltier, W.R. (2009). Closure of the budget of global sea level rise over the GRACE era: the importance and magnitudes of the required corrections for global glacial isostatic adjustment, Quaternary Science Reviews, 28(17-18), pp. 1658-1674.
Pickering, M. D., N. C. Wells, K. J. Horsburgh, and J. A. M. Green (2012), The impact of future sea-level rise on the European Shelf tides, Cont. Shelf Res., 35(0), 1–15, doi:10.1016/j.csr.2011.11.011.
Pollard, D., and R. M. DeConto, 2009: Modelling West Antarctic ice sheet growth and collapse through the past five million years. Nature, 458, 329-332.
Prandi, P., Ablain, M., Cazenave, A., and Picot, N. (2012). Sea level variability in the Arctic Ocean observed by satellite altimetry. Ocean Science Discussions, 8, 2375-2401.
Proshutinsky, A., V. Pavlov, and R. H. Bourke (2001), Sea level rise in the Arctic Ocean, Geophys. Res. Lett., 28(11), 2237–2240, doi:10.1029/2000GL012760.
Proshutinsky, A., I. M. Ashik, E. N. Dvorkin, S. Häkkinen, R. A. Krishfield, and W. R. Peltier (2004), Secular sea level change in the Russian sector of the Arctic Ocean, J. Geophys. Res., 109, C03042, doi:10.1029/2003JC002007.
Purkey, S. G., G. C. Johnson, and D. P. Chambers. (2014). Relative contributions of ocean mass and deep steric changes to sea level rise between 1993 and 2013. Journal of Geophysical Research, 119, 7509-7522, doi:10.1002/2014JC010180.
Rahmstorf, S. (2007). A semi-empirical approach to projecting future sea-level rise. Science, 315, 368–370.
Rhein, M., Rintoul, S.R., Aoki, S., Campos, E., Chambers, D., Feely, R.A., Gulev, S., Johnson, G.C., Josey, S.A., Kostianoy, A., Mauritzen, C., Roemmich, D., Talley, L.D., and Wang, F. (2013): Observations: Ocean. In: Climate Change 2013: The Physical Science Basis. Contribution of Working Group I to the Fifth Assessment Report of the Intergovernmental Panel on Climate Change (Stocker, T.F., D. Qin, G.-K. Plattner, M. Tignor, S.K. Allen, J. Boschung, A. Nauels, Y. Xia, V. Bex and P.M. Midgley (eds.)). Cambridge University Press, Cambridge, United Kingdom and New York, NY, USA.
Richter, K., J.E.Ø. Nilsen, H. Drange (2012a). Contributions to sea level variability along the Norwegian coast for 1960-2010. J. Geophys. Res., 117, doi:10.1029/2009JC007826.
Richter, K., O. H. Segtnan, and T. Furevik (2012b). Variability of the Atlantic inflow to the Nordic Seas and its causes inferred from observations of sea surface height, J. Geophys. Res., 117, C04004, doi:10.1029/2011JC007719.
Richter, K., R. E. M. Riva, H. Drange (2013). Impact of self-attraction and loading effects induced by shelf mass loading on projected regional sea level rise. Geophys. Res. Lett., 40 (1–5), doi: 10.1002/grl.50265
Rignot, E., J. Mouginot, M. Morlighem, H. Seroussi, and B. Scheuchl (2014), Widespread, rapid grounding line retreat of Pine Island, Thwaites, Smith, and Kohler glaciers, West Antarctica, from 1992 to 2011, Geophys. Res. Lett., 41, 3502–3509, doi:10.1002/2014GL060140.
Riva, R. E. M., J. L. Bamber, D. A. Lavallee, and B. Wouters (2010), Sea level fingerprint of continental water and ice mass change from GRACE, Geophys. Res. Lett., 37, L19605, doi:10.1029/2010GL044770

Roblou, L., Lyard, F., Le Hena, M., & Maraldi, C. (2007). X-TRACK, a new processing tool for altimetry in coastal oceans, in Proceedings of the Envisat Symposium 2007, Montreux Switzerland, pp. 23-27 April 2007 .

Roblou, L., Lamouroux, J., Bouard, J., Lyard, F., Le Hena, M., Lombard, A., Marsaleix, P., De Mey, P., and Birol, F. (2011). Post-processing altimeter data towards coastal applications and integration into coastal models., In Coastal altimetry, pp. 217-246, ISBN 978-3–642-12795-3.

Rohling, E. J., K. Grant, M. Bolshaw, A. P. Roberts, M. Siddall, C. Hemleben, and M. Kucera, 2009: Antarctic temperature and global sea level closely coupled over the past five glacial cycles. Nature Geoscience, 2, 500- 504.

Sande, H. and Ravndal, O. R. (2015). Ekstremverdianalyse av vannstandsdata langs norskekysten, Technical Report of the Norwegian Mapping Authority, Hydrographic Service. In prep.

Seneviratne, S.I., N. Nicholls, D. Easterling, C.M. Goodess, S. Kanae, J. Kossin, Y. Luo, J. Marengo, K. McInnes, M. Rahimi, M. Reichstein, A. Sorteberg, C. Vera, and X. Zhang, 2012: Changes in climate extremes and their impacts on the natural physical environment. In: Managing the Risks of Extreme Events and Disasters to Advance Climate Change Adaptation [Field, C.B., V. Barros, T.F. Stocker, D. Qin, D.J. Dokken, K.L. Ebi, M.D. Mastrandrea, K.J. Mach, G.-K. Plattner, S.K. Allen, M. Tignor, and P.M. Midgley (eds.)]. A Special Report of Working Groups I and II of the Intergovernmental Panel on Climate Change (IPCC). Cambridge University Press, Cambridge, UK, and New York, NY, USA, pp. 109-230.

Scherneck, H-G, J. M. Johansson, J. X. Mitrovica, and J. L. Davis (1998), The BIFROST project: GPS determined 3-D displacement rates in Fennoscandia from 800 days of continuous observations in the SWEPOS network, Tectonophysics, 294, 305–321, doi:10.1016/S0040-1951(98)00108-5.

Skjong, M., Næss, A. and Næss, O. E. B (2013). Statistics of extreme sea levels for locations along the Norwegian coast. Journal of Coastal Research, 29-5, 1029-1048, doi: 10.2112/jcoastres-d-12-00208.1

Simpson, M., Breili, K., Kierulf, H. P., Lysaker, D., Ouassou, M., and Haug, E. (2012). Estimates of Future Sea-Level Changes for Norway. Technical Report of the Norwegian Mapping Authority.

Simpson, M., Breili, K., Kierulf, H.P., (2014). Estimates of twenty-first century sea-level changes for Norway. Clim. Dyn. 42, 6613–6629. doi:10.1007/s00382-013-1900-z.

Slangen, A. B. A., van de Wal, R. S. W., Wada, Y., and Vermeersen, L. L. A. (2014). Comparing tide gauge observations to regional patterns of sea-level change (1961–2003). Earth Syst. Dynam., 5, doi:10.5194/esd-5-243-2014.

Smith, A. J. E., Ambrosius, B. A. C. and Wakker, K. F. (2000). Ocean tides from T/P, ERS1, and GEOSAT altimetry. Journal of Geodesy, 74, pp. 399–413.

Stammer, D., 2008: Response of the global ocean to Greenland and Antarctic ice melting. J. Geophys. Res. Oceans, 113, C06022.

Stammer, D., N. Agarwal, P. Herrmann, A. Kohl, and C. R. Mechoso, 2011: Response of a coupled ocean-atmosphere model to Greenland ice melting. Surv. Geophys., 32, 621–642.

Stabell, B., Krzywinski, K. (1978). Strandforskyvningsundersøkelsen. In: Myhre, B. (Ed.), Statfjord Transportation System Project. Ilandføring av olje på Sotra. De arkeologiske undersøkelser 1978. Vindenes. Historisk museum, Universitetet i Bergen, pp. 93–132.

Steffen H, Kaufmann G (2005) Glacial isostatic adjustment of Scandinavia and northwestern Europe and the radial viscosity structure of the Earth's mantle. Geophys J Int 163(2):801–812. doi:10.1111/j.1365-246X.2005.02740.x

Steffen, H., Gitlein,O., Denker,H., Müller,J., Timmen,L., (2009). Present rate of uplift in Fennoscandia from GRACE and absolute gravimetry. Tectonophysics 474(1–2), 69–77, doi:10.1016/j.tecto.2009.01.012.

Steffen H, Wu P (2011) Glacial isostatic adjustment in Fennoscandia - a review of data and modeling. J Geodyn 52(3–4):160–2004. doi:10.1016/j.jog.2011.03.002

Sterl A, van den Brink HW, de Vries H, Haarsma R, van Meijgaard E (2009) An ensemble study of extreme North Sea storm surges in a changing climate. Ocean Sci 5:369–378. doi:10.5194/os-5-369-2009.

Stocker, T.F., D. Qin, G.-K. Plattner, L.V. Alexander, S.K. Allen, N.L. Bindoff, F.-M. Bréon, J.A. Church, U. Cubasch, S. Emori, P. Forster, P. Friedlingstein, N. Gillett, J.M. Gregory, D.L. Hartmann, E. Jansen, B. Kirtman, R. Knutti, K. Krishna Kumar, P. Lemke, J. Marotzke, V. Masson-Delmotte, G.A. Meehl, I.I. Mokhov, S. Piao, V. Ramaswamy, D. Randall, M. Rhein, M. Rojas, C. Sabine, D. Shindell, L.D. Talley, D.G. Vaughan and S.-P. Xie, 2013: Technical Summary. In: Climate Change 2013: The Physical Science Basis. Contribution of Working Group I to the Fifth Assessment Report of the Intergovernmental Panel on Climate Change [Stocker, T.F., D. Qin, G.-K. Plattner, M. Tignor, S.K. Allen, J. Boschung, A. Nauels, Y. Xia, V. Bex and P.M. Midgley (eds.)]. Cambridge University Press, Cambridge, United Kingdom and New York, NY, USA.

Tamisiea, M. E. and Mitrovica. J. X. (2011). The moving boundaries of sea level change: Understanding the origins of geographic variability. Oceanography, 24(2), pp. 24–39, doi:10.5670/oceanog.2011.25.

Tarasov, L., Dyke, A.S., Neal, R.M. and Peltier, W.R. (2012). A data-calibrated distribution of deglacial chronologies for the North American ice complex from glaciological modelling, Earth and Plan. Sci. Let, 315–316, pp. 30–40, doi:10.1016/j.epsl.2011.09.010.
Taylor, K., Stouer, R.J. and Meehl, G.A. (2012) An overview of CMIP5 and the experiment design. Bull Am Meteorol Soc 93(4):485498, doi:10.1175/BAMS-D-11-00094.1
Trenberth, K.E., P.D. Jones, P. Ambenje, R. Bojariu, D. Easterling, A. Klein Tank, D. Parker, F. Rahimzadeh, J.A. Renwick, M. Rusticucci, B. Soden and P. Zhai, 2007: Observations: Surface and Atmospheric Climate Change. In: Climate Change 2007: The Physical Science Basis. Contribution of Working Group I to the Fourth Assessment Report of the Intergovernmental Panel on Climate Change [Solomon, S., D. Qin, M. Manning, Z. Chen, M. Marquis, K.B. Averyt, M. Tignor and H.L. Miller (eds.)].
Tushingham AM, Peltier WR (1991) Ice–3G: a new global model of late Pleistocene deglaciation based upon geophysical predictions of post-glacial relative sea level change. J Geophys Res 96:4497–4523. doi:10.1029/90JB01583
van den Berk, J. and S.S. Drijfhout (2014). A realistic freshwater forcing protocol for ocean-coupled climate models. Ocean Modelling, 81, doi: 10.1016/j.ocemod.2014.07.003
Vasskog, K. et al. (2009), Havnivåstigning. Estimater av framtidig havnivåstigning i norske kystkommuner. Det nasjonale klimatilpasningssekretariatet ved Direktoratet for samfunnssikkerhet og beredskap, september 2009, Tønsberg
Vautard, R., Julien Cattiaux, Pascal Yiou, Jean-Noël Thépaut og Philippe Ciais (2012). Northern Hemisphere atmospheric stilling partly attributed to an increase in surface roughness. Nature Geoscience, 3, doi:10.1038/ngeo979.
Vermeer, M., and S. Rahmstorf (2009). Global sea level linked to global temperature. Proc. Natl. Acad. Sci. U.S.A., 106, 21527–21532.
Vestøl, O. (2006). Determination of postglacial land uplift in Fennoscandia from leveling, tide-gauges and continuous GPS stations using least squares collocation. Journal of Geodesy, 80, pp. 248–258.
Vignudelli, S., Cipollini, P., Gommenginger, C., Gleason, S., Snaith, H.M., Coelho, H., Fernandes, M.J., Lázaro, C., Nunes, A.L., Gómez-Enri, J., Martin-Puig, C., Woodworth, P., Dinardo, S., and Benveniste J. (2011). Satellite altimetry: sailing closer to the coast, in Remote Sensing of the Changing Oceans, Springer, pp. 217-238.
Vignudelli, S., Kostianoy, A.G., Cipollini, P., and Benveniste, J. (Eds.) (2011). Coastal altimetry. Springer.
Vincent, P., Desai, S.D., Dorendeu, J., Ablain, M., Soussi, B., Callahan, P.S., and Haines, B.J. (2003). Jason-1 Geophysical Performance Evaluation. Marine Geodesy, 26, 167-186, doi: 10.1080/714044517.
Volkov, D. L. and Pujol, M.-I. (2012). Quality assessment of a satellite altimetry data product in the Nordic, Barents, and Kara seas. Journal of Geophysical Research, 117, CO3025, doi: 10.1029/2011JC007557.
Wahl, T., Haigh, I.D., Dangendorf, S., and Jensen, J., 2013. Inter-annual and long-term mean sea level changes along the North Sea coastline. In: Conley, D.C., Masselink, G., Russell, P.E. and O'Hare, T.J. (eds.), Proceedings 12th International Coastal Symposium (Plymouth, England), Journal of Coastal Research, 65, pp. 1987-1992.
Christopher S. Watson, Neil J. White, John A. Church, Matt A. King, Reed J. Burgette, Benoit Legresy (2015). Unabated global mean sea-level rise over the satellite altimeter era. Nature Climate Change, doi:10.1038/nclimate2635.
Woodward, R.S. (1888) On the form and position of the sea level with special references to its dependence on superficial masses symmetrically disposed about a normal to the earth's surface. USGS Bull. 48.
Woodworth, P. L. and Player, R. (2003). The permanent service for mean sea level: An update to the 21st century. Journal of Coastal Research, 19, pp. 287–295.
Yin J, Griffies SM, Stouffer RJ (2010) Spatial variability of sea-level rise in the twenty-first century projections. J Clim 23:4585–4607. doi:10.1175/2010JCLI3533.1
Zhao, S., K. Lambeck, and M. Lidberg (2012), Lithosphere thickness and mantle viscosity inverted from GPS-derived deformation rates in Fennoscandia, Geophys. J. Int., 190(1), 278–292, doi:10.1111/j.1365-246X.2012.05454.x.
Østerhus, S., and T. Gammelsrød (1999), The abyss of the Nordic seas is warming, J. Clim., 12, 3297–3304.

Appendix

In this report we provide projections of sea level change and return heights for extreme water levels for all coastal municipalities on mainland Norway.

In general, the sea level change and return heights are given for the administration centre of the municipality, as long as it is at the coast. As the tidal pattern varies significantly along the Norwegian coast, there can be large differences within a municipality. If the return heights or tidal pattern differ largely relative to the administration center within the municipality, one or two additional locations for this municipality have been included. In practice, this means that for any location in a municipality, there can be a 15–20 cm difference between the return heights at that location and the return heights given in Table A.1.2. For the practical use of Tables A.1.2 and A.2.1–3, one should choose the numbers given for the administrative centre, or the location within the municipality with the tidal pattern most similar to the location of interest.

On www.kartverket.no/sehavniva, which is an internet site for tide, sea level and land uplift information, provided by the Norwegian Mapping Authority, it is possible to find return heights and land uplift values for any given position along the Norwegian coast. We recommend that the return heights found in this report are used for planning purposes, as they are the official numbers. An exception would be for the municipalities where return heights are not available, due to insufficient data. For some of these locations, the return levels could become available at www.kartverket.no/sehavniva in the future.

The projections of sea level change and return heights use mean sea level as reference level. Other geospatial information usually refer to other reference levels. In Appendix A.1 we start by presenting the most important reference levels used and some information on the offset values between relevant levels. We then provide return heights for all but two coastal municipalities. In Appendix A.2, we present the projected sea level change for the time periods and scenarios described in the report, at the municipalities.

A.1 Return heights and Land Map Elevation Levels

A.1.1 Overview of important reference levels

Figure A.1 shows how different important reference levels relate to each other, and we discuss the most important levels below. Note in particular that even though heights in maps etc. are normally said to be meters above sea level, the zero level for height on land does not equal mean sea level.

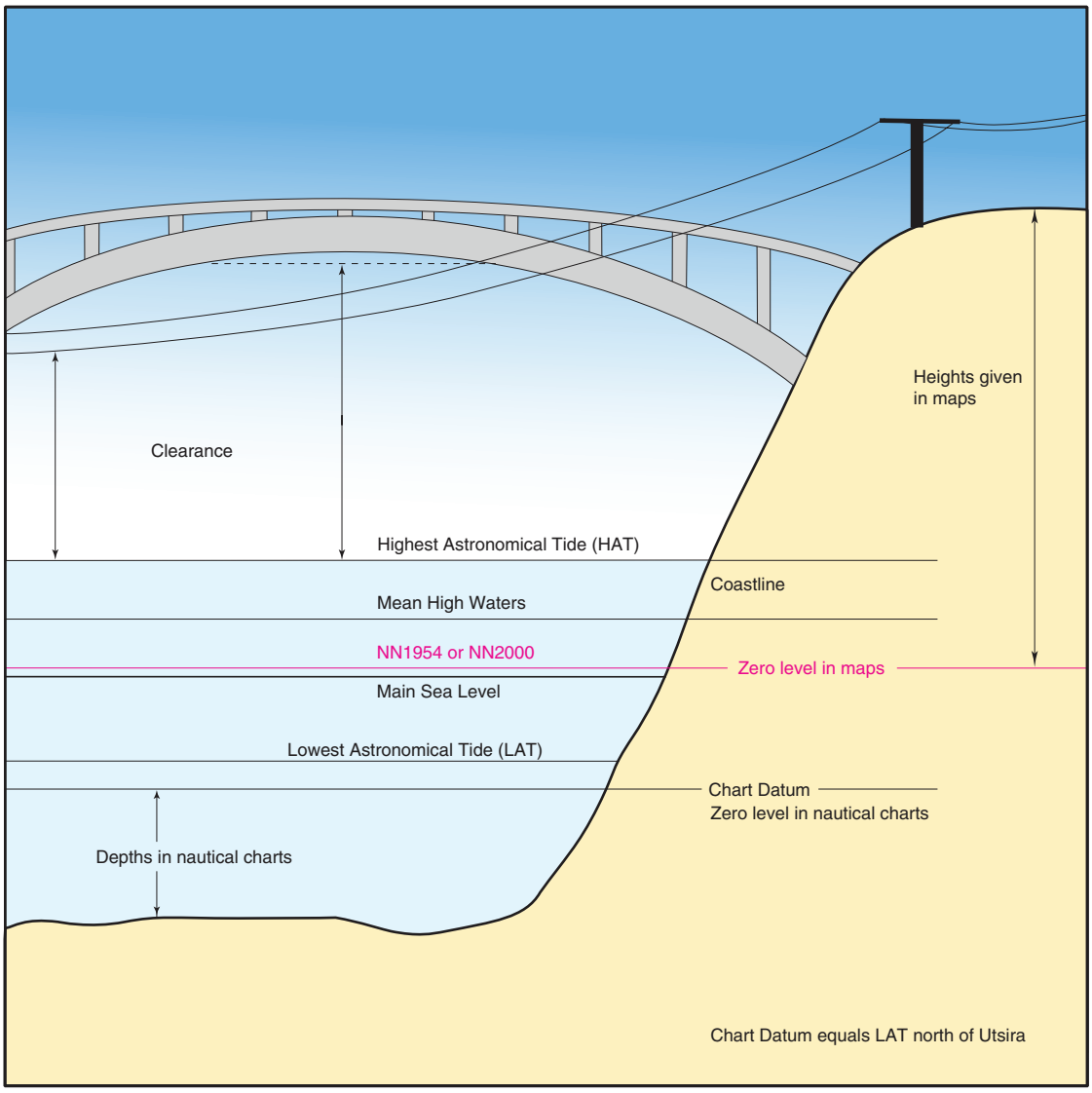

Figure A.1 The relationship between different reference levels.

Mean Sea Level is the average height of the observed surface of the sea over a 19-year period. For consistency purposes, the period used to calculate the mean sea level should be given. All return heights in this report refer to Mean Sea Level (1996–2014), which from September 2015 is the official mean sea level in Norway.

NN1954 / NN2000: Normalnull 1954 (NN1954) and Normalnull 2000 (NN2000) are the names of the two national vertical reference systems currently in use in Norway. NN1954 is the oldest system, as of 2011 it is gradually replaced by NN2000. At the tide gauges along the Norwegian coast the difference between NN1954 and NN2000 varies between -17 cm and 16 cm. The largest difference gradient is found around Vestfjorden in the north of Norway. Across the fjord from Kabelvåg in Lofoten to Narvik, the offset value between the two systems changes from 1 cm in Kabelvåg to 11 cm in Narvik (see Table A.1.1). These differences are mainly due to errors in the old NN1954 height system. The discrepancies between the two systems are significant and must be taken into account in land use planning when considering future sea levels or storm surges. See Appendix A.1.2 on how to transfer heights relative to mean sea level to either NN1954- or NN2000-heights.

The Highest Astronomical Tide (HAT) is defined by the International Hydrographic Organisation as being "the highest tidal level which can be predicted to occur under average meteorological conditions and under any combination of astronomical conditions" (IHO, 2014). In practice HAT is determined by taking the highest predicted tide over a period of 19 years, which ensures that all combinations of astronomical conditions are considered. HAT is thus the highest possible tide not taking into account the effect of storm surges.

The Lowest Astronomical Tide (LAT) is the lowest predictable tide under any combination of astronomical conditions. Similar to HAT, LAT is determined by taking the lowest predicted tide over a period of 19 years.

Chart Datum is the zero level of nautical charts to which all depths are given. For safety reasons, Chart Datum is defined to be a level the actual water level seldom sinks below. North of Utsira, Chart Datum is equal to LAT. For the southern and south-eastern coast where the water level can be completely dominated by the weather effects, Chart Datum is defined to be 20 or 30 cm below LAT.

A.1.2 How to Transfer Heights from Mean Sea Level to NN1954 or NN2000

The projections of sea level and the return heights are all given relative to mean sea level. In order to refer heights given relative to mean sea level to one of the national height systems, an offset must be subtracted. These offsets vary from a few centimetres at some locations to 20–30 cm in others.

The relationship between NN1954/NN2000 and mean sea level is well known at the tide gauges where you are very close to a well established benchmark and where the mean sea level is precisely determined. Table A.1.1 lists the offset values at these locations. Note that you have to subtract the given number to get the correct height in NN1954 or NN2000.

If you are far from a permanent tide gauge, this offset value is usually not very well known. One solution is to interpolate between the two nearest tide gauges. For most locations we can assume the offset found this way has a standard error smaller than 2 cm. Note however, that we have experienced errors with this approach reaching 10 cm, so when correct heights are crucial, this method is not recommended. For precise and reliable determination far from the permanent tide gauges, a temporary tide gauge connected to a reliable benchmark with known heights in the national height system, is the only solution to find the offset. The offset values you find on www.kartverket.no/sehavniva under "Water levels" ("Vannstandsnivå") are for a given location mostly based on interpolation between tide gauges, but for some locations the offset has been updated based on measurement from a temporary tide gauge connected to a reliable bench mark.

Table A.1.1 Offset values for the tide gauges to be used when reducing a height referring to mean sea level to a height in NN1954 or NN2000. Numbers are given in centimetres.

Tide gauge	For NN2000 subtract	For NN1954 subtract
Vardø	25	15
Honningsvåg	22	12
Hammerfest	19	8
Tromsø	18	6
Andenes	15	4
Harstad	17	7
Narvik	12	11
Kabelvåg	11	1
Bodø	12	17
Rørvik	11	19
Trondheim	5	18
Heimsjø	7	8
Kristiansund	6	8
Ålesund	5	3
Måløy	4	1
Bergen	7	-3
Stavanger	9	2
Tregde	9	-2
Helgeroa	6	9
Oscarsborg	2	15
Oslo	3	18
Viker	3	15

A.1.3 Return Heights for all Localities/municipalities

Table A.1.2 lists the 20, 200 and 1000-year return heights for almost all coastal municipalities in Norway. These are the new official numbers. For locations away from a permanent tide gauge the extrapolation approach is different compared to earlier methods, see Chapter 6 for details. Return heights for other periods can be found at www.kartverket.no/sehavniva.

One or two asterisks behind the name of a municipality indicates that there are one or two additional locations listed for this municipality. Please be sure to choose the location that best represents the tidal pattern at your place of interest. Note also the comments and footnotes added to locations.

All numbers are in centimetres above mean sea level (1996–2014). Consult Appendix A.1.2 on how to transfer heights to NN1954 or NN2000 which are the two national height systems used in maps. The closest tide gauge listed in the table may then be useful

Table A.1.2 Return heights in centimetres above mean sea level (1996–2014), with confidence intervals in parentheses. Numbers are given for all but two municipalities, and some have more than one location for which the estimation is done. Names of the closest tide gauge station are given. The table is subdivided into counties.

Municipality	Location	Closest Tide Gauge	20 year return height	200 year return height	1000 year return height
Finnmark					
Sør-Varanger	Kirkenes	VARDØ	229 (219, 236)	246 (232, 255)	257 (239, 268)
Nesseby	Varangerbotn	VARDØ	232 (225, 239)	249 (241, 259)	260 (250, 271)
Vadsø	Vadsø	VARDØ	229 (219, 236)	246 (232, 255)	257 (239, 268)
Vardø	Vardø	VARDØ	219 (212, 226)	237 (228, 246)	248 (237, 258)
Båtsfjord	Båtsfjord	VARDØ	206 (198, 213)	224 (214, 232)	234 (223, 245)
Berlevåg	Berlevåg	VARDØ	198 (190, 205)	216 (204, 225)	227 (213, 237)
Tana	Smalfjord	HONNINGSVÅG	205 (194, 212)	225 (209, 234)	237 (218, 248)
Gamvik	Mehamn	HONNINGSVÅG	201 (190, 208)	221 (205, 230)	233 (214, 244)
Lebesby	Kjøllefjord	HONNINGSVÅG	201 (190, 208)	221 (205, 230)	233 (214, 244)
Nordkapp	Honningsvåg	HONNINGSVÅG	201 (190, 208)	221 (205, 230)	233 (214, 244)
Porsanger	Lakselv	HONNINGSVÅG	215 (204, 222)	235 (219, 244)	247 (228, 258)
Måsøy	Havøysund	HAMMERFEST	196 (186, 202)	214 (199, 222)	225 (206, 234)
Kvalsund	Kvalsund	HAMMERFEST	198 (188, 204)	215 (201, 223)	226 (208, 236)
Hammerfest	Hammerfest	HAMMERFEST	201 (191, 207)	219 (203, 227)	229 (211, 239)
Hasvik	Breivikbotn	HAMMERFEST	201 (191, 207)	219 (203, 227)	229 (211, 239)
Alta	Alta	HAMMERFEST	206 (199, 212)	224 (215, 232)	235 (225, 244)
Loppa	Øksfjord	HAMMERFEST	206 (199, 212)	224 (215, 232)	235 (225, 244)
Troms					
Kvænangen	Burfjord	TROMSØ	216 (209, 220)	233 (225, 239)	244 (234, 250)
Kvænangen	Kjækan	TROMSØ	173 (167, 177)	190 (182, 195)	201 (191, 207)
Nordreisa	Storslett	TROMSØ	214 (208, 219)	232 (223, 237)	243 (233, 249)
Skjervøy	Skjervøy	TROMSØ	216 (209, 220)	233 (225, 239)	244 (234, 250)
Kåfjord	Olderdalen	TROMSØ	216 (209, 220)	233 (225, 239)	244 (234, 250)
Storfjord	Hatteng	TROMSØ	216 (209, 220)	233 (225, 239)	244 (234, 250)
Lyngen	Lyngseidet	TROMSØ	216 (209, 220)	233 (225, 239)	244 (234, 250)
Karlsøy	Hansnes	TROMSØ	212 (205, 216)	229 (221, 235)	240 (230, 246)

Municipality	Location	Closest Tide Gauge	20 year return height	200 year return height	1000 year return height
Karlsøy	Nordvardvika	ANDENES	201 (187, 209)	224 (204, 235)	238 (215, 252)
Tromsø	Tromsø (Sør for Tromsøybrua)	TROMSØ	203 (197, 207)	221 (213, 226)	232 (222, 237)
Tromsø	Ersfjordbotn (Vest for Kvaløya)	ANDENES	190 (177, 199)	214 (194, 225)	229 (205, 242)
Tromsø	Snarby	TROMSØ	213 (206, 217)	230 (222, 236)	241 (231, 247)
Balsfjord	Storsteinnes	TROMSØ	212 (205, 216)	229 (221, 235)	240 (230, 246)
Balsfjord	Mortenhals	HARSTAD	175 (168, 179)	192 (182, 198)	203 (191, 209)
Målselv	Målsnes	HARSTAD	175 (168, 179)	192 (182, 198)	203 (191, 209)
Lenvik	Finnsnes	HARSTAD	176 (169, 180)	193 (183, 199)	204 (192, 210)
Berg	Skaland	ANDENES	186 (173, 195)	210 (191, 221)	226 (202, 238)
Torsken	Gryllefjord	ANDENES	184 (170, 193)	208 (188, 220)	223 (199, 238)
Tranøy	Vangsvik	HARSTAD	176 (169, 180)	193 (183, 199)	204 (192, 210)
Sørreisa	Sørreisa	HARSTAD	176 (169, 180)	193 (183, 199)	204 (192, 210)
Dyrøy	Brøstadbotn	HARSTAD	176 (169, 180)	193 (183, 199)	204 (192, 210)
Salangen	Sjøvegan	HARSTAD	176 (169, 180)	193 (183, 199)	204 (192, 210)
Lavangen	Tennevoll	HARSTAD	176 (169, 180)	193 (183, 199)	204 (192, 210)
Gratangen	Årstein	HARSTAD	176 (169, 180)	193 (183, 199)	204 (192, 210)
Ibestad	Hamnvik	HARSTAD	176 (169, 180)	193 (183, 199)	204 (192, 210)
Skånland	Evenskjer	HARSTAD	183 (176, 187)	200 (190, 206)	211 (198, 217)
Harstad	Harstad	HARSTAD	175 (168, 179)	192 (182, 198)	203 (191, 209)
Kvæfjord	Borkenes	HARSTAD	172 (166, 177)	189 (179, 195)	200 (188, 206)
Nordland					
Andøy	Andenes	ANDENES	184 (170, 193)	208 (188, 220)	223 (199, 238)
Øksnes	Myre	ANDENES	185 (172, 193)	209 (190, 220)	224 (201, 237)
Sortland	Sortland	ANDENES	185 (172, 193)	209 (190, 220)	224 (201, 237)
Bø	Straume	ANDENES	185 (172, 193)	209 (190, 220)	224 (201, 237)
Hadsel	Stokmarknes	ANDENES	185 (172, 193)	209 (190, 220)	224 (201, 237)
Hadsel	Tennstrand	KABELVÅG	247 (231, 256)	273 (251, 284)	289 (263, 302)
Vågan	Svolvær (Sør)	KABELVÅG	245 (230, 254)	271 (249, 282)	287 (260, 300)
Vågan	Laukvika (Nord)	ANDENES	189 (176, 198)	213 (193, 224)	228 (204, 240)
Vestvågøy	Leknes (Sør)	KABELVÅG	241 (225, 249)	267 (245, 278)	283 (257, 295)
Vestvågøy	Eggum (Nord)	ANDENES	185 (172, 193)	209 (190, 220)	224 (201, 237)
Flakstad	Ramberg (Nord)	ANDENES	193 (180, 202)	217 (197, 229)	232 (208, 246)
Flakstad	Nusfjord (Sør)	KABELVÅG	239 (224, 248)	265 (243, 276)	282 (255, 294)
Moskenes	Reine (Sør)	BODØ	227 (218, 233)	249 (237, 256)	262 (248, 271)
Moskenes	Kalkonneset (Nord)	ANDENES	189 (176, 198)	213 (193, 224)	228 (204, 240)
Værøy	Sørland (Sør)	BODØ	219 (211, 225)	242 (230, 249)	255 (241, 264)
Værøy	Flyplass (Nord)	ANDENES	197 (183, 205)	220 (201, 231)	235 (212, 248)
Røst	Røstlandet	BODØ	209 (200, 214)	231 (219, 238)	244 (230, 252)
Lødingen	Lødingen	NARVIK	254 (241, 260)	280 (261, 288)	297 (273, 306)
Tjeldsund	Nedre Fjeldal (Nord)	HARSTAD	183 (176, 187)	200 (190, 206)	211 (198, 217)
Tjeldsund	Ramsund (Sør)	NARVIK	257 (244, 264)	283 (264, 292)	300 (276, 310)
Evenes	Bogen	NARVIK	257 (244, 264)	283 (264, 292)	300 (276, 310)
Narvik	Narvik	NARVIK	259 (246, 265)	285 (265, 294)	302 (277, 311)
Ballangen	Ballangen	NARVIK	257 (244, 264)	283 (264, 292)	300 (276, 310)
Tysfjord	Kjøpsvik	NARVIK	254 (241, 260)	280 (261, 288)	297 (273, 306)
Hamarøy	Presteid (1)	KABELVÅG	248 (233, 257)	274 (252, 285)	290 (263, 303)
Steigen	Leinesfjord	KABELVÅG	241 (225, 249)	267 (245, 278)	283 (257, 295)
Sørfold	Straumen	BODØ	231 (222, 237)	253 (241, 261)	267 (253, 276)
Bodø	Bodø	BODØ	225 (216, 231)	247 (235, 255)	261 (247, 269)
Bodø	Skjerstad	BODØ	172 (162, 178)	194 (180, 202)	208 (191, 218)
Fauske	Fauske	BODØ	173 (164, 179)	196 (181, 204)	210 (192, 219)
Saltdal	Rognan	BODØ	173 (164, 179)	196 (181, 204)	210 (192, 219)
Beiarn	Moldjord (Leirvika) (2)				
Gildeskål	Inndyr	BODØ	223 (215, 229)	245 (233, 253)	258 (244, 267)

Municipality	Location	Closest Tide Gauge	20 year return height	200 year return height	1000 year return height
Meløy	Ørnes	BODØ	220 (212, 226)	242 (230, 250)	255 (241, 264)
Rødøy	Våga	BODØ	219 (211, 225)	242 (230, 249)	255 (241, 264)
Rana	Mo i Rana	RØRVIK	220 (208, 226)	242 (226, 249)	256 (236, 264)
Træna	Husøy	RØRVIK	208 (195, 214)	230 (212, 238)	243 (222, 253)
Lurøy	Lurøy	RØRVIK	213 (202, 219)	235 (219, 243)	248 (230, 257)
Nesna	Nesna	RØRVIK	214 (202, 220)	236 (219, 244)	250 (229, 259)
Leirfjord	Leland	RØRVIK	216 (204, 222)	238 (221, 245)	251 (232, 260)
Hemnes	Bjerka	RØRVIK	218 (206, 224)	240 (224, 248)	254 (234, 263)
Vefsn	Mosjøen	RØRVIK	220 (208, 226)	242 (226, 249)	256 (236, 264)
Dønna	Solfjellsjøen	RØRVIK	211 (199, 218)	233 (216, 241)	247 (226, 256)
Herøy	Silvalen	RØRVIK	216 (204, 222)	238 (221, 245)	251 (232, 260)
Alstahaug	Sandnessjøen	RØRVIK	216 (204, 222)	238 (221, 245)	251 (232, 260)
Vega	Holand	RØRVIK	216 (204, 222)	238 (221, 245)	251 (232, 260)
Vevelstad	Vevelstad	RØRVIK	217 (205, 223)	239 (223, 247)	253 (233, 261)
Brønnøy	Brønnøysund	RØRVIK	216 (204, 222)	238 (221, 245)	251 (232, 260)
Sømna	Vik (Sørvika)	RØRVIK	216 (204, 222)	238 (221, 245)	251 (232, 260)
Bindal	Terråk	RØRVIK	216 (204, 222)	238 (221, 245)	251 (232, 260)
Nord-Trøndelag					
Leka	Sør-Gutvika	RØRVIK	214 (202, 220)	236 (219, 244)	250 (229, 259)
Nærøy	Kolvereid	RØRVIK	210 (198, 217)	232 (215, 240)	246 (225, 255)
Nærøy	Langstranda (Nord-Salten)	RØRVIK	194 (182, 201)	217 (199, 226)	231 (209, 241)
Nærøy	Søråa (Sør-Salten)	RØRVIK	150 (135, 158)	174 (150, 186)	190 (160, 203)
Høylandet	Kongsmoen	RØRVIK	218 (206, 224)	240 (224, 248)	254 (234, 263)
Vikna	Rørvik	RØRVIK	208 (195, 214)	230 (212, 238)	243 (222, 253)
Fosnes	Salsnes	RØRVIK	208 (195, 214)	230 (212, 238)	243 (222, 253)
Namsos	Namsos	RØRVIK	206 (194, 213)	228 (211, 236)	242 (221, 251)
Flatanger	Lauvsnes	RØRVIK	205 (193, 212)	227 (210, 236)	241 (220, 251)
Namdalseid	Sjøåsen	RØRVIK	206 (194, 213)	228 (211, 236)	242 (221, 251)
Verran	Malm	TRONDHEIM	239 (228, 245)	257 (242, 264)	267 (250, 276)
Steinkjer	Steinkjer (For Børgin, see Inderøy)	TRONDHEIM	232 (222, 239)	250 (236, 257)	261 (244, 269)
Inderøy	Straumen (Trondheimsfjorden)	TRONDHEIM	227 (217, 234)	245 (231, 252)	256 (239, 264)
Inderøy	Straumen (Børgin)	TRONDHEIM	150 (142, 158)	165 (154, 176)	174 (161, 187)
Leksvik	Leksvik	TRONDHEIM	224 (214, 230)	241 (228, 249)	252 (236, 260)
Verdal	Verdal	TRONDHEIM	227 (217, 234)	245 (231, 252)	256 (239, 264)
Levanger	Levanger	TRONDHEIM	227 (217, 234)	245 (231, 252)	256 (239, 264)
Frosta	Sørgrenda	TRONDHEIM	221 (210, 227)	238 (224, 245)	249 (233, 257)
Stjørdal	Stjørdalshalsen	TRONDHEIM	221 (210, 227)	238 (224, 245)	249 (233, 257)
Sør-Trøndelag					
Osen	Osen	RØRVIK	205 (193, 212)	227 (210, 236)	241 (220, 251)
Roan	Roan	RØRVIK	205 (193, 212)	227 (210, 236)	241 (220, 251)
Åfjord	Årnes	RØRVIK	205 (193, 212)	227 (210, 236)	241 (220, 251)
Bjugn	Botngård	HEIMSJØ	194 (187, 199)	210 (200, 217)	220 (208, 228)
Bjugn	Høybakken	TRONDHEIM	211 (201, 217)	229 (215, 236)	239 (224, 247)
Frøya	Sistranda	HEIMSJØ	194 (187, 199)	210 (200, 217)	220 (208, 228)
Frøya	Titran	KRISTIANSUND	183 (176, 188)	200 (189, 206)	210 (197, 217)
Ørland	Brekstad	HEIMSJØ	209 (202, 214)	226 (215, 232)	236 (223, 243)
Ørland	Uthaug	HEIMSJØ	194 (187, 199)	210 (200, 217)	220 (208, 228)
Rissa	Rissa	TRONDHEIM	214 (204, 220)	232 (218, 239)	243 (227, 250)
Hitra	Fillan	HEIMSJØ	196 (189, 201)	213 (202, 219)	223 (210, 230)
Hitra	Kvenvær	KRISTIANSUND	183 (176, 188)	200 (189, 206)	210 (197, 217)
Snillfjord	Krokstadøra	HEIMSJØ	195 (188, 200)	212 (201, 218)	222 (209, 229)
Agdenes	Lensvik	TRONDHEIM	217 (207, 224)	235 (221, 242)	246 (229, 254)
Agdenes	Stavøysundet	HEIMSJØ	205 (198, 210)	222 (211, 228)	232 (219, 239)

Municipality	Location	Closest Tide Gauge	20 year return height	200 year return height	1000 year return height
Hemne	Kyrksæterøra	HEIMSJØ	195 (188, 200)	212 (201, 218)	222 (209, 229)
Orkdal	Orkanger	TRONDHEIM	217 (207, 224)	235 (221, 242)	246 (229, 254)
Skaun	Børsa	TRONDHEIM	217 (207, 224)	235 (221, 242)	246 (229, 254)
Melhus	Øysanden (Gran)	TRONDHEIM	217 (207, 224)	235 (221, 242)	246 (229, 254)
Trondheim	Trondheim	TRONDHEIM	221 (210, 227)	238 (224, 245)	249 (233, 257)
Malvik	Hommelvik	TRONDHEIM	221 (210, 227)	238 (224, 245)	249 (233, 257)
Møre og Romsdal					
Smøla	Hopen	KRISTIANSUND	182 (174, 186)	198 (188, 204)	209 (195, 215)
Aure	Aure	KRISTIANSUND	184 (177, 189)	201 (191, 207)	212 (199, 218)
Halsa	Liabøen	KRISTIANSUND	184 (177, 189)	201 (191, 207)	212 (199, 218)
Surnadal	Surnadalsøra	KRISTIANSUND	184 (177, 189)	201 (191, 207)	212 (199, 218)
Kristiansund	Kristiansund	KRISTIANSUND	180 (172, 184)	196 (185, 202)	206 (193, 213)
Tingvoll	Tingvoll	KRISTIANSUND	182 (174, 186)	198 (188, 204)	209 (195, 215)
Sunndal	Sunndalsøra	KRISTIANSUND	185 (178, 190)	202 (191, 208)	213 (199, 219)
Averøy	Kårvåg	KRISTIANSUND	177 (170, 182)	194 (183, 200)	204 (191, 211)
Gjemnes	Batnfjordsøra	KRISTIANSUND	182 (174, 186)	198 (188, 204)	209 (195, 215)
Nesset	Eidsvåg	ÅLESUND	177 (167, 182)	194 (180, 201)	204 (187, 213)
Eide	Eide	KRISTIANSUND	177 (170, 182)	194 (183, 200)	204 (191, 211)
Fræna	Elnesvågen	KRISTIANSUND	175 (167, 179)	191 (179, 197)	201 (187, 208)
Molde	Molde	ÅLESUND	177 (167, 182)	194 (180, 201)	204 (187, 213)
Rauma	Åndalsnes	ÅLESUND	177 (167, 182)	194 (180, 201)	204 (187, 213)
Aukra	Aukrasanden	KRISTIANSUND	175 (167, 179)	191 (179, 197)	201 (187, 208)
Sandøy	Steinshamn	ÅLESUND	173 (164, 179)	190 (176, 198)	201 (183, 210)
Midsund	Midsund	ÅLESUND	174 (166, 180)	191 (181, 199)	202 (190, 211)
Vestnes	Helland	ÅLESUND	177 (167, 182)	194 (180, 201)	204 (187, 213)
Haram	Brattvåg	ÅLESUND	170 (160, 176)	188 (173, 195)	198 (180, 207)
Skodje	Skodje	ÅLESUND	170 (160, 176)	188 (173, 195)	198 (180, 207)
Ørskog	Sjøholt	ÅLESUND	171 (163, 177)	189 (179, 196)	199 (188, 208)
Stordal	Stordal	ÅLESUND	171 (163, 177)	189 (179, 196)	199 (188, 208)
Norddal	Sylte	ÅLESUND	172 (164, 178)	190 (179, 197)	200 (189, 209)
Giske	Valderhaugstranda	ÅLESUND	170 (160, 176)	188 (173, 195)	198 (180, 207)
Ålesund	Ålesund	ÅLESUND	170 (160, 176)	188 (173, 195)	198 (180, 207)
Sykkylven	Aure	ÅLESUND	171 (163, 177)	189 (179, 196)	199 (188, 208)
Stranda	Stranda	ÅLESUND	171 (163, 177)	189 (179, 196)	199 (188, 208)
Ulstein	Ulsteinvik	ÅLESUND	170 (160, 176)	188 (173, 195)	198 (180, 207)
Hareid	Hareid	ÅLESUND	170 (160, 176)	188 (173, 195)	198 (180, 207)
Sula	Langevåg	ÅLESUND	170 (160, 176)	188 (173, 195)	198 (180, 207)
Ørsta	Ørsta	ÅLESUND	170 (160, 176)	188 (173, 195)	198 (180, 207)
Herøy	Fosnavåg	ÅLESUND	169 (161, 175)	187 (176, 194)	198 (186, 206)
Volda	Volda	ÅLESUND	170 (160, 176)	188 (173, 195)	198 (180, 207)
Sande	Larsnes	ÅLESUND	169 (161, 175)	187 (176, 194)	198 (186, 206)
Vanylven	Fiskå (-bygd)	ÅLESUND	169 (159, 174)	186 (172, 194)	197 (180, 206)
Sogn og Fjordane					
Selje	Selje	ÅLESUND	169 (159, 174)	186 (172, 194)	197 (180, 206)
Vågsøy	Måløy	MÅLØY	153 (148, 157)	166 (160, 171)	174 (166, 180)
Eid	Nordfjordeid	MÅLØY	156 (151, 160)	169 (162, 174)	177 (169, 183)
Stryn	Stryn	MÅLØY	157 (152, 161)	170 (163, 175)	178 (170, 184)
Bremanger	Svelgen	MÅLØY	149 (144, 153)	162 (155, 167)	170 (161, 175)
Gloppen	Sandane	MÅLØY	156 (151, 160)	169 (162, 174)	177 (169, 183)
Flora	Florø	MÅLØY	148 (143, 152)	161 (154, 166)	169 (161, 174)
Naustdal	Naustdal	MÅLØY	147 (142, 151)	160 (153, 165)	168 (160, 173)
Luster	Gaupne	BERGEN	141 (136, 144)	153 (147, 158)	160 (153, 166)
Askvoll	Askvoll	MÅLØY	145 (140, 148)	158 (151, 162)	166 (157, 171)
Førde	Førde	MÅLØY	147 (142, 151)	160 (153, 165)	168 (160, 173)

Municipality	Location	Closest Tide Gauge	20 year return height	200 year return height	1000 year return height
Fjaler	Dale	MÅLØY	145 (140, 148)	158 (151, 162)	166 (157, 171)
Gaular	Bygstad	MÅLØY	145 (140, 148)	158 (151, 162)	166 (157, 171)
Balestrand	Balestrand	BERGEN	139 (135, 143)	151 (146, 156)	158 (152, 164)
Leikanger	Hermansverk	BERGEN	139 (135, 143)	151 (146, 156)	158 (152, 164)
Sogndal	Sogndal	BERGEN	140 (137, 143)	152 (150, 157)	159 (157, 165)
Årdal	Årdalstangen	BERGEN	140 (137, 143)	152 (150, 157)	159 (157, 165)
Solund	Hardbakke	MÅLØY	141 (136, 145)	155 (148, 159)	162 (154, 167)
Hyllestad	Hyllestad	MÅLØY	143 (138, 146)	156 (149, 161)	164 (156, 169)
Høyanger	Høyanger	BERGEN	138 (134, 141)	150 (146, 155)	157 (153, 163)
Vik	Vik	BERGEN	139 (135, 143)	151 (146, 156)	158 (152, 164)
Aurland	Aurlandsvangen	BERGEN	140 (137, 143)	152 (150, 157)	159 (157, 165)
Lærdal	Lærdalsøyri	BERGEN	140 (137, 143)	152 (150, 157)	159 (157, 165)
Gulen	Eivindvik	BERGEN	133 (130, 136)	145 (143, 150)	152 (151, 158)
Hordaland					
Fedje	Fedje	BERGEN	130 (126, 133)	142 (136, 147)	149 (142, 155)
Austrheim	Årås	BERGEN	132 (128, 135)	144 (138, 149)	151 (145, 157)
Masfjorden	Masfjordnes	BERGEN	132 (128, 135)	144 (138, 149)	151 (145, 157)
Modalen	Nottveit (1)	BERGEN	131 (126, 134)	143 (137, 147)	150 (143, 156)
Radøy	Manger	BERGEN	129 (125, 132)	141 (135, 146)	148 (141, 154)
Lindås	Knarvik	BERGEN	129 (125, 132)	141 (135, 146)	148 (141, 154)
Vaksdal	Vaksdal	BERGEN	131 (126, 134)	143 (137, 147)	150 (143, 156)
Voss	Bolstadøyri (2)				
Øygarden	Tjeldstø	BERGEN	129 (125, 132)	141 (135, 146)	148 (141, 154)
Meland	Frekhaug	BERGEN	129 (125, 132)	141 (135, 146)	148 (141, 154)
Osterøy	Lonevåg	BERGEN	131 (126, 134)	143 (137, 147)	150 (143, 156)
Fjell	Straume	BERGEN	126 (121, 129)	138 (132, 143)	145 (138, 151)
Askøy	Kleppestø	BERGEN	129 (125, 132)	141 (135, 146)	148 (141, 154)
Bergen	Bergen	BERGEN	129 (125, 132)	141 (135, 146)	148 (141, 154)
Samnanger	Tysse	BERGEN	116 (113, 120)	129 (124, 133)	136 (130, 142)
Kvam	Norheimsund	BERGEN	122 (118, 126)	135 (129, 139)	142 (136, 148)
Granvin	Granvin	BERGEN	124 (120, 127)	136 (131, 141)	143 (137, 149)
Ulvik	Ulvik	BERGEN	124 (120, 127)	136 (131, 141)	143 (137, 149)
Sund	Skogsvåg	BERGEN	122 (118, 125)	134 (129, 139)	142 (135, 147)
Austevoll	Storebø	BERGEN	116 (113, 120)	129 (124, 133)	136 (130, 142)
Os	Osøyro	BERGEN	116 (113, 120)	129 (124, 133)	136 (130, 142)
Fusa	Eikelandsosen	BERGEN	116 (113, 120)	129 (124, 133)	136 (130, 142)
Jondal	Jondal	BERGEN	122 (118, 125)	134 (129, 139)	142 (135, 147)
Ullensvang	Kinsarvik	BERGEN	124 (120, 127)	136 (131, 141)	143 (137, 149)
Eidfjord	Eidfjord	BERGEN	124 (120, 127)	136 (131, 141)	143 (137, 149)
Tysnes	Uggdalseidet	BERGEN	116 (113, 120)	129 (124, 133)	136 (130, 142)
Bømlo	Svortland	BERGEN	112 (109, 116)	125 (120, 129)	132 (127, 137)
Fitjar	Fitjar	BERGEN	116 (113, 120)	129 (124, 133)	136 (130, 142)
Stord	Leirvik	BERGEN	113 (109, 116)	125 (120, 130)	132 (127, 138)
Kvinnherad	Rosendal	BERGEN	114 (110, 117)	126 (121, 130)	133 (128, 139)
Odda	Odda	BERGEN	125 (121, 128)	137 (132, 142)	145 (139, 150)
Sveio	Førde	BERGEN	111 (107, 114)	123 (118, 128)	131 (125, 136)
Etne	Etne	BERGEN	114 (110, 117)	126 (121, 130)	133 (128, 139)
Rogaland					
Haugesund	Haugesund	BERGEN	100 (96, 103)	111 (108, 116)	118 (115, 124)
Vindafjord	Ølen	BERGEN	114 (110, 117)	126 (121, 130)	133 (128, 139)
Vindafjord	Sandeid	STAVANGER	101 (95, 104)	115 (106, 119)	123 (112, 129)
Sauda	Sauda	STAVANGER	101 (95, 104)	115 (106, 119)	123 (113, 129)
Utsira	Nordvik	STAVANGER	104 (99, 107)	118 (110, 122)	126 (116, 132)
Karmøy	Kopervik	STAVANGER	101 (95, 104)	115 (106, 119)	123 (112, 129)
Tysvær	Hervik	STAVANGER	101 (95, 104)	115 (106, 119)	123 (112, 129)

Municipality	Location	Closest Tide Gauge	20 year return height	200 year return height	1000 year return height
Tysvær	Grinde (Grindafjorden og Skjoldafjorden)	STAVANGER	91 (84, 95)	108 (96, 114)	119 (104, 126)
Suldal	Sand	STAVANGER	101 (95, 104)	115 (106, 119)	123 (113, 129)
Bokn	Føresvik	STAVANGER	101 (95, 104)	115 (106, 119)	123 (112, 129)
Finnøy	Judaberg	STAVANGER	101 (95, 104)	115 (106, 119)	123 (112, 129)
Hjelmeland	Hjelmeland	STAVANGER	101 (95, 104)	115 (106, 119)	123 (112, 129)
Kvitsøy	Ydstebøhavn	STAVANGER	101 (95, 104)	115 (106, 119)	123 (112, 129)
Rennesøy	Vikevåg	STAVANGER	101 (95, 104)	115 (106, 119)	123 (112, 129)
Randaberg	Tungenes	STAVANGER	101 (95, 104)	115 (106, 119)	123 (112, 129)
Stavanger	Stavanger	STAVANGER	101 (95, 104)	115 (106, 119)	123 (113, 129)
Strand	Jørpeland	STAVANGER	101 (95, 104)	115 (106, 119)	123 (113, 129)
Sola	Solavika (3)	(STAVANGER)	99 (93, 102)	113 (105, 118)	122 (111, 128)
Sandnes	Sandnes	STAVANGER	101 (95, 104)	115 (106, 119)	123 (113, 129)
Forsand	Forsand	STAVANGER	102 (97, 105)	116 (108, 120)	125 (114, 130)
Klepp	Revtangen (3)	(STAVANGER)	93 (86, 97)	109 (98, 115)	119 (105, 127)
Gjesdal	Frafjord	STAVANGER	102 (97, 105)	116 (108, 120)	125 (114, 130)
Hå	Sirevåg (3)	(STAVANGER)	87 (79, 92)	107 (93, 113)	120 (101, 127)
Eigersund	Egersund (3)	(STAVANGER)	87 (79, 92)	107 (93, 113)	120 (101, 127)
Sokndal	Sogndalsstranda (3)	(STAVANGER)	87 (79, 92)	107 (93, 113)	120 (101, 127)
Vest-Agder					
Flekkefjord	Flekkefjord (3)	(TREGDE)	91 (83, 96)	110 (98, 119)	122 (107, 134)
Kvinesdal	Øye (3)	(TREGDE)	91 (83, 96)	110 (98, 119)	122 (107, 134)
Farsund	Farsund	TREGDE	93 (86, 98)	111 (99, 119)	122 (108, 133)
Lyngdal	Lyngdal (For Lyngdalsfjorden, see Farsund)	TREGDE	93 (86, 98)	111 (99, 119)	122 (107, 132)
Lindesnes	Åvik	TREGDE	95 (88, 100)	112 (101, 120)	124 (109, 133)
Mandal	Mandal	TREGDE	95 (89, 100)	112 (101, 119)	123 (109, 132)
Søgne	Høllen	TREGDE	95 (89, 100)	113 (101, 120)	124 (109, 132)
Kristiansand	Kristiansand	TREGDE	96 (89, 100)	113 (101, 120)	124 (109, 132)
Aust-Agder					
Lillesand	Lillesand	TREGDE	98 (91, 102)	115 (104, 121)	125 (112, 134)
Grimstad	Grimstad	TREGDE	98 (91, 102)	115 (104, 121)	125 (112, 134)
Arendal	Arendal	HELGEROA	126 (112, 135)	151 (129, 163)	168 (139, 182)
Tvedestrand	Tvedestrand	HELGEROA	126 (112, 134)	151 (129, 163)	167 (140, 181)
Risør	Risør	HELGEROA	126 (112, 134)	151 (129, 162)	167 (140, 181)
Telemark					
Kragerø	Kragerø	HELGEROA	126 (112, 134)	151 (129, 162)	167 (140, 181)
Bamble	Langesund	HELGEROA	126 (112, 134)	151 (129, 162)	167 (139, 181)
Porsgrunn	Porsgrunn	HELGEROA	126 (112, 135)	151 (128, 163)	168 (138, 181)
Skien	Rambekk	HELGEROA	126 (112, 135)	151 (128, 163)	168 (138, 181)
Vestfold					
Larvik	Larvik	HELGEROA	126 (112, 134)	151 (129, 162)	167 (139, 180)
Sandefjord	Sandefjord	HELGEROA	126 (112, 134)	151 (129, 162)	167 (139, 180)
Tjøme	Verdens Ende	VIKER	138 (118, 151)	165 (135, 182)	182 (145, 202)
Stokke	Melsomvik	VIKER	138 (118, 151)	165 (135, 182)	182 (145, 202)
Nøtterøy	Årøysund	VIKER	138 (118, 151)	165 (134, 182)	182 (144, 201)
Tønsberg	Tønsberg	VIKER	138 (118, 151)	165 (134, 182)	182 (144, 201)
Horten	Horten	VIKER	139 (118, 152)	166 (134, 184)	183 (144, 205)
Re	Mulodden	VIKER	139 (118, 152)	166 (135, 184)	184 (144, 206)
Holmestrand	Holmestrand	VIKER	139 (118, 152)	166 (135, 184)	184 (144, 206)
Sande	Selvik	VIKER	139 (118, 152)	166 (135, 184)	184 (144, 206)
Svelvik	Svelvik	VIKER	139 (118, 152)	166 (135, 184)	184 (144, 206)
Buskerud					
Drammen	Drammen (Tangen)	VIKER	142 (121, 155)	170 (138, 188)	189 (148, 210)
Lier	Lierstranda	VIKER	142 (121, 155)	170 (138, 188)	189 (148, 210)

Municipality	Location	Closest Tide Gauge	20 year return height	200 year return height	1000 year return height
Røyken	Nærsnes	VIKER	142 (121, 155)	170 (138, 188)	189 (148, 210)
Hurum	Sætre	OSCARSBORG	142 (129, 150)	167 (149, 176)	183 (161, 193)
Oslo					
Oslo	Oslo	OSLO	153 (139, 162)	186 (162, 199)	209 (177, 225)
Akershus					
Asker	Konglungen	OSLO	153 (139, 162)	186 (162, 199)	209 (177, 225)
Bærum	Sandvika	OSLO	153 (139, 162)	186 (162, 199)	209 (177, 225)
Nesodden	Nesoddtangen	OSLO	153 (139, 162)	186 (162, 199)	209 (177, 225)
Oppegård	Svartskog	OSLO	153 (139, 162)	186 (162, 199)	209 (177, 225)
Frogn	Drøbak	OSCARSBORG	142 (129, 150)	167 (149, 176)	183 (161, 193)
Ås	Nesset	OSLO	153 (139, 162)	186 (162, 199)	209 (177, 225)
Vestby	Son	VIKER	139 (118, 152)	166 (135, 184)	184 (144, 206)
Østfold					
Moss	Moss	VIKER	139 (118, 152)	166 (135, 184)	184 (144, 206)
Rygge	Larkollen	VIKER	139 (118, 152)	166 (134, 184)	183 (144, 205)
Råde	Saltnes	VIKER	139 (118, 152)	166 (134, 184)	183 (144, 205)
Fredrikstad	Fredrikstad	VIKER	139 (118, 152)	166 (134, 184)	183 (144, 205)
Sarpsborg	Høysand	VIKER	139 (119, 152)	167 (136, 185)	184 (146, 206)
Hvaler	Skjærhalden	VIKER	139 (118, 152)	166 (135, 184)	183 (146, 205)
Halden	Halden	VIKER	138 (118, 151)	165 (135, 182)	182 (145, 202)

(1) Return heights for the administration centre of this municipality cannot be given due to insufficient data in the area.

(2) Return heights for this municipality cannot be given due to insufficient data in this area.

(3) The estimated return heights in this area have larger uncertainties than for the rest of the coast (cf. explanation in Chapter 6) and should be used with caution.

A.2 Tables for Projected Sea Level Change

The following tables present the projected relative sea level change to 2041–2060, 2081–2100 and 2100, relative to 1986–2005, for each of the three RCPs. The same locations as for the return heights are used, therefore some municipalities have two or three locations listed even though they have very similar or even the same projected sea level changes.

Table A.2.1 Projected sea level change and 5 to 95% ensemble spread for RCP2.6. Averages for three future periods are given. Changes are given relative to the reference period 1986–2005, in centimetres. All coastal municipalities are represented, and some have more than one location for which the estimation is done. The table is subdivided into counties.

RCP2.6		2041–2060			2081–2100			2100		
Municipality	**Location**	**Mean**	**5%**	**95%**	**Mean**	**5%**	**95%**	**Mean**	**5%**	**95%**
Finnmark										
Sør-Varanger	Kirkenes	4	-9	17	2	-2	28	3	-2	31
Nesseby	Varangerbotn	8	-6	21	9	-1	35	10	-1	39
Vadsø	Vadsø	6	-7	20	7	-1	32	8	-2	36
Vardø	Vardø	9	-4	22	12	-1	37	13	-1	41
Båtsfjord	Båtsfjord	11	-2	24	15	-1	40	16	-1	44
Berlevåg	Berlevåg	13	0	26	18	-8	44	20	-8	49
Tana	Smalfjord	10	-3	23	13	-1	39	15	-1	43
Gamvik	Mehamn	14	1	28	20	-6	46	23	-6	51
Lebesby	Kjøllefjord	14	0	27	18	-7	44	20	-8	48
Nordkapp	Honningsvåg	13	0	27	18	-7	44	20	-8	48
Porsanger	Lakselv	7	-6	21	8	-1	33	9	-1	36
Måsøy	Havøysund	14	0	27	18	-7	44	20	-8	48
Kvalsund	Kvalsund	12	-2	27	16	-1	45	19	-1	52
Hammerfest	Hammerfest	14	-1	28	18	-1	47	21	-1	54
Hasvik	Breivikbotn	12	-2	27	17	-1	45	20	-1	50
Alta	Alta	8	-6	23	9	-2	38	12	-2	45
Loppa	Øksfjord	8	-6	23	9	-2	38	12	-2	45
Troms										
Kvænangen	Burfjord	8	-6	22	9	-1	37	12	-1	42
Kvænangen	Kjækan	7	-8	21	7	-2	35	9	-2	39
Nordreisa	Storslett	8	-6	22	9	-1	37	11	-1	41
Skjervøy	Skjervøy	10	-4	24	13	-1	41	15	-1	45
Kåfjord	Olderdalen	7	-7	21	8	-1	36	10	-2	40
Storfjord	Hatteng	6	-9	20	6	-2	33	7	-2	37
Lyngen	Lyngseidet	7	-7	22	9	-1	36	10	-1	41
Karlsøy	Hansnes	11	-3	26	15	-1	43	18	-1	48
Karlsøy	Nordvardvika	10	0	20	12	-5	28	13	-6	33
Tromsø	Tromsø (sør for Tromsøybrua)	7	-3	17	6	-1	23	8	-1	27
Tromsø	Ersfjordbotn (vest for Kvaløya)	9	-1	19	8	-8	25	10	-9	29
Tromsø	Snarby	10	-4	25	14	-1	41	16	-1	46
Balsfjord	Storsteinnes	7	-7	21	7	-1	34	8	-2	37
Balsfjord	Mortenhals	10	-4	24	12	-1	38	13	-1	42
Målselv	Målsnes	9	-5	23	11	-1	37	12	-1	41
Lenvik	Finnsnes	7	-3	17	5	-1	22	6	-1	25
Berg	Skaland	11	1	20	12	-5	29	13	-7	32
Torsken	Gryllefjord	11	1	21	13	-4	30	13	-6	33
Tranøy	Vangsvik	7	-3	17	5	-1	22	7	-1	26
Sørreisa	Sørreisa	5	-5	15	3	-1	20	4	-1	23
Dyrøy	Brøstadbotn	6	-4	16	4	-1	21	5	-1	25
Salangen	Sjøvegan	4	-6	14	0	-1	17	1	-1	20
Lavangen	Tennevoll	3	-7	13	-2	-1	15	-1	-2	18
Gratangen	Årstein	3	-7	13	-2	-1	15	-1	-2	18
Ibestad	Hamnvik	5	-4	15	3	-1	20	3	-1	23
Skånland	Evenskjer	6	-4	15	4	-1	21	4	-1	23
Harstad	Harstad	8	-1	18	8	-9	25	9	-1	28
Kvæfjord	Borkenes	9	-1	19	9	-8	26	10	-1	30
Nordland										
Andøy	Andenes	14	4	23	17	0	34	18	-1	38
Øksnes	Myre	16	1	30	24	-4	51	27	-2	57

RCP2.6		2041–2060			2081–2100			2100		
Municipality	**Location**	**Mean**	**5%**	**95%**	**Mean**	**5%**	**95%**	**Mean**	**5%**	**95%**
Sortland	Sortland	13	-2	28	19	-8	46	22	-8	52
Bø	Straume	16	2	30	24	-3	51	27	-3	56
Hadsel	Stokmarknes	14	-1	28	20	-7	47	23	-7	53
Hadsel	Tennstrand	11	-4	26	16	-1	44	19	-1	49
Vågan	Svolvær (Sør)	11	-4	26	17	-1	44	20	-1	50
Vågan	Laukvika (Nord)	14	0	29	21	-5	48	24	-5	53
Vestvågøy	Leknes (Sør)	16	2	30	24	-3	50	26	-3	56
Vestvågøy	Eggum (Nord)	17	3	31	25	-2	52	28	-1	57
Flakstad	Ramberg (Nord)	17	3	31	25	-2	52	27	-2	57
Flakstad	Nusfjord (Sør)	16	2	30	24	-3	50	26	-3	55
Moskenes	Reine (Sør)	16	2	30	24	-3	51	27	-3	56
Moskenes	Kalkonneset (Nord)	17	3	31	26	-1	53	29	-1	58
Værøy	Sørland (Sør)	16	2	30	24	-2	51	27	-2	56
Værøy	Flyplass (Nord)	16	2	30	25	-2	51	27	-2	57
Røst	Røstlandet	18	4	32	26	0	53	28	0	57
Lødingen	Lødingen	8	-7	23	11	-1	39	14	-1	43
Tjeldsund	Nedre Fjeldal (Nord)	6	-4	15	3	-1	20	3	-1	23
Tjeldsund	Ramsund (Sør)	7	-8	22	9	-1	37	11	-1	41
Evenes	Bogen	3	-6	13	-1	-1	16	-1	-2	18
Narvik	Narvik	3	-1	18	2	-2	30	4	-2	33
Ballangen	Ballangen	4	-1	19	5	-2	32	6	-2	36
Tysfjord	Kjøpsvik	3	-1	19	3	-2	31	5	-2	35
Hamarøy	Presteid	6	-9	21	8	-1	36	10	-1	40
Steigen	Leinesfjord	6	-9	21	8	-1	36	10	-1	40
Sørfold	Straumen	-1	-1	9	-8	-2	9	-9	-2	11
Bodø	Bodø	8	-5	21	8	-1	34	9	-2	38
Bodø	Skjerstad	3	-1	18	2	-2	29	3	-2	33
Fauske	Fauske	1	-1	16	-1	-2	27	1	-2	30
Saltdal	Rognan	0	-1	15	-3	-3	24	-2	-3	28
Beiarn	Moldjord (Leirvika)	3	-1	18	2	-2	30	4	-2	33
Gildeskål	Inndyr	7	-5	20	7	-1	33	8	-2	37
Meløy	Ørnes	8	-5	21	8	-1	34	9	-2	38
Rødøy	Våga	8	-5	21	9	-1	35	10	-1	39
Rana	Mo i Rana	0	-1	14	-4	-2	22	-4	-3	24
Træna	Husøy	11	-2	25	16	-1	42	18	-1	46
Lurøy	Lurøy	7	-7	21	9	-1	34	10	-1	38
Nesna	Nesna	5	-9	19	5	-2	30	6	-2	34
Leirfjord	Leland	4	-9	18	4	-2	29	5	-2	33
Hemnes	Bjerka	1	-1	14	-3	-2	23	-3	-3	25
Vefsn	Mosjøen	2	-1	16	-1	-2	25	0	-2	28
Dønna	Solfjellsjøen	7	-7	20	8	-1	33	9	-1	37
Herøy	Silvalen	7	-7	21	8	-1	33	9	-1	37
Alstahaug	Sandnessjøen	6	-8	19	6	-2	31	7	-2	35
Vega	Holand	6	-7	20	7	-1	33	8	-2	36
Vevelstad	Vevelstad	4	-1	18	3	-2	29	4	-2	32
Brønnøy	Brønnøysund	4	-9	18	3	-2	29	3	-2	32
Sømna	Vik (Sørvika)	4	-9	18	3	-2	29	3	-2	32
Bindal	Terråk	1	-1	15	-3	-2	23	-3	-3	25
Nord-Trøndelag										
Leka	Sør-Gutvika	4	-1	18	2	-2	28	2	-2	31
Nærøy	Kolvereid	4	-1	17	2	-2	28	2	-2	31
Nærøy	Langstranda (Nord-Salten)	4	-1	18	3	-2	29	3	-2	32
Nærøy	Søråa (Sør-Salten)	5	-9	18	4	-2	30	4	-2	33
Høylandet	Kongsmoen	-1	-1	13	-6	-3	20	-7	-3	22
Vikna	Rørvik	6	-8	19	5	-2	31	6	-2	34

RCP2.6		2041–2060			2081–2100			2100		
Municipality	**Location**	**Mean**	**5%**	**95%**	**Mean**	**5%**	**95%**	**Mean**	**5%**	**95%**
Fosnes	Salsnes	4	-1	17	2	-2	28	2	-2	31
Namsos	Namsos	1	-1	15	-2	-2	24	-1	-2	27
Flatanger	Lauvsnes	6	-8	19	5	-2	31	6	-2	34
Namdalseid	Sjøåsen	3	-1	17	1	-2	27	1	-2	30
Verran	Malm	2	-1	16	-2	-2	24	-2	-3	27
Steinkjer	Steinkjer (for Børgin, see Inderøy)	-1	-1	13	-5	-3	20	-5	-3	23
Inderøy	Straumen (Trondheimsfjorden)	0	-1	14	-5	-3	21	-5	-3	23
Inderøy	Straumen (Børgin)	0	-1	14	-5	-3	21	-5	-3	23
Leksvik	Leksvik	2	-1	16	-1	-2	25	-1	-3	28
Verdal	Verdal	-1	-1	13	-7	-3	19	-7	-3	21
Levanger	Levanger	-1	-1	13	-6	-3	20	-6	-3	23
Frosta	Sørgrenda	1	-1	15	-3	-2	23	-3	-3	26
Stjørdal	Stjørdalshalsen	-1	-1	13	-6	-3	20	-6	-3	22
Sør-Trøndelag										
Osen	Osen	7	-7	21	7	-1	33	8	-2	37
Roan	Roan	6	-6	17	5	-1	25	5	-1	26
Åfjord	Årnes	5	-7	16	3	-1	23	2	-1	23
Bjugn	Botngård	6	-6	17	5	-1	25	5	-1	26
Bjugn	Høybakken	5	-7	17	4	-1	24	4	-1	24
Frøya	Sistranda	11	-1	22	13	-6	33	14	-7	34
Frøya	Titran	13	1	25	17	-3	37	18	-4	39
Ørland	Brekstad	6	-6	18	6	-1	25	5	-1	26
Ørland	Uthaug	7	-5	18	7	-1	26	6	-1	27
Rissa	Rissa	4	-8	15	2	-1	21	1	-2	22
Hitra	Fillan	9	-2	21	11	-8	31	11	-1	32
Hitra	Kvenvær	12	0	24	16	-4	36	16	-5	37
Snillfjord	Krokstadøra	7	-6	20	8	-1	33	8	-1	35
Agdenes	Lensvik	4	-7	16	3	-1	23	2	-1	23
Agdenes	Stavøysundet	7	-6	20	8	-1	32	8	-1	35
Hemne	Kyrksæterøra	7	-5	19	7	-1	27	7	-1	28
Orkdal	Orkanger	5	-8	18	4	-2	28	3	-2	30
Skaun	Børsa	4	-9	17	2	-2	26	2	-2	28
Melhus	Øysanden (Gran)	3	-1	16	1	-2	25	0	-2	27
Trondheim	Trondheim	2	-1	15	0	-2	24	-1	-2	25
Malvik	Hommelvik	0	-1	13	-5	-3	21	-6	-3	23
Møre og Romsdal										
Smøla	Hopen	14	0	28	21	-5	47	24	-4	53
Aure	Aure	10	-2	21	12	-7	32	12	-9	33
Halsa	Liabøen	11	-3	25	16	-1	42	19	-1	47
Surnadal	Surnadalsøra	8	-4	19	9	-1	28	8	-1	29
Kristiansund	Kristiansund	14	0	27	21	-5	46	24	-5	52
Tingvoll	Tingvoll	11	-3	24	15	-1	41	18	-1	46
Sunndal	Sunndalsøra	7	-5	19	7	-1	27	7	-1	28
Averøy	Kårvåg	14	0	28	22	-4	47	25	-4	53
Gjemnes	Batnfjordsøra	13	-1	27	20	-6	45	23	-6	51
Nesset	Eidsvåg	11	-3	24	15	-1	41	18	-1	46
Eide	Eide	14	0	28	21	-5	46	24	-4	52
Fræna	Elnesvågen	15	1	28	22	-4	48	25	-3	54
Molde	Molde	14	0	28	21	-5	47	24	-4	52
Rauma	Åndalsnes	11	-3	25	16	-1	42	19	-1	47
Aukra	Aukrasanden	15	1	29	23	-3	48	26	-2	54
Sandøy	Steinshamn	17	3	31	25	1	49	27	0	53
Midsund	Midsund	15	1	29	23	-3	49	27	-2	55
Vestnes	Helland	14	0	28	21	-5	46	24	-5	52

RCP2.6		2041–2060			2081–2100			2100		
Municipality	**Location**	**Mean**	**5%**	**95%**	**Mean**	**5%**	**95%**	**Mean**	**5%**	**95%**
Haram	Brattvåg	16	2	30	24	0	48	26	-1	52
Skodje	Skodje	15	1	28	22	-4	48	25	-3	54
Ørskog	Sjøholt	14	0	28	22	-4	47	25	-4	53
Stordal	Stordal	13	-1	27	20	-6	46	23	-5	51
Norddal	Sylte	12	-2	26	18	-8	43	21	-8	49
Giske	Valderhaugstranda	17	3	30	24	0	48	26	-1	52
Ålesund	Ålesund	16	3	30	24	0	46	25	-1	50
Sykkylven	Aure	15	1	28	22	-4	48	25	-3	54
Stranda	Stranda	13	-1	27	20	-6	46	23	-5	51
Ulstein	Ulsteinvik	17	3	30	24	1	47	26	0	51
Hareid	Hareid	17	3	30	24	1	47	25	-1	51
Sula	Langevåg	17	3	30	24	1	47	25	-1	51
Ørsta	Ørsta	16	3	29	23	0	46	24	-1	50
Herøy	Fosnavåg	17	4	30	25	1	48	26	0	52
Volda	Volda	16	3	29	23	0	46	24	-1	50
Sande	Larsnes	17	3	30	24	1	47	26	0	51
Vanylven	Fiskå(-bygd)	17	3	30	24	1	47	26	0	51
Sogn og Fjordane										
Selje	Selje	17	3	30	24	1	47	26	0	51
Vågsøy	Måløy	17	3	30	24	0	47	25	-1	51
Eid	Nordfjordeid	16	3	29	23	0	46	24	-2	50
Stryn	Stryn	13	-1	27	20	-6	45	23	-6	51
Bremanger	Svelgen	16	3	29	23	0	46	25	-1	50
Gloppen	Sandane	15	2	28	21	-2	44	23	-3	48
Flora	Florø	16	3	29	23	0	46	25	-1	50
Naustdal	Naustdal	15	2	28	22	-2	44	23	-3	48
Luster	Gaupne	9	-3	21	11	-8	31	11	-1	32
Askvoll	Askvoll	15	3	27	21	1	40	22	0	43
Førde	Førde	14	2	26	19	0	39	20	-2	41
Fjaler	Dale	14	2	26	20	0	39	21	-1	42
Gaular	Bygstad	14	2	26	19	0	39	20	-2	41
Balestrand	Balestrand	12	0	24	16	-4	35	16	-6	37
Leikanger	Hermansverk	10	-2	22	13	-7	32	13	-9	34
Sogndal	Sogndal	9	-3	21	11	-8	31	11	-1	32
Årdal	Årdalstangen	7	-5	19	8	-1	27	7	-1	28
Solund	Hardbakke	15	3	27	21	1	40	21	0	43
Hyllestad	Hyllestad	14	2	26	20	0	39	21	-1	42
Høyanger	Høyanger	13	1	25	17	-3	36	17	-4	38
Vik	Vik	11	-1	23	15	-5	34	15	-7	36
Aurland	Aurlandsvangen	9	-3	21	11	-9	30	10	-1	32
Lærdal	Lærdalsøyri	8	-4	20	9	-1	28	8	-1	29
Gulen	Eivindvik	15	3	27	21	1	40	21	0	42
Hordaland										
Fedje	Fedje	15	3	27	21	1	41	22	0	43
Austrheim	Årås	15	3	27	21	1	41	22	0	43
Masfjorden	Masfjordnes	15	3	26	20	1	40	21	0	42
Modalen	Nottveit	14	2	26	19	0	39	20	-2	41
Radøy	Manger	15	3	27	22	2	41	22	1	44
Lindås	Knarvik	16	3	27	22	2	41	23	1	44
Vaksdal	Vaksdal	12	2	22	16	-1	33	18	-1	36
Voss	Bolstadøyri	12	2	22	16	-1	33	18	-1	36
Øygarden	Tjeldstø	15	3	27	22	2	41	23	1	44
Meland	Frekhaug	16	4	27	22	2	41	23	1	44
Osterøy	Lonevåg	15	3	27	21	1	40	22	0	43
Fjell	Straume	16	4	28	23	3	42	24	2	45
Askøy	Kleppestø	16	4	28	23	3	42	24	2	45

RCP2.6		2041–2060			2081–2100			2100		
Municipality	**Location**	**Mean**	**5%**	**95%**	**Mean**	**5%**	**95%**	**Mean**	**5%**	**95%**
Bergen	Bergen	16	4	28	23	3	42	23	2	45
Samnanger	Tysse	12	2	22	16	-1	33	18	-1	36
Kvam	Norheimsund	11	0	20	14	-3	30	15	-3	33
Granvin	Granvin	11	-1	23	14	-5	34	14	-7	35
Ulvik	Ulvik	10	-2	22	12	-7	32	12	-9	33
Sund	Skogsvåg	16	4	28	23	3	42	24	2	45
Austevoll	Storebø	16	4	28	23	3	42	23	2	44
Os	Osøyro	15	4	27	22	2	41	23	1	44
Fusa	Eikelandsosen	12	2	22	16	-1	33	18	-1	36
Jondal	Jondal	10	0	20	14	-3	30	15	-3	33
Ullensvang	Kinsarvik	9	-1	19	11	-6	27	12	-6	30
Eidfjord	Eidfjord	7	-3	17	8	-9	25	9	-9	27
Tysnes	Uggdalseidet	12	2	22	17	0	34	19	0	37
Bømlo	Svortland	16	4	28	23	3	42	24	2	45
Fitjar	Fitjar	16	4	27	22	3	42	23	2	44
Stord	Leirvik	13	2	23	18	1	34	19	1	37
Kvinnherad	Rosendal	11	1	21	15	-2	31	16	-2	35
Odda	Odda	10	0	20	13	-4	30	14	-4	32
Sveio	Førde	16	4	28	23	3	42	23	2	44
Etne	Etne	12	2	22	16	-1	33	18	-1	36
Rogaland										
Haugesund	Haugesund	18	5	31	27	4	50	29	3	54
Vindafjord	Ølen	12	2	22	17	0	34	19	0	37
Vindafjord	Sandeid	12	2	22	17	0	33	19	0	37
Sauda	Sauda	11	1	21	15	-2	31	16	-2	34
Utsira	Nordvik	19	5	32	28	5	50	30	4	55
Karmøy	Kopervik	18	5	31	27	4	50	29	3	55
Tysvær	Hervik	18	5	31	27	4	49	28	3	53
Tysvær	Grinde (Grindafjorden og Skjoldafjorden)	18	4	31	26	3	49	28	2	53
Suldal	Sand	16	3	28	23	0	45	24	-1	49
Bokn	Føresvik	18	5	31	27	4	50	29	3	54
Finnøy	Judaberg	18	4	30	26	4	48	28	3	52
Hjelmeland	Hjelmeland	17	3	29	25	2	46	26	1	51
Kvitsøy	Ydstebøhavn	19	5	32	28	5	50	30	4	55
Rennesøy	Vikevåg	18	5	31	27	5	49	29	4	54
Randaberg	Tungenes	19	6	31	28	6	50	30	5	55
Stavanger	Stavanger	18	5	31	28	5	50	30	4	54
Strand	Jørpeland	17	4	30	26	4	48	28	3	52
Sola	Solavika	19	6	32	29	6	50	30	5	55
Sandnes	Sandnes	18	5	31	27	5	49	29	4	54
Forsand	Forsand	18	5	30	26	4	48	28	3	53
Klepp	Revtangen	19	6	32	29	6	51	31	5	56
Gjesdal	Frafjord	18	5	30	26	4	48	28	3	53
Hå	Sirevåg	19	6	32	29	7	51	31	6	56
Eigersund	Egersund	19	6	32	29	6	51	31	6	56
Sokndal	Sogndalsstranda	19	6	32	29	6	51	32	7	56
Vest-Agder										
Flekkefjord	Flekkefjord	19	5	32	29	6	51	31	6	56
Kvinesdal	Øye	18	5	31	28	5	49	30	5	54
Farsund	Farsund	19	5	32	29	6	51	31	6	56
Lyngdal	Lyngdal (For Lyngdalsfjorden, see Farsund)	18	5	31	28	5	49	30	5	54
Lindesnes	Åvik	18	5	31	27	5	49	30	4	54
Mandal	Mandal	18	4	31	27	4	48	29	4	53

RCP2.6		2041–2060			2081–2100			2100		
Municipality	**Location**	**Mean**	**5%**	**95%**	**Mean**	**5%**	**95%**	**Mean**	**5%**	**95%**
Søgne	Høllen	17	3	30	26	3	47	28	2	52
Kristiansand	Kristiansand	16	3	29	24	2	46	26	1	51
Aust-Agder										
Lillesand	Lillesand	14	1	27	21	-2	43	22	-3	47
Grimstad	Grimstad	13	-1	27	19	-3	41	21	-4	46
Arendal	Arendal	12	-2	26	18	-5	40	19	-6	44
Tvedestrand	Tvedestrand	11	-3	25	16	-6	38	18	-8	42
Risør	Risør	10	-4	23	14	-9	36	15	-1	39
Telemark										
Kragerø	Kragerø	9	-5	22	12	-1	34	13	-1	37
Bamble	Langesund	6	-9	21	8	-1	32	9	-1	37
Porsgrunn	Porsgrunn	6	-9	20	8	-1	31	8	-2	36
Skien	Rambekk	6	-9	21	8	-1	32	9	-1	36
Vestfold										
Larvik	Larvik	5	-9	20	7	-1	30	7	-2	35
Sandefjord	Sandefjord	4	-1	18	4	-2	28	5	-2	32
Tjøme	Verdens ende	4	-1	18	4	-2	27	4	-2	31
Stokke	Melsomvik	3	-1	18	3	-2	26	3	-2	30
Nøtterøy	Årøysund	3	-1	17	2	-2	26	2	-2	30
Tønsberg	Tønsberg	2	-1	17	2	-2	25	2	-2	29
Horten	Horten	1	-1	16	0	-2	23	0	-2	27
Re	Mulodden	1	-1	16	-1	-2	23	-1	-2	27
Holmestrand	Holmestrand	1	-1	16	0	-2	23	0	-2	27
Sande	Selvik	1	-1	15	1	-2	24	0	-2	27
Svelvik	Svelvik	1	-1	15	0	-2	23	-1	-2	25
Buskerud										
Drammen	Drammen (Tangen)	0	-1	14	-1	-2	22	-2	-2	
Lier	Lierstranda	0	-1	14	-1	-2	22	-2	-2	25
Røyken	Nærsnes	0	-1	14	-2	-2	22	-2	-2	24
Hurum	Sætre	0	-1	14	-3	-2	21	-3	-3	24
Oslo										
Oslo	Oslo	-3	-1	12	-7	-3	16	-8	-3	19
Akershus										
Asker	Konglungen	-2	-1	13	-5	-3	18	-6	-3	22
Bærum	Sandvika	-2	-1	13	-6	-3	18	-6	-3	21
Nesodden	Nesoddtangen	-2	-1	12	-7	-3	17	-7	-3	20
Oppegård	Svartskog	-2	-1	13	-6	-3	18	-6	-3	21
Frogn	Drøbak	0	-1	14	-3	-2	21	-3	-3	24
Ås	Nesset	-1	-1	13	-5	-2	19	-5	-3	22
Vestby	Son	1	-1	15	-2	-2	22	-2	-3	26
Østfold										
Moss	Moss	1	-1	15	-1	-2	22	-1	-3	26
Rygge	Larkollen	1	-1	16	-1	-2	23	0	-2	27
Råde	Saltnes	1	-1	16	-1	-2	23	-1	-2	27
Fredrikstad	Fredrikstad	1	-1	16	-1	-2	23	-1	-2	27
Sarpsborg	Høysand	0	-1	14	-3	-2	21	-3	-3	24
Hvaler	Skjærhalden	1	-1	16	0	-2	24	0	-2	27
Halden	Halden	-1	-1	14	-4	-2	20	-4	-3	23

Table A.2.2 Projected sea level change and 5 to 95% ensemble spread for RCP4.5. Averages for three future periods are given. Changes are given relative to the reference period 1986–2005, in centimetres. All coastal municipalities are represented, and some have more than one location for which the estimation is done. The table is subdivided into counties.

RCP4.5		2041–2060			2081–2100			2100		
Municipality	**Location**	**Mean**	**5%**	**95%**	**Mean**	**5%**	**95%**	**Mean**	**5%**	**95%**
Finnmark										
Sør-Varanger	Kirkenes	5	-8	18	11	-15	37	11	-19	41
Nesseby	Varangerbotn	9	-4	21	17	-9	44	18	-12	49
Vadsø	Vadsø	7	-6	20	15	-11	41	16	-14	46
Vardø	Vardø	10	-3	23	19	-7	46	20	-10	51
Båtsfjord	Båtsfjord	12	-1	25	23	-3	49	24	-6	55
Berlevåg	Berlevåg	14	1	27	26	0	53	28	-2	59
Tana	Smalfjord	11	-2	24	21	-6	48	22	-8	53
Gamvik	Mehamn	15	2	28	28	1	55	31	0	62
Lebesby	Kjøllefjord	14	1	28	27	0	53	29	-2	59
Nordkapp	Honningsvåg	14	1	28	27	0	53	29	-2	59
Porsanger	Lakselv	8	-5	21	16	-11	43	17	-13	47
Måsøy	Havøysund	14	1	28	26	0	54	28	-2	59
Kvalsund	Kvalsund	13	-1	27	23	-6	52	25	-7	57
Hammerfest	Hammerfest	14	0	28	25	-4	55	27	-5	59
Hasvik	Breivikbotn	13	-1	27	24	-4	53	26	-7	58
Alta	Alta	9	-5	23	17	-13	46	18	-14	50
Loppa	Øksfjord	9	-5	23	17	-13	46	18	-14	50
Troms										
Kvænangen	Burfjord	9	-5	23	17	-12	45	18	-15	50
Kvænangen	Kjækan	7	-7	21	14	-14	43	15	-17	48
Nordreisa	Storslett	8	-5	22	16	-12	45	17	-15	50
Skjervøy	Skjervøy	11	-3	25	20	-8	49	21	-10	54
Kåfjord	Olderdalen	8	-6	22	15	-13	44	16	-16	49
Storfjord	Hatteng	6	-8	20	13	-15	41	14	-18	46
Lyngen	Lyngseidet	8	-6	22	16	-12	44	17	-15	49
Karlsøy	Hansnes	12	-2	26	23	-5	51	24	-7	57
Karlsøy	Nordvardvika	12	2	22	20	2	39	21	1	41
Tromsø	Tromsø (sør for Tromsøybrua)	9	-1	19	15	-3	34	15	-5	35
Tromsø	Ersfjordbotn (vest for Kvaløya)	10	0	20	17	-1	36	17	-2	37
Tromsø	Snarby	11	-3	25	21	-7	49	22	-10	55
Balsfjord	Storsteinnes	8	-6	22	15	-12	42	15	-15	47
Balsfjord	Mortenhals	10	-3	24	19	-8	47	20	-11	52
Målselv	Målsnes	10	-4	24	18	-9	46	19	-12	51
Lenvik	Finnsnes	8	-2	18	14	-5	33	13	-6	33
Berg	Skaland	12	1	23	20	1	39	21	2	41
Torsken	Gryllefjord	12	2	23	21	2	40	22	2	41
Tranøy	Vangsvik	8	-2	19	14	-4	33	14	-6	34
Sørreisa	Sørreisa	7	-3	17	12	-7	31	11	-8	31
Dyrøy	Brøstadbotn	8	-3	18	13	-5	32	13	-7	32
Salangen	Sjøvegan	5	-5	15	9	-10	28	8	-12	28
Lavangen	Tennevoll	4	-6	14	7	-11	26	6	-13	26
Gratangen	Årstein	4	-6	15	7	-11	26	6	-13	26
Ibestad	Hamnvik	7	-4	17	11	-8	30	11	-8	31
Skånland	Evenskjer	7	-3	18	12	-7	31	12	-8	31
Harstad	Harstad	10	-1	20	16	-3	35	17	-3	37
Kvæfjord	Borkenes	10	0	21	17	-1	36	18	-1	38
Nordland										
Andøy	Andenes	15	4	26	25	6	44	26	7	46
Øksnes	Myre	17	3	30	31	4	58	33	2	64

RCP4.5		2041–2060			2081–2100			2100		
Municipality	**Location**	**Mean**	**5%**	**95%**	**Mean**	**5%**	**95%**	**Mean**	**5%**	**95%**
Sortland	Sortland	14	0	27	26	-1	54	27	-3	58
Bø	Straume	17	3	30	31	3	59	33	2	65
Hadsel	Stokmarknes	14	1	28	27	0	54	28	-2	59
Hadsel	Tennstrand	12	-1	26	24	-3	51	25	-6	56
Vågan	Svolvær (Sør)	13	-1	26	25	-2	52	26	-5	57
Vågan	Laukvika (Nord)	15	2	28	28	1	56	31	0	62
Vestvågøy	Leknes (Sør)	16	3	30	31	4	58	33	3	64
Vestvågøy	Eggum (Nord)	17	4	31	32	5	60	35	5	66
Flakstad	Ramberg (Nord)	17	4	30	32	5	59	35	4	66
Flakstad	Nusfjord (Sør)	16	3	30	31	4	58	33	3	64
Moskenes	Reine (Sør)	17	3	30	31	4	59	34	4	65
Moskenes	Kalkonneset (Nord)	18	4	31	33	6	60	36	5	67
Værøy	Sørland (Sør)	17	4	30	31	5	59	34	4	65
Værøy	Flyplass (Nord)	17	4	30	32	5	59	35	4	66
Røst	Røstlandet	18	5	32	34	7	61	36	6	67
Lødingen	Lødingen	9	-4	23	19	-8	46	20	-11	51
Tjeldsund	Nedre Fjeldal (Nord)	7	-4	18	11	-7	31	12	-8	31
Tjeldsund	Ramsund (Sør)	8	-5	22	17	-10	44	18	-13	49
Evenes	Bogen	5	-6	15	7	-11	26	7	-12	27
Narvik	Narvik	4	-9	18	10	-17	37	10	-21	41
Ballangen	Ballangen	6	-8	19	12	-15	39	12	-18	43
Tysfjord	Kjøpsvik	5	-9	19	11	-16	38	11	-20	42
Hamarøy	Presteid	8	-6	21	16	-11	43	17	-14	48
Steigen	Leinesfjord	8	-6	21	16	-11	43	16	-14	47
Sørfold	Straumen	1	-10	11	0	-19	19	-1	-20	19
Bodø	Bodø	8	-5	21	15	-11	42	17	-13	46
Bodø	Skjerstad	4	-10	18	9	-18	37	9	-21	40
Fauske	Fauske	3	-11	16	7	-20	34	7	-24	38
Saltdal	Rognan	1	-13	15	4	-23	32	4	-27	35
Beiarn	Moldjord (Leirvika)	4	-9	18	10	-17	37	10	-21	41
Gildeskål	Inndyr	8	-5	20	15	-11	41	16	-13	46
Meløy	Ørnes	8	-5	21	15	-11	42	17	-13	46
Rødøy	Våga	8	-4	21	16	-10	43	18	-11	47
Rana	Mo i Rana	1	-12	14	4	-22	30	4	-25	33
Træna	Husøy	12	-1	25	23	-3	49	25	-4	55
Lurøy	Lurøy	8	-5	21	16	-10	42	17	-12	47
Nesna	Nesna	6	-7	19	12	-14	38	13	-16	42
Leirfjord	Leland	5	-8	18	11	-14	37	12	-17	41
Hemnes	Bjerka	1	-12	14	5	-21	31	5	-24	34
Vefsn	Mosjøen	3	-10	16	7	-19	33	7	-22	36
Dønna	Solfjellsjøen	8	-5	21	15	-10	41	16	-13	46
Herøy	Silvalen	8	-5	21	16	-10	42	17	-13	46
Alstahaug	Sandnessjøen	7	-6	19	13	-12	39	14	-15	44
Vega	Holand	7	-6	20	15	-11	41	16	-13	45
Vevelstad	Vevelstad	5	-8	18	11	-15	37	11	-18	40
Brønnøy	Brønnøysund	5	-8	18	11	-15	37	12	-17	41
Sømna	Vik (Sørvika)	5	-8	18	11	-15	37	12	-17	41
Bindal	Terråk	1	-12	14	5	-22	31	5	-24	34
Nord-Trøndelag										
Leka	Sør-Gutvika	4	-9	17	10	-16	36	11	-18	40
Nærøy	Kolvereid	4	-9	17	10	-17	36	11	-19	40
Nærøy	Langstranda (Nord-Salten)	5	-8	18	11	-15	37	12	-17	41
Nærøy	Søråa (Sør-Salten)	5	-8	18	11	-15	37	12	-17	41
Høylandet	Kongsmoen	0	-13	13	2	-25	28	2	-27	31
Vikna	Rørvik	6	-7	19	13	-13	39	14	-15	43

RCP4.5		2041–2060			2081–2100			2100		
Municipality	**Location**	**Mean**	**5%**	**95%**	**Mean**	**5%**	**95%**	**Mean**	**5%**	**95%**
Fosnes	Salsnes	4	-9	17	9	-17	35	10	-19	39
Namsos	Namsos	2	-11	15	6	-20	32	6	-23	35
Flatanger	Lauvsnes	6	-7	19	13	-13	39	14	-15	43
Namdalseid	Sjøåsen	4	-9	17	9	-18	35	9	-20	38
Verran	Malm	2	-11	15	6	-20	32	7	-22	36
Steinkjer	Steinkjer (for Børgin, see Inderøy)	0	-13	13	2	-24	28	2	-27	31
Inderøy	Straumen (Trondheimsfjorden)	0	-13	13	3	-23	29	3	-26	32
Inderøy	Straumen (Børgin)	0	-13	13	3	-23	29	3	-26	32
Leksvik	Leksvik	3	-10	16	7	-19	33	8	-21	37
Verdal	Verdal	-1	-14	12	1	-25	27	1	-28	30
Levanger	Levanger	0	-13	13	2	-24	28	2	-27	31
Frosta	Sørgrenda	2	-11	15	5	-21	31	6	-23	35
Stjørdal	Stjørdalshalsen	0	-13	13	2	-24	28	2	-27	31
Sør-Trøndelag										
Osen	Osen	7	-6	20	15	-11	41	16	-13	46
Roan	Roan	7	-4	18	14	-7	35	15	-8	38
Åfjord	Årnes	6	-5	17	12	-9	33	13	-11	36
Bjugn	Botngård	7	-4	18	14	-7	35	15	-8	38
Bjugn	Høybakken	6	-5	18	13	-8	34	14	-10	37
Frøya	Sistranda	12	0	23	22	1	43	24	0	47
Frøya	Titran	14	3	25	26	4	47	27	3	51
Ørland	Brekstad	7	-4	19	14	-6	35	15	-8	39
Ørland	Uthaug	8	-3	19	15	-6	36	16	-7	39
Rissa	Rissa	5	-6	16	10	-10	31	11	-12	34
Hitra	Fillan	11	-1	22	20	-1	41	21	-2	45
Hitra	Kvenvær	13	2	24	24	3	45	26	2	50
Snillfjord	Krokstadøra	8	-4	20	16	-9	41	17	-11	45
Agdenes	Lensvik	6	-6	17	11	-9	32	12	-11	35
Agdenes	Stavøysundet	8	-4	20	16	-9	41	17	-12	45
Hemne	Kyrksæterøra	8	-3	19	16	-5	37	17	-6	40
Orkdal	Orkanger	5	-7	18	11	-13	36	12	-16	40
Skaun	Børsa	4	-8	17	10	-15	35	10	-18	38
Melhus	Øysanden (Gran)	4	-9	16	8	-16	33	9	-20	37
Trondheim	Trondheim	3	-9	15	7	-17	32	7	-21	36
Malvik	Hommelvik	0	-13	13	3	-23	29	3	-26	32
Møre og Romsdal										
Smøla	Hopen	15	2	28	28	2	53	30	2	59
Aure	Aure	11	0	22	21	0	42	22	-1	46
Halsa	Liabøen	12	-1	25	23	-3	48	25	-4	53
Surnadal	Surnadalsøra	9	-2	20	17	-4	38	18	-5	42
Kristiansund	Kristiansund	15	2	27	27	2	52	30	1	58
Tingvoll	Tingvoll	12	-1	24	22	-3	47	24	-5	52
Sunndal	Sunndalsøra	8	-3	19	16	-5	37	17	-6	40
Averøy	Kårvåg	15	2	28	28	3	53	31	2	59
Gjemnes	Batnfjordsøra	14	1	27	26	1	51	29	0	57
Nesset	Eidsvåg	11	-1	24	22	-4	47	24	-5	52
Eide	Eide	15	2	28	27	2	53	30	1	58
Fræna	Elnesvågen	16	3	28	29	3	54	31	3	60
Molde	Molde	15	2	28	28	2	53	30	2	59
Rauma	Åndalsnes	12	-1	25	23	-3	48	25	-4	53
Aukra	Aukrasanden	16	3	29	29	4	55	32	4	61
Sandøy	Steinshamn	17	4	30	31	6	56	33	6	61
Midsund	Midsund	16	3	29	30	4	55	33	4	61
Vestnes	Helland	15	2	27	27	2	52	30	1	58

RCP4.5		2041–2060			2081–2100			2100		
Municipality	**Location**	**Mean**	**5%**	**95%**	**Mean**	**5%**	**95%**	**Mean**	**5%**	**95%**
Haram	Brattvåg	17	3	30	30	5	55	32	5	60
Skodje	Skodje	16	3	28	29	3	54	32	3	60
Ørskog	Sjøholt	15	2	28	28	3	53	31	2	59
Stordal	Stordal	14	1	27	27	1	52	29	1	58
Norddal	Sylte	13	0	26	24	-1	49	27	-2	55
Giske	Valderhaugstranda	17	4	30	31	6	55	33	5	60
Ålesund	Ålesund	16	4	29	30	6	54	33	6	59
Sykkylven	Aure	16	3	28	29	3	54	32	3	60
Stranda	Stranda	14	1	27	27	1	52	29	1	58
Ulstein	Ulsteinvik	17	4	29	31	7	55	33	7	60
Hareid	Hareid	17	4	29	31	7	54	33	6	59
Sula	Langevåg	17	4	29	31	7	54	33	6	59
Ørsta	Ørsta	16	4	29	30	6	54	32	6	58
Herøy	Fosnavåg	17	5	30	32	8	55	34	7	60
Volda	Volda	16	4	29	30	6	54	32	6	58
Sande	Larsnes	17	4	29	31	7	55	34	7	60
Vanylven	Fiskå(-bygd)	17	4	29	31	7	55	33	7	59
Sogn og Fjordane										
Selje	Selje	17	4	29	31	7	55	33	7	59
Vågsøy	Måløy	17	4	29	31	7	54	33	6	59
Eid	Nordfjordeid	16	4	28	30	6	53	32	5	58
Stryn	Stryn	14	1	27	26	1	51	29	0	57
Bremanger	Svelgen	16	4	29	30	6	54	32	6	59
Gloppen	Sandane	15	3	28	28	4	52	30	4	56
Flora	Florø	16	4	29	30	6	54	32	6	59
Naustdal	Naustdal	15	3	28	28	5	52	31	4	57
Luster	Gaupne	10	-1	21	19	-2	40	20	-2	43
Askvoll	Askvoll	16	4	27	29	8	50	31	8	54
Førde	Førde	15	3	26	27	6	48	29	6	52
Fjaler	Dale	15	4	26	28	7	49	30	7	53
Gaular	Bygstad	15	3	26	27	6	48	29	7	52
Balestrand	Balestrand	12	1	24	24	3	44	25	3	48
Leikanger	Hermansverk	11	0	22	21	0	41	22	0	45
Sogndal	Sogndal	10	-1	21	19	-2	40	21	-2	43
Årdal	Årdalstangen	8	-3	19	16	-5	36	17	-6	39
Solund	Hardbakke	15	4	27	29	8	49	31	8	53
Hyllestad	Hyllestad	15	4	26	28	7	49	30	7	53
Høyanger	Høyanger	13	2	24	25	4	46	27	4	49
Vik	Vik	12	1	23	23	2	43	24	2	47
Aurland	Aurlandsvangen	10	-2	21	19	-2	39	20	-3	42
Lærdal	Lærdalsøyri	8	-3	20	17	-4	37	18	-5	40
Gulen	Eivindvik	15	4	26	28	8	49	31	8	53
Hordaland										
Fedje	Fedje	16	4	27	29	8	50	31	8	54
Austrheim	Årås	16	4	27	29	8	50	31	8	54
Masfjorden	Masfjordnes	15	4	26	28	7	49	31	8	53
Modalen	Nottveit	15	3	26	27	6	48	29	7	52
Radøy	Manger	16	5	27	30	9	50	32	9	54
Lindås	Knarvik	16	5	27	30	9	51	32	9	55
Vaksdal	Vaksdal	14	4	23	25	7	43	28	8	47
Voss	Bolstadøyri	14	4	23	25	7	43	28	8	47
Øygarden	Tjeldstø	16	5	27	30	9	50	32	9	55
Meland	Frekhaug	16	5	27	30	9	51	32	10	55
Osterøy	Lonevåg	16	4	27	29	8	50	31	8	54
Fjell	Straume	17	5	27	31	10	51	33	11	55
Askøy	Kleppestø	17	5	27	31	10	51	33	11	55

RCP4.5		2041–2060			2081–2100			2100		
Municipality	**Location**	**Mean**	**5%**	**95%**	**Mean**	**5%**	**95%**	**Mean**	**5%**	**95%**
Bergen	Bergen	16	5	27	31	10	51	33	11	55
Samnanger	Tysse	14	4	23	25	7	43	28	8	47
Kvam	Norheimsund	13	3	22	23	5	40	25	6	45
Granvin	Granvin	12	0	23	22	1	43	24	1	46
Ulvik	Ulvik	11	-1	22	20	-1	41	22	-1	44
Sund	Skogsvåg	17	5	27	31	10	51	33	11	55
Austevoll	Storebø	16	5	27	31	10	51	33	11	55
Os	Osøyro	16	5	27	30	9	50	32	10	54
Fusa	Eikelandsosen	14	4	24	25	7	43	28	8	47
Jondal	Jondal	12	3	22	23	5	40	25	5	44
Ullensvang	Kinsarvik	11	1	20	20	2	37	22	2	41
Eidfjord	Eidfjord	9	0	19	17	-1	35	19	0	39
Tysnes	Uggdalseidet	14	5	24	26	8	44	29	9	48
Bømlo	Svortland	17	6	28	31	10	51	33	11	55
Fitjar	Fitjar	16	5	27	30	10	51	33	11	55
Stord	Leirvik	15	5	24	26	8	44	29	10	49
Kvinnherad	Rosendal	13	4	23	24	6	41	26	7	46
Odda	Odda	12	2	22	22	4	40	24	5	44
Sveio	Førde	16	5	27	31	10	51	33	11	55
Etne	Etne	14	4	23	25	7	43	28	8	47
Rogaland										
Haugesund	Haugesund	19	6	31	35	11	58	38	11	63
Vindafjord	Ølen	14	5	24	26	8	44	29	9	48
Vindafjord	Sandeid	14	5	24	26	8	43	29	9	48
Sauda	Sauda	13	3	22	23	6	41	26	6	45
Utsira	Nordvik	19	7	31	36	12	59	39	12	64
Karmøy	Kopervik	19	6	31	35	11	58	38	12	64
Tysvær	Hervik	18	6	30	34	10	57	37	11	62
Tysvær	Grinde (Grindafjorden og Skjoldafjorden)	18	6	30	34	10	57	37	10	62
Suldal	Sand	16	3	28	30	7	53	33	7	58
Bokn	Føresvik	19	6	31	35	11	58	38	11	63
Finnøy	Judaberg	18	5	30	33	10	56	36	10	62
Hjelmeland	Hjelmeland	17	4	29	32	8	54	34	8	60
Kvitsøy	Ydstebøhavn	19	7	31	36	12	59	39	12	64
Rennesøy	Vikevåg	18	6	30	35	11	57	38	11	63
Randaberg	Tungenes	19	6	31	35	12	58	38	12	64
Stavanger	Stavanger	19	6	31	35	12	58	38	12	63
Strand	Jørpeland	18	5	30	33	10	56	36	10	62
Sola	Solavika	19	7	31	36	12	58	39	13	64
Sandnes	Sandnes	18	6	30	35	11	57	38	12	63
Forsand	Forsand	18	5	30	34	10	56	37	10	62
Klepp	Revtangen	19	7	31	36	13	60	39	13	65
Gjesdal	Frafjord	18	5	30	34	10	56	37	10	62
Hå	Sirevåg	19	7	31	36	13	59	40	13	65
Eigersund	Egersund	19	7	31	36	13	59	39	13	65
Sokndal	Sogndalsstranda	20	7	32	37	13	59	40	14	65
Vest-Agder										
Flekkefjord	Flekkefjord	19	7	31	36	13	59	39	13	64
Kvinesdal	Øye	19	6	31	35	12	58	38	12	63
Farsund	Farsund	19	7	31	36	13	59	39	13	64
Lyngdal	Lyngdal (For Lyngdalsfjorden, see Farsund)	19	6	31	35	12	58	38	12	63
Lindesnes	Åvik	18	6	31	35	12	57	38	11	63
Mandal	Mandal	18	5	30	34	11	57	37	11	62

RCP4.5		2041–2060			2081–2100			2100		
Municipality	**Location**	**Mean**	**5%**	**95%**	**Mean**	**5%**	**95%**	**Mean**	**5%**	**95%**
Søgne	Høllen	18	5	30	33	10	56	36	10	61
Kristiansand	Kristiansand	17	4	29	32	9	55	35	9	60
Aust-Agder										
Lillesand	Lillesand	15	2	27	29	5	51	31	5	56
Grimstad	Grimstad	14	1	26	27	4	50	29	3	54
Arendal	Arendal	13	0	25	26	2	48	27	1	53
Tvedestrand	Tvedestrand	12	-1	25	24	1	47	26	-1	51
Risør	Risør	11	-2	23	22	-2	44	23	-4	48
Telemark										
Kragerø	Kragerø	9	-3	22	20	-4	42	21	-6	46
Bamble	Langesund	7	-6	20	16	-9	40	17	-11	45
Porsgrunn	Porsgrunn	7	-7	20	15	-10	39	16	-12	44
Skien	Rambekk	7	-6	20	16	-9	40	17	-11	45
Vestfold										
Larvik	Larvik	6	-7	19	14	-11	39	15	-13	43
Sandefjord	Sandefjord	5	-9	18	12	-13	36	13	-16	41
Tjøme	Verdens ende	5	-9	18	11	-14	35	12	-16	40
Stokke	Melsomvik	4	-10	17	10	-15	34	11	-18	39
Nøtterøy	Årøysund	4	-10	17	10	-15	34	10	-18	38
Tønsberg	Tønsberg	3	-10	16	9	-16	33	10	-19	38
Horten	Horten	2	-11	15	7	-18	31	8	-21	36
Re	Mulodden	2	-11	15	7	-18	31	8	-21	35
Holmestrand	Holmestrand	2	-11	15	7	-18	31	8	-21	36
Sande	Selvik	2	-11	15	8	-17	32	8	-20	36
Svelvik	Svelvik	2	-11	14	7	-18	31	7	-21	35
Buskerud										
Drammen	Drammen (Tangen)	1	-12	14	6	-19	30	6	-22	34
Lier	Lierstranda	1	-12	14	6	-18	30	6	-22	34
Røyken	Nærsnes	1	-12	14	6	-19	30	6	-23	34
Hurum	Sætre	1	-13	14	4	-21	29	5	-24	33
Oslo										
Oslo	Oslo	-2	-15	11	0	-25	24	0	-29	28
Akershus										
Asker	Konglungen	-1	-14	13	2	-23	27	2	-26	30
Bærum	Sandvika	-1	-15	12	2	-23	26	2	-27	29
Nesodden	Nesoddtangen	-1	-15	12	1	-24	25	1	-28	29
Oppegård	Svartskog	-1	-14	12	2	-23	26	2	-27	30
Frogn	Drøbak	1	-13	14	5	-21	29	5	-24	33
Ås	Nesset	0	-14	13	3	-22	27	3	-26	31
Vestby	Son	2	-12	15	6	-19	30	6	-22	34
Østfold										
Moss	Moss	2	-12	15	6	-19	31	7	-22	35
Rygge	Larkollen	2	-11	15	7	-18	31	8	-21	35
Råde	Saltnes	2	-11	15	7	-18	31	7	-21	35
Fredrikstad	Fredrikstad	2	-11	15	7	-18	31	8	-21	35
Sarpsborg	Høysand	1	-13	14	5	-21	29	5	-24	33
Hvaler	Skjærhalden	2	-11	16	7	-18	32	8	-21	36
Halden	Halden	0	-13	13	4	-21	28	4	-25	32

Table A.2.3 Projected sea level change and 5 to 95% ensemble spread for RCP8.5. Averages for three future periods are given Changes are given relative to the reference period 1986–2005, in centimetres. All coastal municipalities are represented, and some have more than one location for which the estimation is done. The table is subdivided into counties.

RCP8.5		2041–2060			2081–2100			2100		
Municipality	**Location**	**Mean**	**5%**	**95%**	**Mean**	**5%**	**95%**	**Mean**	**5%**	**95%**
Finnmark										
Sør-Varanger	Kirkenes	9	-4	23	27	-5	60	32	-5	69
Nesseby	Varangerbotn	13	-1	26	33	1	67	38	1	76
Vadsø	Vadsø	12	-2	25	32	0	64	36	0	74
Vardø	Vardø	14	0	28	36	3	69	41	4	79
Båtsfjord	Båtsfjord	16	3	30	40	8	72	45	9	82
Berlevåg	Berlevåg	18	4	32	43	10	76	48	11	86
Tana	Smalfjord	15	1	29	37	4	71	41	4	80
Gamvik	Mehamn	19	5	33	44	11	78	50	12	88
Lebesby	Kjøllefjord	19	4	33	43	10	76	48	11	86
Nordkapp	Honningsvåg	19	4	33	43	10	76	48	11	86
Porsanger	Lakselv	12	-3	27	32	-1	66	36	-2	75
Måsøy	Havøysund	18	3	34	42	9	77	47	9	87
Kvalsund	Kvalsund	17	2	33	39	6	75	44	6	84
Hammerfest	Hammerfest	19	3	34	42	8	77	47	9	86
Hasvik	Breivikbotn	17	1	33	40	6	75	45	7	85
Alta	Alta	14	-2	29	33	-1	68	37	-1	77
Loppa	Øksfjord	14	-2	29	33	-1	68	37	-1	77
Troms										
Kvænangen	Burfjord	12	-4	28	33	-1	68	37	-1	76
Kvænangen	Kjækan	11	-5	27	31	-3	66	34	-3	74
Nordreisa	Storslett	12	-3	28	32	-1	67	36	-1	76
Skjervøy	Skjervøy	15	-1	30	36	3	71	41	3	80
Kåfjord	Olderdalen	12	-4	27	31	-2	66	35	-2	74
Storfjord	Hatteng	10	-5	26	29	-5	63	32	-5	71
Lyngen	Lyngseidet	12	-3	27	32	-2	66	35	-2	75
Karlsøy	Hansnes	16	1	31	38	5	73	43	6	82
Karlsøy	Nordvardvika	15	4	27	35	10	61	38	9	69
Tromsø	Tromsø (sør for Tromsøybrua)	12	1	24	29	5	55	32	3	63
Tromsø	Ersfjordbotn (vest for Kvaløya)	13	2	25	32	7	57	34	6	65
Tromsø	Snarby	15	0	30	37	3	71	41	4	80
Balsfjord	Storsteinnes	12	-3	27	31	-2	64	34	-2	72
Balsfjord	Mortenhals	15	0	30	35	3	69	39	3	77
Målselv	Målsnes	14	-1	29	34	2	68	38	2	76
Lenvik	Finnsnes	11	0	23	28	4	54	31	2	61
Berg	Skaland	15	4	28	35	11	60	38	10	67
Torsken	Gryllefjord	16	4	28	36	12	61	38	11	68
Tranøy	Vangsvik	12	0	23	29	4	54	31	3	62
Sørreisa	Sørreisa	10	-1	22	26	2	52	29	0	59
Dyrøy	Brøstadbotn	11	0	23	28	3	53	30	1	61
Salangen	Sjøvegan	8	-3	20	23	-1	49	25	-3	56
Lavangen	Tennevoll	7	-4	19	21	-3	47	23	-5	54
Gratangen	Årstein	8	-4	19	22	-3	48	24	-5	54
Ibestad	Hamnvik	10	-2	22	26	2	51	28	0	57
Skånland	Evenskjer	11	-1	23	26	3	51	28	1	58
Harstad	Harstad	13	1	25	31	7	56	34	6	63
Kvæfjord	Borkenes	14	2	26	32	9	57	35	7	64
Nordland										
Andøy	Andenes	18	6	30	40	16	65	43	16	73
Øksnes	Myre	21	6	36	46	15	80	51	15	89

RCP8.5		2041–2060			2081–2100			2100		
Municipality	**Location**	**Mean**	**5%**	**95%**	**Mean**	**5%**	**95%**	**Mean**	**5%**	**95%**
Sortland	Sortland	18	3	33	42	10	75	46	10	84
Bø	Straume	21	6	36	47	14	81	52	16	90
Hadsel	Stokmarknes	19	4	34	43	11	76	47	11	85
Hadsel	Tennstrand	16	1	32	39	7	71	43	7	81
Vågan	Svolvær (Sør)	17	1	32	39	8	72	44	8	81
Vågan	Laukvika (Nord)	19	4	34	44	13	77	49	14	86
Vestvågøy	Leknes (Sør)	20	6	35	47	15	79	52	17	89
Vestvågøy	Eggum (Nord)	21	7	36	48	17	81	54	18	91
Flakstad	Ramberg (Nord)	21	7	35	48	16	81	53	18	90
Flakstad	Nusfjord (Sør)	20	6	35	47	15	79	52	16	89
Moskenes	Reine (Sør)	21	6	35	47	16	80	52	17	90
Moskenes	Kalkonneset (Nord)	22	7	36	49	17	82	54	19	92
Værøy	Sørland (Sør)	21	6	35	47	16	80	53	17	90
Værøy	Flyplass (Nord)	21	7	35	48	16	80	53	17	90
Røst	Røstlandet	22	8	37	49	18	82	54	19	91
Lødingen	Lødingen	13	-2	29	34	2	66	38	2	75
Tjeldsund	Nedre Fjeldal (Nord)	10	-1	22	26	3	51	28	1	58
Tjeldsund	Ramsund (Sør)	12	-3	28	32	1	64	36	0	73
Evenes	Bogen	8	-4	20	22	-1	47	24	-4	53
Narvik	Narvik	8	-7	23	25	-7	57	28	-8	65
Ballangen	Ballangen	9	-6	25	27	-4	59	30	-6	68
Tysfjord	Kjøpsvik	9	-6	24	26	-5	58	29	-7	66
Hamarøy	Presteid	12	-4	27	31	0	63	35	-1	72
Steigen	Leinesfjord	12	-4	27	31	-1	63	34	-2	72
Sørfold	Straumen	4	-8	16	15	-8	40	16	-1	46
Bodø	Bodø	12	-2	26	31	1	63	36	1	71
Bodø	Skjerstad	8	-7	23	24	-7	57	27	-9	65
Fauske	Fauske	7	-9	22	22	-9	54	25	-1	62
Saltdal	Rognan	5	-1	20	19	-1	52	22	-1	59
Beiarn	Moldjord (Leirvika)	8	-7	23	25	-7	57	28	-8	65
Gildeskål	Inndyr	12	-2	26	31	0	62	35	1	71
Meløy	Ørnes	12	-2	26	31	1	63	36	1	71
Rødøy	Våga	13	-1	27	32	2	64	37	3	72
Rana	Mo i Rana	5	-1	19	20	-1	50	23	-1	58
Træna	Husøy	16	2	30	39	9	70	44	9	79
Lurøy	Lurøy	12	-2	27	32	2	63	36	2	71
Nesna	Nesna	10	-5	24	28	-2	59	32	-2	67
Leirfjord	Leland	9	-5	24	27	-3	58	31	-3	66
Hemnes	Bjerka	5	-9	20	21	-9	51	24	-1	59
Vefsn	Mosjøen	7	-8	21	23	-7	53	26	-8	61
Dønna	Solfjellsjøen	12	-3	26	31	1	62	35	1	70
Herøy	Silvalen	12	-3	26	31	2	62	36	2	70
Alstahaug	Sandnessjøen	10	-4	25	29	-1	60	33	-1	68
Vega	Holand	11	-3	26	31	1	61	35	1	70
Vevelstad	Vevelstad	9	-6	23	27	-3	57	30	-4	65
Brønnøy	Brønnøysund	9	-5	23	27	-3	58	31	-3	66
Sømna	Vik (Sørvika)	9	-5	23	27	-3	58	31	-3	66
Bindal	Terråk	6	-9	20	21	-1	52	24	-1	59
Nord-Trøndelag										
Leka	Sør-Gutvika	9	-6	23	26	-4	57	30	-4	65
Nærøy	Kolvereid	9	-6	23	26	-5	57	30	-4	65
Nærøy	Langstranda (Nord-Salten)	9	-5	23	27	-3	58	31	-3	66
Nærøy	Søråa (Sør-Salten)	10	-5	24	27	-3	58	32	-2	67
Høylandet	Kongsmoen	4	-1	18	18	-1	49	21	-1	56
Vikna	Rørvik	10	-4	25	29	-1	60	33	-1	68

RCP8.5		2041–2060			2081–2100			2100		
Municipality	**Location**	**Mean**	**5%**	**95%**	**Mean**	**5%**	**95%**	**Mean**	**5%**	**95%**
Fosnes	Salsnes	8	-6	23	25	-5	56	29	-5	64
Namsos	Namsos	6	-8	21	22	-8	53	25	-9	60
Flatanger	Lauvsnes	10	-4	25	29	-1	60	33	-1	68
Namdalseid	Sjøåsen	8	-6	22	25	-6	56	29	-5	64
Verran	Malm	7	-8	21	22	-8	53	26	-8	61
Steinkjer	Steinkjer (for Børgin, see Inderøy)	4	-1	19	18	-1	49	21	-1	56
Inderøy	Straumen (Trondheimsfjorden)	5	-1	19	19	-1	50	22	-1	57
Inderøy	Straumen (Børgin)	5	-1	19	19	-1	50	22	-1	57
Leksvik	Leksvik	7	-7	21	23	-7	54	27	-7	62
Verdal	Verdal	4	-1	18	17	-1	48	20	-1	55
Levanger	Levanger	4	-1	18	18	-1	49	21	-1	56
Frosta	Sørgrenda	6	-8	20	21	-9	52	25	-9	60
Stjørdal	Stjørdalshalsen	4	-1	18	18	-1	49	21	-1	56
Sør-Trøndelag										
Osen	Osen	12	-3	26	31	1	62	36	2	71
Roan	Roan	11	-2	24	30	6	55	34	5	63
Åfjord	Årnes	10	-3	23	28	4	53	31	3	60
Bjugn	Botngård	11	-2	24	30	6	55	34	5	63
Bjugn	Høybakken	10	-2	23	29	5	54	32	4	62
Frøya	Sistranda	16	3	28	38	14	63	42	14	72
Frøya	Titran	18	5	31	42	17	68	46	18	76
Ørland	Brekstad	11	-1	24	31	6	56	34	6	63
Ørland	Uthaug	12	-1	25	31	7	56	35	7	64
Rissa	Rissa	9	-4	22	27	2	52	30	1	59
Hitra	Fillan	15	2	27	36	12	61	40	12	69
Hitra	Kvenvær	17	4	30	40	15	66	45	16	74
Snillfjord	Krokstadøra	12	-2	26	32	4	62	36	4	70
Agdenes	Lensvik	10	-3	22	28	3	53	31	3	60
Agdenes	Stavøysundet	12	-2	26	32	3	62	36	4	69
Hemne	Kyrksæterøra	12	-1	25	32	8	57	36	8	65
Orkdal	Orkanger	10	-4	23	28	-1	57	31	-1	65
Skaun	Børsa	9	-5	22	26	-3	55	29	-3	63
Melhus	Øysanden (Gran)	8	-6	22	25	-4	54	28	-5	61
Trondheim	Trondheim	7	-7	21	24	-5	53	27	-6	60
Malvik	Hommelvik	5	-1	19	19	-1	50	22	-1	57
Møre og Romsdal										
Smøla	Hopen	18	4	32	44	14	74	49	15	84
Aure	Aure	15	2	28	37	13	62	41	13	70
Halsa	Liabøen	15	1	29	39	9	69	44	9	79
Surnadal	Surnadalsøra	13	0	26	33	9	58	37	9	66
Kristiansund	Kristiansund	17	4	31	43	14	73	49	14	84
Tingvoll	Tingvoll	14	1	28	38	9	68	43	8	78
Sunndal	Sunndalsøra	12	-1	25	32	8	57	36	7	65
Averøy	Kårvåg	18	4	32	44	15	74	50	15	85
Gjemnes	Batnfjordsøra	17	3	31	42	13	72	48	13	83
Nesset	Eidsvåg	14	1	28	38	8	67	43	8	78
Eide	Eide	18	4	31	44	14	73	49	14	84
Fræna	Elnesvågen	18	5	32	45	15	75	50	16	85
Molde	Molde	18	4	31	44	14	74	49	15	84
Rauma	Åndalsnes	15	1	29	39	9	69	44	9	79
Aukra	Aukrasanden	19	5	32	45	16	75	51	17	86
Sandøy	Steinshamn	21	6	35	48	18	77	53	20	87
Midsund	Midsund	19	5	33	46	16	76	52	17	87
Vestnes	Helland	18	4	31	43	14	73	49	14	84

RCP8.5		2041–2060			2081–2100			2100		
Municipality	**Location**	**Mean**	**5%**	**95%**	**Mean**	**5%**	**95%**	**Mean**	**5%**	**95%**
Haram	Brattvåg	20	5	35	47	17	76	52	19	86
Skodje	Skodje	18	5	32	45	15	75	50	16	86
Ørskog	Sjøholt	18	4	32	44	15	74	50	15	85
Stordal	Stordal	17	3	31	43	13	72	48	14	83
Norddal	Sylte	16	2	30	40	11	70	46	11	81
Giske	Valderhaugstranda	20	5	35	47	18	76	52	19	86
Ålesund	Ålesund	20	6	35	46	19	74	51	20	83
Sykkylven	Aure	18	5	32	45	15	75	50	16	86
Stranda	Stranda	17	3	31	43	13	72	48	14	83
Ulstein	Ulsteinvik	21	7	35	47	19	75	52	21	84
Hareid	Hareid	21	6	35	47	19	75	51	20	83
Sula	Langevåg	21	6	35	47	19	75	51	20	83
Ørsta	Ørsta	20	6	34	46	18	74	51	20	82
Herøy	Fosnavåg	21	7	35	48	20	76	53	21	84
Volda	Volda	20	6	34	46	18	74	51	20	82
Sande	Larsnes	21	7	35	47	19	75	52	21	84
Vanylven	Fiskå(-bygd)	21	6	35	47	19	75	52	21	83
Sogn og Fjordane										
Selje	Selje	21	6	35	47	19	75	52	21	83
Vågsøy	Måløy	21	6	35	47	19	75	52	20	83
Eid	Nordfjordeid	20	6	34	46	18	74	50	19	82
Stryn	Stryn	17	3	31	42	13	72	48	13	83
Bremanger	Svelgen	20	6	34	46	18	74	51	20	83
Gloppen	Sandane	19	5	33	44	17	72	49	18	81
Flora	Florø	20	6	34	46	18	74	51	20	83
Naustdal	Naustdal	19	5	34	45	17	72	49	18	81
Luster	Gaupne	14	0	27	36	11	61	40	12	68
Askvoll	Askvoll	20	6	33	46	21	70	51	22	79
Førde	Førde	18	5	32	44	19	69	49	21	77
Fjaler	Dale	19	6	32	45	20	69	50	21	78
Gaular	Bygstad	19	5	32	44	19	69	49	21	77
Balestrand	Balestrand	16	3	30	40	15	65	45	17	73
Leikanger	Hermansverk	15	1	28	38	13	62	42	14	70
Sogndal	Sogndal	14	1	27	36	11	61	40	12	68
Årdal	Årdalstangen	12	-2	25	32	7	57	36	8	64
Solund	Hardbakke	19	6	33	45	20	70	50	22	79
Hyllestad	Hyllestad	19	6	32	45	20	69	50	21	78
Høyanger	Høyanger	17	4	30	42	17	66	46	18	75
Vik	Vik	16	3	29	39	15	64	44	16	72
Aurland	Aurlandsvangen	14	0	27	35	11	60	39	11	68
Lærdal	Lærdalsøyri	12	-1	26	33	8	58	37	9	65
Gulen	Eivindvik	19	6	33	45	20	70	50	22	78
Hordaland										
Fedje	Fedje	20	6	33	46	21	71	51	23	79
Austrheim	Årås	20	6	33	46	21	71	51	22	79
Masfjorden	Masfjordnes	19	6	32	45	20	70	50	22	78
Modalen	Nottveit	19	5	32	44	19	69	49	21	77
Radøy	Manger	20	6	33	46	21	71	51	23	80
Lindås	Knarvik	20	7	33	47	22	71	52	23	80
Vaksdal	Vaksdal	17	6	29	42	20	64	47	21	73
Voss	Bolstadøyri	17	6	29	42	20	64	47	21	73
Øygarden	Tjeldstø	20	7	33	46	22	71	51	23	80
Meland	Frekhaug	20	7	33	47	22	72	52	24	80
Osterøy	Lonevåg	20	6	33	46	21	70	51	22	79
Fjell	Straume	21	8	33	48	24	72	53	26	81
Askøy	Kleppestø	21	8	33	48	24	72	53	26	81

RCP8.5		2041–2060			2081–2100			2100		
Municipality	**Location**	**Mean**	**5%**	**95%**	**Mean**	**5%**	**95%**	**Mean**	**5%**	**95%**
Bergen	Bergen	20	8	33	48	23	72	53	26	80
Samnanger	Tysse	17	6	29	42	20	64	47	21	73
Kvam	Norheimsund	16	4	27	40	18	61	45	18	70
Granvin	Granvin	16	2	29	39	14	64	43	15	71
Ulvik	Ulvik	14	1	28	37	12	62	41	13	69
Sund	Skogsvåg	21	8	33	48	24	72	53	26	81
Austevoll	Storebø	20	8	33	48	23	72	53	25	80
Os	Osøyro	20	7	33	47	23	71	52	25	79
Fusa	Eikelandsosen	17	6	29	42	20	64	47	21	73
Jondal	Jondal	16	4	27	39	17	61	44	18	70
Ullensvang	Kinsarvik	14	3	26	37	15	58	41	15	67
Eidfjord	Eidfjord	13	1	24	34	12	56	39	12	65
Tysnes	Uggdalseidet	18	6	29	43	21	65	48	22	74
Bømlo	Svortland	21	8	33	48	24	72	54	26	81
Fitjar	Fitjar	20	7	33	48	23	72	53	25	80
Stord	Leirvik	18	6	30	43	21	65	49	22	74
Kvinnherad	Rosendal	17	5	28	41	19	62	46	20	72
Odda	Odda	15	4	27	39	17	60	44	17	70
Sveio	Førde	20	8	33	48	23	72	53	25	80
Etne	Etne	17	6	29	42	20	64	47	21	73
Rogaland										
Haugesund	Haugesund	22	9	36	53	25	80	59	27	90
Vindafjord	Ølen	18	6	29	43	21	64	48	22	74
Vindafjord	Sandeid	18	6	29	43	21	64	48	22	74
Sauda	Sauda	16	5	28	40	18	62	45	19	71
Utsira	Nordvik	23	9	36	53	26	81	60	28	91
Karmøy	Kopervik	23	9	36	53	25	80	59	28	90
Tysvær	Hervik	22	8	35	51	24	78	58	27	88
Tysvær	Grinde (Grindafjorden og Skjoldafjorden)	22	8	35	52	24	79	58	26	89
Suldal	Sand	19	6	33	48	20	74	54	23	84
Bokn	Føresvik	22	9	36	53	25	80	59	27	90
Finnøy	Judaberg	21	8	35	51	24	77	58	26	88
Hjelmeland	Hjelmeland	20	7	34	49	22	76	56	25	86
Kvitsøy	Ydstebøhavn	23	9	36	53	26	81	60	28	91
Rennesøy	Vikevåg	22	8	35	52	25	78	59	28	89
Randaberg	Tungenes	22	9	36	53	26	79	60	29	90
Stavanger	Stavanger	22	8	36	52	25	79	59	28	90
Strand	Jørpeland	21	8	35	51	24	77	57	26	88
Sola	Solavika	23	9	36	53	26	80	60	29	90
Sandnes	Sandnes	22	8	36	52	25	79	59	28	89
Forsand	Forsand	21	8	35	51	24	78	58	27	88
Klepp	Revtangen	23	10	37	54	26	81	61	29	92
Gjesdal	Frafjord	21	8	35	51	24	78	58	27	88
Hå	Sirevåg	23	9	37	54	27	80	61	30	91
Eigersund	Egersund	23	9	36	54	27	80	61	30	91
Sokndal	Sogndalsstranda	23	10	36	54	28	80	62	31	92
Vest-Agder										
Flekkefjord	Flekkefjord	23	9	36	54	27	80	62	31	92
Kvinesdal	Øye	22	8	36	53	26	79	60	29	90
Farsund	Farsund	23	9	36	54	27	80	62	31	92
Lyngdal	Lyngdal (For Lyngdalsfjorden, see Farsund)	22	8	36	53	26	79	60	29	90
Lindesnes	Åvik	22	8	36	53	26	79	60	29	90
Mandal	Mandal	22	8	35	52	25	78	59	28	89

RCP8.5		2041–2060			2081–2100			2100		
Municipality	**Location**	**Mean**	**5%**	**95%**	**Mean**	**5%**	**95%**	**Mean**	**5%**	**95%**
Søgne	Høllen	21	7	35	51	24	78	57	23	90
Kristiansand	Kristiansand	21	7	34	50	23	77	56	22	89
Aust-Agder										
Lillesand	Lillesand	19	5	32	47	19	73	52	18	85
Grimstad	Grimstad	17	3	31	45	18	71	52	21	82
Arendal	Arendal	16	2	30	44	17	70	50	19	81
Tvedestrand	Tvedestrand	16	1	29	42	15	68	49	17	79
Risør	Risør	14	0	28	40	12	66	46	15	76
Telemark										
Kragerø	Kragerø	13	-1	27	38	11	64	44	13	74
Bamble	Langesund	11	-3	25	33	4	62	40	6	73
Porsgrunn	Porsgrunn	10	-4	25	33	3	62	39	5	72
Skien	Rambekk	11	-4	25	33	4	62	40	6	73
Vestfold										
Larvik	Larvik	10	-4	24	32	2	61	38	4	71
Sandefjord	Sandefjord	9	-6	23	29	0	58	35	1	68
Tjøme	Verdens ende	8	-6	22	29	-1	58	35	1	68
Stokke	Melsomvik	8	-7	22	28	-2	57	34	0	67
Nøtterøy	Årøysund	7	-7	21	27	-2	56	33	-1	66
Tønsberg	Tønsberg	7	-7	21	27	-3	56	33	-1	66
Horten	Horten	6	-8	20	25	-5	54	30	-4	63
Re	Mulodden	6	-9	20	25	-5	53	30	-4	63
Holmestrand	Holmestrand	6	-8	20	25	-5	54	30	-4	63
Sande	Selvik	5	-9	19	26	-3	54	31	-3	64
Svelvik	Svelvik	5	-9	19	25	-4	53	30	-4	63
Buskerud										
Drammen	Drammen (Tangen)	4	-1	18	24	-5	52	29	-5	62
Lier	Lierstranda	4	-1	18	24	-5	52	29	-5	62
Røyken	Nærsnes	4	-1	18	24	-6	52	29	-5	62
Hurum	Sætre	4	-1	18	22	-8	51	27	-7	60
Oslo										
Oslo	Oslo	2	-1	16	18	-1	47	23	-1	56
Akershus										
Asker	Konglungen	3	-1	17	20	-1	49	25	-9	58
Bærum	Sandvika	3	-1	17	19	-1	48	24	-1	57
Nesodden	Nesoddtangen	2	-1	16	19	-1	47	24	-1	57
Oppegård	Svartskog	3	-1	17	20	-1	48	25	-9	58
Frogn	Drøbak	4	-1	18	22	-8	51	28	-6	61
Ås	Nesset	3	-1	17	21	-9	49	26	-8	59
Vestby	Son	5	-9	19	24	-6	52	29	-5	62
Østfold										
Moss	Moss	5	-9	19	24	-6	53	29	-5	62
Rygge	Larkollen	6	-9	20	25	-5	53	30	-4	63
Råde	Saltnes	6	-9	20	25	-5	53	30	-4	63
Fredrikstad	Fredrikstad	6	-9	20	25	-5	53	30	-4	63
Sarpsborg	Høysand	4	-1	18	22	-8	51	28	-6	61
Hvaler	Skjærhalden	6	-8	20	25	-5	54	31	-3	64
Halden	Halden	4	-1	18	21	-8	50	27	-7	60

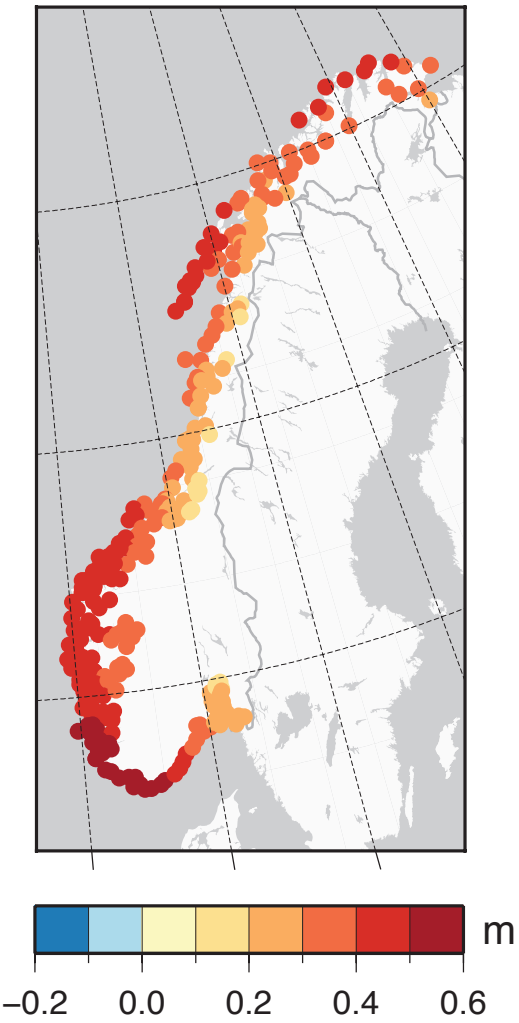

The graphic shows the most likely relative sea level changes by the end of the century in a high emission scenario.

Simpson, M. J. R., J. E. Ø. Nilsen, O. R. Ravndal, K. Breili, H. Sande, H. P. Kierulf, H. Steffen, E. Jansen, M. Carson and O. Vestøl (2015). Sea Level Change for Norway: Past and Present Observations and Projections to 2100. Norwegian Centre for Climate Services report 1/2015, ISSN 2387-3027, Oslo, Norway.

Kartverket

NERSC Nansensenteret

Bjerknes Centre for Climate Research